Doctoral theses at NTNU, 2020:297

Evgenii Salganik

Thermodynamic scaling of ice ridge consolidation

Doctoral thesis

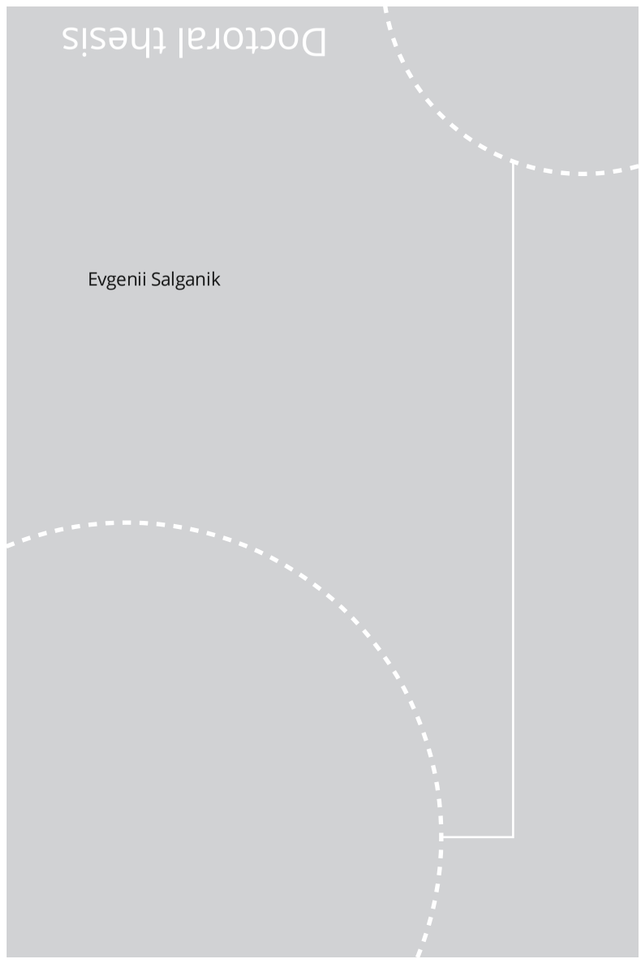

ISBN 978-82-326-4942-6 (printed ver.)
ISBN 978-82-326-4943-3 (electronic ver.)
ISSN 1503-8181

NTNU
Norwegian University of
Science and Technology

NTNU
Norwegian University of Science and Technology
Thesis for the Degree of
Philosophiae Doctor
Faculty of Engineering
Department of Civil and Environmental
Engineering

Doctoral theses at NTNU, 2020:297

NTNU

Evgenii Salganik

Thermodynamic scaling of ice ridge consolidation

Thesis for the Degree of Philosophiae Doctor

Trondheim, September 2020

Norwegian University of Science and Technology
Faculty of Engineering
Department of Civil and Environmental Engineering

NTNU
Norwegian University of
Science and Technology

NTNU
Norwegian University of Science and Technology

Thesis for the Degree of Philosophiae Doctor

Faculty of Engineering
Department of Civil and Environmental Engineering

ISBN 978-82-326-4942-6 (printed ver.)
ISBN 978-82-326-4943-3 (electronic ver.)
ISSN 1503-8181

Doctoral theses at NTNU, 2020:297

Printed by NTNU Grafisk senter

Abstract

Laboratory and field experiments together with analytical and numerical simulations were performed to study the scaling of the ice ridge consolidation. Such experiments and corresponding thermodynamic models are an important method for describing and predicting morphological, physical, and mechanical properties of the consolidated layer, corresponding atmospheric heat fluxes, and structural loads.

The laboratory-scale experiments covered ice ridges, grown from freshwater, seawater, and water-ethanol solution with different types of morphology including with parallel blocks. Such morphology was used to decrease effects from the ridge inhomogeneity, and to increase the measurement accuracy of the ridge macroporosity and the ice thickness. This allowed for separate investigations of the effects from the other ridge parameters including block thickness, ice initial temperature, and the ridge sail height. The effect of the faster growth rate of the consolidated layer over the level ice for small-scale ridges observed experimentally was found to be related to the difference in convective-conductive coupling for the two types of ice, which can be increased by the extended ridge sail surfaces. The experiments with water-ethanol ice showed no significant difference in consolidation rates with the freshwater ice ridges.

The full-scale experiments covered saline ice ridges artificially made from the surrounding level ice. This method allowed us to increase the accuracy of the macroporosity and initial ice temperature values. The results of the field measurements confirmed the thickness overestimation based on the measured temperature profile in the ridge blocks in comparison to the ridge voids. This thickness overestimation was also observed in small-scale experiments. The effect of slower consolidation rates for the full-scale ridges during the initial phase observed experimentally was found to be related to the significant deviation of those ridges from the homogeneous approach.

Simulations of the ridge consolidation were performed using a two-dimensional finite element method with the moving boundary and the discrete rubble blocks. It was validated by the performed laboratory and field experiments for different scales and different types of ice. It allowed deeper investigations of the effects from the ridge sail, rubble block initial temperature and thickness, ridge keel, and the thickness estimation methods for the consolidated layer. It has also been able to describe the scale-effects in the previous ridge experiments. The simulations helped to provide insight into the analysis of the ice ridge thermal investigations, the estimation algorithms for the consolidated layer thickness, and on the distribution of the heat transfer through the different ridge parts. The difference between fresh and saline ice growth was equally important for level ice and ice ridges, but its values were becoming significant during the initial and warming phases.

The analytical model of ridge consolidation was also formulated and validated using numerical simulations, field, and laboratory experiments. This model also allows to consider sail height, block thickness, initial ice temperature, ice salinity, and snow thickness, but cannot consider the thermal inertia. This analytical ridge model could be used for the prediction of the consolidated layer thickness in the probabilistic analysis of ice actions on structures.

Contents

Preface

This thesis is submitted to the Norwegian University of Science and Technology (NTNU) for partial fulfillment of the requirements for the degree of philosophiae doctor.

This doctoral work was performed at the Department of Civil and Environmental Engineering, NTNU, Trondheim and the Department of Arctic Technology of the University Centre in Svalbard, UNIS, with Professor Knut V. Høyland as the main supervisor and with co-supervisors Professor Aleksey Marchenko and Professor Aleksey Shestov.

This thesis was financed by the Research Council of Norway (RCN) through NTNU's Research Centre for Sustainable Arctic Marine and Coastal Technology (SAMCoT CRI), the partners of SAMCoT, and by the HAVOC project also supported by RCN.

Acknowledgments

As John Donne wrote “No man is an island entire of itself…”, most of the scientific work couldn’t be real without the unconditional trust of the society, without collaborations of people truly believing in the importance of their research fields, without infinite islands of different topics connected via bridges to form a continent of the future sustainable civilization.

I am grateful to my supervisor Knut Vilhelm Høyland for letting me work on this inspiring topic. His experience, comments, and suggestions have been very valuable together with his organization of many interesting collaborations and experiments. I thank my co-supervisor Aleksey Shestov for his experience, and a lot of help with fieldwork, laboratory work, equipment, and safety. I thank my second co-supervisor Aleksey Marchenko for the inspiration, for his lectures and his amazing focus on science. I am very grateful for the collaboration with Sönke Maus, his broad knowledge and interest in using new technologies and techniques. I would also like to thank Sveinung Løset, the leader of our research Centre, for his enthusiasm, knowledge, and organizing skills. I also thank my master’s degree supervisor Karl Shkhinek. Our numerous scientific discussions, his belief in me, and his help in becoming a researcher cannot be forgotten.

I also appreciate the collaboration with Aalto University and VTT via the HYDRALAB+ project and their help with organizing ice tank experiments. Many thanks to the Arctic Technology department and the logistics department of the University Centre in Svalbard for helping with laboratory and fieldwork activities. I am also very thankful for the great atmosphere and kindness of my colleagues from the “basement” of the Norwegian University of Science and Technology.

Declaration of Authorship

This thesis consists of an overview and the following 6 publications (Appendices 1–6). Two papers have been submitted to journals; one has been published; one is under review. Four papers have been submitted to conference proceedings; three have been published; one is under review.

Paper 1. Salganik, E., Høyland, K.V., Shestov, A., 2017. Thermodynamics and consolidation of ice ridges for laboratory scale. Proceedings of the International Conference on Port and Ocean Engineering under Arctic Conditions (POAC), Busan, Korea, paper no. 78.

The paper describes laboratory experiments on the consolidation of saline ice ridges and different methods of estimation macroporosity and consolidated layer thickness. The first author was responsible for planning and performing the experimental work, analyzing the obtained data, developing thermodynamic models, and writing the manuscript. Aleksey Shestov helped to perform the experimental work. Knut Høyland contributed to the paper by giving valuable comments and by assisting in the writing process.

Paper 2. Salganik, E., Høyland, K.V., 2018. Thermodynamics and Consolidation of Fresh Ice Ridges for Different Scale and Configuration. Proceedings of the 24th International Association for Hydro-Environment Engineering and Research (IAHR) International Symposium on Ice, Vladivostok, Russia, paper no. 38.

The paper describes laboratory experiments on the consolidation of freshwater ice ridges and describes both analytical and numerical models of that process. The first author designed experiments, analyzed the results, formulated models, and wrote most of the paper. Knut Høyland contributed to the paper by giving valuable comments and by assisting in the writing process.

Paper 3. Salganik, E., Høyland, K.V., Shestov, A., Løset, S., Heijkoop, A.-N., 2019. Medium-scale consolidation of artificial ice ridge – Part I: surface temperature, thickness and mechanical properties. Proceedings of the International Conference on Port and Ocean Engineering under Arctic Conditions (POAC), Delft, Netherlands, paper no. 82.

The paper describes the field experiment on the consolidation of saline ice ridge and describes both analytical and numerical models of that process. The first author analyzed the obtained data, performed additional laboratory worked, helped to perform the experiment, developed thermodynamic models, and wrote most of the paper. Aleksey Shestov and Sveinung Løset designed and performed the experiment. Anne-Niekolai Heijkoop contributed to the paper by helping with artificial ridge formation. Knut Høyland contributed to the paper by giving valuable comments and by assisting in the writing process.

Paper 4. Salganik, E., Høyland, K.V., Maus, S., 2020. Consolidation of fresh ice ridges for different scales. Cold Regions Science and Technology. vol. 171., https://doi.org/10.1016/j.coldregions.2019.102959

The paper describes laboratory experiments on the consolidation of freshwater ice ridges and

describes both analytical and numerical models of that process, investigating the role of surface roughness, blocks thickness, and initial temperature on consolidation rates. The first author designed experiments, analyzed the results, formulated models, and wrote most of the paper. Sönke Maus contributed to the paper by giving valuable comments and suggestions, helping with laboratory experiments, and by assisting in the writing process. Knut Høyland contributed to the paper by assisting in the writing process.

Paper 5. Salganik, E., Høyland, K.V., Shestov, A. Medium-scale experiment in consolidation of an artificial sea ice ridge in Van Mijenfjorden, Spitsbergen. Submitted to Cold Regions Science and Technology, under revision.

The paper describes the deeper analysis of field experiment on the consolidation of saline ice ridge, reviews the application of different thermodynamic models, describes methods for indirect estimation of experiment key parameters, formulate algorithms and explains uncertainties of consolidated layer thickness estimation, describes analytical and numerical models of that process using different atmospheric models. The first author analyzed the obtained data, performed additional laboratory worked, helped to perform the experiment, developed thermodynamic models, and wrote most of the paper. Aleksey Shestov contributed to the paper by designing and performing field experiment. Knut Høyland contributed to the paper by giving valuable comments and by assisting in the writing process.

Paper 6. Salganik, E., Ervik, Å., Heinonen, J., Høyland, K.V., Perälä, I., Puolakka, O., Shestov, A., van den Berg, M. Experiments in scaled ice ridge and structure interaction in Aalto ice tank: thermodynamics of ethanol ice. Submitted to Proceedings of the 25th International Association for Hydro-Environment Engineering and Research (IAHR) International Symposium on Ice, Trondheim, Norway, under revision.

The paper presents the basin experiments in ice-structure interaction with ice ridge build from the model ice produced from a water-ethanol solution. The first author was responsible for performing laboratory experiments, analyzing the obtained data, developing thermodynamic models, and writing the manuscript. Åse Ervik, Jaakko Heinonen, Ilkka Perälä, Otto Puolakka, Aleksey Shestov, and Marnix van den Berg contributed to the paper by helping to perform the experimental ice basin work. Knut Høyland contributed to the paper by giving valuable comments and by assisting in the writing process.

Notations

Fixed symbols

A_c	Sail cross-section area
c	Cloud fraction
c_a	Specific heat capacity of the air
c_b	Specific heat capacity of the liquid brine
c_i	Specific heat capacity of the fresh ice
c_s	Specific heat capacity of the snow
c_{si}	Specific heat capacity of the sea ice
C_e	Eddie coefficient for latent heat of evaporation
C_s	Eddie coefficient for sensible heat
e	Vapor pressure
h	Ice thickness
h_0	Initial ice thickness
h_c	Thickness of the consolidated layer
h_i	Thickness of fresh ice
h_k	Keel depth
h_s	Thickness of snow
h_{si}	Thickness of sea ice
H_{si}	Enthalpy of sea ice
H	Heat transfer coefficient
H_{ia}	Convectional heat transfer coefficient
$H_{ia,eff}$	Effective heat transfer coefficient
k_b	Thermal conductivity of liquid brine
k_i	Thermal conductivity of fresh ice
k_s	Thermal conductivity of snow
k_{si}	Thermal conductivity of sea ice
l	Length of the sail
L_e	Specific latent heat of vaporization
L_i	Specific latent heat of water
L_r	Effective specific latent heat of water for the ridge
m_i	Mass fraction of ice
q	Heat flux
q_a	Convective heat flux through the air
q_c	Conductive heat flux through the ice
q_e	Latent heat flux of evaporation
q_f	Heat flux through the ridge sail
q_{LW}	Net longwave radiative flux
q_r	Effective heat flux through the ridge
q_s	Sensible heat flux
q_{SW}	Net shortwave radiative flux

q_v	Heat flux through the ridge void
q_w	Heat flux from the water
P	Sail top perimeter
P	Atmospheric pressure
R	Degree of consolidation h_c/h_i
R	Thermal resistance
RH	Relative humidity
R_{norm}	Ridge normalization factor
s	Height of the sail
S_b	Salinity of the liquid brine
S_c	Salinity of the consolidated layer
S_i	Bulk salinity of the sea ice
S_r	Salinity of the unconsolidated rubble
S_w	Salinity of the seawater
t	Time
T	Temperature
T_0	Initial ice temperature
T_a	Air ambient temperature
T_b	Temperature of the block at the bottom of the consolidated layer
T_{as}	Air-snow interface temperature
T_{base}	Temperature of the sail base
T_f	Liquid freezing temperature
T_s	Air-ice interface temperature
T_{si}	Snow-ice interface temperature
v_i	Volume fraction of ice
v_n	Normal velocity of the ice-water interface
V_w	Wind speed
w	Ridge block width
w_v	Ridge void width
Z	Solar zenith angle
α	Albedo of ice or snow
ε	Longwave emissivity of snow
ε^*	Effective emissivity of the atmosphere
ϵ_f	Fin performance
η	Ridge macroporosity
η_0	Ridge initial macroporosity
θ_b	Dimensionless block temperature at the bottom of the consolidated layer
ρ_a	Density of the air
ρ_b	Density of the liquid brine
ρ_i	Density of the fresh ice
ρ_s	Density of the snow
ρ_{si}	Density of the sea ice

σ_f	Flexural strength of the level ice
σ_c	Uniaxial compressive strength of the consolidated layer
σ_i	Uniaxial compressive strength of the level ice

Abbreviations

CL	Consolidated layer
FDD	Freezing degree-days
FDH	Freezing degree-hours
LI	Level ice

1 Introduction

1.1 Background and motivation

Ice ridges are occupying a significant portion of polar sea ice. Sea ice can be divided into undeformed level ice and deformed ice features including ice ridges. Ridges are formed by shearing, bending, or compression of sea ice driven by wind and currents. Typical ice ridges consist of above water sail and underwater keel. Voids between underwater ice blocks are usually slowly freezing from above forming a consolidated layer under atmospheric cooling. The fraction of these liquid voids in an ice ridge can be characterized by a value of macroporosity. The thickness of this consolidated layer can be several times larger than surrounding undeformed level ice. In the absence of icebergs, ice ridges are forming design loads on ships, ports, lighthouses, platforms, bridges, and other offshore and coastal structures.

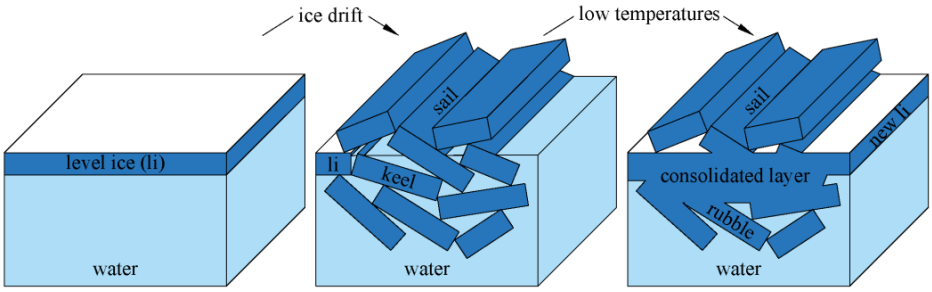

Figure 1. Schematic formation of an ice ridge from level ice and its further consolidation process, featuring main parts of an ice ridge: above water sail, underwater keel, consisting out of consolidated layer and unconsolidated rubble. The development of the consolidated layer is of interest in this thesis.

Ice ridge classification includes first-year ridges and multi-year ridges which managed to survive a summer melt season. Multi-year ridges are usually fully consolidated, but the fraction of multi-year ice in Arctic regions is decreasing and their development will not be covered in this work. Evaluation of structural loads from ice ridges is described in some standards including ISO 19906 (2019), meanwhile, load calculation requires knowledge of many ridge parameters and highly depends on the design thickness of the consolidated layer and its mechanical strength.

The consolidated layer thickness is usually measured by mechanical (Leppäranta and Hakala, 1992) or thermal drilling (Kharitonov, 2008) or from the ridge vertical temperature profile (Høyland, 2007). These methods can be used both in full-scale and in a laboratory. In small-scale, a model ridge can be just lifted from the water which can give a profile of the consolidated layer with a much higher resolution. Figure 1 shows an illustration of a consolidated layer development and gives a feeling of how uneven its bottom surface can be.

Ridging can occur almost at any time during the cold season, so the consolidation process of a first-year ridge can take many months. To conduct a field experiment on consolidation, it is important to perform some type of thickness measurements several times during most of the ridge development. A few field studies describe the seasonal development of the consolidated

layer (Blanchet, 1998; Høyland, 2007; Shestov et al., 2018). One field study in the Baltic sea (Leppäranta et al., 1995) report observations of ridge formation date. Unfortunately, most of these studies report only average values of consolidated layer thickness, which include the additional thickness of unconsolidated rubble. Meanwhile, Høyland (2002) reported a 26 % higher values of the consolidated layer thickness obtained by drilling than by temperature profile analysis. Timco and Burden (1997) analyzed the maximum, minimum, and average thickness of the consolidated layer and found thickness variability larger than 3. Such a large variance confirms that to validate a ridge solidification model, a stricter definition of consolidated layer thickness is required.

A small-scale series of laboratory experiments were performed by Timco and Goodrich (1988), and showed a different behavior of consolidation rates in comparison with fieldwork results. The existing thermodynamic models of ice ridges by Leppäranta and Hakala (1992) and Marchenko (2008) were not validated experimentally for different scales. Additionally, existing ridge models are describing the rubble as a continuum homogeneous media and are not considering local inhomogeneities as well as sail and snow distribution.

Any model of ridge consolidation should be based on the thermodynamic models of level ice. Consolidated layer thickness is often compared with a thickness of surrounding level ice as in engineering standards (ISO 19906, 2019) or field investigations (Leppäranta and Hakala, 1992). Even advanced models of ice growth are often not able to describe field measurements (Maykut, 1986).

This motivates us to design experiments in ridge consolidation with a more controlled environment and morphology, limiting the number of factors influencing the ice growth rate. It also motivates us to use a discontinuous approach with ridge modelled with separate blocks and voids. This discontinuous approach might help us to provide more of an understanding of the phenomena behind ice ridge consolidation and corresponding inhomogeneities leading to the variety observed in many experiments.

1.2 Research approach

This research was conducted by obtaining and analyzing field and laboratory measurements of ice ridge thermal, morphological, and mechanical properties, analyzing existing full-scale measurements of ice ridge consolidation, analytical and numerical modelling of ice ridge consolidation. Laboratory and numerical experiments in ridge consolidation were performed with two different geometries: with vertically oriented and with randomly oriented ice blocks. The first method allowed to increase the accuracy of macroporosity measurements, while the second method allowed to have more natural ridge morphology.

The ridge consolidation process was modelled using the finite element method using three different materials: ice, water, and snow. The position of the ice-water moving boundary was defined by the energy balance condition.

1.3 Objectives and scope

The main objectives of this thesis are to study the seasonal development of first-year ridge

consolidated layer in different scales, formulate and validate ridge thermodynamic models using data from laboratory and field experiments, quantify uncertainties of the experiments in ice ridge consolidation. Thermodynamic models aim to be able to explain the results of experiments in consolidation for different scales, as well as to be considering features of ice ridges including snow accumulations, sail height, block thickness, orientation and initial temperature, ice salinity and inhomogeneity.

The scope of the work is the following:

- Conduct laboratory experiments in the consolidation of freshwater small-scale ridges and investigate main parameters governing consolidated layer growth including freezing time, air temperature, macroporosity, sail height, initial block temperature, and block thickness.
- Formulate a one-dimensional analytical model and two-dimensional numerical model of ridge consolidation, which should be validated by small-scale laboratory and large-scale fieldwork experiments. Such models should be applicable for both freshwater and saline ice ridges, as well as for both laboratory and natural conditions.
- Design and conduct field experiments in the consolidation of a saline large-scale ridge with minimal uncertainties in initial conditions including ridge building time, initial block temperature, and ridge macroporosity. Investigate additional governing parameters and mechanisms in comparison to freshwater laboratory conditions including snow thickness, ice salinity, longwave, and shortwave radiation. Compare experimental results with predictions of developed analytical and numerical models.
- Conduct ice tank experiments in ice-structure interaction with ridges produced from model ice, compare results of ridge consolidation with predictions from analytical and numerical models. Perform laboratory experiments allowing to compare consolidation rates between ice grown from freshwater and a dopant water solution.
- Perform and analyze mechanical experiments with saline level ice and ice ridges in both small- and large scales.

1.4 Thesis structure

This thesis includes a collection of papers, provided in Appendices 1–6. Following the introduction, presented in Chapter 0, four chapters provide a summary of each of the four research topics approached in this thesis. To divide a whole topic, we define a matrix of scale ridge research.

- First, scales of our interest can be divided into two main categories: small-scale ridges, which can be created in ice tanks and cold laboratories, and large-scale ridges, which can be mainly found in nature. It is our goal to describe which processes are similar and which are different in both scales.

- Second, materials of our interest are freshwater ice ridges and ice ridges grown from a certain solution, mainly seawater. Freshwater ridges can be found in freshwater seas and other reservoirs, seawater ridges can be found in most of the polar regions, as well as can be produced in some basins and laboratories, while for mechanical scaling

ridges can be also produced from the other water solutions.

- Third, what type of scaling is our main interest: geometrical or mechanical, and how they are interconnected via freezing time and temperature.

The structure of this work is following described above matrix for the type of ridge scaling. Chapter 2 covers the geometrical scaling of ice thickness for freshwater ridges in small-scale laboratory experiments. Such experiments in ridge consolidation (growth of consolidated layer thickness) can have the most controlled environment and simplest boundary conditions in comparison to the other parts of the ridge scaling matrix. This can be explained by a completely known ridge morphology and consolidation time, while boundaries provide no external currents and no significant effect of radiation, and freshwater ice is a material with well-known and almost temperature-independent thermodynamic parameters. This part of the study includes laboratory experiments, which allowed us to validate both analytical and numerical models of freshwater consolidation. Additionally, these models were extended for a larger scale to check their validity based on the fieldwork experimental results from other researchers.

Chapter 3 is related to medium-scale ridges grown from saline seawater in field conditions. In this chapter I will cover general differences between laboratory and field conditions, between small- and large-scale top surface heat balance, how to account the presence of snow above the ridge, which data is required to estimate radiative balance, and which uncertainties we have to account when dealing with any ridge consolidation model validation. This chapter will also cover a description of artificial ridge building as well as an explanation of such experiment benefits in comparison with a standard ridge related field campaign. In that chapter I will also describe a difference between saline and fresh ice growth models and when these models can give significantly different predictions for the same meteorological conditions.

Chapter 4 is related to model ice, basin-scale experiment performed in Aalto university ice tank, and laboratory experiments in ridge consolidation covering differences between ice grown from freshwater and water-ethanol solution. It describes the main principles of basin experiment scaling, ridge production, and solidification of ice grown from water-ethanol solution.

Chapter 5 describes my investigations in mechanical characteristics of ice ridges and their comparison with similar characteristics of the surrounding level ice. It will cover the results of uniaxial compression tests of samples from both small- and large-scale saline ice ridges and surrounding level ice.

The structure of the thesis is shown in Figure 2.

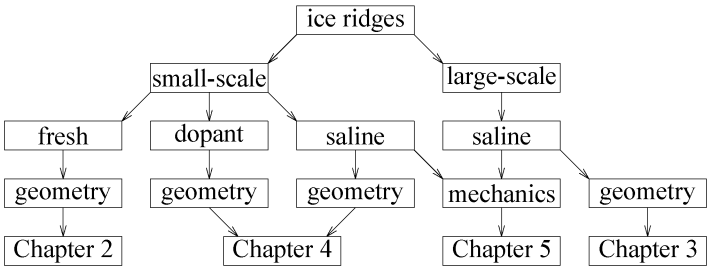

Figure 2. Structure of the doctoral study, following different geometrical sizes, different water solutions and different types of scaling.

2 Consolidation of small-scale freshwater ridges in laboratory conditions

This chapter summarizes analyses and results from laboratory experimental data collected at NTNU cold laboratory in 2018. Setup and results of experimental studies of small-scale consolidated layer growth are presented in the conference paper (Appendix 2). Validation of analytical and numerical thermodynamic models based on these experiments is presented in the full-length paper (Appendix 4).

2.1 Introduction

Ice covers in rivers, lakes, seas and oceans deform due to wind and current actions and ice ridges are forming. Ridges consist of a sail and a keel above and below the water level. Just after the ridge formation its keel consists of ice blocks and water-filled voids described by the ridge macroporosity. Later due to atmospheric cooling, the ridge keel consolidates by downward freezing of these voids and forming the consolidated layer.

Consolidation of ice ridges can be studied in the field, but these investigations are time-consuming and are usually unable to provide data about the ridge formation process and initial conditions before consolidation. Many of the parameters governing consolidation process are unknown or quite uncertain: initial macroporosity, initial size, orientation, salinity and temperature of broken ice blocks forming the ridge, and thickness of the snow above the ridge.

The consolidation process occurs over different timescales for rivers, lakes, seas and Arctic regions. The seasonal development of the consolidated layer was described by Blanchet (1998), Høyland (2002), Leppäranta et al. (1995) and Strüb-Klein and Høyland (2011). It is important to predict the thickness of the consolidated layer for different timescales. In order to conduct controlled experiments with well-known initial conditions and reasonably short duration small-scale experiments in laboratories and ice tanks are often conducted. In such experiments, the physical dimensions are reduced with a geometric scale factor. For experiments with ice-structure interaction corresponding scaling of mechanical parameters is required and performed using different techniques involving ice warming, using of dopants and spraying (Franz von Bock und Polach and Ehlers, 2015; Palmer and Dempsey, 2009). A theory of thermodynamic scaling for ice ridges is not yet developed and previous models did not include scale effects (Lepparanta and Leppäranta, 1993), while they were observed in laboratory (Timco and Goodrich, 1988) and field (Blanchet, 1998; Høyland, 2002a; Leppäranta et al., 1995) experiments.

Most of natural ice ridges are grown from a saline water and are formed from sea ice blocks, consisting out of a mixture of coexisting solid and liquid phases. It makes its thermodynamic and mechanical properties more complex and strongly dependent on their liquid fraction, being a function of ice salinity and temperature. It is important to understand how ice salinity is affecting ice growth rates and how are they different between freshwater and saline ice. It was shown by Griewank and Notz (2013) that different salinity profiles could change large-scale ice thickness prediction by less than 4 %. For laboratory experiments Notz (2005) showed that the growth rate of saline ice cooled from above is close to that of fresh ice. For small-scale ice ridges Timco and Goodrich (1988) found no difference between level ice and ridge

consolidation for fresh water and ethylene-glycol-aliphatic-detergent-sugar (EG/AD/S) water solution. Høyland (2002) have found similar consolidation rates for ridges formed in Baltic and Greenland Seas with different salinities of 3 ppt and 34 ppt correspondingly. Large-scale ice growth rate is proportional to the value of the square route of thermal conductivity divided by the density and latent heat (Stefan, 1891), while the difference in this value between two types of ice is less than 4 % (Notz, 2005; Schwerdtfeger, 1963; Yen, 1981).

Based on previous experimental studies in small-scale ridge consolidation and after some experience with saline ridges made from randomly oriented ice blocks (Appendix 1), it was decided that it is important to design a new type of experiment with smaller uncertainties in its initial conditions.

First, we used freshwater ice instead of most common in nature saline ice. Most thermodynamic parameters of freshwater ice are almost temperature independent (Notz, 2005). It helps to eliminate effective sensible heat and temperature dependent latent heat outside of simple analytical models: for a common sea ice salinity of around 5 ppt its solid fraction at freezing point is only 85 %. It makes important to keep ice temperature after the experiment undisturbed, which is not practical for laboratory experiments. Sensible heat itself can be included into analytical solution (Adams et al., 1960), but only in case of temperature independent governing parameters, which is not true for sea ice.

Second, we used ridge morphology with parallel ice blocks instead of randomly oriented blocks. It solves many complications with quantification of experimental governing parameters. With parallel blocks a location of consolidated layer part with minimum thickness is predefined. Ridge macroporosity is easy to estimate from the volume of rubble blocks and ice tank volume. But more importantly, with parallel blocks macroporosity is constant over ridge depth. It means that every timestep a cross section of voids to be frozen has the same area. This approach allows to use average value of macroporosity for validation of any analytical or numerical model using such experiments. For small-scale experiments even errors of linear size direct measurements of block, void and consolidated layer thicknesses gives significant errors, comparable to the effects from additional parameters, governing consolidation rates. Dimensions of small-scale ridges were chosen to be similar with previously performed basin test with ice ridges (Repetto-Llamazares, 2010).

There are several alternatives for parallel block morphology. Small-scale ridge can be formed from blocks of identical width placed in a planar box. It will allow to estimate macroporosity as a function of depth from underwater cameras. It allows blocks to be randomly oriented, but it also creates additional complications and uncertainties with underwater ice-water edge detection and presenting analytical solution of consolidation with depth dependent macroporosity.

2.1.1 Size effect in previous studies

The rate of ice growth in ridges depends on many the meteorological factors including air temperature T_a, water freezing temperature T_f, wind speed, long and shortwave radiation, snow thickness, ice thickness and macroporosity. During melting season, the oceanic fluxes are also becoming important. Some of these parameters are not easy to measure. When it comes to the

analysis of ridge consolidation, it is practical to compare rates of ice growth in the ridge and of the surrounding level ice due to identical meteorological conditions. The main difference between ridge and level ice growth conditions can be in snow thickness, but this parameter is easy to measure during fieldwork and easy to include into thermodynamic model. This assumption of the same surface fluxes was used by Leppäranta and Hakala (1992). For that they introduced a non-dimensional factor R by dividing the thickness of the consolidated layer h_c with the surrounding level ice thickness h_i. In their model this factor should be constant during ridge consolidation, being a function of only ridge macroporosity η as

$$R = h_c/h_i = \eta^{-0.5} \quad (1)$$

Meanwhile, the level ice surrounding a ridge may be (a) level ice from which the ridge has formed, (b) level ice that started forming in a lead created by ridge formation, or (c) thicker level ice of a different ice floe (Figure 3). For each of these cases an initial value of the factor R will be different. In the field it is often difficult to determine the origin of investigated level ice. This explains complications with fieldwork analysis using the factor R and advantages of laboratory experiments where the initial thicknesses are known.

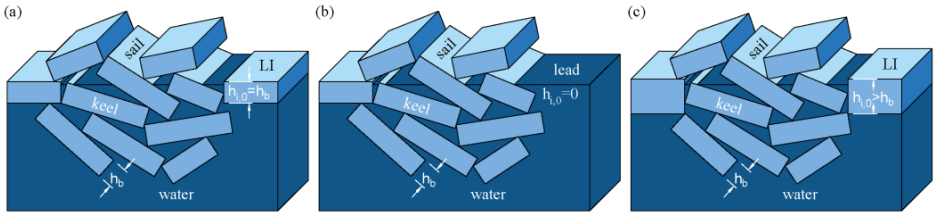

Figure 3. Scheme of an ice ridge with block thickness h_b formed from uniform level ice with thickness $h_{i,0} = h_b$ (a), formed close to a newly formed lead with zero ice thickness $h_{i,0} = 0$ (b), and formed from closure of a lead by a thicker level ice $h_{i,0} > h_b$ (c).

Different scale experimental studies in ridge consolidation show that the ratio of the consolidated layer to level ice thickness R approach a similar asymptotic value. For small-scale laboratory experiments factor R was decreasing (Figure 4a), while for large-scale field investigations it was increasing in time (Figure 4b).

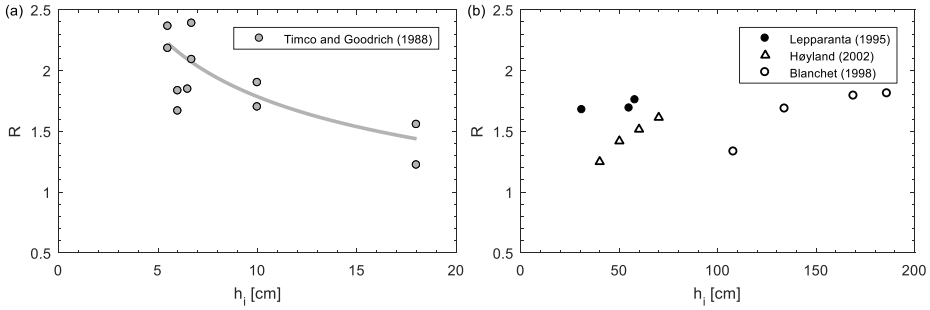

Figure 4. The ratio of the consolidated layer to level ice thicknesses R vs level ice thickness h_i from laboratory experiments by Timco and Goodrich (1988) (a) and from field data by Leppäranta et al. (1995), Høyland (2002) and Blanchet (1998) (b).

This trend was similar for both freshwater and model EG/AD/S ice with dopants for small-scale (Timco and Goodrich, 1988) and for ridges grown from water with both high salinity like in Spitsbergen fjords (Høyland, 2002a) and Beaufort Sea (Blanchet, 1998) and low salinity like in the Gulf of Bothnia (Leppäranta et al., 1995).

2.2 Methods

2.2.1 Laboratory experiments

Laboratory experiments were performed to study the influence of the block size, block orientation, block initial temperature and surface roughness on the consolidation rate. Fresh ice was cut into pieces, cooled down to the temperature T_0, placed in the water tank with side thermal insulation, and frozen under air temperature T_a of -15 °C (Figure 5a). Ice blocks were parallel to minimize errors of the ridge macroporosity measurements. The ridge block thickness was 2, 4 or 6 cm, the initial ice block temperature was -1, -15 or -24 °C, the surface roughness was characterized by the sail height s, which varied in the range 0–3 cm, block orientation was vertical or inclined by 30° to water surface. The initial macroporosity η_0 was calculated from the block width w and void width w_v as $w_v/(w + w_v)$. Thermistor strings with minimum sensor spacing of 1.5 cm were installed vertically to measure temperatures. The consolidated layer thickness h_c was assumed to be the minimum thickness of newly formed ice (Figure 5b).

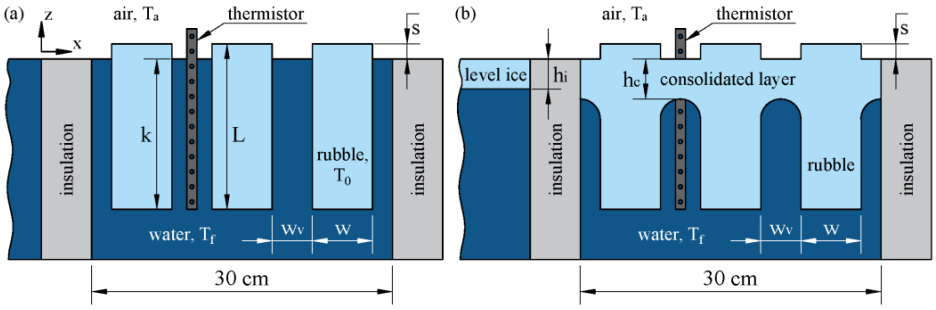

Figure 5. Experimental setup with vertical ice blocks before (a) and after (b) consolidation.

2.2.2 Analytical solution

The freezing rate of fresh ice in a laboratory is mainly governed by air temperature and wind speed. In contrast to field conditions, forced convection is the main heat transfer mechanism for small-scale laboratory conditions. The efficiency of laboratory cooling system can be characterized by the convectional heat transfer coefficient H_{ia}, while the corresponding heat transfer can be expressed as a function of the temperature difference between the ice surface and the air via Newton's law of cooling:

$$q_a = H_{ia}(T_s - T_a) \tag{2}$$

The conductive heat flux q_c depends on the bottom and top surface temperatures T_f and T_s and its thickness h_i according to the Fourier's law as

$$q_c = -k_i\,\partial T/\partial z \cong k_i\left(T_f - T_s\right)/h_i \tag{3}$$

Assuming equality of latent, conductive and convective fluxes, level ice thickness development can be expressed as:

$$h_i = \left(\frac{2k_i}{\rho_i L_i}\left(T_f - T_a\right)t + \left(\frac{k_i}{H_{ia}}\right)^2\right)^{0.5} - \frac{k_i}{H_{ia}} \tag{4}$$

For field conditions there are methods to estimate heat transfer coefficient H_{ia} from the measured wind speed V_w (Adams et al., 1960). For laboratory conditions this approach was not validated. Instead, we estimated H_{ia} using Eq. (4) and back-calculated its value from experimentally measured values of level ice thickness h_i, corresponding freezing time t and average in time air temperature T_a.

In previous publications ice ridges are assumed as a homogeneous media with small pores that are evenly distributed in its volume. For such a ridge, we must freeze only the liquid fraction η inside the ridge volume (Leppäranta, 1993):

$$L_r = L_i\eta \tag{5}$$

Thus, consolidated layer thickness analytical solution for homogeneity assumption is:

$$h_c = \left(\frac{2k_i}{\rho_i L_i \eta}\left(T_f - T_a\right)t + \left(\frac{k_i}{H_{ia}}\right)^2\right)^{0.5} - \frac{k_i}{H_{ia}} \tag{6}$$

Using Eq. (4) and Eq. (6) we can predict thickness of level ice and consolidated layer for different laboratory conditions, freezing time and ridge macroporosity η. In order to include the effect of different initial temperature of ice blocks T_0, we can assume that all the negative sensible heat stored in those blocks $c_i\left(T_f - T_0\right)$ transforms into the new ice growth after the contact with water at its freezing temperature T_f. Corresponding change in ridge macroporosity from its initial value η_0 to its value after the initial phase η can be found as (assuming no heat flux from the water):

$$\eta = \eta_0 - (1 - \eta_0)\frac{c_i\left(T_f - T_0\right)}{L_i} \tag{7}$$

Sail is a two-dimensional feature even in our simplified model ridge morphology. Heat transfer through a rough surface is affected by two factors: additional thermal resistance from the thicker ice layer, which should decrease heat flux, and additional interface area, which should increase heat flux. Theory of extended surfaces (Incropera et al., 2013) can be applied to solve problem. A finned surface includes thermal conduction through the fin and thermal convection at its surfaces. It can be described by its thickness w, length l (assumed infinitely large in our model) and height s, which define two main parameters: top perimeter $P = 2(w + l)$ and cross-section area $A_c = wl$. The heat transfer equation of a uniform fin cross-section in vertical direction can be defined as:

$$\frac{d}{dz}\left(A_c\frac{dT}{dx}\right)-\frac{H_{ia}P}{k_iA_c}(T-T_a)=0 \tag{8}$$

The temperature at the base of the fin can be defined as $T(0)=T_b$, and the boundary condition at the top surface $HA_c(T(s)-T_a)=-k_iA_c dT/dx|_{z=s}$. Vertical heat flux through the sail q_f is equal to:

$$q_f=\sqrt{H_{ia}Pk_iA_c}(T_b-T_a)\frac{\sinh ms+(H_{ia}/mk_i)\cosh ms}{\cosh ms+(H_{ia}/mk_i)\sinh ms}, \tag{9}$$

where $P=2(w+l)$ is the top perimeter area of the sail, $A_c=wl$ is the cross-section area of the sail, T_{base} is the temperature at the base of the sail, $m=\sqrt{H_{ia}P/k_iA_c}$ is the constant, l is the sail length perpendicular to the cross-section area.

The temperature distribution above the consolidated layer can be expressed as:

$$\frac{T-T_a}{T_{base}-T_a}=\frac{\cosh m(s-z)+(H_{ia}/mk_i)\sinh m(s-z)}{\cosh ms+(H_{ia}/mk_i)\sinh ms} \tag{10}$$

The effective heat flux through the sail can be compared with the heat flux of a flat surface via a fin performance defined as:

$$\epsilon_f=\frac{q_f}{H_{ia}A_c(T_{base}-T_a)} \tag{11}$$

Fin performance allows to compare effect of ridge sail on the ridge consolidation from this analytical solution and from experimental results.

The value of the experimental effective heat transfer coefficient $H_{ia,eff}$ can be found from the directly measured interface temperatures and ice thickness using the equality of convective and conductive heat fluxes (Eq. (2) and (3) as:

$$H_{ia,eff}=\frac{k_i(T_f-T_s)}{h_i(T_s-T_a)} \tag{12}$$

The value of analytical effective heat transfer coefficient $H_{ia,eff}$ can be found from Eq. (9) and Eq. (11) as:

$$H_{ia,eff}=\frac{(T_s-T_a)(w+w_v)}{q_fw+q_vw_v} \tag{13}$$

One of the goals of scaling is to normalize solution providing a scale-independent factor. For that purpose, we can use Eq. (4) and (6) and introduce a normalized solution, allowing for comparison between experiments with a different heat transfer coefficient H_{ia}, ridge initial macroporosity η_0 and level ice thickness h_i:

$$R_{norm} = \left(\frac{h_c(h_c + 2k_i/H_{ia})}{h_i(h_i + 2k_i/H_{ia})} \eta_0 \right)^{0.5} \quad (14)$$

Figure 5b defines the main morphological parameters of the model ridge. Some factors influencing the consolidation rates, including block thickness w and keel depth h_k, are not included in the analytical model and are not normalized. Their effect can be considered only using experimental and numerical approaches.

2.2.3 Numerical model

There are two main mathematical models for modelling of solidification: the fixed domain method and the front tracking method (Liu and Chao, 2006). Widely used fixed domain method is the effective specific heat method, which uses a single material for both liquid and solid by including the latent heat in the temperature-dependent-specific heat value. This method is not accurate for the materials with large values of the specific heat and when the two phases are in thermal equilibrium. The front tracking method, in contrast, includes separate materials for liquid and solid, allowing to have an exact position of phase-change interface, and it was chosen for analysis in our experiments. The ridge consolidation process was modelled in two-dimensions using the finite element analysis simulation software COMSOL Multiphysics 5.3a.

The position of the ice-water boundary was defined by the Stefan energy balance condition, where the difference in heat fluxes in two materials is equal to the amount of new solid formed or melted

$$\rho_i L_i v_n = k_i \frac{\partial T}{\partial n} - q_w, \quad (15)$$

where v_n is normal velocity of the ice-water interface, $\partial T/\partial n$ is normal derivative of the ice temperature at the interface, and q_w is the heat flux from the water.

The heat flux balance at the air-ice interface is:

$$H_{ia}(T_a - T_s) = k_i \left(\frac{\partial^2 T}{\partial x^2} + \frac{\partial^2 T}{\partial z^2} \right) \quad (16)$$

Heat diffusion within the ice is described as:

$$\rho_i c_i \frac{\partial T}{\partial t} = k_i \left(\frac{\partial^2 T}{\partial x^2} + \frac{\partial^2 T}{\partial z^2} \right) \quad (17)$$

Boundary conditions of our numerical model were identical to ones in experiments and in analytical model. Thermal boundary conditions were defined as thermal insulation at the sides and at the bottom, and as external convection with a constant heat transfer coefficient H_{ia} at the air-ice interface. These numerical simulations were performed to study the effect of the initial block temperature, block width and length, sail height, and porosity on ice growth. The numerical model setup was identic to the experimental setup shown in Figure 5.

2.3 Results

2.3.1 Analysis of laboratory experiments

Results of level ice thickness measurements plotted against FDD or $\int(T_f - T_a)\,dt$ are presented in Figure 6a. A time-averaged heat transfer coefficient H_{ia} was estimated as 20 W/m^{2}K in our laboratory using Eq. (4). The consolidated layer thickness plotted in the same way together with the level ice thickness is shown in Figure 6b together with results of analytical model from Eq. (6) for the minimum and maximum values of ridge macroporosity for our laboratory experiments.

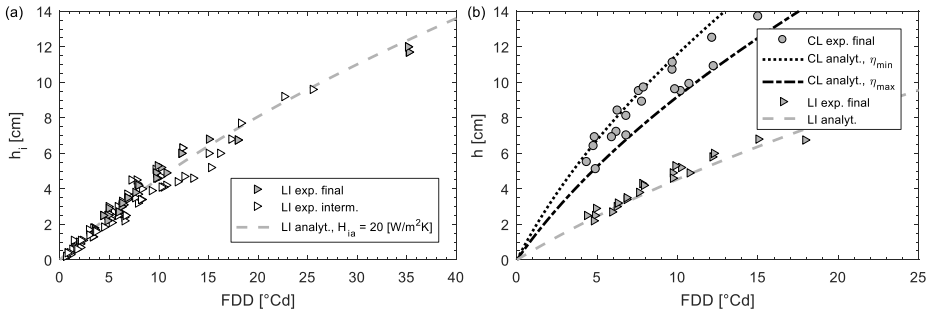

Figure 6. Level ice thickness h_i (a) and thickness of level ice and the consolidated layer h (b) vs freezing-degree days FDD from experiments and from the analytical model for minimum and maximum experimental ridge porosities η_{min} and η_{max}.

One of the main assumptions of our analytical and numerical models is that the value of the heat transfer coefficient H_{ia} is the same for the level ice and for the ridge. This assumption was confirmed experimentally by estimation of the effective heat transfer coefficient $H_{ia,eff}$ for level ice and for ridges using measured values of interface temperatures and ice thickness at the end of experiments. The convective boundary condition from Eq. (2) using heat transfer coefficient H_{ia} is applied to horizontal, vertical and inclined ice top surfaces. This is complicated to measure experimentally, so only the effective heat transfer coefficient $H_{ia,eff}$ can be estimated from the measured temperatures and thickness. Figure 7a shows that for the ridge experiments with sail height smaller than 1.5 cm the values of estimated effective heat transfer coefficient $H_{ia,eff}$ were close to the values for the level ice. A comparison of analytical and experimental estimates of $H_{ia,eff}$ for the ridges with different sail heights and corresponding ratio of top surface and cross-section area is presented in Figure 7b. The ratio of top surface and cross-section area was found from the experimentally measured sail height s, block w and void width w_v as $(2s + w + w_v)/(w + w_v)$. Small-scale sails added additional top surfaces for ridges with increasing heat fluxes.

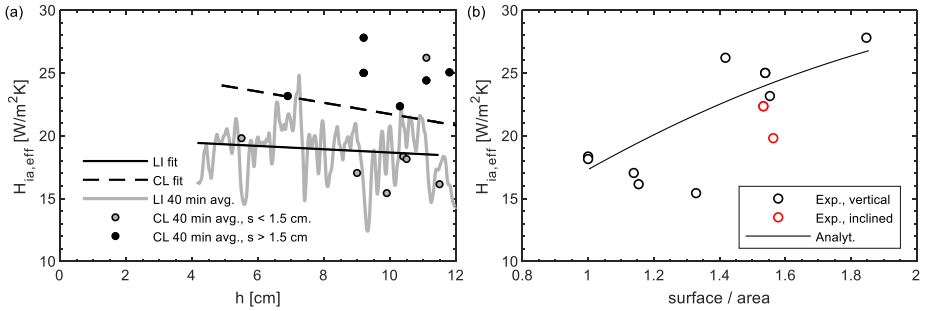

Figure 7. Experimental values of the effective heat transfer coefficient $H_{ia,eff}$ from temperature and thickness measurements using Eq. (12) vs the ice thickness h for the level ice and ridge experiments (a) and comparison of experimental and analytical values of $H_{ia,eff}$ values for model ridges vs the ratio of sail surface and cross-section area (b) using Eq. (13).

Block thickness effect was approached using experiments and numerical simulations. Usage of normalization factor from Eq. (14) allowed to compare experimental results with different macroporosities. Two-dimensional numerical simulations with different block thicknesses indicated that the deviation of analytical solution from observations was a consequence of the variable block thicknesses, a two-dimensional effect that was well-captured by the numerical model (Figure 8a). The R_{norm} values approached equilibrium faster for thinner blocks, while a peak in R_{norm} values was reached when level ice had grown to approximately the size of the voids w_v. Figure 8b shows an extension of the numerical results for a larger range of scales.

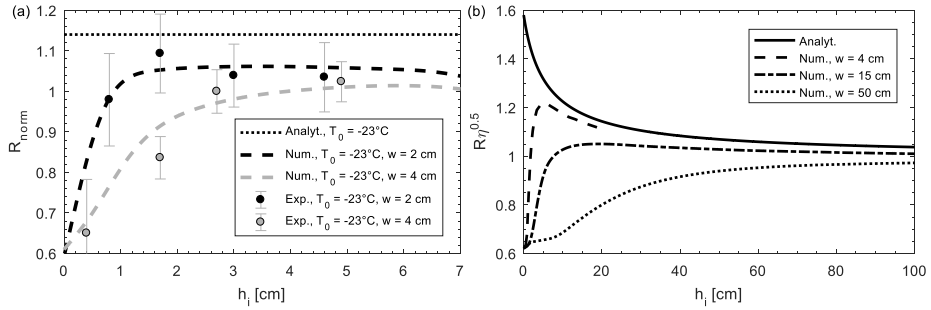

Figure 8. Values of R_{norm} (a) and $R\eta^{0.5}$ (b) vs the level ice thickness h_i for different block thicknesses w in experiments and in numerical simulations.

The effect of the initial ice temperature and sail height, with increasing consolidation for increasing sail heights and decreasing initial temperatures (Figure 9) was also confirmed by similar experimental and numerical results. The effect on R_{norm} values from an increasing sail height of 3 cm was equivalent to the effect from a decreasing initial temperature of -23 °C.

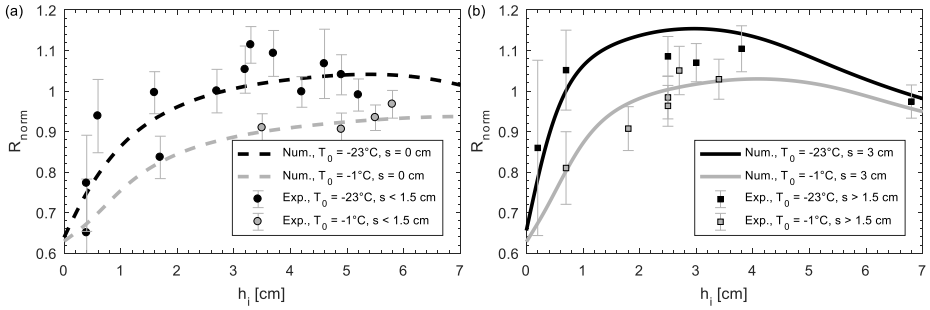

Figure 9. Temperature effect on the R_{norm} values for experiments with a small (a) and large (b) sail.

The initial macroporosity η_0 is the main parameter defining the difference between a ridge and level ice consolidation. The effect of both macroporosity and the heat transfer coefficient is considered in R_{norm}. Lower values of the heat transfer coefficient H_{ia} led to a more significant scale effect for similar ice thicknesses (Figure 10).

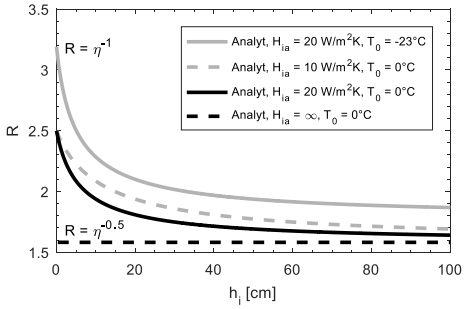

Figure 10. Ratio of consolidated layer and level ice thicknesses $R = h_c/h_i$ vs level ice thickness h_i for the analytical solution from Eq. (4), (6) and (7) and initial macroporosity η_0 of 0.4 for the different initial block temperatures T_0 and heat transfer coefficient H_{ia}.

Experiments in consolidation should be reproducible for ridges with different macroporosities and for laboratories with different heat transfer coefficients. A perfect normalization can be characterized by the absence of effects on normalized factor from changing its input parameters. By varying the macroporosity values η_0 obtained by changing the block size and by varying the heat transfer coefficient values in our numerical model we confirmed the validity of normalization using factor R_{norm}. For simulations with different initial macroporosity, the heat transfer coefficient was 20 W/m^{2}K (Figure 11a), while for simulations with varying heat transfer coefficient, the initial macroporosity was 0.4 (Figure 11b).

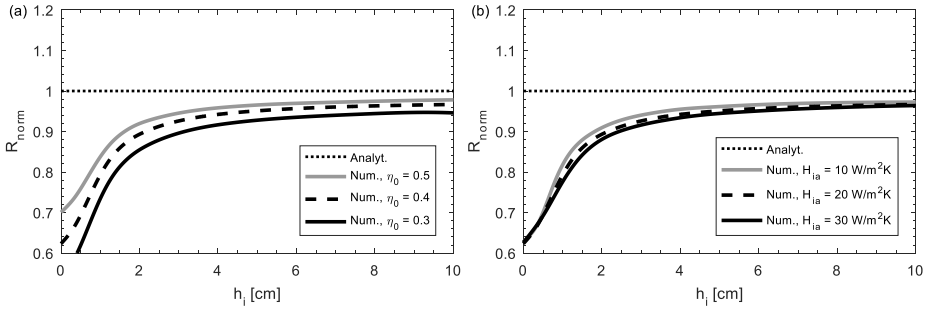

Figure 11. R_{norm} vs the level ice thickness h_i for different porosities (a) and different heat transfer coefficients H_{ia} (b).

Usage of R_{norm} factor provides the possibility of comparing the experiments in different scales with different initial macroporosities and heat transfer coefficients expecting R_{norm} values approaching a value of 1.

2.4 Discussion

Normalization of experiments in ridge consolidation proposed in previous studies (Leppäranta and Hakala, 1992) was found to be not applicable for small scales (Figure 10). Proposed analytically derived factor R_{norm} allows to normalize such experiments. Instrumental errors of proposed experiments with simplified geometry (Figure 9) are small enough for investigating of effects from additional parameters of model ridges including sail height, block initial temperature and block thickness.

The consolidation process can be divided into several phases. The initial phase starts immediately after ridging, when the level ice and consolidated layer are growing at almost the same rate, and the R value is 1. This phase ended when values of R started to approach the value of η^{-1} (Figure 8b). The end of this phase usually occurs when the level ice reaches approximately the void width value and R reaches the maximum value. During the following main phase, R can be described by the presented analytical solution from Eq. (6). It slowly decreased and approached its equilibrium value of $\eta^{-0.5}$.

In the introduction of this chapter we already covered existing experiments in ridge consolidation and their limitations, mainly related to the unknown ridging time and uncertainties in the macroporosity values. Several assumptions for our model's application for those experiments. Like in our laboratory experiments, we estimated time averaged heat transfer coefficient H_{ia} from the described experimental dependency of level ice thickness from FDD. In case of fieldwork data, this coefficient included not only air, but also snow thermal resistance, which depends on snow thickness and snow thermal conductivity. Due to limited information about these parameters, the value of the heat transfer coefficient H_{ia} was assumed to be constant during these experiments. Time of ridging was estimated using the reported values of block thickness, assuming the ridging occurred when the level ice thickness reached the value of block thickness. For the experiments by Høyland (2002) ridge macroporosity was measured. For the experiment by Blanchet (1998) we assumed the ridge macroporosity of 0.25 using fieldwork investigations by Pavlov et al. (2016). For the basin experiments by Timco and Goodrich

(1988), the ridge porosity of 0.5 was estimated from the block length and thickness ratio using the experimental correlation of Surkov and Truskov (2003).

Our analytical and numerical models provided accurate predictions of consolidation development (Figure 12a). Our small-scale results were similar to those of by Timco and Goodrich (1988), which confirms that our experimental setup is applicable for the small-scale consolidation investigations (Figure 12b).

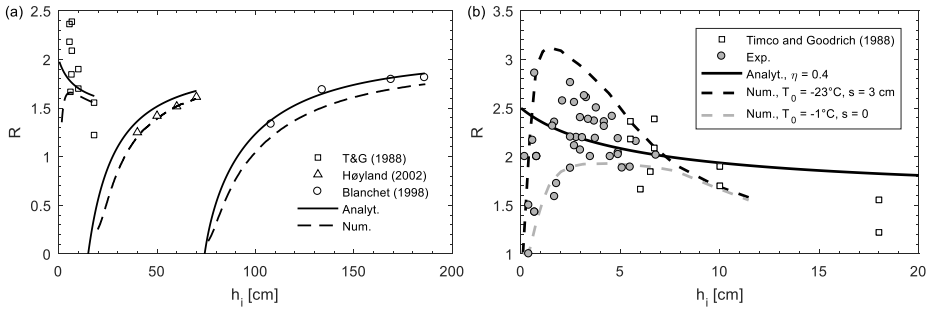

Figure 12. Comparison of *R* values from experiments by Timco and Goodrich (1988), Blanchet (1988), and Høyland (2002) and from analytical and numerical solutions for initial experimental conditions for large scales (a) and small scales (b).

The application of our models to experiments in different scales shows that previously observed size-effects can be explained by our analytical approach better than by previous models of ridge consolidation.

2.5 Conclusions and recommendations

This chapter covers experimental work in small-scale freshwater ridge consolidation and provides analytical and numerical models, which can describe obtained experimental results and can be extended for larger scales. The main findings are summarized as follows:

- The analytical model of ice ridge solidification, which can explain observed scale effects on consolidated layer growth, is presented. It allows the comparison of experiments for ridges with different porosities, ice block initial temperatures, subjected to air with different convectional heat transfer coefficients using the introduced normalization factor R_{norm}. The ratio of the consolidated layer and surrounding level ice thickness based on that solution mainly depended on the ridge macroporosity η, starting at the value of η^{-1} and approaching $\eta^{-0.5}$ for thick ice.
- The new configuration of laboratory experiments in ridge consolidation was described to improve the accuracy of the main parameters governing that process. In the provided experiments, the consolidated layer reached a thickness up to 2.2–2.8 times greater than level ice for the ridge macroporosity η of 0.4, close to the described analytical model predictions of η^{-1}.
- A numerical model, which was able to predict effects on the consolidation rates from sail height, block thickness, block initial temperature and macroporosity, was described and validated using the provided experiments. The sail height had a

significant effect on the small-scale consolidation, leading to up to a 40 % thicker consolidated layer for the sail height of 3 cm compared to the level area. This phenomenon was observed in both experiments and numerical simulations, and it contrasts with typical observations for large-scale ridges.

- Both experiments and numerical simulations confirmed that the consolidated layer thickness was initially growing slower than predicted by the analytical solution. The analytical solution was approached when the thickness of ice growing in voids reached the thickness of the ridge blocks.

Experimental fieldwork in large-scale consolidation of saline ice ridge is described in the following Chapter 3. Laboratory and basin thermodynamic experiments with saline and model ice produced from randomly oriented ice blocks are described in Chapter 4, while mechanical investigations of saline ridges in different scales are covered in Chapter 5.

3 Field consolidation of medium-scale saline ridge

This chapter summarizes thermodynamic analyses and results from the medium-scale field experiment performed in Van Mijenfjorden in 2017. The setup and results of the field study of medium-scale consolidated layer growth are presented in the conference paper (Appendix 3). Validation of analytical and numerical thermodynamic models based on this experiment are presented in the journal paper (Appendix 5).

3.1 Introduction

In the previous chapter we described our experiments in the consolidation of freshwater small-scale ice ridges and thermodynamic models allowing to describe their results. It was shown that our models can also describe the results of existing experiments in larger scales in contrast to previously developed ridge consolidation models (Leppäranta and Hakala, 1992). Meanwhile, previous studies reported that the measurements of such experiments have a large variance (Høyland, 2002a; Timco and Burden, 1997), and not all the key parameters for ridge consolidation were reported in existing fieldwork observations. In this study thickness of the consolidated layer h_c is defined as a minimum of newly formed ice between ice (Figure 13).

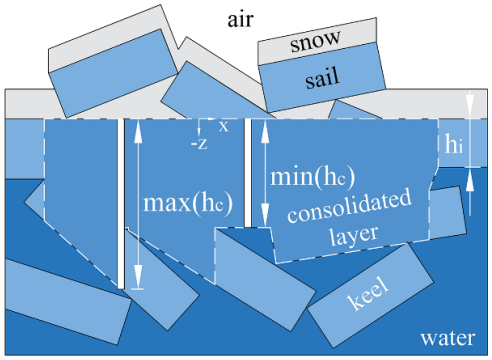

Figure 13. Ridge cross-section with maximum and minimum consolidated layer thickness h_c.

As was mentioned in Chapter 2, there is a limited amount of field experiments, allowing for validation of a thermodynamic model (Table 1). The only field experiment with a known starting time of ridge consolidation was described by Leppäranta et al. (1995). In that experiment the thickness of the consolidated layer was measured using mechanical drilling, which can significantly overestimate thickness, estimated using temperature data (Høyland, 2002a). In the longest existing field measurements by Blanchet (1998) macroporosity, snow thickness, and ridging time were not measured. In three different experiments by Høyland (2002) most of the key parameters for ridge consolidation were measured, but experiments covered only later stages of consolidation, while the ridging time was unknown.

Table 1. Summary of field experiments in ridge consolidation

Study	t [d]	FDD	h_i [m]	h_c [m]	η	h_s [m] (LI/CL)	Location
Høyland (2002)	71	985	0.95-1.16	1.19-1.61	0.33	0.4 / 0.45	Svalbard
Høyland (2002)	56	680	0.65-0.75	0.91-1.13	0.35	0.3 / 0.4	Svalbard
Høyland (2002)	28	134	0.45-0.55	0.50-0.71	0.38	0.05 / 0.1	Baltic Sea
Blanchet (1998)	150	2407	1.08-1.86	1.44-3.37	-	-	Beaufort Sea
Leppäranta et al. (1995)	87	600	0.15-0.58	0.00-1.02	0.32	0.02-0.22	Baltic Sea
Salganik et al. (2019)	66	716	0.50-0.99	0.00-1.20	0.36	0.07 / 0.07	Svalbard

The motivation for the new fieldwork was to perform an experiment in consolidation allowing to know the ridge building time, initial volume and temperature of the blocks, snow thickness development, and consolidated layer thickness using several measuring techniques. For that purpose, it was decided to build an artificial middle-scale ridge close to the weather station allowing to have precise meteorological observations.

Another motivation was to compare results from a simple one-dimensional analytical and two-dimensional numerical model to quantify errors originated from analytical simplifications and assumptions. Advanced numerical models for ridge consolidation exist (Høyland, 2002b; Marchenko, 2008), but these are difficult to use in probabilistic design where for example different climate scenarios need to be considered and thousands of simulations should be run to quantify structural reliability. The traditional solution is based upon modifying the latent heat in Stefan's law with the rubble macro-porosity (Leppäranta and Hakala, 1992). In the simplest form, this solution neither takes into account the snow cover nor the atmospheric boundary layer (the air), but modifications to include these can easily be done. However, the effect of the real three-dimensional bottom and top surfaces of the consolidated layer is not included.

Medium-scale solidification experiments provide the unique advantage of accurately measured parameters such as initial macroporosity, initial block temperature, and salinity, and freezing time. It reduces error in crucial parameters for the solidification process, which includes radiation, air natural, and forced convection, conduction through snow and ice, and phase change. Saline ice has a polycrystalline structure with salt brine inclusions between crystals. Thus, any temperature or salinity change leads to the change of sea ice solid fraction. In this chapter, we define and validate a simple analytical solidification model suitable for transient air temperature, wind speed, and snow thickness. The field experiment was intended to compare thermodynamics and development of physical and mechanical parameters of level ice and consolidated layer.

3.2 Methods

3.2.1 Field experiment

The field experiment in the consolidation of artificial saline ice ridge was performed during 66 days from 25 February 2017 until 2 May 2017 in Vallunden lagoon, Van Mijenfjorden, Svalbard (Lu et al., 2019; Salganik et al., 2019a). We cut 55 blocks with an average salinity of 3.8 ppt from 50 cm thick ice using trencher, totally 11.4 m^3 of ice, to make a ridge. The average block temperature was -7.8 °C. The blocks were dumped from the ramp into the basin of 3.0 m by 4.9 m made in the ice cover using rope and snowmobile (Figure 14).

During 4 visits we collected information about ice temperature, salinity, and density vertical

profiles. Ridge morphology was investigated by collecting 3 vertical cores during the visit 1 and 12 vertical cores at visit 4. The value of initial macroporosity was estimated based on the volume of ice blocks measured during visit 1 before ridge building and final ridge volume measured during visit 4. The final volume of the ridge was estimated using keel depth and sail height values from 12 cores drilled during visit 4.

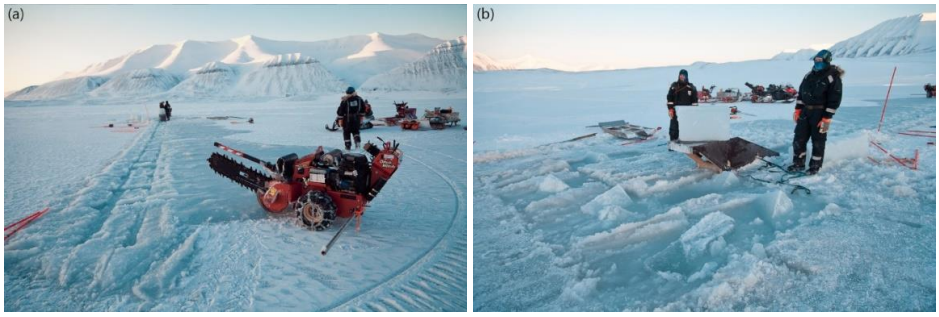

Figure 14. Feeding channel (a) and ridge formation using the ramp (b).

The temperature in the ridge and the surrounding level ice was measured every 10 minutes using thermistor strings. Level ice initially had 7 cm freeboard and its temperature profile was logged until March 18. In the ridge sail with 15 cm freeboard temperature was measured until the end of the experiment on May 4. Three cores were used to measure initial parameters of level ice during visit 1. During all 4 visits of the experimental site following parameters were measured for level ice and model ridge: ice and snow thickness, ice salinity, and density vertical profiles. The salinity and density profiles had a vertical resolution of 5 cm.

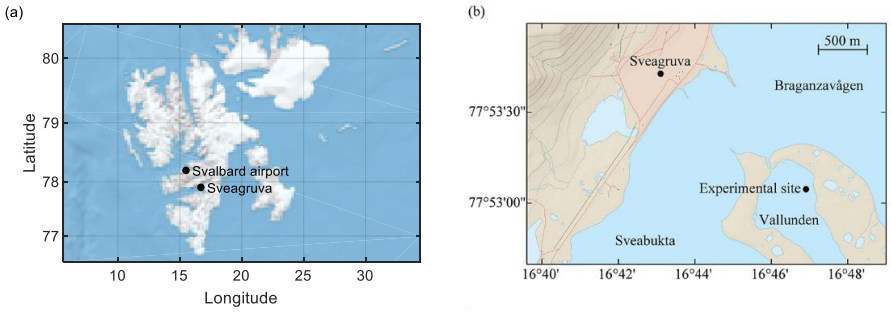

Figure 15. Weather stations location in Svalbard (a) and experimental site location in Van Mijenfjorden (b).

Ice thermodynamic parameters including heat capacity, thermal conductivity, latent heat, and solid fraction were calculated from Notz (2005). Data from weather stations in Svalbard were collected using web service eklima.no by the Norwegian Meteorological Institute. Information about air temperature, humidity, and wind speed was received from the closest weather station 99760 Sveagruva, located 2 km from the experimental site. Missing local direct measurements of cloudiness data were received from 99840 Svalbard airport weather station 40 km from the experimental site. Local cloudiness at the experimental site was received from the Icosahedral

Nonhydrostatic (ICON) Modelling Framework by the German Weather Service.

Ice thickness between four visits was estimated from temperature measurements below the upper 20 cm. All the sensors with temperature values lower than a chosen threshold of 0.5 °C were considered frozen. The highest and lowest measurement points were used for linear extrapolation of temperature profile to obtain ice thickness value. The sensitivity of this method to the chosen threshold will be described in the results.

In this section we will also describe input data for the application of our thermodynamic models, including atmospheric data from weather stations or remote sensors, and physical parameters of ice. Average cloudiness c measured at Svalbard airport weather station was 0.63 during the experimental time. The Icosahedral Nonhydrostatic (ICON) Modelling Framework showed the average cloud cover of 0.57 for Svalbard airport and 0.58 for Sveagruva. The average air temperature at Sveagruva weather station during the experiment was -12.6 °C, 0.3 °C warmer than the historical value for March and April (Førland et al., 1997). The average relative humidity RH was 0.75 for both Sveagruva and Svalbard airport weather stations. The average wind speed at Sveagruva during the experiment was 4.7 m/s.

Level ice and model ridge salinity profiles from the cores drilled at visits 1 and 4 are shown in Figure 16. The level ice salinity after 66 days increased from 3.8 ppt to 4.6 ppt, the consolidated layer final salinity was 4.1 ppt. Based on the observed vertical shift in level ice salinity profiles, it can be argued that 4 cm of ice formed above the initial top surface during warm periods in the later stage of the experiment.

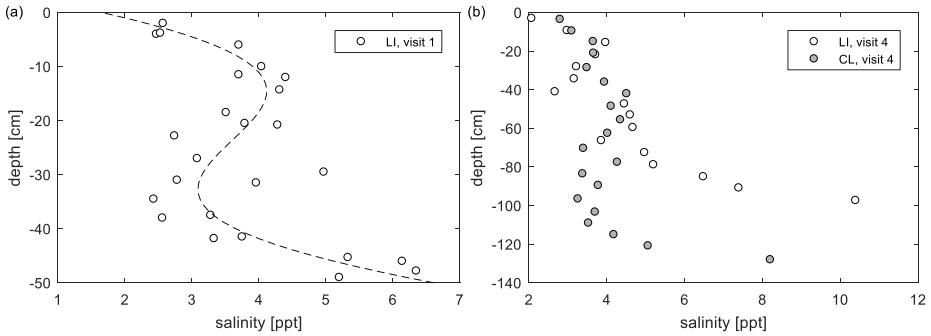

Figure 16. Salinity profiles for visit 1 (a) and visit 4 (b).

Relative brine volume was estimated using in-situ measurements of ice temperature, salinity, density and water freezing temperature T_f (Cox and Weeks, 1983). Values of the relative brine volume are presented for level ice at visit 1 for initial in-situ temperature, and water freezing temperature (Figure 17a) and for level ice and consolidated layer for the in-situ temperature at visit 4 (Figure 17b). Both level ice and the consolidated layer had the final value of 8 % liquid volume fraction (Figure 17b) and 2 % gas volume fraction.

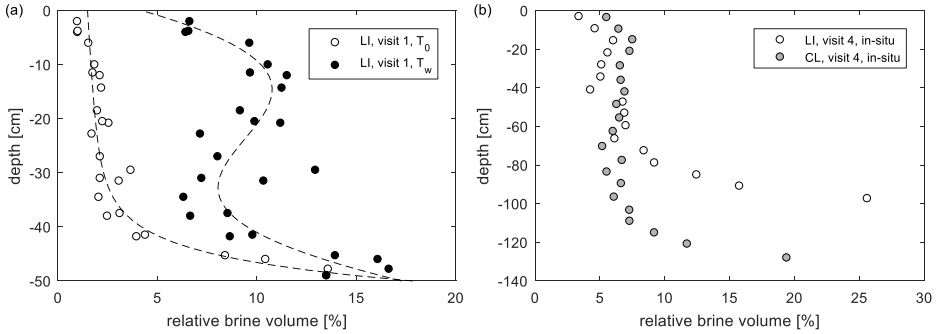

Figure 17. Relative brine volume profiles for in-situ and water freezing temperatures at visit 1 (a) and in-situ temperatures at visit 4 (b).

During the experiment level ice grew from 50 cm to 99 cm, the consolidated layer grew up to 120±12 cm. The development of level ice and consolidated layer draft is presented in Figure 18a: from the drilling during 4 visits and from the vertical temperature profiles measured by thermistors. Snow thickness above the level ice varied in the range 2–11 cm, snow thickness above the ridge was in the range 0–13 cm.

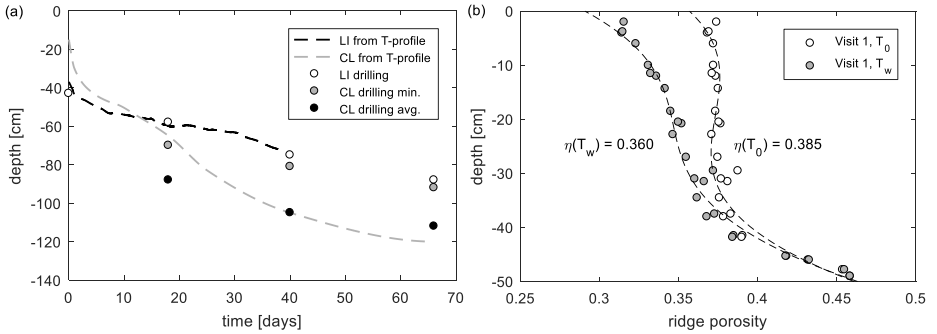

Figure 18. Ice draft development (a) and ridge porosity profile for visit 1 at in-situ and water temperature (b).

Figure 18b shows the ridge total porosity values estimated for measured level ice in-situ and water temperature, salinity, and density. The average value of the ridge total porosity should decrease from 0.39 to 0.36 due to block average initial temperature of -7.8 °C. The value of initial macroporosity was found from ridge morphology at visits 1 and 4 (Figure 19).

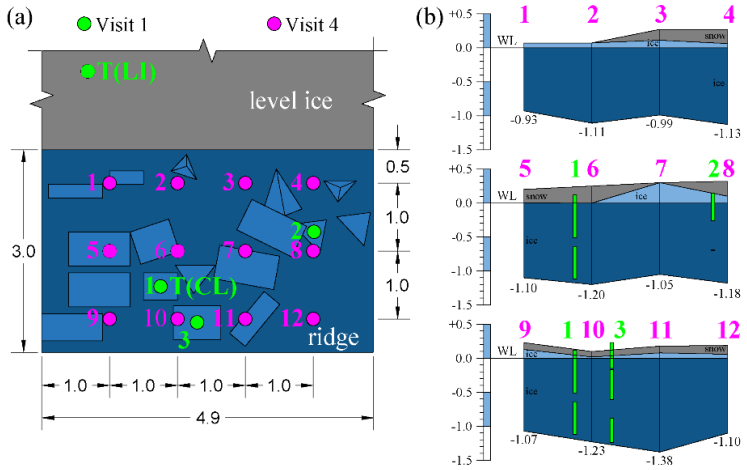

Figure 19. Ridge plan (a) and vertical profiles (b) during visits 1 and 4 from ice drilling.

Table 2. Temporal evolution of the main level ice and model ridge parameters

Parameter	Visit			
	1	2	3	4
Number of LI/CL cores	3/0	0/2	0/4	1/12
Min. CL thickness [m]	0.00	0.78	0.97	1.00
Avg. CL thickness [m]	-	0.96	1.13	1.20
LI thickness [m]	0.50	0.65	0.82	0.99
CL snow thickness [m]	0.00	0.13	0.07	0.09
LI snow thickness [m]	0.02	0.11	0.02	0.05
CL salinity [ppt]	3.8	4.2	3.8	4.1
LI salinity [ppt]	3.8	-	-	4.6
FDD [°d]	705	915	1228	1421
Ridge macroporosity	0.36	-	-	0.00

Table 2 presents the main physical and morphological parameters of level ice and model ridge during 4 visits, as well as accumulated freezing indexes in FDD.

3.2.2 Sea ice growth modelling

3.2.2.1 Atmospheric fluxes

We have used two analytical and numerical models to calculate the growth of level ice and the consolidated layer. The analytical models are one-dimensional, and they assume infinitely fast thermal diffusion in contrast to more accurate two-dimensional numerical models. All the four models require the following input of ice and snow parameters:

- Snow: thickness, thermal conductivity.
- Level ice: salinity, gas volume, thickness.
- Ridges: macroporosity; block initial temperature, salinity, gas volume, and thickness; sail size, consolidated layer salinity, gas volume, and thickness.

The heat exchange with the atmosphere was modelled in two ways. Firstly with a simple convective flux, and secondly with a model including radiation and turbulence (Maykut, 1986).

In the convective model the atmospheric flux q_a is defined from Newton's law of cooling (Eq. (2), where the convective heat transfer coefficient H_{ia} is a function of the wind speed V_w and can be found as (Adams et al., 1960):

$$H_{ia} = \max\left(11.6, 5.7V_w^{0.8}\right) \tag{18}$$

The radiative model includes longwave and shortwave radiation, sensible and latent heat fluxes. Radiation fluxes are not proportional to the difference between snow top surface and air ambient temperatures $T_{as} - T_a$ and cannot be included in the total model in the form of temperature-independent resistance as for convective model. This model requires the following meteorological data:

- LW radiation: air temperature, humidity, cloudiness.
- SW radiation: cloudiness, surface albedo (Shine, 1984).
- Turbulent fluxes: air temperature, wind speed (Smith, 1988).

The top surface heat flux balance can be written as (Maykut, 1986):

$$q_{LW} + q_{SW} + q_s + q_e + q_c = 0, \tag{19}$$

where q_{LW} is the net longwave radiation, q_{SW} is the net shortwave radiation, q_s is the sensible heat flux, q_e is the latent heat flux, q_c is the conductive flux through the ice and snow. The net longwave radiation can be calculated as (Maykut, 1986):

$$q_{LW} = \varepsilon\sigma T_{as}^4 - \varepsilon^*\sigma T_a^4, \tag{20}$$

where $\varepsilon = 0.99$ is the snow longwave emissivity, σ is the Stefan-Boltzmann constant, T_{as} and T_a are the air-snow interface and air ambient temperatures, and ε^* is the effective emissivity for the atmosphere, which can be found as (Maykut, 1986):

$$\varepsilon^* = 0.7855(1 + 0.2232\, c^{2.75}), \tag{21}$$

where c is the fractional cloud factor.

Alternatively, the net longwave radiation from the ocean surface can be found as (Rosati and Miyakoda, 1988):

$$q_{LW} = -\delta\sigma T_a^3\left(T_a\left(0.254 - \frac{0.0066}{132.22}e_a\right)(1 - C_l c) + 4(T_{as} - T_a)\right), \tag{22}$$

where $\delta = 0.95$ is the emissivity of the sea surface relative to the black body, e_a is the near-surface vapor pressure at air ambient temperature T_a, $C_l = 0.8$ is the cloud coefficient.

The net shortwave radiation q_{SW} can be found as (Shine, 1984):

$$q_{SW} = (1 - \alpha)\Phi_c \frac{S\cos^2 Z}{0.0455 + 1.2\cos Z + (1 + \cos Z)10^{-5}e_a}, \tag{23}$$

where α is the albedo of ice or snow, Φ_c is the cloud correction factor, S is the solar constant, and Z is the solar zenith angle.

Cloud correction factor Φ_c can be calculated as (Laevastu, 1960):

$$\Phi_c = 1 - 0.6c^3 \tag{24}$$

Sensible and latent heat fluxes can be found as (Maykut, 1986):

$$q_s = \rho_a c_a C_s V_w (T_a - T_{as}), \tag{25}$$

$$q_e = 0.622 \rho_a L_e C_e V_w \, (e_a - e_{s0})/P, \tag{26}$$

where ρ_a is the density of the air, c_a is the specific heat of the air, C_s and C_e are the bulk transfer coefficients for sensible and latent heat, V_w is the wind speed at the reference height, L_e is the latent heat of vaporization, RH is the relative humidity, e_{s0} is the saturation vapor pressure at surface temperature T_{as}, P is the total atmospheric pressure.

The vapor pressure e can be expressed through the saturation vapor pressure e_s at the given temperature and relative humidity RH as:

$$e = RH \cdot e_s \tag{27}$$

The saturation vapor pressure e_s at the given temperature T can be found as (Tsonis, 2007):

$$e_s = 611 \exp(19.83 - 5417/(T + 273.15)) \tag{28}$$

The bulk transfer coefficients for sensible and latent heat C_s and C_e mainly depends on wind speed and the temperature difference between surface and air $T_{as} - T_a$. For surfaces warmer than air these coefficients are usually in the range of $(1 \ldots 2) \cdot 10^{-3}$ for the elevation of 10 m (Smith, 1988) or can be assumed to be $1 \cdot 10^{-3}$ (Rosati and Miyakoda, 1988).

The conductive flux through the ice and the snow q_c can be found as:

$$q_c = \frac{k_s k_i}{k_s h_i + k_i h_s} \left(T_f - T_{as}\right) \tag{29}$$

Finally, the equilibrium snow top surface temperature T_{as} for the radiative model can be found numerically from Eq. (19).

3.2.2.2 Analytical 1-D resistive level ice model

Analytical solution for freshwater level ice and consolidated layer laboratory growth was presented in Chapter 2. Several corrections and improvements are required to analyze field experiments with saline ice. For field experiments, many meteorological parameters are changing in time including air temperature, wind speed, and snow thickness, so the differential form of a solution is preferable over an integral form.

This model allows simulating the growth of level ice with a uniform snow cover in steady-state conditions with a convective atmospheric flux. The growth rate depends on how the temperature difference between air and water is distributed between insulating layers of air, snow, and ice. Three thermal resistances define temperature profile in level ice: air R_a, snow R_s, and ice R_i (Figure 20b). The sum of all thermal resistances or the total system thermal resistance is showing how much heat can be transported in time from the water to the air. We will start with a convective model of atmospheric fluxes, defining the value of the air thermal resistance R_a. To find the vertical heat flux q at any time we should know air and water temperatures T_a and T_f, and the values defining three thermal resistances: snow thickness h_s and thermal conductivity k_s, ice thickness h_i and ice thermal conductivity k_i, and convective heat transfer coefficient H_{ia}:

$$q = \frac{T_a - T_{as}}{R_a} = \frac{T_{as} - T_{si}}{R_s} = \frac{T_{si} - T_f}{R_i} = \frac{T_a - T_f}{R_a + R_s + R_i}; \quad (30)$$

$$R_a = 1/H_{ia}\,; \quad (31)$$

$$R_s = h_s/k_s\,; \quad (32)$$

$$R_i = h_i/k_i, \quad (33)$$

where T_{as} and T_{si} are the air-snow and snow-ice interface temperatures.

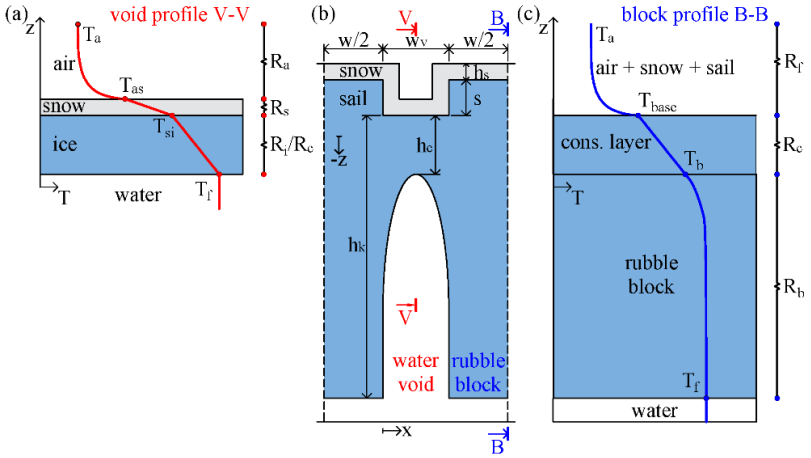

Figure 20. Sketch of geometry used in analytical and numerical models of a ridge, w is the block width, w_v the void width, h_s the snow thickness, s is the sail height, h_k is the keel depth, and h_c the minimum thickness of the consolidated layer (b) and thermal resistance model for the level ice and ridge void (a) and for the ridge block (c).

Convective heat transfer coefficient H_{ia} can be estimated from the measured wind speed from Eq. (18), the snow thermal conductivity depends on snow density (Calonne et al., 2011), ice thermal conductivity slightly depends on its salinity and temperature (Schwerdtfeger, 1963), and the snow and ice thicknesses and should be measured manually or estimated from the measured vertical temperature profiles. Ice thermal conductivity can be estimated from its

temperature and periodically measured salinity profiles (for our experiment) or sea ice desalinization model (Griewank and Notz, 2013). There is a very weak dependence of drift snow temperature on its thermal conductivity (Sturm et al., 1997).

The more advanced radiative model has been also used in this analytical resistive model. Its corresponding thermal resistance can be found from Eq. (19) and (30) as:

$$R_a = \frac{T_a - T_{as}}{q_a} = \frac{T_a - T_{as}}{q_{LW} + q_{SW} + q_s + q_e} \tag{34}$$

The interface temperature T_{as} can be found numerically to satisfy condition from Eq. (30).

The dependence of snow thermal conductivity on its density has a large variance and requires accurate density measurements. We suggest estimating snow thermal conductivity values from the measured snow thickness and vertical temperature profile in snow and ice as:

$$k_s = \frac{(T_{si} - T_f)}{(T_{as} - T_{si})} \frac{k_i h_s}{h_i} \tag{35}$$

One of the ways to validate this model is to compare the estimated and measured values of heat fluxes. In transient conditions, temperature distribution will be the following described ratios with a time lag defined by the thermal inertia of snow and ice layers.

We can also use the analytical resistive model with convective or radiative atmospheric flux for ice growth estimation. The results of these predictions can be validated using experimentally measured ice thickness from drilling or estimated from the vertical temperature profile. Assuming no oceanic flux from the water and no thermal inertia, the gas-free fresh (pure) ice growth can be estimated from meteorological data including air temperature, wind speed, and snow thickness as:

$$\rho_i L_i \frac{dh_i}{dt} = \frac{T_f - T_a}{R_a + R_s + R_i} \tag{36}$$

Saline ice has different thermal properties and corresponding thermal response. Its thermal inertia can be divided into specific heat of pure ice and brine, and change of solid fraction at different temperatures, which requires freezing or melting of pure ice inside sea ice. The values of sea ice enthalpy account for both effects as:

$$H_{si} = -L_i m_i - m_i \int c_i dT - (1 - m_i) \int c_b dT \tag{37}$$

The solid mass fraction of sea ice can be found as:

$$m_i = 1 - \frac{S_i}{S_b} \tag{38}$$

The sea ice solid volume fraction can be found as:

$$v_i = \frac{1 - \frac{S_i}{S_b}}{1 + \frac{S_i}{S_b}\left(\frac{\rho_i}{\rho_b} - 1\right)} \tag{39}$$

The thermal conductivity of sea ice is equal to (Notz, 2005):

$$k_{si} = v_i k_i + (1 - v_i) k_b, \tag{40}$$

The heat capacity of sea ice per unit mass c_{si} can be approximately estimated as (Notz, 2005):

$$c_{si} = c_i - L_i \frac{\alpha S_i}{T^2}, \tag{41}$$

where $\alpha = -0.05411$ is the liquidus slope.

The density of sea ice was found as (Notz, 2005):

$$\rho_{si} = v_i \rho_i + (1 - v_i) \rho_b, \tag{42}$$

The density of pure cab be found from (Pounder, 1966) as:

$$\rho_i = 916.8 - 0.1403 \cdot T \tag{43}$$

The thermal conductivity of pure ice cab found from Yen (1991) as:

$$k_i = 2.21 - 1.00 \cdot 10^{-2} T + 3.44 \cdot 10^{-5} T^2 \tag{44}$$

Pure ice heat capacity can be found as (Weast, 1977):

$$c_i = 2112.2 + 7.6973 \cdot T \tag{45}$$

The latent heat of fusion L_i of water is 333.5 kJ/kg (Feistel and Hagen, 1998). The enthalpy value for ice with any temperature and salinity distribution is defining how much energy should be extracted from the water for its solidification and cooling (Figure 21). The low solid fraction of warm sea ice can lead to faster growth in comparison to Stefan equation and pure ice growth: for the salinity of 5 ppt warm ice at water freezing temperature requires 15 % less negative energy to be formed.

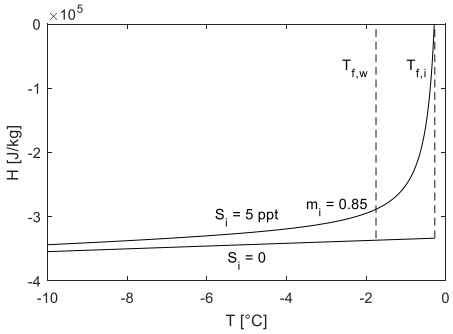

Figure 21. Saline and fresh ice enthalpy vs temperature.

The difference between the top and bottom heat fluxes in ice is spent on ice heating or cooling. The thickness of saline ice can be estimated from pure ice thickness h_i found from Eq. (36) as:

$$h_{si} = h_i \frac{\rho_i L_i}{\rho_{si} \Delta H_{si}} \tag{46}$$

Such an analytical model, which ignores time delay in thermal diffusion, can give errors when the air temperature is quickly moving towards the water freezing point. This error can be eliminated only by solving diffusion equations for snow and saline ice layers. The difference between analytical and numerical predictions will be presented in the study results.

3.2.2.3 Analytical 1-D resistive ridge model

Ridge consolidation has many similarities with level ice growth, but there are some vital differences: a) the ridge keel is porous with a macroporosity η while the level ice grows from pure liquid and b) the ridge has the spatial inhomogeneous top and bottom surfaces. The macroporosity may be adjusted for by modifying the latent heat using Eq. (5). This assumption is valid for homogeneous ridges with small voids. In a sketch of a simplified ice ridge (Figure 20b) its macroporosity is defined as $w_v/(w_v + w)$.

The top ridge surface characterized by its height s gives a locally changing ratio of thermal resistances and the total area via which heat is extracted to the air. Ridge sails also change the distribution of snow, creating accumulations and snow-free surfaces. The top surface of ridge sails can be significantly colder while the sail temperature at the water level can be warmer than in sail free consolidated layer (Leppäranta et al., 1995). In our model, we assume that snow thickness is the same on the top and the sides of ice blocks.

Thermodynamics of ridge sail is mainly affected by two factors: additional thermal resistance from the thicker ice layer, which should decrease heat flux below water level, and additional air-snow or air-ice interface area, which should increase heat flux below water level. For that problem, we have applied the theory of extended surfaces (Incropera et al., 2013), described in Section 2.2.2. To apply this theory for our model, the thermal resistance of a ridge sail should be defined as:

$$R_f = (T_{base} - T_a)A_c/q_f \tag{47}$$

For snow-free ice, the thermal resistance of air is equal to the turbulence resistance $1/H_{ia}$. When there is snow on the top of the ice, the combined heat transfer coefficient for air and snow H can be estimated as:

$$H = \left(\frac{1}{H_{ia}} + \frac{h_s}{k_s}\right)^{-1} \tag{48}$$

This value of H should be used instead of H_{ia} in Eq. (8)-(11).

The bottom surface of an ice ridge is also inhomogeneous. Here we define two different vertical one-dimensional heat fluxes, up from a void (Figure 20b) and through a block (Figure 20c). The model assumes that sail exists only on top of blocks. The heat fluxes up from a ridge void q_v can be found as:

$$q_v = \frac{T_f - T_a}{R_a + R_s + R_c}; \tag{49}$$

$$R_c = h_c/k_i, \tag{50}$$

where R_c is the thermal resistance of the consolidated layer.

The heat flux in the ridge block q_b can be found as:

$$q_b = \frac{T_f - T_a}{R_f + R_c + 0.5 \cdot R_b}, \tag{51}$$

where R_f is the sail thermal resistance, R_b is the rubble block thermal resistance defined as:

$$R_b = \frac{w}{4k_i}\left(\frac{\pi}{2} - 1\right) \tag{52}$$

This thermal resistance of ice block R_b is changing the temperature at the bottom level of the consolidated layer, making blocks colder than water freezing point T_f.

The total heat flux through the ridge voids and blocks is equal to the latent flux:

$$q_r = q_v\eta + q_b(1 - \eta) = \rho_i L_r \frac{dh_c}{dt} \tag{53}$$

The difference in temperature profiles between ridge voids and blocks is making experimental thickness estimation from the temperature profile more complicated, as well as analysis of heat fluxes due to ridge inhomogeneity.

3.2.3 Numerical model

Our two-dimensional numerical thermodynamic model of saline ice ridge is based on the freshwater ice model (Section 2.2.3) with following modifications: thermodynamic parameters

of freshwater ice solid and liquid phases were substituted with of saline ice (Section 3.2.2.2), an additional layer of snow was added, and snow top surface thermal boundary condition was modified according to the description of convective and radiative models (Section 3.2.2.1).

The heat flux balance at the air-snow interface for the convective model is described as follows:

$$H_{ia}(T_a - T_{as}) = k_s\left(\frac{\partial^2 T_s}{\partial x^2} + \frac{\partial^2 T_s}{\partial z^2}\right) \tag{54}$$

Heat diffusion within the snow and ice is described by

$$\rho_{s,i} c_{s,i} \frac{\partial T_{s,i}}{\partial t} = k_{s,i}\left(\frac{\partial^2 T_{s,i}}{\partial x^2} + \frac{\partial^2 T_{s,i}}{\partial z^2}\right) \tag{55}$$

The numerical model includes a thin initial ice thickness h_0 of 5 cm at the air-water interface (Figure 20a). For unknown snow density ρ_s we used the value of 374 kg/m^3, obtained from measurements taken during the winter end on Svalbard (Sand et al., 2003). Snow specific heat capacity c_s was assumed to be equal to of pure ice c_i. Saline ice thermodynamic parameters were taken from Notz (2005). Other values including seawater density, specific heat, coefficient of thermal expansion, latent heat of fusion, and water kinematic viscosity were obtained using the Gibbs SeaWater Oceanographic Toolbox of TEOS-10 (Millero, 2010).

3.3 Results

We will describe thermodynamic effects from the main differences between level ice and ice ridge including ridge sail, snow on its top, ridge rubble, and ridge inhomogeneity (section 3.3.1). After that, we will also describe details of the consolidation experiment and how general conclusions can help with its analysis and model validation (sections 3.3.2-3.3.5).

3.3.1 Sail and rubble effects using analytical and numerical models

It was shown in Section 2.3.1 analytically and numerically that for small-scale ridges not covered by snow sail presence is increasing consolidation rates. Large scale-ridges has wider sail blocks that are leading to less efficient heat transfer. The presence of snow decreases the combined air and snow heat transfer coefficient H from Eq. (48), making extended surfaces more efficient. Below we examine how the snow cover affects the analytical solution of the surface flux (by the fin performance ϵ_s in Eq. (11) and further, apply the two-dimensional numerical solution (Section 3.2.3). The analytical solution for the fin performance shows that it increases with increasing snow thickness, and for snow thicknesses above 1 cm it predicts that the presence of a sail increases the heat flux compared to the same snow cover of flat ice (Figure 22). Our numerical simulations confirm the general trend of the increasing effect of thicker snow.

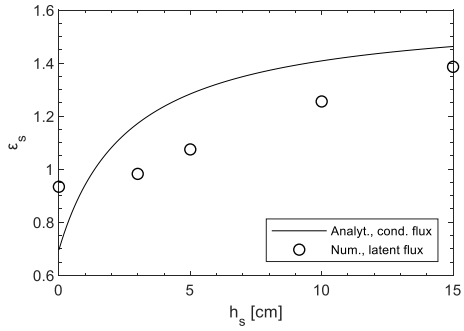

Figure 22. Sail performance ϵ_s vs snow thickness h_s for 15 cm sail height and 50 cm sail width from the analytical sail model and its effect on consolidated layer thickness from the numerical convective model.

The lower surface of the consolidated layer is also important. Level ice thickness can be estimated from its temperature profile as the ice temperature is always less than equal to T_f, and the water below always warmer than equal to T_f. For the profile through a ridge block (B-B in Figure 20) it is not so easy as the consolidated layer end somewhere inside an ice block. The spatial resolution of temperature measurements combined with the non-linear temperature profile close to the bottom and the daily variations in the top makes it necessary to extrapolate. We have chosen to extrapolate a linear temperature profile, skipping the upper 20 cm, and to define the bottom node as follows: the bottom node is the lowest node in which the temperature is less than equal to $T_f - \Delta T$, where ΔT is an arbitrary threshold.

Figure 23 shows vertical temperature profiles through the consolidated layer after 1 and 25 days of consolidation. For each point in time, it shows temperature profiles for cases where the consolidated layer ends in a void and a rubble block as well as the corresponding thickness estimation of the consolidated layer using a threshold $\Delta T = 1$ °C. The figure illustrates differences in the estimated thicknesses Δh_c up to 0.2 m, and since our definition of the consolidated layer (Figure 13) corresponds with the one derived from a void, we call this difference a thickness overestimation Δh_c.

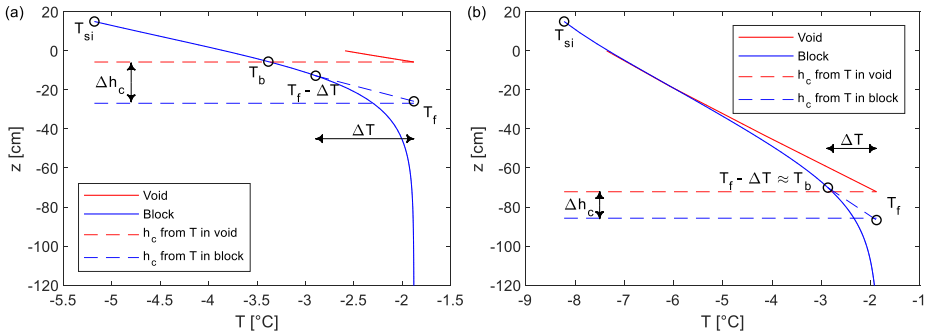

Figure 23. Temperature profiles in ridge void and block after 1 day (a) and after 25 days (b) of consolidation from the numerical model.

Numerical simulations of this overestimation were performed for different sail height and snow thickness. The thickness overestimation decreased with increasing consolidated layer thickness and depended on sail and snow (Figure 24a). A dimensionless block temperature θ_b can be defined as:

$$\theta_b = \frac{T_f - T_b}{T_f - T_{si}} = \frac{\Delta T_b}{\Delta T_c + \Delta T_b}, \tag{56}$$

where T_b is the temperature at the block center at the bottom level of the consolidated layer with minimum thickness (Figure 23).

The thickness overestimation Δh_c depends on the block temperature T_b (Figure 23a) as:

$$\frac{\Delta h_c}{h_c}(\Delta T = \Delta T_b) = \theta_b \tag{57}$$

From the resistive analytical model described in section 3.2.2.3, the dimensionless block temperature θ_b is defined by the block thickness w, and the consolidated layer thickness h_c as:

$$\theta_b = \frac{R_b}{R_c + R_b} = \left(1 + \frac{7h_c}{w}\right)^{-1} \tag{58}$$

The condition $\Delta T = \Delta T_b$ is complicated to use for the thickness estimation in experiments because it requires knowledge of the consolidated layer thickness. For the smaller thresholds $\Delta T < \Delta T_b$ the values of the thickness overestimation are larger and cannot be described by the resistive model. The larger thresholds $\Delta T > \Delta T_b$ correspond with smaller overestimations but can dramatically increase errors of the temperature profile extrapolation, especially for the initial phase of the consolidation. Thus, it is recommended to use threshold range close to the ΔT_b for the later stages of the consolidation. For our experiments ΔT_b lays in the range between $(T_f - T_{si})/5$ and $(T_f - T_{si})/10$ during the most of the time (Figure 24b).

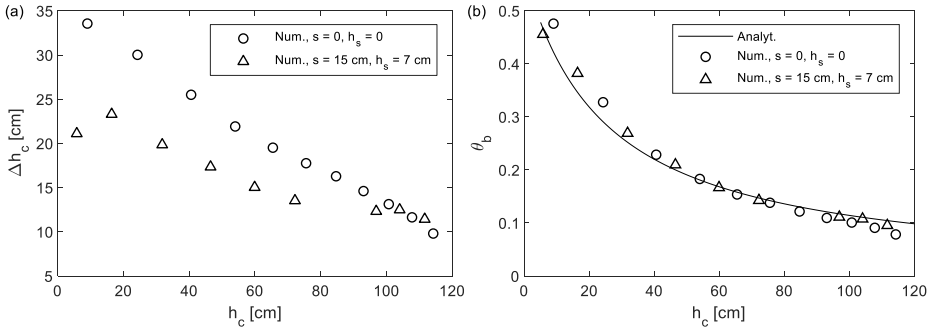

Figure 24. The thickness overestimation Δh_c for the consolidated layer based on temperature profiles from numerical modelling using $\Delta T = 1$ ℃ (a) and block bottom dimensionless temperature θ_b based on numerical and analytical models (b).

As can be seen from Figure 23, large-scale ridges are inhomogeneous and vertical temperature gradient can be significantly different for different parts of an ice ridge. It can be important for the validation of an analytical consolidation model because almost any analytical model is only able to describe average heat flow through different parts or even through the whole ice ridge.

3.3.2 Top surface heat balance

The experimental values of the air thermal resistance were much smaller than thermal resistances of both ice and snow: the average air temperature was only 0.3 °C lower than the measured top surface temperature of snow, while the average difference between the top and bottom surface temperatures was 4.1 °C for snow and 8.3 °C for ice.

We would like to examine how the analytical models (Section 3.2.2.1) with two different atmospheric fluxes (convective and or radiative) predict the air-snow temperature T_{as}. We assume that the meteorological and ice experimentally measured parameters were known including air temperature, ice salinity, temperature, and define a temperature difference over the air boundary layer $\Delta T_a = T_{as} - T_a$. More uncertain parameters including snow thickness and thermal conductivity were assumed unknown. The radiative model is more complicated and to estimate its sensitivity to the uncertainty of the three following aspects were examined:

- Longwave radiation model: Maykut (1986), Rosati and Miyakoda (1988).
- Cloudiness: from the weather station in Longyearbyen, from ICON model for Svea.
- Turbulent heat transfer coefficient: Smith (1988), Rosati and Miyakoda (1988).

The air-snow temperature predicted by the two atmospheric flux models are given in Figure 25a and shows that the convective model predicts a warmer snow surface. For a convective model from its definition a snow/ice top surface temperature T_{as} can't be colder than air temperature T_a, when air is also colder than water. Such temperature distribution is known as ground inversion, was observed during our experiment, but can be described only using the radiative model. Figure 25b shows ΔT_a derived directly from the level ice measurements and for the two models based on meteorological data and experimentally measured conductive heat flux q_c using Eq. (19) and Eq. (30).

The turbulent heat transfer coefficient has a relatively small effect of 2 % of the heat flux. Averaged over time difference between analytical and experimental values of ΔT_a was in the range of -2.5…0.6 °C for different parametrization giving the best fit for the models of Maykut (1986), Smith (1988) and cloudiness data from the Longyearbyen weather station. A simple convective model by Adams et al. (1960) gave a difference of 1.7 °C (Figure 25b).

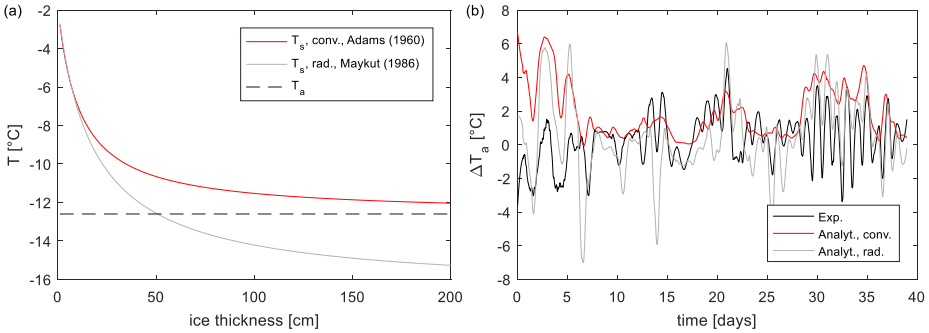

Figure 25. Top surface temperature T_s vs ice thickness h_i (a) and the difference between the top surface and air temperatures ΔT_a from the level ice experiment, radiative and convective analytical models based on experimentally measured conductive heat flux q_c and meteorological data (b).

Radiative models can predict top surface temperatures more accurately, but an error of the convective model is small enough considering its simplicity.

3.3.3 Snow conditions

Snow thickness above level ice and the consolidated layer were measured directly during four visits. The snow thermal conductivity value of 0.21 Wm^{-2} was obtained based on both level ice and ridge temperature profile and four in-situ measurements of snow thickness requested the fit heat flux balance using Eq. (35). Further, the reverse task can be solved. Assuming a constant snow thermal conductivity and knowing ice temperature profile, snow thickness in time during the experiment was estimated (Figure 26) and further used in numerical modelling. Both for level ice and model ridge snow thickness was considerably low except days 12–21.

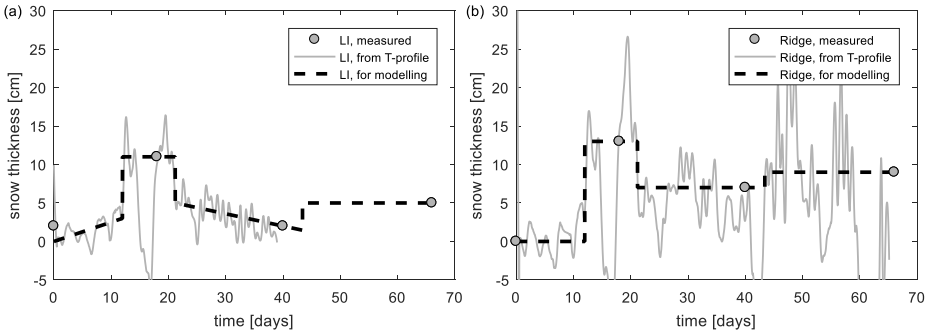

Figure 26. Snow thickness above level ice (a) and consolidated layer (b) vs time.

3.3.4 Vertical heat fluxes

The main parameters of air and snow were estimated in two previous sections from our field measurements. It is of interest to see how our thermodynamic models can predict heat fluxes found experimentally from ice temperature, density, and salinity vertical profiles. Analytically and numerically estimated heat fluxes are based on meteorological data and measured or estimated ice and snow thermodynamic parameters. Average heat fluxes in level ice calculated

using convective and radiative models are 7 % and 3 % lower than from the experiment (Figure 27a).

Modelling and validation of heat fluxes for ridges are much more complicated due to its inhomogeneity. Figure 27b shows the results of our two analytical models of ridge consolidation with "flat" morphology (without a sail). The "flat" analytical radiative model gives 6 % higher flux than experimentally estimated, the convective model gives 5 % lower flux. There is a difference between average fluxes in voids and blocks. In our numerical radiative model, the average heat flux in the void was 22.6 W/m^2, while the average flux in the block was 19.3 W/m^2, closer to the experimental heat flux of 19.0 W/m^2. In the numerical model simulations, the largest heat flux increase is only observed in the vicinity of sail walls, while heat fluxes in the middle of the block and void are almost equal.

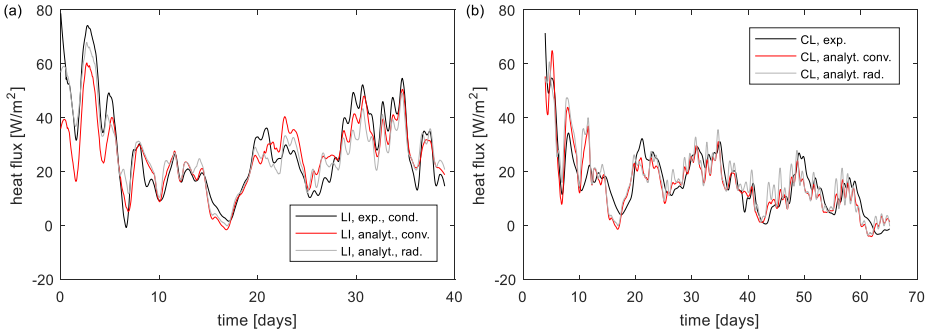

Figure 27. Vertical heat fluxes from the experiment, convectional, and radiative analytical models in level ice (a) and the ridge (b).

As a summary, our analytical and numerical models are predicting heat fluxes equally accurate for level ice and ridges, while the more advanced radiative model is performing slightly better than convective (Table 3).

3.3.5 Ice thickness

The thickness of level ice from the experimental measurements at visit 4 was 99 cm including an additional 4 cm grown on its top surface. Our convective and radiative analytical models predicted thickness of 95 and 102 cm (Figure 28a), while the same numerical models gave 94 and 95 cm. The experimental thickness of the consolidated layer was 120 cm, convective and radiative analytical models gave 113 and 123 cm (Figure 28b), numerical models gave 114 and 120 cm. The numerical models predicted lower thickness due to considering ice thermal inertia. The numerical radiative model gave the closest values to the experimental thickness for both level ice and consolidated layer.

As it was described before (Section 3.3.1) thickness estimation based on the measured temperature profile measured in the block can give values of the consolidated layer thickness higher than its minimum values. In our experiment we also observed this effect. It was eliminated in the thickness range of 50-65 cm and after 112 cm corresponding to the ridge void locations (Figure 28b).

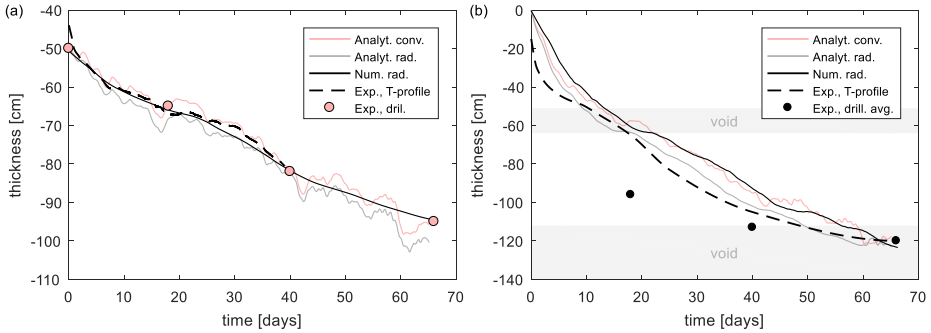

Figure 28. Level ice (a) and consolidated layer (b) thickness vs time.

In general, it can be concluded, that convective models are underestimating ice growth, while radiative models are giving values closer to experimental thicknesses (Table 3).

Table 3. Ice thickness and mean vertical heat flux values after visit 4 (visit 3)

Ice type	Model	s [m]	h analyt. [m]	h num. [m]	h exp. [m]	q analyt. [W/m^2]	q num. [W/m^2]	q exp. [W/m^2]
LI	Conv.	0	0.95	0.94	0.95	20.3 (25.9)	19.9 (27.0)	(27.9)
	Rad.	0	1.02	0.95		21.2 (27.0)	20.9 (28.3)	
CL	Conv.	0	1.13	1.14	1.20	20.3	20.3	19.0
	Rad.	0	1.23	1.20		21.6	21.0	
	Conv.	0.15	1.21	1.16		21.4	19.4	
	Rad.	0.15	-	1.23		-	22.2	

For the evaluation of the thickness overestimation, we used the thickness prediction of our numerical radiative model as a reference (Figure 28b). The calculated experimental thickness overestimation was in the range of 0–25 cm or 0–5 cm/°C with a significant drop when the consolidated layer was growing in voids (Figure 29a). The values of thickness overestimation based on temperature profiles from our numerical modelling were slightly higher. The temperature effect on thickness overestimation was almost constant, scale effect was considerably low (Figure 29b).

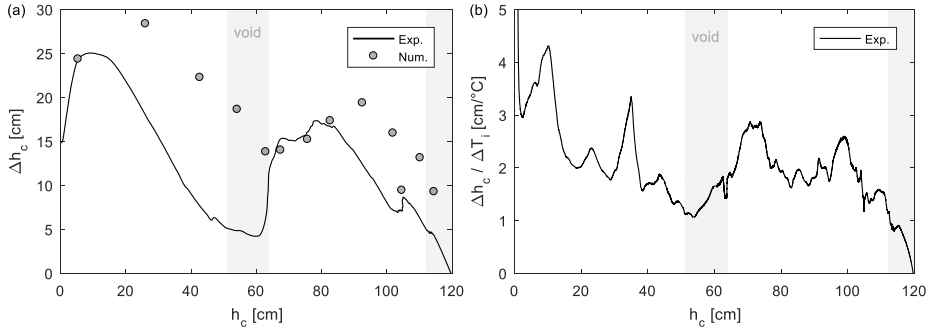

Figure 29. Total thickness overestimation Δh_c (a) and its values per temperature difference in ice $\Delta T_i = T_{si} - T_f$ (b) vs consolidated layer thickness.

3.4 Discussion

3.4.1 Validation of consolidation models

A ridge thermodynamic model can be usually validated using experimental temperature profiles or experimental coring profiles. Accuracy of both methods is limited by inhomogeneity of the bottom surface of the consolidated layer. Previous studies (Blanchet, 1998; Høyland, 2002a; Timco and Burden, 1997) showed that the consolidated layer thickness measurements from coring have too large variability and errors to be suitable for validation of a consolidation model. For example, Høyland (2002) reported 26 % larger values of consolidated layer thickness measurements performed by drilling than by temperature profile analysis. Timco and Burden (1997) analyzed maximum, minimum, and average consolidated layer thickness for 25 ridges and found thickness variability larger than 3. This study attempted to show limitations and errors which can be observed in the analysis of ridge temperature and thickness, estimated from these measurements.

In contrast to experimental measurements, a consolidation model can give only a value of minimum thickness not including the thickness of ice blocks, partly frozen into the consolidated layer. A simple condition of an ice and water boundary, where the temperature is equal to the water freezing point, would give thickness including ice blocks, inside which ice temperature is exponentially approaching freezing temperature. This condition is not providing values of interest (minimum consolidated layer thickness) and it also requires accurate equipment to distinguish small temperature differences. As it was shown in the study, it is possible to use more advanced conditions of the ice-water interface, but even such algorithms can give overestimated values of consolidated layer thickness.

Another way to validate the consolidation model is to compare the values of vertical heat fluxes. But heat fluxes are affected by local conditions more than thickness values. And to analyse temperature profile it is important to know its exact location, which is especially complicated for underwater ridge parts. Due to the semi-elliptical shape of an ice-water interface for ridges (Salganik et al., 2020) measured vertical heat fluxes are not always equal to the latent heat fluxes related to the change of consolidated layer thickness.

Radiative models are generally predicting faster ice growth. Meanwhile, the difference between predictions of radiative and convective models can be significantly lowered due to the presence of shortwave radiation. This explains why both radiative and convective numerical models accurately predict ice growth.

There are numerous ways of snow thickness distribution over an ice ridge which can influence effects from a sail on consolidation rates. We presented both results of analytical and numerical models with and without a sail, meanwhile, due to experimental uncertainties including thickness overestimation, it is hard to say, if the models with a sail accurately described its effect. To analyse the temperature profile above the waterline, it is necessary to have a physical model of a ridge sail.

We used two parameters for consolidation model validation: heat fluxes and ice thickness. The accuracy of heat flux measurements was limited by the accuracy of thermistors and the evaluation of thermal conductivity value from the ice temperature, salinity, and gas volume. The accuracy of consolidated layer thickness was limited by the ridge inhomogeneity and accounting of unconsolidated rubble into total ice thickness.

3.5 Conclusions and recommendations

A medium-scale sea ice ridge was produced in the Van Mijen fjord, Svalbard during the winter of 2017. The thickness and properties of the level ice that was used to make the ridge were measured and thermistor-strings were installed in the ridge and the neighboring level ice. The ridge was visited four times for drilling and sampling. The experimental results provided enough information for accurate growth prediction and validation of ridge consolidation models.

One-dimensional analytical model using the thermal resistance concept was described and applied for both level ice and ridge consolidation. A detailed description of the model application for usage with meteorological data and basic parameters from several visits of the experimental site was provided. The described analytical model can predict heat fluxes inside the consolidated layer quite accurately allowing fast analysis of experimental data or predictions. The radiative top surface heat balance model gives more accurate results than the convective model but requires more input parameters.

It was observed in the experiment, that the temperature profile could give overestimated values of the consolidated layer thickness depending on the profile location. Potential reasons were described and confirmed with both experiment and numerical simulations.

Main results of the chapter can be summarized as:

- The analytical resistive ridge model with convective atmospheric flux captures the relevant phenomena well and could be used for prediction of the consolidated layer thickness in probabilistic analysis of ice actions on structures.
- During 66 days with the average air temperature of -12.6 °C the level ice grew from 50 to 99 cm; the consolidated layer of the ridge with the ridge macro-porosity of 0.36 grew up to 120 cm.
- The model including the radiative terms predicted heat fluxes in level ice and ridge better than the convective model but required more input data.
- Vertical temperature profiles through the consolidated layer and further into respectively a void and an ice block may result in estimations of the consolidated layer thickness with the difference up to the half-block thickness.
- The difference between fresh and saline ice growth is equally important for level ice and ice ridges, but it becomes significant only during the warming phase.

4 Consolidation of small-scale dopant ridges in laboratory and basin conditions

This chapter summarizes analyses and results from laboratory experimental data collected at UNIS cold laboratory in 2016-2017, from basin tests performed at Aalto ice tank in 2019, and at NTNU ice laboratory in 2020. Setup and results of laboratory studies of saline small-scale consolidated layer growth are presented in the conference paper (Appendix 1). Setup and results of laboratory and ice basin studies of small-scale consolidated layer growth from water-ethanol solution are presented in the conference paper (Appendix 6).

4.1 Introduction

Chapter 2 covered a consolidation of a small-scale ice ridge produced from freshwater parallel ice blocks in laboratory conditions. As it was described, such a simplification allows more controlled experimental validation of ridge thermodynamic models. Meanwhile, such morphology is not realistic for natural ridges and not practical for ice-structure interaction experiments. So, with all additional uncertainties, it is of interest to investigate the consolidation of ridges made of randomly oriented blocks made from dopant ice.

The model tests with ice are usually performed to study ice-structure or ice-ship interaction. Due to practical reasons, the ice thickness is usually in a small range, where its mechanical properties are well documented by the basin personnel. Usually, at small scales, ice strength is strongly dependent on the cooling time after its formation (Chapter 5). First-year ice ridges in model tests are usually produced from the level ice with a thickness of 3-9 cm and scaling factor of 20–50. After reaching a required thickness, level ice is broken into blocks and pushed into a smaller section of an ice tank to form a model ridge. Its consolidated layer can be formed by further cooling or by ice rafting (Repetto-Llamazares, 2010).

For model tests with ice ridges and ice-structure interaction, three main types of dopants are commonly used: sodium chloride, EG/AD/S, and ethanol. The presence of a dopant allows easier control of ice mechanical properties by changing its temperature and corresponding solid fraction, as well as it refines grain size. There are also a few level model ice types. In some basins including Hamburg Ship Model Basin, and Aker Arctic, sodium chloride water solution is used together with bottom ice growth. EG/AD/S dopant is used at NRC Ottawa Ice tank (Timco, 1986), ethanol dopant is used at the Aalto university ice basin (von Bock und Polach et al., 2013), where ice is growing from the top.

There is a limited amount of studies dealing with the consolidation of basin-scale ridges. Timco and Goodrich (1988) presented results of EG/AD/S model ice ridge consolidation with the range of thickness of 10-30 cm and compared thickness values from direct measurements and temperature profiles analysis. ITTC (1999) recommend scaling the consolidation time as the square of the geometric scaling factor like the Stefan equation of ice growth.

There are also a few studies presenting results of level ice solidification from different water-based solutions. It can be explained by only a 4 % difference between sea ice growth predictions with different salinity profiles (Griewank and Notz, 2013). Meanwhile, saline level ice, cooled from below due to the absence of the ice desalinization process, is growing faster than fresh ice

in laboratory scales (Notz, 2005). This process is gravitationally stable like the consolidation of water-ethanol solution. Saline ice is expelling salt, so its bulk salinity is lower than the salinity of the water from which it was formed. A mixture of water and ethanol is lighter than pure water, so there is no reason to expect differences in ethanol concentration of solid and liquid. This might lead to a high liquid fraction at the bottom of ethanol ice and faster ice growth in comparison to saline ice.

This motivates us to perform experiments in ridge consolidation using similar techniques including ridge formation and usage of a dopant. This can prove that our thermodynamic model works for that type of ice ridges.

4.2 Methods

4.2.1 Laboratory experiments with saline ice

We performed six laboratory experiments with different initial block temperature and two-dimensional ridge configuration (Figure 30). One 4 cm thick vertical layer of ice blocks were partly thermally insulated from sides and from the bottom by 1 cm thick acrylic walls. The acrylic box has a void of 58x58x4 cm.

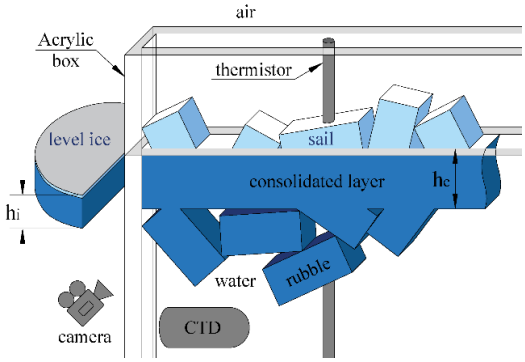

Figure 30. Experimental setup for 2D configuration used in UNIS cold laboratory.

Sea ice blocks of 8x4x4 cm were put into the acrylic box placed in the middle of 1000 liter tank with saline water. Vertical temperature profile was measured using thermistor strings, while seawater salinity and temperature were measured using CTD sensors. Ridge initial macroporosity and consolidated layer thickness were obtained by underwater camera image processing. The thickness of the level ice and the consolidated layer, water freezing temperature, and salinity of water below level ice were manually measured by a ruler, thermometer (Ebro TFX 410-1), and conductivity meter (Mettler Toledo SG7-FK2). After experiments, ridges were taken from the water tank for geometrical, temperature, density, and salinity measurements. Sea ice density ρ_{si} was measured by hydrostatic weighing in kerosene (Pustogvar and Kulyakhtin, 2016).

4.2.2 Ice tank experiments

The model tests were performed in the ice tank of Aalto University. It is a 40 m by 40 m basin with 2.8 m water depth equipped with a cooling system and a carriage. The model ice used for

ridge blocks was granular fine-grained ice produced by spraying the basin water from the moving carriage at -10 °C. After reaching a design ice thickness of 4 cm, the air temperature was lowered to -12 °C. A target model ice flexural strength of 50 kPa was obtained by ice warming. Froude scaling was used with a geometric scale factor as well as a flexural strength scale factor as 15. Norströmsgrund lighthouse was used as a prototype for the cylindrical structure. A total of three level ice sheets were produced, one ridge per ice sheet was built.

Table 4. Main parameters of experiments in Aalto ice tank for basin- and full scale.

Parameter	Basin scale	Full scale
Level ice thickness h_i	4 cm	0.6 m
Keel depth h_k	40 cm	6 m
Sail height s	8 cm	1.2 m
Target flexural strength σ_f	50 kPa	0.75 MPa
Cylinder diameter	50 cm	7.5 m

Model ice was produced from pure water with a 0.3 % fraction of ethanol. Ice density for the floe 1 was 950 kg/m^3. Ridge block thickness was 4 cm for all 3 ice floes. Structure moving speed was 2 cm/s. Ethanol-water liquidus temperature was -0.12 °C based on its phase diagram.

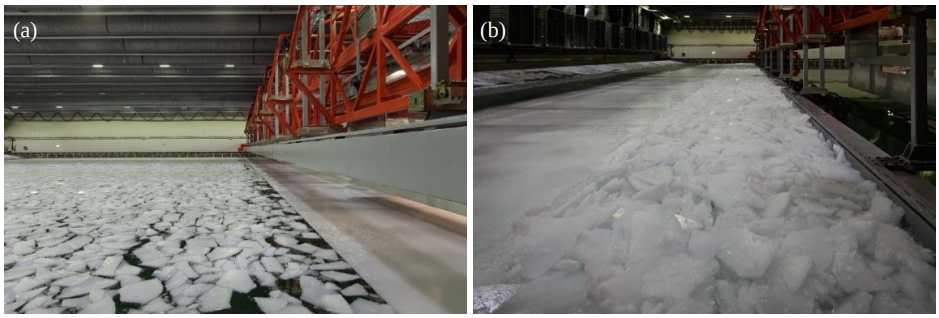

Figure 31. Ridge produced from floe 1 before (a) and after (b) ridge building in Aalto ice tank.

Air temperature development is presented for different stages of the experiment together with measured values of level ice flexural strength (Figure 32 and Figure 33a). The first stage was spraying, when model ice was produced and then cooled down to reach a certain value of the flexural strength. After the measurement of the mechanical properties, level ice could be tempered at freezing temperature or warmed to reach a preferable value of strength. When the target strength was reached, a part of level ice was broken with carriage (Figure 31a), and a ridge was produced from that ice by moving broken ice using pushing plates and anchoring surrounding level ice (Figure 31b). After that, ice-structure interaction tests with unconsolidated ridge were performed. It followed by the ridge consolidation at -12 °C and following ridge warming. When the flexural strength of the level ice was measured again, the ice-structure interaction test was performed with the consolidated ridge.

The average keel depth of 40 cm was measured only for the floe 3 by vertical profiling. The average measured sail height was 8 cm. Ridge 3 was produced from 40 m by 24 m ice floe with 4 cm thickness. Based on the volume of sail, keel, and initial ice for the ridge production we estimated ridge initial macroporosity of 0.31.

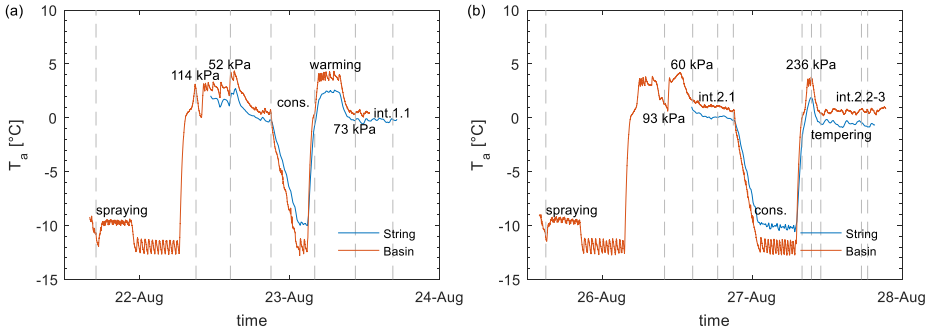

Figure 32. Air temperature timeline for ice floe 1 (a) and 2 (b) and measured flexural strength for experiments in Aalto ice tank.

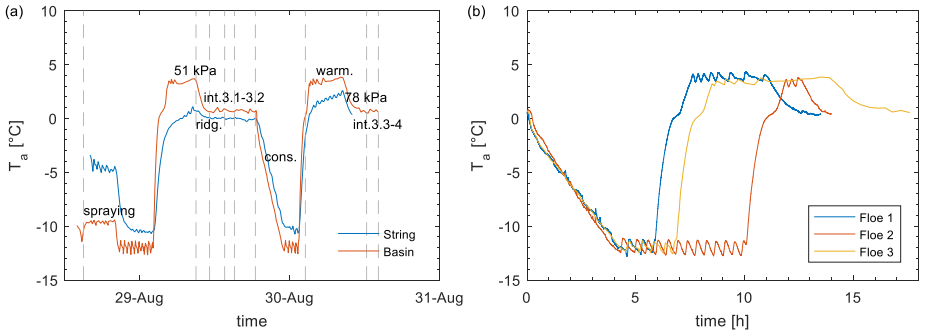

Figure 33. Air temperature timeline for ice floe 3 (a) and ridge consolidation stage (b) and measured flexural strength for experiments in Aalto ice tank.

Two thermistor strings were installed in the old and new level ice and two strings were installed in the ridge. The length of each thermistor string is 40 cm, the minimum sensor spacing is 1.3 cm, the time step was set to 10 minutes. We used strings from GeoPrecision GmbH with TNode EX sensors with 0.1 °C accuracy. The heat flux above the ice top surface was measured using the heat flux plate Hukseflux HFP01-05 for the ice floe 3.

For the basin tests, the value of the heat transfer coefficient H_{ia} was estimated from the measured convective heat flux q_a and the ice thickness h_i assuming equal convective and conductive fluxes as:

$$H_{ia} = \left(\frac{T_f - T_a}{q_a} - \frac{h_i}{k_i}\right)^{-1} \tag{59}$$

Thermodynamic results of the basin tests will be compared with the results of our analytical and numerical models of level ice and ridge consolidation (Section 2.2.2).

4.2.3 Laboratory experiments with ethanol ice

Laboratory experiments in the consolidation of ice ridges formed from freshwater and 0.3 % ethanol solution were performed at the air temperature of -17 °C. Ice was grown in two cylindrical water tanks with a diameter of 30 cm and side insulation. Ice ridges were grown

inside additional polystyrene insulation forming water voids of 18x10 cm horizontal cross-section. The thickness of vertical blocks, forming ridges, was 4 cm, the ridge initial macroporosity was approximately 33 %. We preformed 9 level ice and 16 ridge experiments to study the freezing process of both liquids under the same external thermal conditions. The experiment configuration was close to the described in Section 2.2.1.

Ice ridges were equipped with two thermistor strings each: one in the middle of the void and one in the middle of the block. Ice blocks for different experiments had an initial temperature of -15 °C or -1 °C. After the end of each experiment, we measured the thickness of the consolidated layer and surrounding level ice using a ruler.

4.3 Results

4.3.1 Laboratory experiments with saline ice

The key parameters of the performed tests are presented in Table 5. The heat transfer coefficient H_{ia}, based on direct level ice thickness and air temperature values (Eq. (4), was 20 W/m^{2}K. The average initial ridge macroporosity was 0.4, the initial block temperature was in the range from -11.7 to -2.7 °C.

Table 5. Summary of 2D laboratory experiments in saline ice ridge consolidation performed at UNIS in 2016-2017.

№	T_0	η_0	S_r	S_c	$S_{w,0}$	FDD	h_i	h_c	R
-	°C	-	ppt	ppt	ppt	°Cd	cm	cm	-
1	-2.7	0.41	7.0	3.7	20.2	15.4	5.5	7.5	1.15
2	-7.9	0.49	7.0	6.2	22.0	11.0	4.6	8.0	1.74
3	-6.4	0.38	7.0	4.8	24.1	29.3	9.5	12.9	1.36
4	-9.5	0.45	2.1	3.3	10.2	33.9	10.8	16.4	1.34
5	-11.7	0.35	2.1	1.6	8.7	24.5	9.1	14.9	1.32
6	-4.6	0.30	2.1	2.2	9.7	19.1	9.5	15.0	1.27

The location of the ice-water interface estimated from video analysis was in a good agreement with the measured vertical temperature profile (Figure 34a). The temperature gradient in the consolidated layer was two times higher at the top ice surface than at the bottom surface. During the experiments, the ice top surface temperature T_s was significantly warmer than the air temperature T_a (Figure 34b).

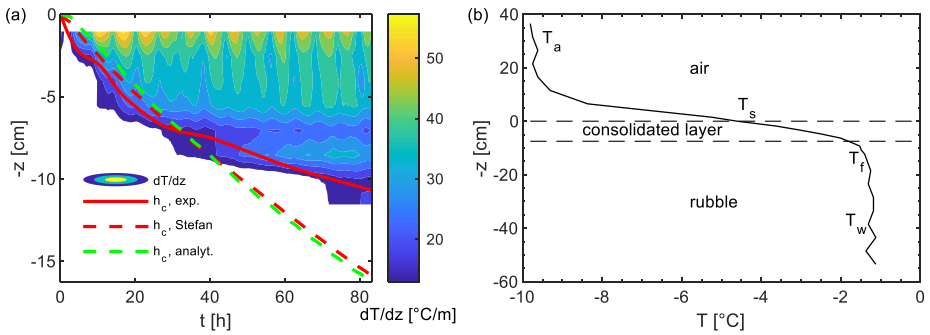

Figure 34. Temperature gradient and temperature in time and space: vertical temperature gradient dT/dz vs time t and water depth z. The red solid curve is the consolidated layer thickness h_c from video analysis, the red dashed curve represents h_c prediction from Stefan's condition using experimental ice top surface temperature T_s (Eq. (15) and the green dashed curve represents h_c prediction from the measured FDD (Eq. (6) and the temperature profile of model ridge after t = 40 h (b) for experiment 3 performed in UNIS cold laboratory.

The values of the initial macroporosity were estimated using images taken before the experiments (Figure 35a). Its vertical distribution is important for ice growth analysis and its values could have significant deviations from average values (Figure 35b). Without considering low values at the box corners macro-porosity for experiment 3 was in the range of 0.12–0.26.

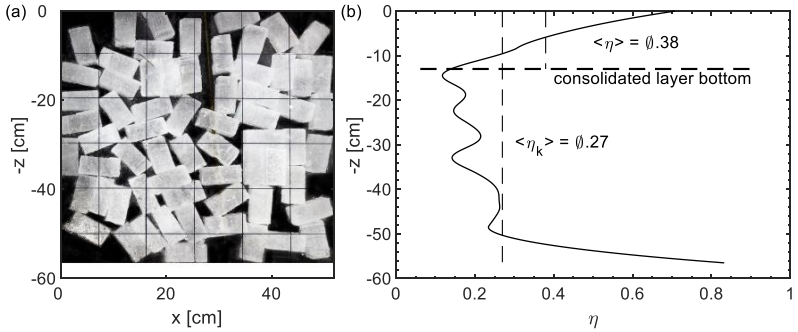

Figure 35. Initial rubble configuration (a) and initial macroporosity distribution η_0 vs depth z (b) for experiment 3 performed in UNIS cold laboratory.

For lower rubble initial temperature T_0 experiments gave higher values of R than for higher temperatures. The results can be normalized using the analytical solution from Eq. (1) via the values of $R\sqrt{\eta_0}$ (Figure 36a).

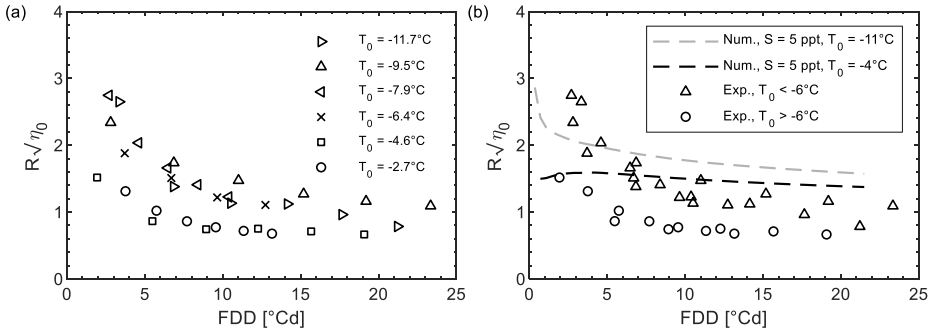

Figure 36. Values of $R\sqrt{\eta_0}$ vs FDD for experiments with different initial block temperature T_0 (a) and from numerical simulations of the ridge with macroporosity of 0.4, the salinity of 5 ppt, and two different initial block temperatures T_0 for the experiments in UNIS cold laboratory.

The strong decreasing trend of $R\sqrt{\eta_0}$ experimental values cannot be explained using 2D

numerical modelling (Figure 36b) using the sea ice thermodynamic model described in Section 3.2.3. This difference can be caused by the absence of side insulation in our experiments, which can be observed by non-linearity of the temperature profiles in the consolidated layer (Figure 34b). The analytical model predictions of consolidation were close to the estimation of ice growth based on the measured top surface temperature gradient and Stefan's condition (Figure 34a).

4.3.2 Ice tank experiments

The directly measured old level ice thickness was in the range of 40–45 mm. These measurements were performed during the flexural strength tests. The estimations from the temperature profiles in that ice had similar values (Figure 37a). During the end of the consolidation phase, we measured the presence of a thin layer of supercooled water under the old level ice, which disappeared after the start of the warming phase.

Table 6. Measured with ruler and estimated ice thickness for tests in Aalto ice tank [mm]

Ice type / Ice sheet	Sheet 1	Sheet 2	Sheet 3
New LI	22 / 20 (T)	20 (T)	20 (T)
Old LI	41-45	40-41	40-42
CL	15 / 20 (T)	40 / 40 (T)	25 / 25 (T)

The estimated from the temperature data consolidated layer thickness was 20 mm for floe 1, 40 mm for floe 2, and 25 mm for floe 3 (Figure 37b).

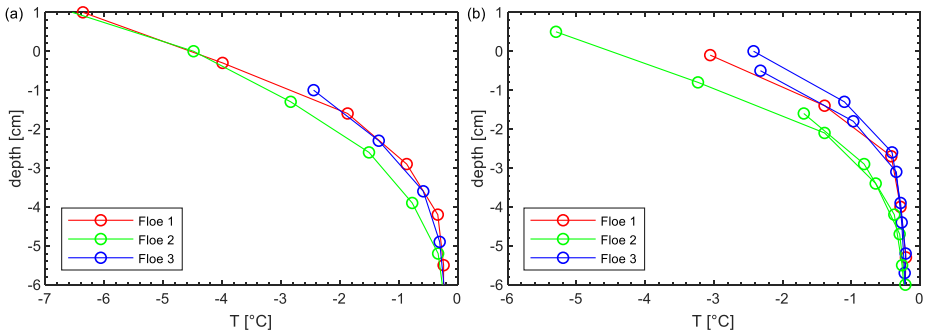

Figure 37. Old level ice (a) and ridge (b) coldest temperature profiles during consolidation for the experiment in Aalto ice tank.

Thickness values of different ice types measured directly using ruler and estimated from temperature profiles (T) are presented in Table 6. Those measured and estimated thickness values are in good agreement with the results of numerical modelling, presented in the next section.

4.3.3 Laboratory experiments with ethanol ice

For the analysis of the temperature data of basin tests, it is important to understand, which ice thicknesses we might expect to observe in ice, grown form water-ethanol solution (alcohol ice). During our basin experiments, we had ridge consolidation with freezing indexes of 50, 62, and 101 FDH at the air ambient temperature of -12 °C (Figure 33b). The values of heat flux above

the level ice measured during spraying is giving heat transfer coefficient value of approximately 10 W/m^{2}K for the basin experiments. For these values according to our analytical solution (Eq. (4) we can expect freshwater level ice thickness of 6 and 12 mm for 50 and 100 FDH respectively. For the ridge porosity of 0.31 the estimated thickness of the freshwater consolidated layer using Eq. (6) is 17 and 34 mm for 50 and 100 FDH.

Freshwater level ice growth is a well-studied process. Thin ice growth is governed by the value of the heat transfer coefficient H_{ia}, which can be found experimentally for laboratory conditions using Eq. (4). The described laboratory experiments were performed to check the relation between fresh and ethanol ice growth for both level ice and ridges. It was found that level ice grown from the ethanol solution is growing 15 % faster and consists of two parts: strong consolidated upper part and weak dendritic lower part. The thickness of the bottom dendritic layer had the value of approximately half of the total ice thickness (Figure 38a). The measured thickness was 6 mm and 9 mm (50 FDH), 12 mm, and 16 mm (100 FDH) correspondingly for freshwater and ethanol level ice. For the same conditions consolidated layer thickness was 23 mm and 27 mm (51 FDH), 50 mm, and 48 mm (100 FDH) for freshwater and ethanol solution. The average ridge macroporosity for these laboratory experiments was 0.32. Opposite to level ice, ridges from ethanol solution didn't have a weak dendritic layer and were growing as fast as fresh ice (Figure 38b).

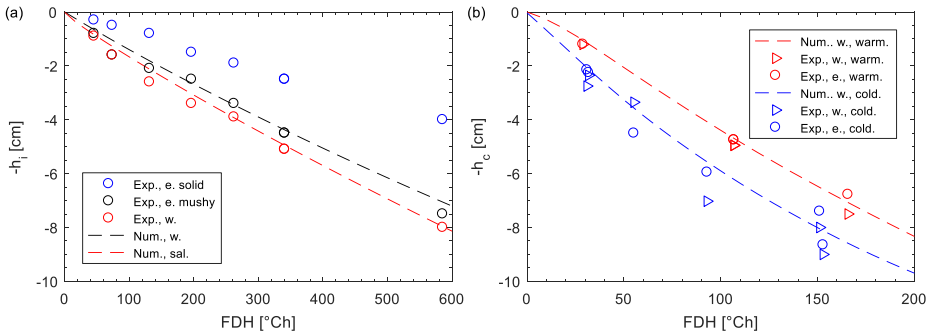

Figure 38. Level ice (a) and consolidated layer thickness (b) vs FDH for laboratory experiments and numerical simulations for NTNU ice laboratory.

The value of the heat transfer coefficient H_{ia} for NTNU laboratory was estimated from the level ice growth observation to be 13 W/m^{2}K. For the level ice growth in the vicinity of the model ridge, the heat transfer was around 15 W/m^{2}K, slightly higher due to larger surface roughness (Figure 39a).

Table 7. Laboratory and basin experimental values of ice thickness for NTNU ice laboratory and Aalto ice tank compared with analytical and numerical thickness estimation using heat transfer coefficient H_{ia}=10 W/m^{2}K.

Floe	Type	FDH	Solution	*h*, basin	*h*, lab.	*h*, analyt.	*h*, num.
-	-	[°Ch]	-	[mm]	[mm]	[mm]	[mm]
1	LI	50	w.	-	8	6	6

Floe	Type	FDH	Solution	*h*, basin	*h*, lab.	*h*, analyt.	*h*, num.
-	-	[°Ch]	-	[mm]	[mm]	[mm]	[mm]
			e.	20	9	8	8
2		101	w.	-	12	12	11
			e.	20	16	15	15
3		62	w.	-	8	7	7
			e.	20	9	9	10
1	CL	50	w.	-	23	17	11
			e.	15	27	20	16
2		101	w.	-	50	34	26
			e.	40	48	39	36
3		62	w.	-	23	21	14
			e.	25	27	24	21

For the considered scale of experiments, the higher value of the heat flux coefficient will give around 30 % faster growth for laboratory conditions than for the ice tank. For example, for 50 and 100 FDD, level ice thickness would be 7.5 mm instead of 5.8 mm and 14.7 mm instead of 11.5 mm. Measured in laboratory conditions consolidated layer thickness was 27 mm and 48 mm for ethanol solution and the same freezing indexes (Table 7). These values are larger than the temperature sensor spacing of 13 mm so we can expect to measure ice thickness in the basin experiment with reasonable accuracy (Figure 40).

In full-scale measurements, indirect thickness estimation from the vertical temperature profile is a trivial process due to a significant temperature difference between ice top and bottom surfaces. For the smaller scales, most of the temperature changes are occurring in the air inside the thermal boundary layer. Thickness estimation from the temperature profile is limited by temperature sensors spacing. At least two sensors should be frozen and be considerably colder than the liquid freezing point. As can be seen, achievable sensor spacing can be easily not enough to estimate thicknesses of newly formed level ice for the considered range of freezing time.

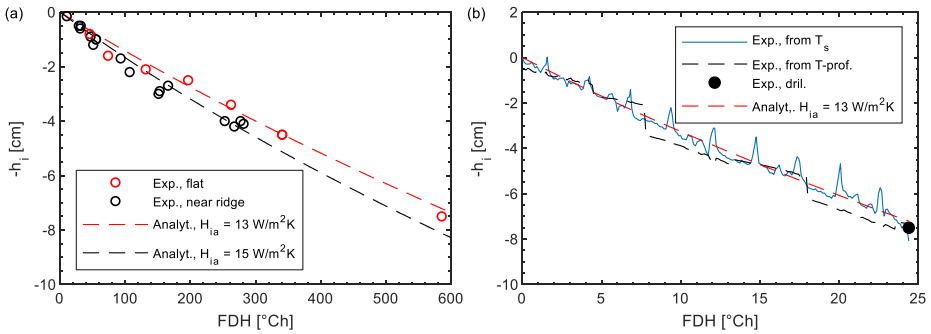

Figure 39. Freshwater level ice thickness vs FDH for experiments with different surface roughness using direct thickness measurements (a) and from different thickness estimation algorithms during a single experiment (b) for NTNU ice laboratory.

Assuming the constant value of the heat transfer coefficient it is possible to estimate ice

thickness from its measured surface temperature for almost any thickness range (Figure 39b). Examples of experimental and analytical temperature profiles for 50 and 100 FDH at the end of experiments are presented in Figure 40. It shows the difference between temperatures in the ridge voids and blocks, which can lead to the thickness overestimation of approximately 2 cm for the block profiles. This experimentally confirms the thickness overestimation theory presented in Chapter 3.

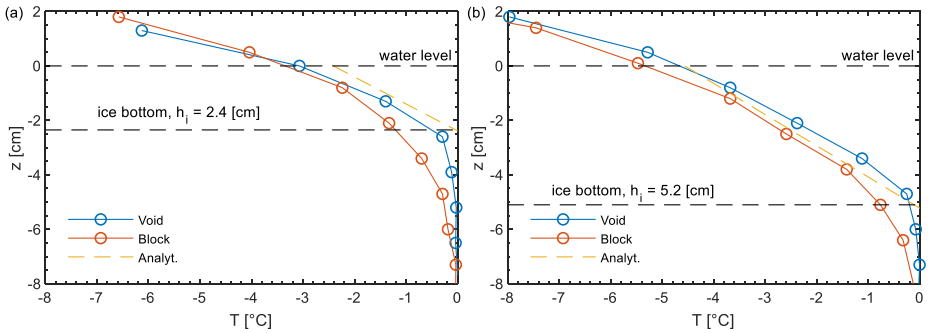

Figure 40. Temperature profiles of freshwater ridges at the end of laboratory experiments with 50 FDH (a) and 100 FDH (b) for NTNU ice laboratory.

We performed a comparison of level ice growth from freshwater and 0.3 % ethanol solution in identic thermal conditions and found that ethanol level ice is growing approximately 15 % faster than freshwater level ice. This difference was close to the difference between saline and fresh ice growth based on our numerical model for 0.3 % salinity for both liquid and solid parts (Figure 38a).

Additionally, ethanol ice had a dendritic structure with dendrites occupying approximately 50 % of the total ice thickness, while freshwater ice has a planar thermodynamically stable interface. The same ice structure was not observed during experiments with ethanol ridges: the consolidated layer didn't have a large layer of dendrites. According to the performed thin sections and similarly to the numerical simulations, the ice growth in ridges occurs mostly in a horizontal direction, allowing to overcome the supercooled layer of liquid.

We did not find any significant difference in experimental consolidation rates between freshwater and ethanol ridges. Both ridges produced from warm (-1 °C) and cold (-15 °C) blocks were freezing close to the results of our analytical and numerical models of a freshwater ridge for the FDH lower than 200 °Ch (Figure 38b).

The experiments with warm blocks can be well described by the analytical solution even for larger scales. For the cold blocks, the consolidated layer thickness is usually underestimated analytically for the initial stages of experiments and overestimated for the larger scales (Figure 41a).

The results of laboratory experiments for cold blocks can be only explained if some part of the initial block sensible heat goes not to porosity change but consolidated layer growth (Figure 41b). For the analysis, we used two factors: the ratio of consolidated layer and level ice

thickness $R = h_c/h_i$ and corresponding normalized factor R_{norm} from Eq. (14).

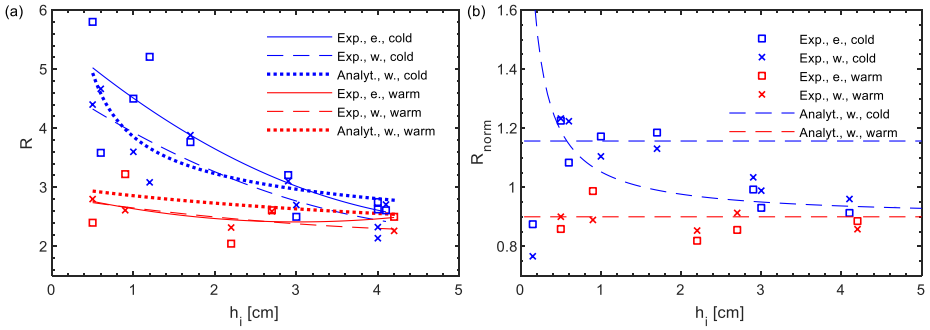

Figure 41. R (a) and R_{norm} (b) factors vs level ice thickness from the laboratory experiments and the analytical solution for NTNU ice laboratory.

The grain size was estimated using thin sections presented in Figure 42. Freshwater level ice had grains around 5 mm, ethanol level ice had slightly smaller grains of 4 mm. Newly formed ice in the consolidated layer had much finer grains around 1 mm for both freshwater and ethanol ridges.

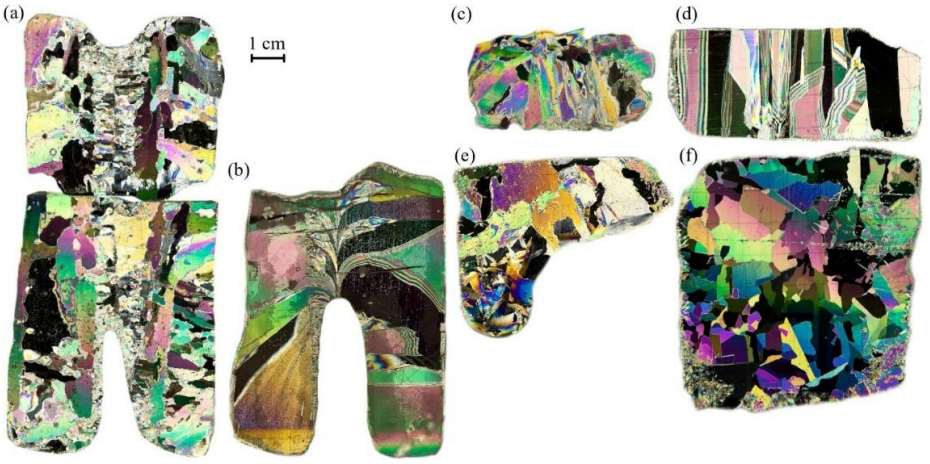

Figure 42. Vertical thin section of ethanol ridge (a), freshwater ridge (b), ethanol level ice (c), freshwater level ice (d), horizontal thin section of ethanol level ice (e), freshwater level ice (f) for NTNU ice laboratory.

4.4 Discussion

4.4.1 Laboratory experiments with saline ice

The experimental results confirmed a significance of the scale-effect, making ridge consolidation faster for smaller scales in comparison to the level ice growth rates. It also confirmed the significance of the effect from the block initial temperature for saline ice ridges. The values of factor R approached values $1/\sqrt{\eta_0}$, but significantly faster than from our analytical and numerical models (Figure 36b).

The deeper analysis of the experiments with two-dimensional configuration, thin side acrylic insulation, and random ice block orientation revealed their disadvantages. They were designed to have transparent walls to provide the visual information about the ridge morphology, which can give accurate values of the ridge macroporosity and the consolidated layer thickness. Meanwhile, the lack of the side insulation changes the thermal boundary conditions, when the bottom part of the consolidated layer below the surrounding level ice is not insulated from its sides, like in natural conditions, but exposed to the seawater at its freezing point. Additionally, differences in block thickness created small gaps between ice blocks and acrylic walls, allowing lateral freezing and horizontal heat fluxes in the bottom part of the consolidated layer. The significance of these effects was observed from the non-linearity of the temperature profile in the consolidated layer (Figure 34a). The consolidation rates of these experiments deviated from the solution by assuming, that the conductive heat flux, estimated from the ice top surface temperature, seawater freezing point, and its thickness, is equal to the latent heat flux (Stefan's equation).

Additional complications of the experimental analysis were coming from a large variability of the macroporosity values over the ridge depth (Figure 35b), mainly caused by the corner effects from the insulation acrylic box. It is limiting the comparison of different experiments, requires additional image processing, and complicates analytical and numerical models for experimental validation.

The combination of complicated thermal boundary conditions and ridge morphology gives a motivation to redesign experiments in small-scale ridge consolidation to make them easier to process and to be replicated using analytical and numerical models. Such an experimental design is described in Section 2.2.1.

4.4.2 Ice tank experiments

Basin tests with ice-structure interaction provide a unique chance to have a scaled experiment with load measurements. But there are many uncertainties in ridge morphological parameters, which can make an analysis of the interaction in comparison to the full scale complicated. One of these parameters is the thickness of the consolidated layer. Laboratory experiments validated with analytical and numerical modelling were performed to provide more accurate predictions of consolidation rates for similar conditions to the performed basin experiment.

The measurements of the consolidated layer thickness for the ridges produced in ice basins include a lot of uncertainties due to the high ratio of measuring methods errors and ranges of thickness. Direct measurements are complicated because basin-scale ridge from ethanol ice is too fragile so it can't be lifted from the liquid. Model ice is also not providing enough resistance to perform ice drilling suitable for ridge profiling.

Temperature profiles can also be used, but their measurements could be influenced by several factors: the local sail height, the local keel depth, and the vertical position of a thermistor. The sail height is believed to be the key factor: it is hard to measure during installation, while sail height is usually several times larger than consolidated layer thickness. The presence of keel blocks submerged into a consolidated layer can make the temperature profile non-linear. Both sail and keel presence can lead to an overestimation of the consolidated layer thickness.

Another important value which is hard to measure with good precision is a ridge macroporosity. For our basin tests, it was estimated from the cross-sectional profiles of keel depth, average sail height, and initial ice volume before ridge production. Tuhkuri (2002) showed a large variability of ridge macroporosity values for similar ridging conditions in the Aalto ice basin.

4.4.3 Laboratory experiments with ethanol ice

The experiments showed differences and similarities between the consolidation of ice grown from freshwater and ethanol solution. The experiments with level ice confirmed that gravitational stability is leading to the increasing ice growth rates, while for gravitationally unstable interfaces this effect on the growth rate is insignificant in comparison to one of freshwater ice. The similar effects on growth rates were measured by Notz (2005). In his experiment rates of the gravitationally stable upward growth of sea ice were significantly higher than for the gravitationally unstable downward growth, which was like the rates for the freshwater ice.

The experiments showed that the difference in growth rates between those two types of ice are smaller than uncertainties and instrumental errors for experiments with ice ridges. It was observed that the effect of the initial block temperature on ridge consolidation rates is decreasing after the initial phase of the consolidation. When the consolidated layer thickness is reaching the values of the block thickness, the effect of the initial block temperature is becoming insignificant.

4.5 Conclusions and recommendations

This chapter covers experimental work in small-scale saline and ethanol ridge consolidation and provides analytical and numerical models, which can describe obtained experimental results. The main findings are summarized as follows:

- The small-scale ice ridges grown from pure water and water-ethanol solution have similar consolidation rate and similar grain size of the newly formed ice.
- The low initial temperature of ice blocks forming a saline or ethanol ridge can increase consolidation rates up to 2-3 times, but this effect is becoming small when the consolidated layer thickness is reaching the value of the block thickness.
- The laboratory experiments in ridge consolidation confirmed that ridge inhomogeneity can lead to the overestimation of the consolidated layer thickness based on the temperature profile, measured in an ice block in comparison to the one from the ridge void. As in the results of the large-scale numerical model, the value of this overestimation is larger than half block thickness depending on the chosen algorithm of thickness estimation.
- Experiments in the consolidation of small-scale ridges consisting of randomly oriented blocks produce too large experimental errors to be suitable for the validation of analytical and numerical ridge thermodynamic models.

5 Mechanical characteristics of saline ice ridges in different scales

This chapter summarizes results from experiments performed in UNIS cold laboratory in 2017-2018 and field experiment performed in Sveagruva, Svalbard in 2017. The results of laboratory studies in sea ice small-scale consolidation are presented in the conference paper (Appendix 1). The results of the field experiment are presented in the conference paper (Appendix 6).

5.1 Introduction

A structural load from the consolidated layer of an ice ridge mainly depends on the ice thickness, ice strength, and the type of failure (Ervik et al., 2019). Meanwhile, the ice strength also depends on several factors including its temperature, salinity, grain structure and size, freezing time, stress state, load orientation, and strain rate.

The dependency of the level ice uniaxial strength on its microporosity values was investigated by Timco and Frederking (1990) and Moslet (2007). Similar data were obtained for the sea ice ridges by Shafrova and Høyland (2008), and Høyland (2007). They also showed that the consolidated layer horizontal strength was 1.5 times higher than of level ice, while the strongest samples were in the middle part of the consolidated layer.

For the laboratory model ridges, Kioka et al. (2001) have found similar strength for the consolidated layer in both vertical and horizontal directions, opposite to the strength of level ice. They also found a significant size-effect for the uniaxial compression tests in the sample diameter range 5-30 cm: smaller ridge samples were up to two times stronger.

5.2 Methods

5.2.1 Small-scale laboratory experiments

The preparation of laboratory experiments in saline ice ridge consolidation is described in Section 4.2.1. The tank was filled with the water having initial salinity $S_{w,0}$, the model ridge was made from previously grown level ice with initial salinity S_r cut in the horizontal direction. The level ice and the consolidated layer from six consolidation tests were taken from the water tank after experiments, cooled down to -10 ℃, cut into horizontally oriented 10x4x4 cm specimens, and uniaxially compressed under the constant strain rate of 10^{-3} Hz. Depth, linear dimensions, temperature, density, and salinity were measured for each specimen. Rubble block orientation was measured for the samples from the consolidated layer using image processing (Figure 43). The compression rig provided force and displacement measurements for each mechanical test. The density was measured before the compression using hydrostatic weighing in kerosene (Pustogvar and Kulyakhtin, 2016), the salinity and temperature were measured after the compression using conductivity meter (Mettler Toledo SG7-FK2) and thermometer (Ebro TFX 410-1). The compressive strength σ was defined as a ratio of the maximum load and the initial cross-sectional area. The brine and gas volumes forming the microporosity were estimated from the measured temperature, density, and salinity from Cox and Weeks (1983).

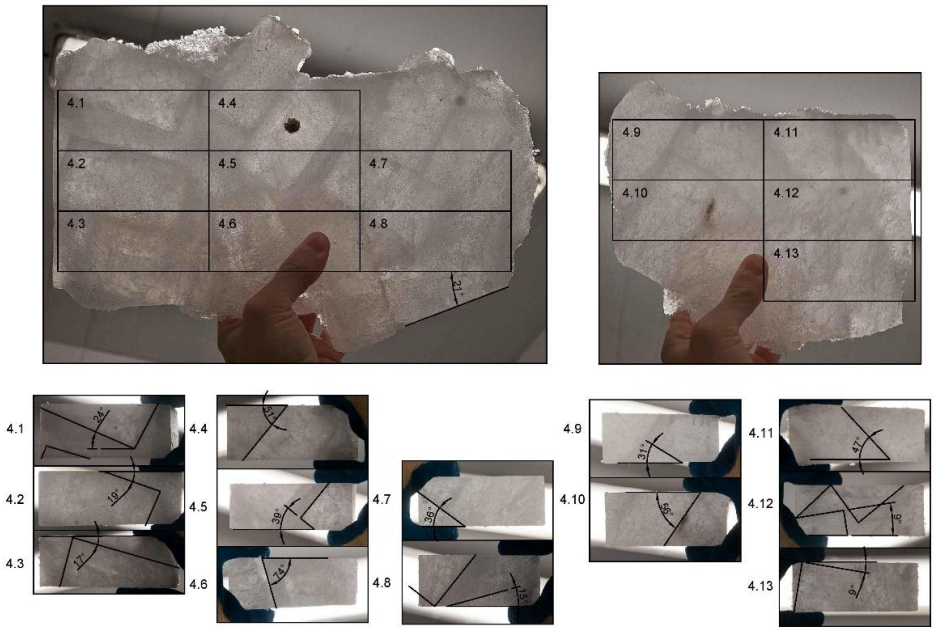

Figure 43. Block orientation for the specimens from the consolidated layer of the test run 4.

In total 26 and 65 specimens were compressed during experiments in 2017 and 2018 from the consolidated layer, level ice, and rubble.

5.2.2 Large-scale field experiments

The investigations of the ice mechanical parameters were part of the field experiment described in Section 3.2.1. In that experiment we created a full-scale artificial ice ridge from the 50 cm thick level ice in Van Mijenfjorden, Svalbard, and investigated its consolidation for 66 days. After the ridge creation, we made three more visits to the experimental site and performed 71 in-situ and laboratory uniaxial compression tests. The specimens had 7.2 cm diameter and 17.5 cm length, and they were compressed under the constant strain rate of 10^{-3} Hz. The compression rig is described by Moslet (2007). We measured their density before the compression using the hydrostatic weighing method, and their temperature and salinity after the compression.

We collected 12 vertical and horizontal level ice samples during visit 2, and 4 vertical level ice and 17 vertical ridge samples during visit 4. Tests with these samples were performed in the lab at the temperature -10 °C. During visit 3 we performed 38 in-situ compression tests including 32 for level ice and 6 for the ridge.

5.3 Results

5.3.1 Small-scale laboratory experiments

The average parameters for each experimental run are presented in Table 8. The first three experiments were performed with liquid salinity of 9.5 ppt, while in the other three runs the

liquid salinity was 31.9 ppt, close to the seawater. The average salinity of the level ice was 21 % higher than of the consolidated layer.

Table 8. Summary of 2D laboratory experiments in sea ice ridge consolidation and mechanics performed at UNIS in 2017-2018.

Run	Samples	$S_{w,0}$	S_r	S_i	S_c	h_i	h_c	σ_i	σ_c
-	-	ppt	ppt	ppt	ppt	cm	cm	MPa	MPa
1	4	10.2	2.2	3.4	4.1	10.8	16.4	2.2	2.4
2	2	8.7	2.2	-	1.6	9.1	14.9	-	4.6
3	20	9.7	2.1	2.1	2.4	9.5	15.0	3.5	3.5
4	28	29.1	7.1	9.8	9.1	8.2	12.0	2.4	2.3
5	22	31.2	6.9	8.9	6.8	3.8	11.2	2.5	3.0
6	15	35.5	6.9	12.2	9.1	4.0	9.2	2.0	2.2

The strength of a specimen depends on many factors including its temperature, salinity, and consolidation time. For small-scale experiments a loss of liquid brine during sample extraction and cutting is inevitable. The gas volume of the samples from the consolidated layer was 83 % higher than from the level ice, while their microporosity was only 11 % higher.

The common practice is to correlate strength with the macroporosity, a sum of fractional gas and brine volumes. The average compressive strength of the consolidated layer strength was 5 % higher than of level ice and 28 % higher than of unconsolidated rubble. The strength values were linearly decreasing with the growth of the macroporosity for all types of ice (Figure 44a). While strength values were close for the consolidated layer and level ice, the standard deviation was 2.4 and 1.4 times higher for the consolidated layer for run 1-3 and 4-6 correspondingly.

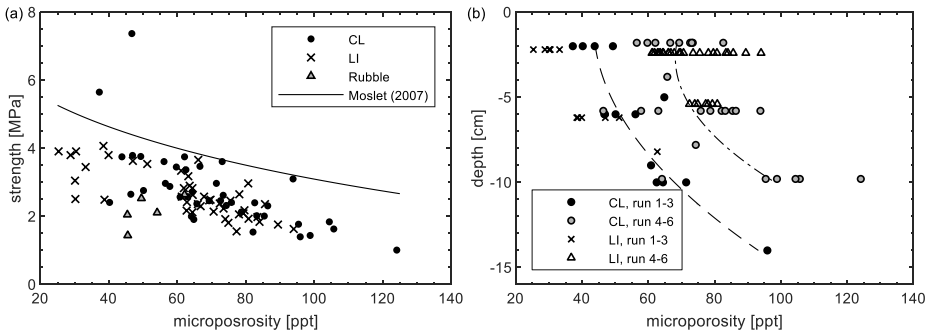

Figure 44. The uniaxial horizontal strength vs microporosity for our experiments and maximum level ice strength fit from Moslet (2007) (solid line) (a) and the depth vs ice microporosity at -10 ℃ with the corresponding fit for run 1-3 (dashed line) and run 4-6 (dash-dot line) (b).

The ice upper layers were stronger due to salt expulsion and corresponding lower values of microporosity (Figure 45).

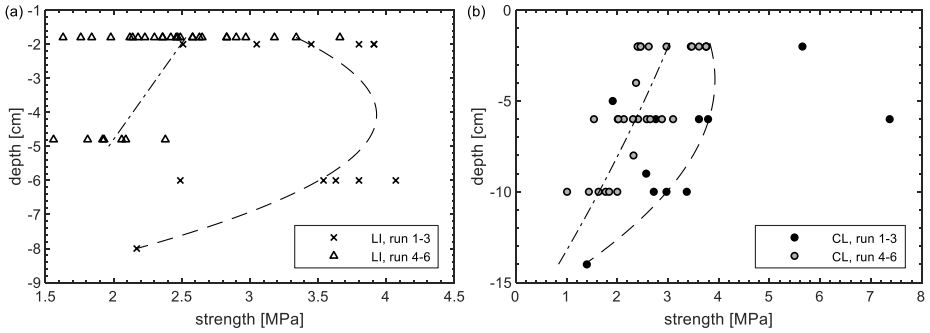

Figure 45. The depth vs the ice strength for the level ice (a) and the consolidated layer (b) with the corresponding fit for run 1-3 (dashed line) and for run 4-6 (dash-dot line).

The average block inclination inside the consolidated layer was 29°. We have found no correlation between block orientation and the strength of the consolidated layer with inclusions of those blocks. For runs 4-6 the average consolidated layer strength for the depth of 0-4 cm was 3.0 MPa, for 4-8 cm it was 2.4 MPa, and for 8-12 cm it was 1.7 MPa (Figure 46b).

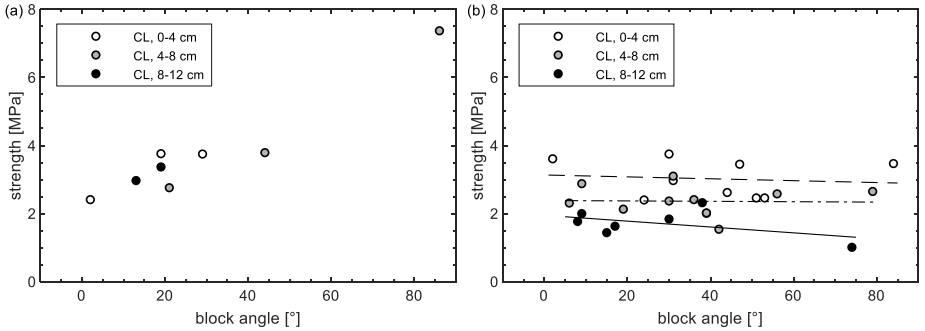

Figure 46. The block orientation vs the strength of the consolidated layer for run 1-3 (a) and 4-6 and fit for the depth of 0-4 cm (dashed line), 4-8 cm (dash-dot line), and 8-12 cm (solid line) (b).

5.3.2 Large-scale field experiments

Results of in-situ and laboratory uniaxial compression experiments, performed during visits 2, 3, and 4, are presented in Figure 47. The in-situ average compression strength of horizontal level ice samples during visit 3 was 3.2 MPa, and 8.1 MPa for vertical level ice samples. Horizontal samples from the consolidated layer had a strength of 4.4 MPa, and 6.1 MPa for vertical samples from the consolidated layer.

In laboratory conditions at the temperature of around -10 °C, the average strength of horizontal level ice samples was 4.5 MPa at visit 2, vertical strength was 7.7 MPa at visit 2, and 5.0 MPa at visit 4. The vertical consolidated layer strength was 5.9 MPa.

The strength of level ice for visit 2 was measured in different directions for horizontal samples:

for EW direction it was 6.0 MPa, for NS it was 3.4 MPa, for 45° to NS it was 4.2 MPa.

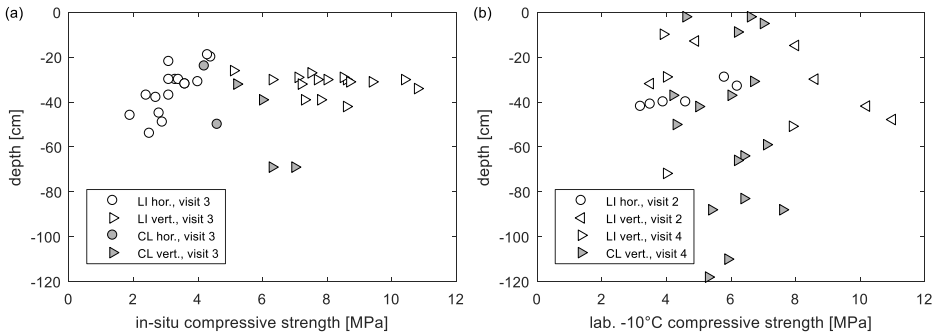

Figure 47. Depth vs uniaxial compressive strength for in-situ (a) and -10 °C (b) temperatures.

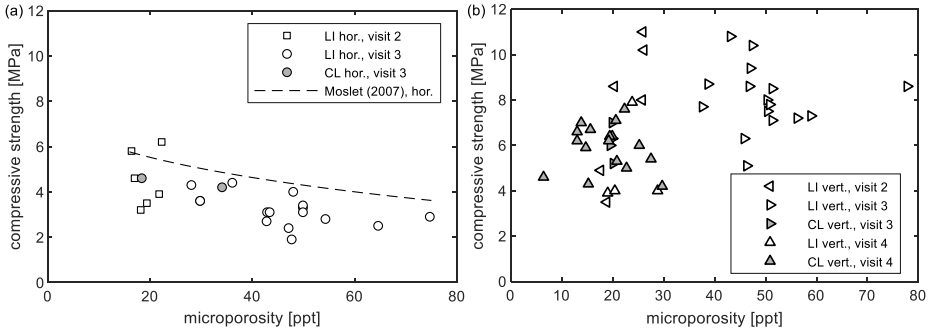

Figure 48. Uniaxial compressive strength for horizontal (a) and vertical (b) samples vs microporosity.

The samples from the ridge had a much higher percentage of failures in a ductile way in contrast to level ice. The results of the splitting test for the ridge is described in Lu et al., 2019.

5.4 Discussion

The values of the level ice strength in our laboratory experiments in their relation to the microporosity were similar to the field study results from Moslet (2007). The freezing time after the ice formation was found to be the key factor governing both ice salinity and compressive strength, all laboratory-scale samples were tested at -10 °C. It was also confirmed by the absence of the correlation between the consolidated layer strength and orientation of the blocks forming the consolidated layer. The strength of the newly formed ice in the ridge void appeared to be governing the total strength of the consolidated layer for the laboratory tests. The newly formed ice might be less mechanically consolidated than rubble blocks and therefore might have smaller strength. Like for the salt expulsion, the ice strength was growing until a certain threshold and then was remaining constant. For our horizontal samples from the level ice and the ridge, this threshold was close to 4 MPa (Figure 45). It also shows that without thermal scaling, the mechanical scaling is hardly possible. The size of our specimens was close to the size of rubble blocks allowing us to investigate the mechanical properties of the whole

consolidated layer, not its separate parts.

Strength relations of the consolidated layer and the level ice in the presented field experiment in Svalbard are in a good agreement with the field results from Shafrova and Høyland (2008). The size of the samples used for the compression tests was much smaller than the size of the blocks forming the artificial ice ridge. The results of such tests, in contrast to the laboratory scales, can only characterize a strength of separate parts of the ridge including rubble blocks and newly formed ice in between. The horizontal strength of the consolidated layer was larger than the strength of the level ice probably because it mostly consists out of inclined rubble blocks. The strength of the inclined block should be in between the level ice horizontal and vertical strength, which was observed in our experiments. It shows the general difference between small- and large-scale ridge investigations using uniaxial compression and the importance of scaled mechanical experiments as well as full-scale mechanical investigations.

While the small-scale mechanical experiments with small-scale characterize a mechanical resistance of a large volume of the consolidated layer, the small-scale experiments with full-scale ridges can characterize the resistance of its parts. Such results can be influenced by the dominant proportion of the rubble blocks inside the consolidated layer.

The temperature of the laboratory tests was chosen -10 ℃ as a generally accepted standard temperature for the compression tests. For small-scale ridges this temperature also appears to be practical, warmer samples from the consolidated layer tend to lose a lot of brine and to break in the vicinity of block surfaces. In order to investigate parameters of mechanically scaled and warmed ice, it is more practical to use methods allowing to leave ice flowing in the water. That gives a possibility not to lose brine as well as to avoid additional damage from sample cutting.

5.5 Conclusions and recommendations

Series of laboratory and field experiments were performed to study mechanical properties of the ridges in different scales. In total 91 tests were completed for small-scale ridges and 71 tests for the full-scale ridge. Samples from small-scale ridges had dimensions of 10x4x4 cm, while in large-scale we compressed 7.2 cm diameter cylinders.

The results showed that small-scale compression tests represent different ridge parameters depending on the ridge scale. For the small-scale ridges, it describes the strength of several blocks frozen together. For the full-scale ridge, the results of the uniaxial compression tests described strength of each separate part of the consolidated layer, which consists of the weaker newly formed ice and stronger and inclined blocks. The main findings are summarized as follows:

- The block orientation has no correlation with the compressive strength of the consolidated layer for the small-scale saline ridges. The total strength of blocks and newly formed ice was comparable with the horizontal strength of the level ice.
- The small-scale uniaxial compressive strength of the full-scale ridge lays between the strength of the surrounding level ice in horizontal and vertical directions. This can be explained by the range of block inclination forming the ridge.
- The strength of the small-scale saline ridge depends on the consolidation time and

decrease towards ice bottom like for the level ice despite all ice being tested at -10°C. The lowest strength values were always at the bottom part of the ice. After a certain consolidation time, each layer of ice is reaching a maximum value of the mechanically consolidated ice, which was around 4 MPa for our tests with saline ice.

- The strength of the full-scale ridge has a weaker correlation with depth than the surrounding level ice.

6 Conclusions and future work

6.1 Conclusions

In this thesis experimental, analytical, and numerical studies on ice ridge consolidation in different scales were performed. The studies were carried out to study the size-effect on the growth rate of the ridge consolidated layer in laboratory and field conditions. In numerical modeling, the emphasis was put on interpreting the ice ridge consolidation through experimental results. The modeling methods used were based on the discontinuous description of the ridge material in contrast to the homogeneous approach of the analytical approach.

The main original findings and features presented in this thesis are as follows:

1. The effect of a faster growth rate of the consolidated layer over the level ice for small-scale ridges observed experimentally was investigated, and it was found to be related to the difference in convective-conductive coupling for the two types of ice, which can be increased by the extended ridge sail surfaces. This can explain a significantly thicker consolidated layer in relation to the surrounding level ice for small-scale ridges (Paper 2).
2. The effect of slower consolidation rates for full-scale ridges during the initial phase observed experimentally was found to be related to the significant deviation of those ridges from the homogeneous approach commonly used for the ridge thermodynamic models. This effect increases together with the increase of rubble block thickness and can be validated only using ridge discontinuous description (Paper 4).
3. A numerical thermodynamic model for an ice ridge consolidation based on the moving boundary method was developed and implemented. This model considers ridge sail, ridge keel, rubble block thickness, snow distribution, radiative and turbulent upper boundary fluxes, and ice salinity, and was validated using field and laboratory experiments (Papers 4 and 5).
4. The overestimation of the consolidated layer thickness from the measured temperatures was observed in experiments in small- and large scales and was related to the significant horizontal heat fluxes in ridges, described using the numerical thermodynamic model of the ridge (Papers 5 and 6).
5. The difference in growth rate between fresh, saline, and dopant ice in different scales was investigated, and it was found that there is no significant difference between ridge consolidation for these materials during its main phase, while deviations occur during the initial and the warming phases of the consolidation (Papers 5 and 6).

6.2 Future work

Ice ridges come with more complicated morphology as was used in most of the laboratory studies that were used for validation of the presented thermodynamic models. Future work should include more detailed investigations on how ridge morphology, block length, keel depth, and macroporosity distribution might influence its thermodynamics and which numerical methods could be used for these investigations.

Most of the field studies about ice ridge consolidation cover only the main phase of the

consolidation and a small amount of decay phase. Future work should include more both field and laboratory investigations on ice ridge melting, the corresponding transformation of the ridge morphology, and redistribution of salt. Additionally, future fieldwork experiments should require more detailed investigation and measurements of snowpack and radiation heat fluxes. These measurements can decrease errors coming from the external to ice atmospheric forcing and uncertainties of atmospheric and snowpack parametrizations.

Since the scale models of ice ridges often involve mechanical scaling under warm temperature conditions, experimental work on the strength of the consolidated layer at warm conditions should be performed to check conclusions valid for the specimens at the standard for mechanical testing colder conditions. It would make the interpretation easier to performed mechanical experiments with undisturbed ridges using indenters or punch tests.

References

Adams, C.M., French, D.N., Kingery, W.D., 1960. Solidification of Sea Ice. J. Glaciol. 3, 745–761. https://doi.org/10.3189/S0022143000018050

Blanchet, D., 1998. Ice loads from first-year ice ridges and rubble fields. Can. J. Civ. Eng. 25, 206–219. https://doi.org/10.1139/l97-073

Calonne, N., Flin, F., Morin, S., Lesaffre, B., Du Roscoat, S.R., Geindreau, C., 2011. Numerical and experimental investigations of the effective thermal conductivity of snow. Geophys. Res. Lett. 38, 1–6. https://doi.org/10.1029/2011GL049234

Cox, G.F.N., Weeks, W.F., 1983. Equations for Determining the Gas and Brine Volumes in Sea-Ice Samples. J. Glaciol. 29, 306–316. https://doi.org/10.3189/S0022143000008364

Ervik, Å., Nord, T.S., Høyland, K. V., Samardzija, I., Li, H., 2019. Ice-ridge interactions with the Norströmsgrund lighthouse: Global forces and interaction modes. Cold Reg. Sci. Technol. 158, 195–220. https://doi.org/10.1016/j.coldregions.2018.08.020

Feistel, R., Hagen, E., 1998. A Gibbs thermodynamic potential of sea ice, Cold Regions Science and Technology. https://doi.org/10.1016/S0165-232X(98)00014-7

Førland, E.J., Hanssen-Bauer, I., Nordli, P.Ø., 1997. Climate statistics and longterm series of temperature and precipitation at Svalbard and Jan Mayen, DNMI-Rapport, Klima.

Franz von Bock und Polach, R.U., Ehlers, S., 2015. On the Scalability of Model-Scale Ice Experiments. J. Offshore Mech. Arct. Eng. 137, 051502. https://doi.org/10.1115/1.4031114

Griewank, P.J., Notz, D., 2013. Insights into brine dynamics and sea ice desalination from a 1-D model study of gravity drainage. J. Geophys. Res. Ocean. 118, 3370–3386. https://doi.org/10.1002/jgrc.20247

Høyland, K. V., 2007. Morphology and small-scale strength of ridges in the North-western Barents Sea. Cold Reg. Sci. Technol. https://doi.org/10.1016/j.coldregions.2007.01.006

Høyland, K. V., 2002a. Consolidation of first-year sea ice ridges. J. Geophys. Res. 107, 3062. https://doi.org/10.1029/2000JC000526

Høyland, K. V., 2002b. Simulations of the consolidation process in first-year sea ice ridges. Cold Reg. Sci. Technol. 34, 143–158. https://doi.org/10.1016/S0165-232X(02)00002-2

Incropera, F.P., DeWitt, D.P., Bergman, T.L., Lavine, A.S., 2013. Principles of heat and mass transfer, Water. https://doi.org/10.1016/j.applthermaleng.2011.03.022

ISO 19906, 2019. Petroleum and natural gas industries - Arctic offshore structures, International Standard. https://doi.org/10.5594/J09750

Kharitonov, V. V., 2008. Internal structure of ice ridges and stamukhas based on thermal drilling data. Cold Reg. Sci. Technol. 52, 302–325. https://doi.org/10.1016/j.coldregions.2007.04.020

Kioka, S., Takeuchi, T., Yasunaga, Y., Saeki, H., 2001. The Physical Properties of Consolidated Ridge Ice Modeled as Frozen Rubble. pp. 79–90. https://doi.org/10.1007/978-94-015-9735-7_7

Laevastu, T., 1960. Factors affecting the temperature of the surface layer of the sea. Comment. Phys. Math. 25.

Leppäranta, M., Hakala, R., 1992. The structure and strength of first-year ice ridges in the Baltic Sea. Cold Reg. Sci. Technol. 20, 295–311. https://doi.org/10.1016/0165-232X(92)90036-T

Leppäranta, M., Lensu, M., Kosloff, P., Veitch, B., 1995. The life story of a first-year sea ice ridge. Cold Reg. Sci. Technol. 23, 279–290. https://doi.org/10.1016/0165-232X(94)00019-T

Lepparanta, M., Leppäranta, M., 1993. A review of analytical models of sea-ice growth. Atmos. - Ocean 31, 123–138. https://doi.org/10.1080/07055900.1993.9649465

Liu, Y.-C., Chao, L.-S., 2006. Modified Effective Specific Heat Method of Solidification Problems. Mater. Trans. 47, 2737–2744. https://doi.org/10.2320/matertrans.47.2737

Lu, W., Shestov, A., Løset, S., Salganik, E., Høyland, K., 2019. Medium-scale Consolidation of Artificial Ice Ridge-Part II: Fracture Properties Investigation by a Splitting Test, Proceedings of the 25th International Conference on Port and Ocean Engineering under Arctic Conditions, Delft, The Netherlands.

Marchenko, A., 2008. Thermodynamic consolidation and melting of sea ice ridges. Cold Reg. Sci. Technol. 52, 278–301. https://doi.org/10.1016/j.coldregions.2007.06.008

Maykut, G.A., 1986. The Surface Heat and Mass Balance, in: The Geophysics of Sea Ice. Springer US, Boston, MA, pp. 395–463. https://doi.org/10.1007/978-1-4899-5352-0_6

Millero, F.J., 2010. Equation of State of Seawater. Oceanography 23, 18–33. https://doi.org/10.5670/oceanog.2010.21.COPYRIGHT

Moslet, P.O., 2007. Field testing of uniaxial compression strength of columnar sea ice. Cold Reg. Sci. Technol. 48, 1–14. https://doi.org/10.1016/j.coldregions.2006.08.025

Notz, D., 2005. Thermodynamic and fluid-dynamical processes in sea ice. University of Cambridge.

Palmer, A., Dempsey, J., 2009. Model tests in ice, in: Proceedings of the 20th International Conference on Port and Ocean Engineering under Arctic Conditions. pp. POAC09-40.

Pavlov, V.A., Kornishin, K.A., Efimov, Y.O., Mironov, E.U., Guzenko, R.B., Kharitonov, V. V., 2016. Peculiarities of consolidated layer growth of the Kara and Laptev Sea ice ridges. Neft. Khozyaystvo - Oil Ind.

Pounder, E.R., 1966. The Physics of Ice. Am. J. Phys. https://doi.org/10.1119/1.1973537

Pustogvar, A., Kulyakhtin, A., 2016. Sea ice density measurements. Methods and uncertainties. Cold Reg. Sci. Technol. 131, 46–52. https://doi.org/10.1016/j.coldregions.2016.09.001

Repetto-Llamazares, A.H. V., 2010. Review on Model Ice Ridges. 20th IAHR Int. Symp. Ice, Lathi, Finland, June 14 to 18, 2010 1–14.

Rosati, A., Miyakoda, K., 1988. A General Circulation Model for Upper Ocean Simulation. J. Phys. Oceanogr. 18, 1601–1626. https://doi.org/10.1175/1520-0485(1988)018<1601:agcmfu>2.0.co;2

Salganik, E., Høyland, K.V., Maus, S., 2020. Consolidation of fresh ice ridges for different scales. Cold Reg. Sci. Technol. 171. https://doi.org/10.1016/j.coldregions.2019.102959

Salganik, E., Høyland, K.V., Shestov, A., Løset, S., Heijkoop, A.-N., 2019a. Medium-scale consolidation of artificial ice ridge-Part I: surface temperature, thickness and mechanical properties, in: Proceedings of the 25th International Conference on Port and Ocean Engineering under Arctic Conditions, Delft, The Netherlands.

Salganik, E., Høyland, K.V., Shestov, A., Løset, S., Heijkoop, A.N., 2019b. Medium-scale consolidation of artificial ice ridge – part i: Surface temperature, thickness and mechanical properties, in: Proceedings of the International Conference on Port and Ocean Engineering under Arctic Conditions, POAC.

Sand, K., Winther, J.G., Maréchl, D., Bruland, O., Melvold, K., 2003. Regional variations of snow accumulation on Spitsbergen, Svalbard, 1997-99. Nord. Hydrol. https://doi.org/10.2166/nh.2003.0026

Schwerdtfeger, P., 1963. The Thermal Properties of Sea Ice. J. Glaciol. 4, 789–807. https://doi.org/10.1017/S0022143000028379

Shafrova, S., Høyland, K. V., 2008. Morphology and 2D spatial strength distribution in two Arctic first-year sea ice ridges. Cold Reg. Sci. Technol. https://doi.org/10.1016/j.coldregions.2007.05.011

Shestov, A., Høyland, K., Ervik, Å., 2018. Decay phase thermodynamics of ice ridges in the Arctic Ocean. Cold Reg. Sci. Technol. 152, 23–34. https://doi.org/10.1016/j.coldregions.2018.04.005

Shine, K.P., 1984. Parametrization of the shortwave flux over high albedo surfaces as a function of cloud thickness and surface albedo. Q. J. R. Meteorol. Soc. https://doi.org/10.1002/qj.49711046511

Smith, S.D., 1988. Coefficients for sea surface wind stress, heat flux, and wind profiles as a function of wind speed and temperature. J. Geophys. Res. Ocean. 93, 15467–15472. https://doi.org/10.1029/JC093iC12p15467

Stefan, J., 1891. Ueber die Theorie der Eisbildung, insbesondere über die Eisbildung im Polarmeere. Ann. Phys. https://doi.org/10.1002/andp.18912780206

Strüb-Klein, L., Høyland, K., 2011. One season of a 1st year sea ice ridge investigation–Winter 2009. Proc. 21st Int. Conf. Port Ocean Eng. under Arct. Cond.

Sturm, M., Holmgren, J., König, M., Morris, K., 1997. The thermal conductivity of seasonal snow. J. Glaciol. 43, 26–41. https://doi.org/10.1017/S0022143000002781

Surkov, G.A., Truskov, P.A., 2003. Parameters of hummock-forming blocks of ice. Proc. 17th Int. Conf. Port Ocean Eng. under Arct. Cond. 2003. Trondheim, Norway. 2, 87–102.

Tests, M., Predictions, F.S., Wake, F.S., Factors, M.C., Data, I., Data, O., Example, T., Analysis, U., With, C., Scale, F., 1999. ITTC – Recommended Procedures ITTC – Test Methods for Model Ice Properties. ReVision.

Timco, G.W., 1986. EG/AD/S: A new type of model ice for refrigerated towing tanks. Cold Reg. Sci. Technol. https://doi.org/10.1016/0165-232X(86)90032-7

Timco, G.W., Burden, R.P., 1997. An analysis of the shapes of sea ice ridges. Cold Reg. Sci. Technol. https://doi.org/10.1016/S0165-232X(96)00017-1

Timco, G.W., Frederking, R.M.W., 1990. COMPRESSIVE STRENGTH OF SEA ICE SHEETS ABSTRACT A model has been developed for predicting the 17, 227–240.

Timco, G.W., Goodrich, L.E., 1988. Ice rubble consolidation. Proc. 9th Int. Symp. Ice, Int. Assoc. Hydraul. Eng. 1, 537–548.

Tsonis, A.A., 2007. An Introduction to Atmospheric Thermodynamics, An Introduction to Atmospheric Thermodynamics. Cambridge University Press, Cambridge. https://doi.org/10.1017/CBO9780511619175

Tuhkuri, J., 2002. Laboratory tests on ridging and rafting of ice sheets. J. Geophys. Res. 107, 1–14. https://doi.org/10.1029/2001jc000848

von Bock und Polach, R., Ehlers, S., Kujala, P., 2013. Model-scale ice - Part A: Experiments. Cold Reg. Sci. Technol. 94, 74–81. https://doi.org/10.1016/j.coldregions.2013.07.001

Weast, R.C., 1977. CRC Handbook of Chemistry and Physics, 57th Edition, Handbook of Chemistry and Physics.

Yen, Y.-C., 1981. Review of Thermal Properties of Snow, Ice, and Sea Ice. CRREL Rep. 81-10 1–27.

A.1. Paper 1

Thermodynamics and consolidation of ice ridges for laboratory scale.

Salganik, E., Høyland, K.V., Shestov, A.

Proceedings of the International Conference on Port and Ocean Engineering under Arctic Conditions (POAC), Busan, Korea, paper no. 78., 2017.

POAC'17
Busan, KOREA

Proceedings of the 24th International Conference on
Port and Ocean Engineering under Arctic Conditions
June 11-16, 2017, Busan, Korea

Thermodynamics and Consolidation of Ice Ridges for Laboratory Scale

Evgenii Salganik[1,2], Knut Vilhelm Høyland[1], Aleksey Shestov[1,2]
[1] Sustainable Arctic Marine and Coastal Technology (SAMCoT), Centre for Research-based Innovations (CRI), Norwegian University of Science and Technology, Trondheim, Norway
[2] The University Centre in Svalbard, Longyearbyen, Norway

ABSTRACT

First-year ice ridge interaction with structures often gives highest loads and can be modelled in controlled environment in ice basins. Five laboratory experiments were performed to study model-scale first-year ice ridge development. Effect of initial rubble temperature on consolidated level growth was observed. For both ridges with low and high initial rubble temperatures, consolidated layer was 2–4 times thicker than surrounding level ice at the initial phase of experiment. At the main phase of consolidation this ratio approaches lower equilibrium value of 1.2–1.7 of level ice thickness that is also depends on initial rubble temperature. Non-linear sea ice specific heat capacity can change consolidation development that results in sufficient difference from ice thickness prediction using Leppäranta (1993) and Ashton (1989) approaches.

Observed ratios of air, ice top and bottom surface temperatures can be used for consolidated layer thickness predictions in laboratory conditions using obtained heat transfer coefficient H_{ia}.

During the main phase vertical conductive heat flux at the top of consolidated layer was about two times higher than heat flux at the bottom part due to sea ice cooling. Latent heat flux was slightly lower than vertical conductive heat flux at the bottom of consolidated layer due to natural water convection.

Consolidated layer bulk salinity was always lower than salinity of surrounding level ice for provided experiments. This difference was becoming larger after melting phase.

This study can be approach for better understanding of the main differences between thermodynamics of model-scale and full-scale ice ridges.

KEY WORDS: Ice, ridges, thermodynamics, consolidation, laboratory.

INTRODUCTION

Increasing level of transportation and exploration in the Arctic enhance the significance of ice loads on coastal and offshore structures. Loads from ice ridges often give highest quasi-static loads. In contrast with level ice, loads from ice ridges depends on several that are hard to measure directly in field.

The thickness of consolidated layer h_c is one of these and because of uncertain data the load estimation may become inaccurate. Analysis of mesoscale experiments requires good

understanding of aspect ratio effect on stress distributions. However, it is possible to model ice-structure interaction with controlled key parameters in ice basins.

Mechanical scaling traditionally involves decreasing of both ice strength and elastic parameters. This originates from studies of icebreakers advancing through level ice where inertia and gravity forces both play key roles. It is not obvious that the gravity contribution is necessary for relatively slow interaction between ice ridges and fixed structures. One of the main problems connected to mechanical scaling is that in vicinity of the melting point not only strength and elastic parameters are changing but also mechanisms of ice failure and applicability of elastic material model.

Thermodynamics of ice ridge governs both the thickness and the strength of consolidated layer, two key parameters for ice ridge load determination: ISO/FDIS/19906 (2010) recommends modelling the consolidated layer of ice ridges as thick level ice, even though it may have different salinity, ice texture and temperature profile.

Laboratory experiments were provided to understand how controlled consolidation parameters (air and water temperature, initial ice temperature, dopant fraction and time) could affect both consolidated layer thickness and salinity for laboratory scale.

The main goal of this study is to investigate ridge consolidation process because ratios of different thermal processes (conduction, convection, solidification, salt expulsion and initial rubble sensible heat at temperature T_0) is different for different scales while laboratory scale is used for basin tests and full scale is used for collecting and verification of ice ridge thermal, mechanical and geometrical parameters.

RIDGE CONSOLIDATION THEORY

Full-scale ridge development usually consists of three main phases: initial, main and decay (Høyland and Liferov, 2005). For laboratory scale, initial phase (when ice rubble temperature T_0 is lower than freezing point of surrounding water T_f) can continue during significant part of the whole experiment time (Chen and Høyland, 2016). For adiabatic conditions, realized in an ice rubble, the change of initial keel macro-porosity $\Delta\eta$ for fresh ice is equal to:

$$\Delta\eta = (1-\eta)\frac{c_i\left(T_f - T_0\right)}{L_i} = (1-\eta)Ste, \quad (1)$$

where η is the initial rubble macro-porosity, c_i is the fresh ice specific heat capacity, L_i is the latent heat of ice, Ste is the Stefan number.

Change of keel macro-porosity $\Delta\eta$ for saline ice is higher due to change of ice micro-porosity during temperature change and so that strongly depends on freezing temperature of surrounding water (Schwerdtfeger, 1963):

$$\Delta\eta = (1-\eta)\frac{\int_{T_0}^{T_f} c_{si}(T)dT}{L_{si}}, \quad (2)$$

where c_{si} is the sea ice specific heat capacity, L_{si} is the latent heat of sea ice.

Heat convection in the water initiated by solidification can decrease saline ice growth rate providing heat flux around 280 W/m^2 in the beginning of initial phase and around 90 W/m^2 in the late phase for ice initial temperature of 35°C (Chen and Høyland, 2016). That corresponds to heat transfer coefficient H_{iw} of 8 W/m^{2}K for the initial phase.

Forced and natural air convection affects consolidation rate by governing ice top surface temperature T_s depending on ice thickness h and ice surface roughness, air temperature T_a and circulation, and water freezing temperature T_f. Biot number represents ratio of conduction resistance within a solid ice to the external convection resistance offered by the surrounding air (Bergman, et al., 2011):

$$Bi = \frac{H_{ia}h}{k_i} = \frac{T_f - T_s}{T_a - T_s}, \tag{3}$$

where H_{ia} is the heat transfer coefficient, h is the ice thickness, k_i is the ice thermal conductivity.

Recommended values of heat transfer coefficient H_{ia} are in the range of 10–30 W/m^{2}K for still air and 6.7 m/s wind speed correspondingly (Ashton, 1989).

Ice thickness under assumption of linear temperature profile and no water convection can be calculated from the top ice surface T_s and the water freezing temperature T_f as (Stefan, 1891):

$$h(t) = \sqrt{h(t_0)^2 + \frac{2k_i}{\rho_i L_i}\int_{t_o}^{t}(T_f - T_s)dt}, \tag{4}$$

where k_i is the ice thermal conductivity, ρ_i is the ice density, L_i is the latent heat of ice.

The surface temperature T_s can be significantly higher than the air temperature T_a for thin ice growth. Under assumption of equal convective heat flux to the atmosphere and conductive heat flux through the ice Ashton (1989) derived an equation for the ice thickness, based on values of air temperature T_a, water freezing point T_f, and heat transfer coefficient H_{ia}:

$$h(t) = \sqrt{\frac{2k_i}{\rho_i L_i}(T_f - T_a)t + \left(\frac{k_i}{H_{ia}}\right)^2} - \frac{k_i}{H_{ia}} \tag{5}$$

Consolidated layer growth can be calculated assuming reduced value of the ice latent heat multiplied by the value of macro-porosity η (Leppäranta, 1993):

$$L_c = \eta L_i \tag{6}$$

This equation is valid only under assumption of constant macro-porosity in the ridge keel part that will consolidate.

EXPERIMENTAL SETUP

A series of laboratory experiments were performed with different initial rubble temperature and different thermal boundary conditions: 2D and 3D configurations (Figure 1). One vertical layer of ice rubble partly insulated from sides and from the bottom by acrylic walls was used at 2D configuration. Plastic net with 30x30 cm horizontal cross-section was filled with ice rubble at 3D configuration. Two sides of the plastic net were thermally insulated during run 4 and there was no insulation of model ridge at run 5.

Ice for model ridges was prepared in 1000 L water tank and cut into pieces of 8x4x4 cm (run 1, 2, 3 and 5) and 7x5x3 cm (run 4). Then transparent acrylic box (2D) or plastic net (3D) with ice rubble at initial temperature was placed in the middle of the tank with water at the freezing point. Two of the models (run 1 and 5) went through transition zone from consolidation to

melting. Air temperatures were in the range of -(4–15)°C during initial and main phases of consolidation and around +5°C during decay phase. Amount of freezing degree-days ($FDD_{air} = \int(T_a - T_w)dt$) was in the range of 11–30°Cd. Initial water salinity $S_{w,0}$ was in the range of 20–34 ppt, rubble salinity $S_{i,0}$ was 3.8–7.0 ppt for different experiment runs.

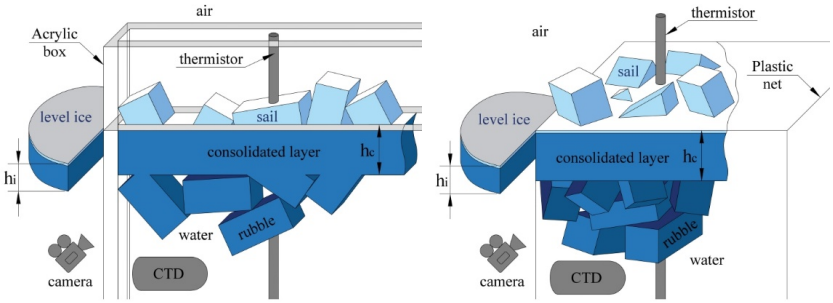

Figure 1. Experimental setup for 2D (left) and 3D (right) configurations

Thermistor strings and CTD (electrical conductivity, temperature and depth) sensors measured vertical temperature profile in air, consolidated layer, rubble, water, and water salinity and freezing temperature. Initial macro-porosity and consolidated layer thickness of 2D model ridges were obtained by underwater camera image processing. Freezing and upper surface temperatures of ridges were assumed equal to the temperature values measured by thermistor string at the bottom and the top surface of consolidated layer. Level ice thickness, water freezing temperature and salinity of water below level ice bottom surface were manually measured by ruler, thermometer (Ebro TFX 410-1) and conductivity meter (Mettler Toledo SG7-FK2).

Consolidated layer thickness was measured manually after each experiment. Initial macro-porosity of 3D model ridges was obtained from manually measured keel volume and number of rubble blocks. Evolution of consolidated layer and corresponding freezing temperatures were obtained from analysis of vertical temperature profiles from thermistors.

Two types of thermistor strings were used: 100 cm length thermistor string with metal cover and 15 cm length negative temperature coefficient thermistor string with plastic cover (Chen and Høyland, 2016).

After experiments, model-scale ridges were taken from water tank for geometrical, temperature, density and salinity measurements. Sea ice density ρ_{si} was measured by hydrostatic weighing in paraffin (Pustogvar and Kulyakhtin, 2016).

RESULTS

Key initial parameter's values and experiment results after a main consolidation phase are presented in Table 1. The ratio of consolidated layer h_c and level ice thickness h_i is called degree of consolidation $R = h_c/h_i$. It can be estimated from experimental data and also can be derived using Stefan's predictions $R^{Ste} = h_c^{Ste}/h_i^{Ste}$ based on measured consolidated layer surface temperatures and initial macro-porosity of consolidated layer η.

For lower rubble initial temperature for both 2D and 3D experiments give higher degree of consolidation in comparison to Stefan's predictions. Average values of heat transfer coefficient

H_{ia}, derived from consolidated layer top and bottom surfaces and air temperatures using equation (3), were higher for experiments with colder initial rubble. At the same moment heat transfer coefficient H_{ia}, based on direct level ice thickness and air temperature values, was around 20 W/m^{2}K for all provided experiments.

Table 1. Consolidation experiments summary

N	Type	T_0	η	$\Delta\eta$	$S_{i,0}$	$S_{w,0}$	FDD_{air}	H_{ia}	h_i	h_i^{Ste}	h_c	h_c^{Ste}	R	R^{Ste}	R/R^{Ste}
-	-	°C	-	-	ppt	ppt	°Cd	W/m^{2}K	cm	cm	cm	cm	-	-	-
1	2D	-2.7	0.41	0.20	7.0	20.2	15.4	7.0	6.5	4.2	7.5	6.6	1.15	1.57	0.73
2	2D	-7.9	0.49	0.25	7.0	22.0	11.0	15.0	4.6	6.1	8.0	8.7	1.74	1.43	1.22
3	2D	-6.4	0.38	0.25	7.0	24.1	29.3	22.0	9.5	13.7	12.9	20.5	1.36	1.50	0.91
4	3D	-17.6	0.47	0.21	5.0	24.0	15.1	20.0	9.0	9.3	11.9	13.6	1.32	1.46	0.90
5	3D	-3.0	0.31	0.04	3.8	34.2	29.5	7.0	13.5	18.1	18.0	32.3	1.33	1.78	0.75

Both ice top and bottom surface temperatures of consolidated layer are different from level ice temperatures due to different ratios of conduction and convection, and due to different growth rate and salt expulsion for 2D and 3D configurations. Consolidated layer average vertical temperature gradient was almost constant during experiment time while values of the gradient were significantly higher at the top ice surface than at the bottom surface. For typical vertical temperature profile, the air temperature was significantly lower than ice top surface temperature while ice bottom temperature was slightly lower than water temperature below (Figure 2).

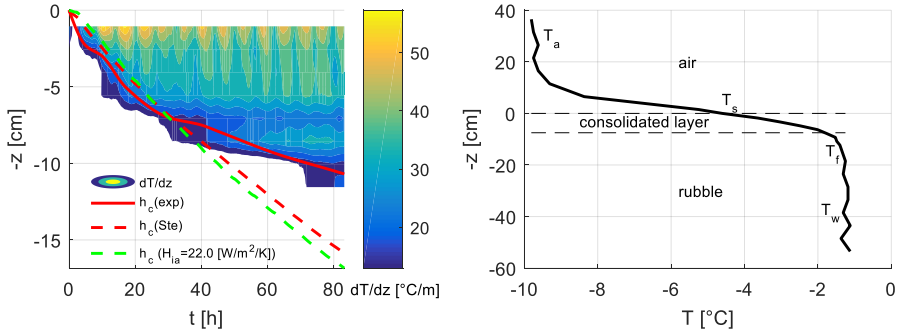

Figure 2. Temperature and temperature gradients in time and space: a) Vertical temperature gradient dT/dz vs time t and water depth z. Red solid curve is h_c from video analysis, red dashed curve represents h_c prediction from Stefan's equation and green dashed curve represents h_c prediction from Ashton's equation using heat transfer coefficient of 22 W/m^{2}K and b) temperature profile of model ridge after t = 40 h (right) for run 3 (2D)

Macro-porosity measurements are complex for volumetric (3D) ice ridges while image processing can give its values for planar (2D) consolidation experiments. Initial macro-porosity vertical distribution is important for ice growth analysis and its values could have significant deviations from average values. Without taking into account low values at the box corners macro-porosity for run 3 was in the range of 0.12–0.26 (Figure 3).

For thin ice growth, difference between air and water freezing temperature is usually much higher than difference between ice top and bottom surface temperatures. For provided experiments ratio between accumulated $FDD_{air} = \int (T_a - T_w) dt$ and $FDD_{ice} = \int (T_s - T_f) dt$ was in the range of 1.7–2.4 during experiments.

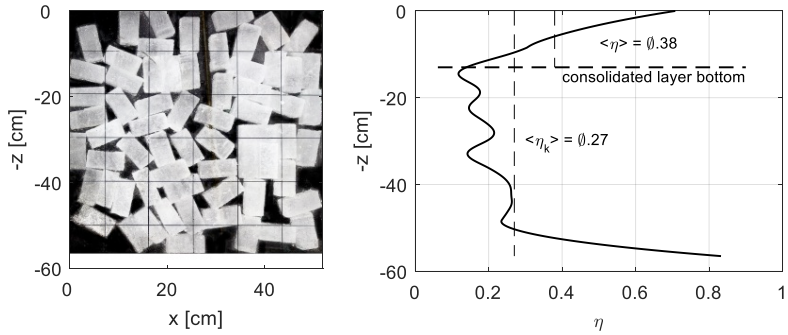

Figure 3. Initial rubble configuration (left) and macro-porosity distribution η vs water depth z (right) for run 3

Ratio of consolidated layer and level ice thicknesses, called degree of consolidation R, is a convenient way to represent ridge development. To neglect different ice growth rate for different macro-porosities η for different experiments and their stages, ratios of experimental and analytical degree of consolidation are presented at the Figure 4. Analytical values are based on Stefan's equation for ice growth, measured surface and water freezing temperatures and latent heat of fusion for consolidated layer $L_{i,c} = \eta L_i$.

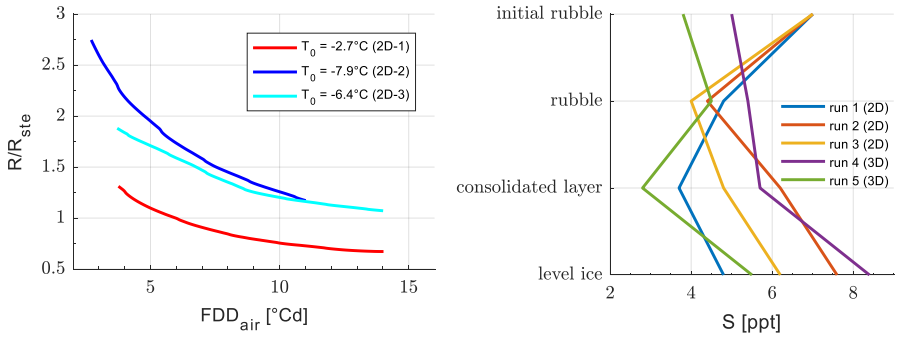

Figure 4. Ratio of experimental and analytical degree of consolidation vs FDD_{air} for 2D experiments with different initial rubble temperatures T_0 (left) and salinity of level ice, initial ridge rubble, consolidated layer and surrounding level ice (right)

Ice salinity usually depends on water salinity and ice growth rate. Consolidated layer was more saline than surrounding level ice (Figure 4). After decay phase, consolidated layer was becoming less saline than rubble and almost two times less saline than level ice. That means that ice consolidated layer had almost two times less micro-porosity than level ice around model ice ridge after the main phase. Bulk ice salinity was linearly decreasing during freezing.

Air content of sail is close to air content of consolidated layer top while air content of

consolidated layer bottom is close to air content of rubble. Average air contents of level ice and consolidated layer are close. Density of model ridge rubble was slightly lower than density of level ice and consolidated layer.

DISCUSSION

After short time of consolidation, less than 5°Cd, consolidated layer thickness was almost 2 times higher than thickness value predicted only by initial rubble macro-porosity in comparison to level ice thickness (Figure 4). This effect was decreasing in time, and consolidated layer thickness started approaching equilibrium value that also depends on initial rubble temperature. For initial rubble temperatures close to water freezing point, this value is around 0.7 for both 2D and 3D experiments. For lower initial temperatures values of R/R^{Ste} are higher for 2D configuration than for 3D.

It is possible to estimate change of initial macro-porosity $\Delta\eta$ based on values of the rubble initial temperature, the sea ice specific heat capacity, the sea ice latent heat and initial rubble porosity η using equation (2). Ratio of R/R^{Ste} can be estimated from macro-porosity as:

$$\frac{R}{R^{Ste}} = \sqrt{\frac{\eta}{\eta - \Delta\eta}} \tag{7}$$

It is assumed that heat diffusion in the rubble is fast enough to form new ice before consolidated layer significant growth. For provided experiments, values of estimated ratios of R/R^{Ste} were in the range of 1.1–1.7. However, this assumption cannot explain higher R/R^{Ste} experimental values during initial phase. It also does not account heat loss due to water convection and ice cooling that can explain slower ice growth at the late stages of experiments.

Two main processes govern consolidated layer growth rate: extraction of initial sensible energy $\int cdT$ due to temperature increase and upper surface cooling by air convection. First process strongly depends on ice rubble salinity. New ice is forming faster around fresh ice (for several hours depending on ice rubble size) but saline ice can store higher amount of energy to form new ice around it due to non-linear sea ice specific heat capacity c_{si} and sea ice thermal conductivity k_{si}. Fourier number can be used for dimensionless analysis of described heat transfer.

Second governing process is consolidation due to cooling from above. This process also depends on ice salinity because for high values of saline ice specific heat capacity significant amount of heat should be spent on sea ice cooling so less heat can be available for ice formation. It can be seen from non-linear ice vertical temperature gradient profile during provided experiments.

Cooling can decrease effect of initial macro-porosity change because ice at freezing temperatures of surrounding contains sufficient amount of brine that should be partly frozen after cooling. It should be said that for engineering or basin test application consolidated layer thickness at the air temperature equal to the surrounding water freezing temperature is a value of interest. It is also a convenient value for experimental analysis because all the energy stored in initial rubble should be spent on consolidation process not on cooling.

Another complication of consolidated layer formation analysis is the effect that due to lower permeability and slow solute diffusion water salinity near consolidation surface is significantly higher than initial water salinity that leads to less amount energy that could be extracted from cold rubble.

According to Chen and Høyland (2016) for ice surrounded by fresh water, amount of new formed fresh ice around saline ice $\Delta V/V$ is 48 % higher than for fresh ice: 26 % and 16 % respectively. This value corresponds to the volume change $\Delta V/V$ calculated from sea ice specific heat capacity values by Schwerdtfeger (1963) including total melting of initial saline ice:

$$\frac{\Delta V}{V} = \frac{\int_{T_0}^{T_f} c_{si}(T)dT}{L_i} = \frac{\int_{-35}^{-0.13} c_{si}(T)dT}{L_i} = 1.34, \quad (8)$$

where $T_f = -0.13℃$ is the freezing temperature of sea ice with salinity of 2.65 ppt.

The test results prove that initial rubble temperature changes not only initial degree of consolidation values but also its values during cooling. This degree of consolidation value depends on ratio of initial rubble temperature and consolidated layer temperature at the end of experiment. It can be confirmed by the fact that degree of consolidation values after decay phase (when consolidated layer temperature is close to water freezing point) were approaching $1/\sqrt{\eta}$ values (and $R/R^{Ste} = 1$) for experiments with high rubble initial temperature.

For experiment runs 2 and 3 with rubble initial temperatures of -7.9°C and -6.4°C degree of consolidation values are approaching values $1/\sqrt{\eta}$ because these temperatures are relatively close to final consolidated layer surface temperatures of -4.0°C and -5.4°C respectively.

These assumptions can explain why consolidated layer growth is faster at the beginning and slower after initial phase (Figure 2).

During the main phase vertical conductive heat flux at the top of consolidated layer $(k_{si}dT/dz|_{z=0+})$ is about two times higher than heat flux at the bottom part $\left(k_{si}dT/dz|_{z=h_c-}\right)$ while this difference accounts for ice cooling. Latent heat flux $(\rho_{si}L_{i,c}\, dh_c/dt)$ is at the same moment slightly lower than vertical conductive heat flux at the bottom of consolidated layer. This difference accounts for water convection that is not considered at Stefan's condition:

$$\rho_{si}L_{i,c}\, dh_c/dt = k_{si}dT/dz|_{z=h_c-} \quad (9)$$

Lower initial rubble temperature also leads to higher ratio of conduction resistance to the external convection air resistance. While thin level ice growth is governed by air convection, consolidated layer growth is also controlled by initial sensible energy. However, for full-scale first-year ice ridges difference between sail surface temperature and air temperature is insignificant (Shestov and Ervik, 2016).

2D experiments give easily accessible data of macro-porosity distribution that is very valuable for consolidation analysis. 3D configuration provides realistic thermal boundary conditions with insulation along imaginable model ridge axis, without insulation at water-keel boundaries and realistic permeability of rubble. There is no perfect insulation at ridge sides for 2D configuration. It creates addition heat fluxes oriented not in vertical direction. Permeability difference leads to higher difference in level ice and consolidated layer bottom surface temperatures due to higher water bulk salinity around rubble inside 2D box.

Consolidated layer bulk salinity was always lower than salinity of surrounding level ice. This difference was becoming larger after melting phase. It could be critical for scale-model mechanical experiments because ice strength is governed by salinity and temperature while thinner level ice is more saline and its temperature have to decrease faster than for thicker consolidated layer.

CONCLUSIONS

Five laboratory experiments were performed to study model-scale ridge development. Effect of initial rubble temperature on consolidated level growth was observed during initial and main phases of ridge formation. For both ridges with low and high initial rubble temperatures, consolidated layer was 2–4 times thicker than surrounding level ice at the initial phase of experiment. At the main phase of consolidation this ratio approaches lower equilibrium values in the range of 1.2–1.7 that is also depends on initial rubble temperature. Effect of non-linear sea ice specific heat capacity on degree consolidation was described in order to explain sufficient difference from ice thickness prediction using Leppäranta (1993) and Ashton (1989) approaches.

Difference in ratio of conduction resistance within a solid ice to the external convection resistance offered by the surrounding air was observed for level ice and consolidated layer formed from a rubble of different initial temperatures. Observed ratios of air, ice surface and water freezing temperatures can be used for consolidated layer thickness predictions for laboratory conditions using obtained heat transfer coefficient H_{ia}.

During the main phase vertical conductive heat flux at the top of consolidated layer was about two times higher than heat flux at the bottom part due to ice cooling and high non-linear values of sea ice specific heat capacity. Latent heat flux was slightly lower than vertical conductive heat flux at the bottom of consolidated layer due to natural water convection.

2D and 3D experimental configurations and their advantages and potential method uncertainties of usage for consolidation process study were described.

Effect of different consolidation conditions for level ice and rubble was observed during experiments. Consolidated layer bulk salinity was always lower than salinity of surrounding level ice for provided experiments. This difference was becoming larger after melting phase that could be critical for scale-model mechanical experiments because ice strength is governed by salinity and temperature while thinner level ice is more saline and its temperature have to decrease faster than for thicker consolidated layer.

This study can be approach for better understanding of the main differences between thermodynamics of model-scale and full-scale ice ridges and for the development of ridge consolidation model. Future consolidation studies have to take into account main effects governing this process: air convection above ice surface, salt expulsion and diffusion below consolidated layer, initial sensible energy, macro-porosity distribution and non-linear specific heat capacity of sea ice during bulk salinity development.

ACKNOWLEDGEMENTS

The authors wish to acknowledge the support of the Research Council of Norway through the Centre for Research-based Innovation, SAMCoT, and the support of the SAMCoT partners. The authors wish to acknowledge the economic support of the Research Council of Norway through the project “Field studies and modelling of sea state, drift ice, ice actions and methods of icebergs management on the Arctic shelf, 2015-2017 (FIMA)”. The logistics and Arctic Technology department at UNIS are acknowledges for helping during laboratory experiments.

REFERENCES

Ashton G.D., 1989. Thin Ice Growth. *Journal of Water Resources Research*. Vol. 25, No. 3. pp. 564–566.

Bergman, T.L., Incropera, F.P. and Lavine, A.S., 2011. *Fundamentals of heat and mass transfer*. John Wiley & Sons.

Chen, X. and Høyland, K.V., 2016. Laboratory Work on Heat Transfer in Submerged Ice, Theory, Experimental Setup and Results. *Proceedings the 23rd IAHR International Ice Symposium on Ice*, Ann Arbor, USA.

Høyland, K.V., Liferov, P., 2005. On the initial phase of consolidation. *Cold Regions Science and Technology*. (41, 1), pp. 49-59.

Høyland, K.V., 2002. Consolidation of first-year sea ice ridges. *Journal of geophysical research*. 107(C6): 3062.

ISO/FDIS/19906, 2010. Petroleum and natural gas industries - Arctic offshore structures. Standard.

Leppäranta, M., 1993. A review of analytical models of sea- ice growth. *Atmosphere-Ocean*, 31, pp. 123-138.

Pustogvar, A. and Kulyakhtin, A., 2016. Sea ice density measurements. Methods and uncertainties. *Cold Regions Science and Technology*. vol. 131.

Schwerdtfeger, P., 1963. The thermal properties of sea ice. *Journal of Glaciology*, 4: pp. 789-807.

Shestov, A. and Ervik, Å., 2016. Studies of Drifting Ice Ridges in the Arctic Ocean during May-June 2015, Part II. Thermodynamic properties and melting rate. *Proceedings the 23rd IAHR International Ice Symposium on Ice*, Ann Arbor, USA.

Stefan, J., 1891. Uber die Theorie der Eisbildung, insbesondere uber die Eisbildung im Polarmeere, *Annalen der Physik und Chemie*, 42, pp. 269-286.

A.2. Paper 2

Thermodynamics and Consolidation of Fresh Ice Ridges for Different Scale and Configuration.

Salganik, E., Høyland, K.V.

Proceedings of the 24th International Association for Hydro-Environment Engineering and Research (IAHR) International Symposium on Ice, Vladivostok, Russia, paper no. 38, 2018.

International Association for Hydro-Environment Engineering and Research
Supported by Spain Water and IWHR, China

24th IAHR International Symposium on Ice
Vladivostok, Russia, June 4 to 9, 2018

Thermodynamics and Consolidation of Fresh Ice Ridges for Different Scale and Configuration

Evgenii Salganik[1], Knut Vilhelm Høyland[1]
[1]*Sustainable Arctic Marine and Coastal Technology (SAMCoT), Centre for Research-based Innovations (CRI), Norwegian University of Science and Technology, Trondheim, Norway*
Department of Civil and Environmental Engineering, NTNU, 7491, Trondheim, Norway
evgenii.salganik@ntnu.no, knut.hoyland@ntnu.no

Ice ridges are formed from deformed ice under atmospheric cooling. Interaction of first-year ice ridges with structures often gives highest loads. This process can be modelled in ice basins under controlled environment in contrast to field experiments, where most key parameters for consolidation analysis are unknown or uncertain. A series of experiments have been conducted to study model-scale fresh ice ridge development. The effect of initial rubble size, temperature, and configuration on consolidated level growth was observed in experiments and described analytically. Scale-dependent model was developed, taking into account main thermodynamic processes governing model-scale fresh ridge consolidation: conduction in the ice, sensible heat storage in the ice and convection in the air. Results of numerical and analytical models and experiments showed that consolidated layer growth was significantly faster than level ice for small-scale experiments. This difference is governed not only by the ridge initial macro-porosity (volumetric liquid fraction) and temperature but also by block length, width, freeboard, and orientation. Experimental setup and instrumentation are described providing measuring techniques for the convectional heat transfer coefficient, consolidated layer and level ice thickness, and heat fluxes at the newly formed ice and initial ice rubble.
This study provides the understanding of the main differences between the thermodynamics of fresh model-scale and full-scale ice ridges. It can be a basis for saline ridge consolidation analysis, where there is a presence of solution gradients in both ice and water underneath. Study results can provide additional information about data that should be collected in future field investigations and laboratory experiments, and about parameters that could be controlled to perform basin tests with necessary and realistic model-scale ridge configuration.

Introduction

In recent years, the part of deformed sea ice is increasing. Physical parameters of broken ice features can be studied in the field, but these investigations are time-consuming and usually cannot provide data about ridge formation process, initial conditions before consolidation, and about potential full-scale loads on offshore structures and vessels. It literally means that almost all the parameters governing consolidation process are unknown or quite uncertain: initial macro-porosity, initial size, orientation, salinity and temperature of broken ice blocks (rubble) forming the ridge, and thickness of the snow above the ridge.

Scale basin tests can be used for the design of new structures. However, scale models of ice ridges also have disadvantages: complications with scaling down of ice microstructure, mechanical properties and performing natural ridge formation. Significant scaling of ice mechanical properties is possible only using dopants, which makes solidification process more complicated because of temperature dependent liquid fraction of model ice. According to Griewank and Notz (2013), the dopant concentration in growing ice depends strongly on an experimental scale and dopant density at different temperatures and concentrations. The research goal is to study ice ridge solidification in different scales to be able to predict its growth rate in basin and laboratory tests and to provide a better understanding of ridge thermodynamics in general.

Theory

Consolidation is mainly governed by ridge thermodynamics, most of the information can be received from thermistor strings. However, thermistors usually provide data about temperature distribution in one dimension while ridge consolidation is a multidimensional process. The temperature profile in the air above the ice is non-linear in the range of boundary layer. Ice surface temperature depends on the ratio between conduction in the ice and convection in the air, so it can be estimated from temperature gradient in ice and convectional heat transfer coefficient H_{ia} mainly depending on air velocity. The temperature profile in the ice during freezing is usually non-linear because some part of higher heat flux at the top surface is covering the amount of sensible heat to cool down the ice with growing thickness to transport heat.

According to Griewank and Notz (2013), sensible heat changes the ice growth insignificantly so in most cases linear temperature profile can be assumed. It is a weak assumption for fresh ice ridges and even weaker assumption for sea ice ridge, because during ridge solidification not only newly formed ice but also surrounding rubble should be cooled down to the equilibrium temperature profile. Temperature profile from voids can provide information about consolidated layer ice growth, while profiles from ice rubble can tell about the heat that is stored, extracted and conducted through it. The difference between these two profiles can show how strong heat fluxes in the horizontal direction are. The consolidated layer thickness h_c is assumed as the minimum thickness of newly formed ice after ridging process. The ratio of the consolidated layer and surrounding level ice thickness is called the degree of consolidation $R = h_c/h_i$.

In previous publications and engineering standards, ice ridges are usually assumed as a homogeneous media with small pores evenly distributed in its volume. This simplification provides a simple one-dimensional solution of consolidation problem based on the amount of

freezing degree-days and initial macro-porosity η_0 where the ratio between the consolidated layer and surrounding level ice thicknesses is $h_c/h_i = 1/\sqrt{\eta_0}$ (Leppäranta, 1993). Coupling of conduction in the ice, convection in the air and additional sensible heat needed for rubble cooling can be implied to this solution (Adams et al., 1960) giving significant scale effect of level ice and consolidated layer growth rate ratio (Fig. **3**). This solution is correct for small and mostly horizontally oriented blocks. Level ice h_i and consolidated layer thickness h_c can be found as:

$$\Delta T dt = \frac{1}{2}\rho L dh_i \left(\frac{h_i}{k} + \frac{1}{H_{ia}}\right)\left(1 + \sqrt{1 + \frac{4}{3}\frac{c_p \Delta T}{L}\left(\left(\frac{H_{ia}h_i}{k}\right)^3 - 1\right)\Big/\left(\frac{H_{ia}h_i}{k}\right)^3}\right); \quad (1)$$

$$\Delta T dt = \frac{1}{2}\rho L_c dh_c \left(\frac{h_c}{k} + \frac{1}{H_{ia}}\right)\left(1 + \sqrt{1 + \frac{4}{3}\frac{c_p \Delta T}{L}\left(\left(\frac{H_{ia}h_c}{k}\right)^3 - 1\right)\Big/\left(\frac{H_{ia}h_c}{k}\right)^3}\right); \quad (2)$$

$$L_c = L\eta_0, \quad (3)$$

where t is the freezing time; ΔT is the difference between water freezing and air ambient temperatures; ρ is the ice density; L is the ice latent heat; L_c is the latent heat of consolidated layer; k is the ice thermal conductivity, and c_p is the ice specific heat capacity.

This analytical approach is valid if the ice ridge can be described as a homogeneous media. Full-scale ridge development consists of three main phases: initial, main and decay (Høyland and Liferov, 2005). The initial phase of ridge consolidation can be included into the described analytical model by varying the value of initial porosity η_0. According to Chen and Høyland (2016) only 80 % of specific heat energy of 20 cm thick ice block can be transferred to the new ice formation. This correction was used to evaluate the value of initial porosity change $\Delta\eta = \eta - \eta_0$ for the analytical mode:

$$\Delta\eta = 0.8(1 - \eta)\frac{c_p(T_f - T_0)}{L} \quad (4)$$

Convectional heat transfer coefficient H_{ia} for steady laboratory conditions can be back-calculated from equation (1) using experimental level ice thickness for corresponding time and air temperatures.

Experimental setup

Twenty tests were conducted to study the influence of rubble blocks scale, orientation and initial temperature on consolidation rate. Fresh ice was cut into pieces with a prescribed size of $L \times w \times 10$ cm, cooled down to the chosen temperature T_0, placed into the water tank with side thermal insulation, and frozen under laboratory conditions with air temperature T_a of -15°C (Fig. **1**). Ice blocks were vertical or inclined by 30° from water level surface. The thickness of ice blocks w was 2, 4 and 6 cm; the length L was 15 cm and 25 cm. The initial thickness for both level ice and the consolidated layer was 0, the initial water temperature was 0°C, the initial ice blocks temperature was -1, -15 and -24°C. The size of side insulation box was 10x30x25 cm. Above water block height varied for different tests in the range of 0–3 cm. Two thermistor

strings with the length of 100 cm and 15 cm were installed to measure water, ice and air temperatures. Initial macro-porosity values η_0 were close to 0.4 and were obtained from photo images. In the full-scale ridges, macroporosity values are in the range of 11–45 % (Høyland, 2007). Both level ice and consolidated layer thicknesses were measured directly after each experiment.

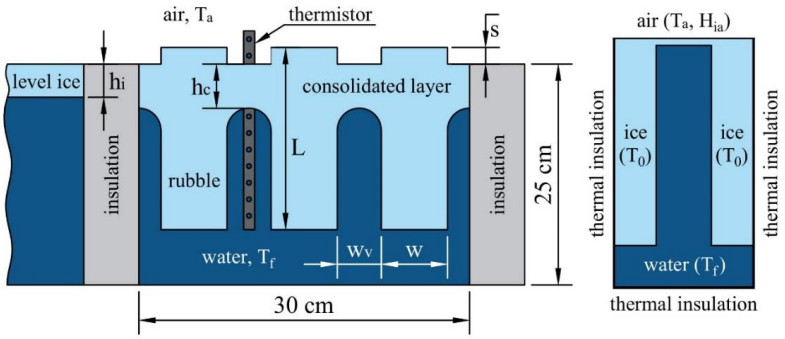

Fig. 1. Scheme of the experimental setup and numerical model setup at starting time.

a) b)

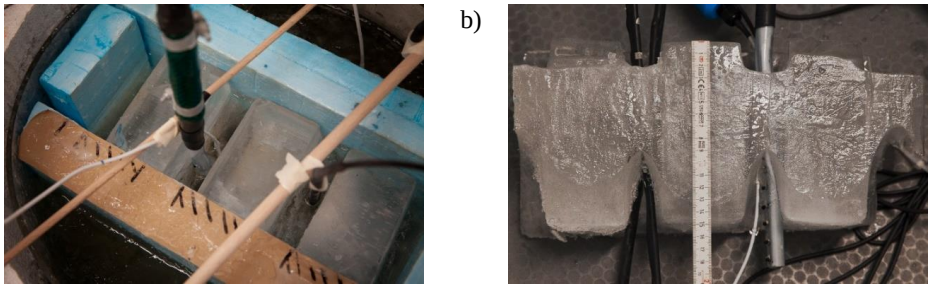

Fig. 2. a) Experimental setup and b) model ridge after consolidation.

Numerical model

The ridge consolidation process was modelled using finite element analysis simulation software COMSOL Multiphysics 5.2a. Two materials, fluid water, and solid ice, were used. Heat transfer in fluid and laminar flow packages were coupled for water simulation. The position of the ice-water boundary was defined by Stefan energy balance condition, where the difference of heat fluxes in two materials is equal to the amount of new solid formed or melted (Alexiades et al., 2003). This model requires following material parameters: thermal conductivity, heat capacity, density, the coefficient of thermal expansion, latent heat of fusion and kinematic viscosity. These values were obtained using the Gibbs SeaWater Oceanographic Toolbox of TEOS-10 (Feistel et al., 2010) and from Schwerdtfeger (1963). Thermal boundary conditions were defined as thermal insulation from sides of ice and bottom of the water, and as external convection with a constant heat transfer coefficient H_{ia} at the top. The value of $H_{ia} = 20\,W/m^2K$ was used based on level ice growth rate in the laboratory.

Results

Ice growth rate depends both on air ambient temperature T_a and heat transfer coefficient H_{ia}, so it is practical to present consolidation process as a function of level ice thickness h_i via degree of consolidation $R = h_c/h_i$. It is also practical to present experimental results normalized over different ridge porosities η_0 as $R\sqrt{\eta_0}$. This factor shows the difference between idealized consolidated layer thickness, which is $1/\sqrt{\eta_0}$ times larger than of surrounding level ice, and actual thickness of the consolidated layer from the experiments or from the model. Values of $1/\sqrt{\eta_0}$ for h_c/h_i can be only realized with following assumptions: infinite heat transfer coefficient H_{ia}, zero thermal inertia $c_p\Delta T$, and infinitely small block size. Consolidation factor $R\sqrt{\eta_0}$ with these assumptions is equal to 1 (Fig. **3**a).

Analytical solution, described in equation (2), is based on homogeneity assumption, and, according to the provided experiments, significantly overestimates consolidation when level ice thickness h_i is smaller than the distance between blocks $w_v = w\eta_0/(1-\eta_0)$ (Fig. **3**b).

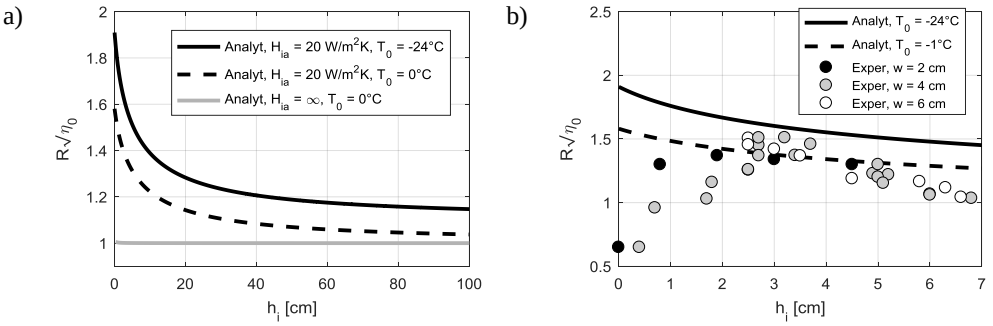

Fig. 3. Ratio of consolidated layer and level ice thickness $R = h_c/h_i$ multiplied by the square root of initial porosity $\sqrt{\eta_0}$ vs level ice thickness h_i a) for large scales and analytical solution and b) for small-scale experimental and analytical values.

For experiments with thinner ice blocks, consolidation layer thickness is faster approaching the analytical solution. Numerical modelling results can explain lower values of consolidation $R\sqrt{\eta_0}$ for later stages of experiments: solidification rate is slower when consolidation layer thickness is approaching to the values of block length L, solidification rate is higher for larger above water block height s or sail of the model ridge (Fig. **4**).

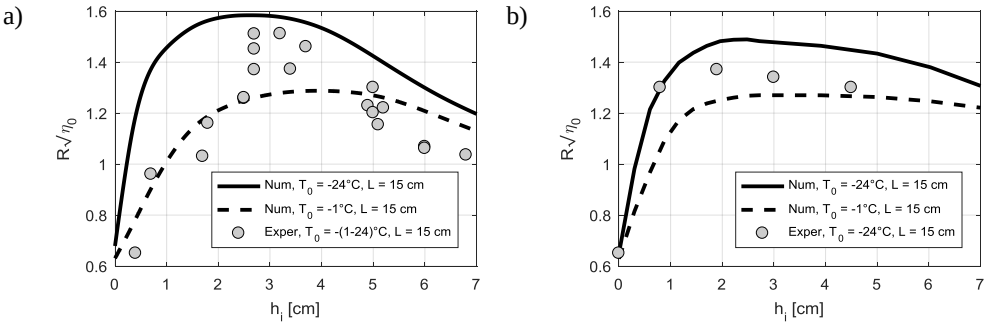

Fig. 4. Product of the degree of consolidation and square root of porosity $R\sqrt{\eta_0}$ vs level ice thickness h_i from numerical simulations and from experiments a) for 4 cm wide blocks and b) 2 cm wide blocks.

In the 1D analytical model, the block length L is infinitely large and there is no sail. There is no significant effect on experimental consolidation rate from block orientation and initial temperature. At the same time, both analytical and numerical models are predicting maximum experimental values of consolidation $R\sqrt{\eta_0}$ only with taking into account block initial temperature T_0. For all the provided experiments consolidated layer was up to 2.2–2.8 times thicker than surrounding level ice while the idealized solution for porosity value of 0.4 gives values of $R = 1.6$.

Discussion

According to numerical and experimental results not only initial ice thickness and temperature, but also block length and sail height, are affecting ridge consolidation rate. Consolidated layer thickness from simulations and experiments is approaching 1D analytical solution from equation (2) after surrounding level ice is reaching values close to ridge block thickness w. When the consolidated layer thickness is close to the ridge block length L, growth rate is becoming slower than according to the analytical solution. Presence of above water ice (ridge sail) is changing the initial ratio between convection and conduction and increasing consolidation rate.

The strong effect from initial ice temperature was not observed in experiments, but according to simulation results, extraction of sensible energy $c_p(T_f - T_0)$ during initial phase has a significant effect on consolidation process. The effect of initial rubble temperature on consolidation ratio $R\sqrt{\eta_0}$ is scale dependant. According to analytical solution for consolidated layer growth and initial porosity change from equation (4), simulation results are converging to 1D model if only some part of the initial sensible energy is going to be spent on new ice growth. These values are also scale dependant: 70 % and 60 % of sensible energy for 4 cm blocks and 15 cm.

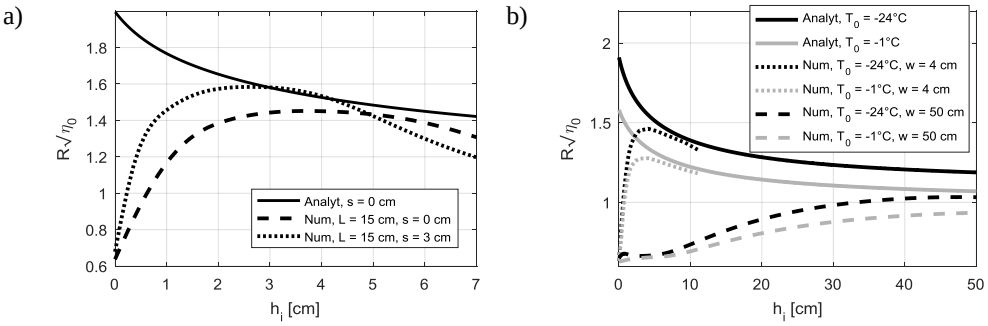

Fig. 5. Product of the degree of consolidation and square root of porosity $R\sqrt{\eta_0}$ vs level ice thickness h_i a) for $w = 4$ cm, $T_0 = -24℃$ and different sail height s and b) for 4 cm and 50 cm wide blocks from 1D analytical solution and from numerical simulations.

During the initial stage, consolidated layer with vertically oriented blocks is growing as fast as surrounding level ice (Petrich et al., 2007), while during the main phase its thickness is close to the scale-dependent 1D analytical solution from.

Conclusions

Analytical solution for one-dimensional fresh ice ridge consolidation is provided showing the significantly faster growth of consolidated layer in comparison to surrounding level ice for smaller scales. Experiments were conducted showing that this scale effect is significantly stronger for thinner ice blocks. Finite element model for ridge consolidation in different scale and configuration is described and confirmed by experimental data. For all the provided experiments consolidated layer was up to 2.2–2.8 times thicker than surrounding level ice. When the consolidated layer thickness is close to the ridge block length, the growth rate is becoming slower than according to the one-dimensional analytical solution. Presence of above water ice (ridge sail) is increasing consolidation rate. Study results can be used for basin-scale experiments and full-scale ridge investigations.

Acknowledgements

The authors wish to acknowledge the support of the Research Council of Norway through the Centre for Research-based Innovation, SAMCoT, and the support of the SAMCoT partners.

References

Adams, C. M., French D.N. and Kingery W. D., 1960. Solidification of sea ice. Journal of Glaciology, 3(28), 745-760.

Alexiades, V., Hannoun N., and Mai, T.Z., 2003. Tin Melting: Effect of Grid Size and Scheme on the Numerical Solution," Proc. 5th Mississippi State Conf. Differential Equations and Computational Simulations, pp. 55–69.

Ashton G.D., 1989. Thin Ice Growth. Journal of Water Resources Research. Vol. 25, No. 3, pp. 564–566.

Chen, X. and Høyland, K.V., 2016. Laboratory Work on Heat Transfer in Submerged Ice, Theory, Experimental Setup and Results. Proceedings the 23rd IAHR International Ice Symposium on Ice, Ann Arbor, USA.

Feistel, R., Wright D. G., Jackett D. R., Miyagawa K., Reissmann J. H., Wagner W., Overhoff U., Guder C., Feistel A. and Marion G. M., 2010. Numerical implementation and oceanographic application of the thermodynamic potentials of water, vapour, ice, seawater and air. Part 1: Background and equations. Ocean Science, 6, 633 – 677.

Griewank, P. J. and Notz, D., 2013. Insights into brine dynamics and sea ice desalination from a 1-D model study of gravity drainage. Journal of Geophysical Research: Oceans, 118(7):3370–3386.

Høyland, K.V., Liferov, P., 2005. On the initial phase of consolidation. Cold Regions Science and Technology. (41, 1), pp. 49-59.

Høyland, K.V., 2007. Morphology and small-scale strength of ridges in the North-western Barents Sea. Cold Reg. Sci. Technol. 48 (3), 169–187.

Leppäranta, M., 1993. A review of analytical models of sea- ice growth. Atmosphere-Ocean, 31, pp. 123-138.

Petrich, C., Langhorne P. J., and Sun Z. F., 2007. Formation and structure of refrozen cracks in land-fast first-year sea ice. Journal of Geophysical Research: Atmospheres, 112:C04006.

Salganik, E., Høyland, K. V. and Shestov A., 2017. Thermodynamics and Consolidation of Ice Ridges for Laboratory Scale. Proceedings – International Conference on Port and Ocean Engineering under Arctic Conditions.

Schwerdtfeger, P., 1963. The thermal properties of sea ice. J. Glaciol. 789–807.

A.3. Paper 3

Medium-scale consolidation of artificial ice ridge – Part I: surface temperature, thickness and mechanical properties.

Salganik, E., Høyland, K.V., Shestov, A., Løset, S., Heijkoop, A.-N.

Proceedings of the International Conference on Port and Ocean Engineering under Arctic Conditions (POAC), Delft, Netherlands, paper no. 82, 2019.

Proceedings of the 25th International Conference on
Port and Ocean Engineering under Arctic Conditions
June 9-13, 2019, Delft, The Netherlands

Medium-scale consolidation of artificial ice ridge – Part I: surface temperature, thickness and mechanical properties

Evgenii Salganik[1,2], Knut Vilhelm Høyland[1], Aleksey Shestov[2], Sveinung Løset[1], Anne-Niekolai Heijkoop[2,3]
[1] Sustainable Arctic Marine and Coastal Technology (SAMCoT), Centre for Research-based Innovations (CRI), Norwegian University of Science and Technology, Trondheim, Norway
[2] The University Centre in Svalbard, Longyearbyen, Norway
[3] Delft University of Technology, Delft, Netherlands

ABSTRACT

This paper is describing preparations and methods of medium-scale ridge consolidation experiment and development of ridge and surrounding level ice morphological, thermal, and mechanical characteristics for the experiment, performed in 2017 in Svalbard. It is also providing analysis and modelling of freezing rates and surface temperatures.

In February–May of 2017 for 66 days, experiment on ice ridge consolidation was performed in seawater Vallunden Lake connected with Van Mijen Fjord. 55 ice blocks were cut from level ice of 50 cm thickness and placed into the open water basin of 4.9 m by 3.0 m. Both level ice and artificial ridge were equipped with temperature sensors. During 3 visits, manual measurements of uniaxial strength in vertical and horizontal directions, salinity, gas volume, ice and snow thickness were performed for both level ice and ridge consolidated layer. 42 level ice and 25 ridge small-scale compression tests were completed in situ and in laboratory conditions.

The surface temperature of level ice was significantly warmer than of the ridge during most of the experiment, while the average snow thickness was higher for the ridge. During the experiment, 717°Cd were accumulated, and level ice grew from 50 cm up to 99 cm while the consolidated layer grew up to 120 cm. The analysis of the difference in consolidated layer thickness from temperature profiles in the ridge voids and blocks is given. The uniaxial compressive strength of the consolidated layer was between vertical and horizontal level ice strength for both in situ and laboratory tests.

KEY WORDS: Ice; Ridges; Solidification; Thermodynamics; Fieldwork.

NOMENCLATURE

c_b	Specific heat capacity of the brine [$Jkg^{-1}K^{-1}$]
c_i	Specific heat capacity of the ice [$Jkg^{-1}K^{-1}$]
h_i	Ice thickness [m]
h_s	Snow thickness [m]

h_{si} Sea ice thickness [m]

k_i Thermal conductivity of the ice [$Wm^{-1}K^{-1}$]

k_s Thermal conductivity of the snow [$Wm^{-1}K^{-1}$]

m_i Mass fraction of ice

q Heat flux [W/m^2]

H_{ia} Air convectional heat transfer coefficient [$Wm^{-2}K^{-1}$]

H_{si} Specific sea ice enthalpy [J/kg]

L_i Specific latent heat of pure ice [J/kg]

S_i Bulk salinity of ice [°C]

T_a Air ambient temperature [°C]

T_{as} Air-snow interface temperature [°C]

T_f Water freezing temperature [°C]

T_{si} Snow-ice interface temperature [°C]

η_t Ridge total porosity

ρ_i Pure ice density [kg/m^3]

ρ_{si} Sea ice density [kg/m^3]

INTRODUCTION

According to the definition of the WMO (1970), an ice ridge is a line or wall of broken ice forced up by pressure. Ridges usually consist of three parts: the sail, the consolidated layer, and the unconsolidated rubble. A significant part of loads on offshore structures and vessels is coming from the consolidated layer (Ervik et al., 2019). Høyland (2002) defined three phases of ridge consolidation: initial, main and decay. End of the initial phase is when the unconsolidated part is at the water freezing temperature. The thickness of level ice and the consolidated layer is the main value of interest for structural loads. It can be measured by mechanical drilling or from vertical temperature profile.

There are only several ridge consolidation models (Leppäranta et al., 1995), confirmed by observations with accurately measured conditions and initial parameters. Seasonal development of consolidated layer was described by Blanchet (1998), Høyland (2002), and Shestov et al. (2018).

Timco and Goodrich (1988), and Salganik and Høyland (2018) provided data about basin-scale experiments in ridge consolidation. Meanwhile, small-scale experiments cannot provide confidence in large-scale models due to the significant difference in the importance of separate mechanisms of heat transfer and significant simplifications in laboratories including the absence of snow. Ashton (1989) showed the difference between thin and thick fresh ice growth.

The consolidated layer is usually growing from the initial phase with zero minimum ice thickness until thicknesses larger than of surrounding ice. This means that ridge solidification includes a large range of scales and ratios of thermal resistances.

The consolidation process is usually characterized by the ratio of the consolidated layer and level ice thicknesses called a degree of consolidation. Natural ridging process can occur at

any time throughout the season. This makes the ratio of the number of cold days when level ice and consolidated layer are growing random. The common way to describe ridge consolidation via its degree of consolidation is practical for engineering purposes, but not so useful for solidification model validation due to sensitivity to the initial level ice thickness at the moment of ridging.

Medium-scale solidification experiments are providing the unique advantage of accurately measured parameters such as initial macro-porosity, initial block temperature and salinity, and freezing time. It minimizes error in key parameters for the solidification process, which includes air natural and forced convection, conduction through snow and ice, and phase change. Saline ice is a composite material, so any temperature or salinity change leads to the change of sea ice solid fraction. In natural conditions, solidification includes also warming, described by Shestov et al. (2018). In this paper, we are trying to define and validate a simple analytical solidification model suitable for transient air temperature, wind speed, and snow thickness. The aim of the field experiment was to compare thermodynamics and development of physical and mechanical parameters of level ice and consolidated layer.

Level ice growth in steady-state conditions depends on how the temperature difference between air and water is distributed between insulating layers of air, snow, and ice. For slow changes of boundary conditions, the temperature gradient at the bottom of ice depends on the ice top surface temperature and its thickness. Three thermal resistances define temperature profile and the total system thermal resistance is showing how much heat can be transported in time from the water to the air:

$$q = \frac{T_a - T_{as}}{R_a} = \frac{T_{as} - T_{si}}{R_s} = \frac{T_{si} - T_f}{R_i} = \frac{T_a - T_f}{R_a + R_s + R_i}; \quad (1)$$

$$R_a = 1/H_{ia}\,; \quad (2)$$

$$R_s = h_s/k_s\,; \quad (3)$$

$$R_i = h_i/k_i\,; \quad (4)$$

In transient conditions, temperature distribution will be following described ratios with a time lag defined by the thermal inertia of snow and ice. Thermal inertia for saline ice can be divided into specific heat of pure ice and brine, and change of solid fraction at different temperatures, which requires freezing or melting of pure ice inside sea ice. The sum of both effects can be presented via the enthalpy of sea ice:

$$H_{si} = -L_i m_i - m_i \int c_i dT - (1 - m_i) \int c_b dT \quad (5)$$

Enthalpy values at different temperatures illustrate the difference from simplified ice growth known as Stefan equation of ice growth: depending on ice temperature and salinity only a certain mass fraction should be frozen, while additional negative heat should be spent to adjust ice temperature to a certain temperature profile. Zero value of enthalpy can be chosen arbitrarily and assumed zero at sea ice freezing point.

The enthalpy value for ice with any temperature and salinity distribution is defining how much energy should be extracted from the water for its solidification and cooling (Figure 1). As can be seen, enthalpy difference can be higher or lower than pure ice latent heat. Pure ice and brine sensible heat are decreasing sea ice growth at low temperatures in comparison to the Stefan equation. In contrast, the low solid fraction of warm sea ice can lead to faster growth in comparison to Stefan equation and pure ice growth. For salinity of 5 ppt warm ice at water freezing temperature requires 15 % less negative energy to be formed.

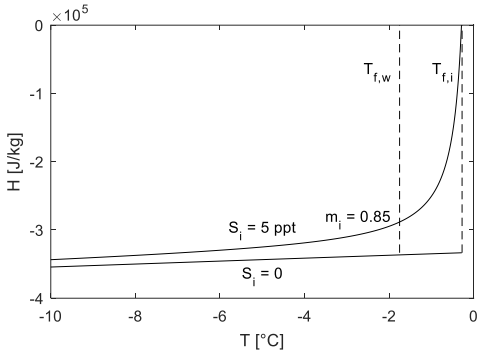

Figure 1. Saline and fresh ice enthalpy vs temperature.

The difference between the top and bottom heat fluxes in ice is spent on ice heating or cooling. When ice is thick enough, the bottom heat flux depends only on average top surface temperature.

Assuming no oceanic flux from the water, the pure ice growth can be estimated as:

$$\rho_i L_i \, dh_i/dt = -k_i \, \partial T/\partial z \tag{6}$$

Assuming no thermal inertia, the pure ice growth can be estimated from meteorological data including air temperature, wind speed, and snow thickness:

$$\rho_i L_i \frac{dh_i}{dt} = -k_i \frac{T_{si} - T_f}{h_i} = \frac{T_a - T_f}{R_a + R_s + R_i} \tag{7}$$

For the field data analysis, usage of the bottom ice boundary for heat flux calculation can be impractical due to high uncertainties in salinity and temperature profiles, while only the change of total ice volume is the main value of interest. According to Griewank and Notz (2013), different salinity profiles can change the ice growth prediction by less than 4 %. The thickness of saline ice including sensible heat can be estimated from pure ice thickness without sensible heat from the solid volume fraction as:

$$h_{si} = h_i \frac{\rho_i L_i}{\rho_{si} \Delta H_{si}} \tag{8}$$

This simple analytical model, which ignores time delay in thermal diffusion, can give errors when the air temperature is quickly moving towards seawater freezing point. This error can be eliminated only by solving diffusion equations for snow and saline ice layers assuming external convection from the air. The difference between analytical and numerical predictions will be presented in the results of this study.

Ridge consolidation has many similarities with level ice growth. Meanwhile, there are following critical differences: ridge is a porous media consisting out of 60–80 % of ice staying at the seawater freezing temperature under the bottom of the consolidated layer. Leppäranta and Hakala (1989) suggested considering this difference by assuming the value of ridge effective latent heat as:

$$L_r = \eta_t L_i \tag{9}$$

The vertical temperature gradient can be assumed homogeneous for ridges with small voids, but in natural scale, voids between ice blocks are in the range of consolidated layer thickness. Due to this inhomogeneity, horizontal heat fluxes are occurring inside ice ridges (Leppäranta et al., 1995), and ice-water interface has ellipse shape where new ice is forming (Petrich et al., 2007).

Another difference is the presence of large above water ice called sail in ice ridges, which is the locally changing ratio of thermal resistances and the total area via which heat is extracted to the air. The sail presence is caused by the trapezoidal shape of ridge keel and large underwater volume in comparison to level ice.

Ridge sail is also changing the distribution of snow, creating accumulations and snow-free surfaces. It is making top surface conduction to be a purely 3D problem in contrast to level ice. These factors are changing thermal resistance of ridge sail and its top surface temperature, making the analysis of field data much more complicated due to the difference in temperatures of different parts of the consolidated layer. Leppäranta et al. (1995) observed that the top of the ridge could be significantly colder while the sail temperature at the water level can be warmer than in sail free consolidated layer. Meanwhile, the 1D analytical model can be used for both void and block parts of the ridge, assuming the sum of these heat fluxes is spent for the new ice formation.

METHODS

The field experiment in the artificial ridge consolidation was performed during 66 days from 25 February 2017 until 4 May 2017 in Lake Vallunden in the Van Mijenfjorden in Svalbard. Lake Vallunden is a seawater lake connected with the seawater fjord by a small 100 m long channel (Marchenko and Morozov, 2013). The ridge was made of 55 blocks from 50 cm thick ice, totally 11.4 m^3 of ice. The average initial level ice salinity was 3.8 ppt (Figure 4a) and the average initial block temperature was -7.8°C. A basin 3.0 m by 4.9 m was made in the level ice cover, and the blocks were damped into this basin. The ice blocks were cut in the feeding channel using trencher (Figure 2a). After that, the blocks were placed into the water basin using rope, ramp, and snowmobile (Figure 2b).

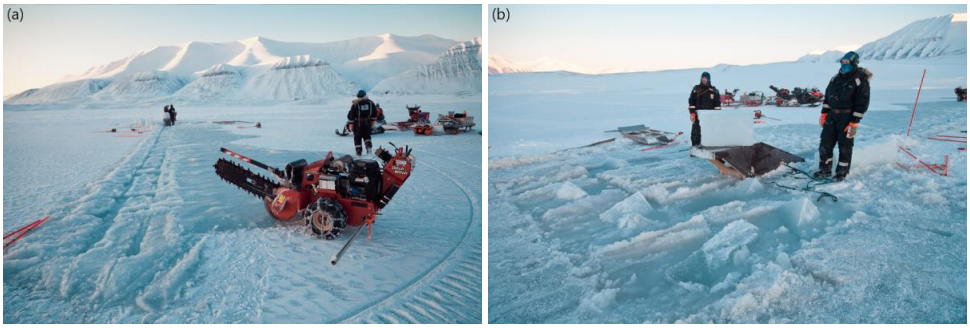

Figure 2. Feeding channel (a) and ridge formation using the ramp (b).

The following information was collected during 4 visits: temperature, salinity, density profiles, and uniaxial compressive strength. During the 1st visit 3 vertical cores were collected to investigate ridge morphology, and 12 vertical cores were collected at the 4th visit.

Both level ice and ridge were instrumented with thermistor strings. The ridge thermistor string was placed in the borehole 1 during the visit 1, the level ice thermistor was placed close to the ridge (Figure 3b). The top surface temperature of the ridge with 15 cm freeboard, the top surface temperature of level ice with 7 cm freeboard and air ambient temperature are shown at Figure 3a. Ice thickness was measured by drilling during 4 visits and was also estimated from vertical temperature profiles from thermistors (Figure 6a).

Sea ice thermodynamic parameters including heat capacity, thermal conductivity, latent heat and solid fraction were calculated from Notz (2005). Air convectional heat transfer coefficient as a function of the wind speed was estimated from Adams (1960), with the

average value for the time of experiment of 21 $Wm^{-2}K^{-1}$. Air ambient temperature and wind speed values were received from the Sveagruva meteorological station.

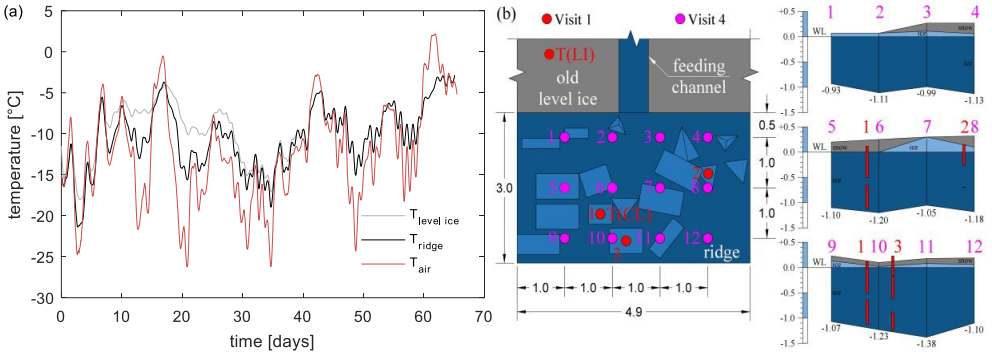

Figure 3. Air, level ice and ridge top surface temperatures (a) and ridge profiles (b)

Three cores were used to measure initial parameters of level ice from each the ridge was formed (Figure 4a). One core of the level ice and of the ridge were used for salinity and density profiles at the visit 4 (Figure 4b). The vertical resolution of salinity and density profiles was 5 cm.

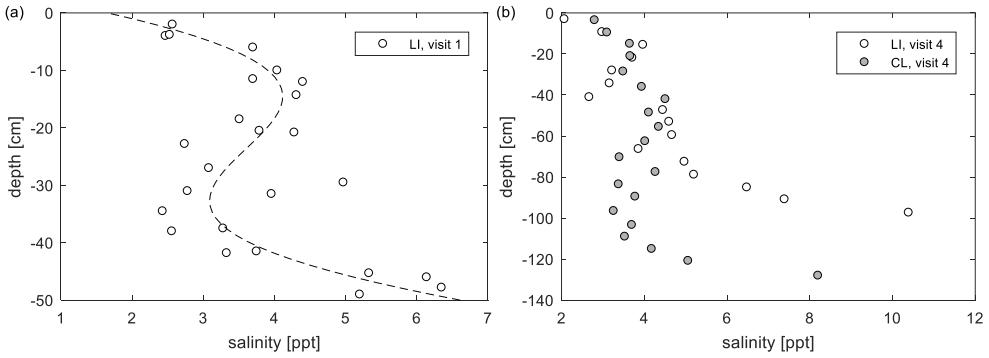

Figure 4. Salinity profiles for visit 1 (a) and for visit 4 (b).

12 vertical and horizontal level ice samples for uniaxial compression were collected during visit 2. 4 vertical level ice and 17 vertical ridge samples were also collected during visit 4. Tests with these samples were performed in the lab at a temperature near -10°C. 38 in-situ compression tests were performed during visit 3, including 32 for level ice and 6 for the ridge.

The numerical simulations of level ice and ridge consolidation were performed with finite element analysis simulation software COMSOL Multiphysics 5.3a using the front tracking method. The position of the ice-water boundary was defined by Stefan energy balance condition, where the difference of heat fluxes in two materials is equal to the amount of new solid formed or melted.

RESULTS

Brine volume (Figure 5a) was estimated for ice initial temperature and freezing temperature of the surrounding water in the formed ridge (Cox and Weeks, 1983). Ridge initial macro-porosity of 0.36 was estimated from the total volume of ice blocks, and from sail and keel elevations obtained from drilling (Figure 3b).

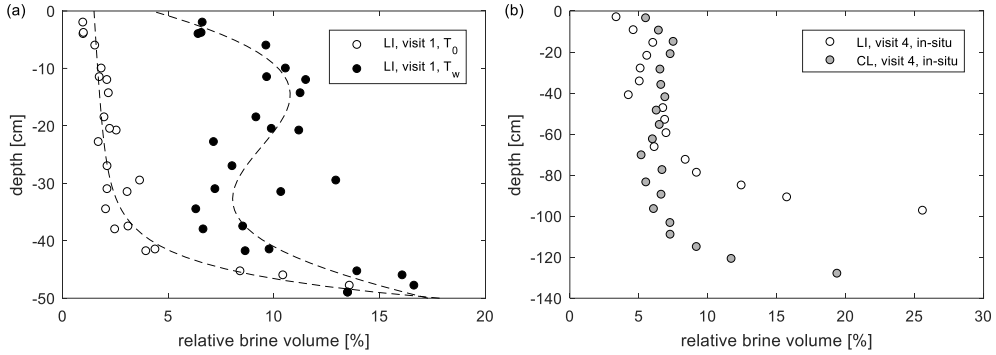

Figure 5. Relative brine volume profile for in-situ and water temperatures for visit 1 (a) and for visit 4 (b).

The average air temperature during consolidation experiment was -12.6°C from both meteorological station and upper sensor of the thermistor string. Average freeboard at visit 4 was 7 cm for level ice and 8 cm for the ridge. During the time of the experiment level ice grew from 50 cm to 99 cm, while the consolidated layer grew up to 120±12 cm (Figure 6a). The level ice salinity after 66 days changed from 3.8 ppt to 4.6 ppt, consolidated layer final salinity was 4.1 ppt (Figure 5b).

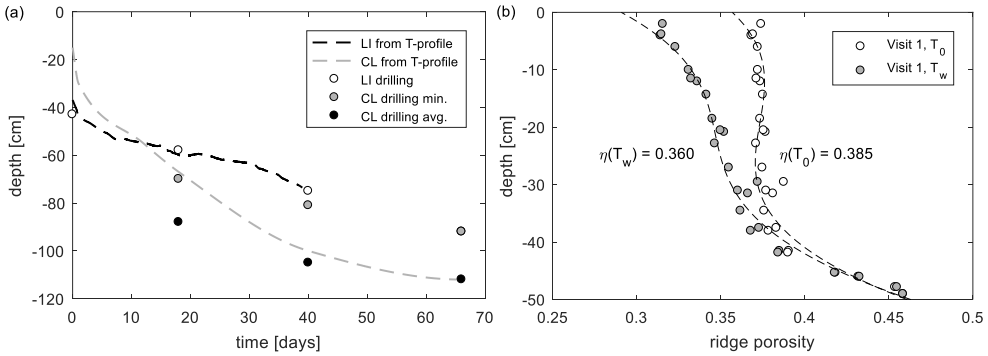

Figure 6. Ice thickness development (a) and ridge porosity profile before and after the initial phase of consolidation (b).

Due to block average initial temperature of -7.8°C, the ridge total porosity including brine and gas volumes should decrease from 0.39 to 0.36 under the assumption of salt conservation (Figure 6b).

The snow thermal conductivity value of 0.21 Wm^{-2} was calculated from the level ice temperature profile to fit thermal resistance values for measured snow thickness (Figure 7a). Snow resistance values can be used for estimation of snow thermal conductivity for four visits when the snow thickness was measured. For the whole time of the experiment, the snow resistance data can show the exact time of snow thickness change. The snow thermal resistance above the ridge with 15 cm sail was 2.2 times lower than snow thermal resistance above level ice for measured snow thicknesses and the same snow thermal conductivity of 0.21 W/m^2 (Figure 7b).

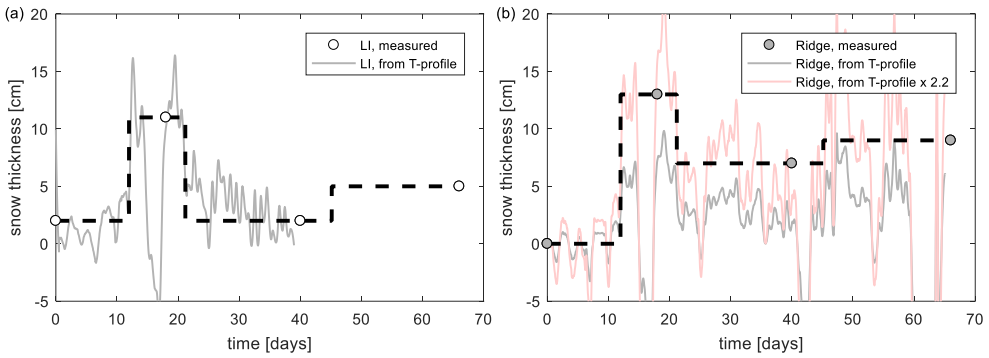

Figure 7. Snow thickness above level ice (a) and consolidated layer (b) vs time.

The analytical model allows accurately predicting level ice growth (Figure 8a). Top surface freezing is not included in the model. Based on salinity profiles at visit 1 and 4 (Figure 5a and b), around 4 cm was formed above the initial top surface.

Level ice thickness from direct measurements at visit 4 was 99 cm, while our analytical model predicted the thickness of 95 cm (Figure 8a). The numerical model result was 2 % larger than of analytical. The observed consolidated layer thickness was 120 cm, and 116 cm from the analytical model (Figure 8b). The numerical model result was 122 cm.

At the visit 4 salinity, density and temperature of level ice and consolidated layer were measured, giving 8 % of liquid volume fraction (Figure 5b) and 2 % of gas volume fraction. The analytical model final liquid volume fraction was 9 % for both level ice and consolidated layer.

Table 1. Evolution of the main level ice and consolidated layer properties

Property	Visit number			
	1	2	3	4
Number of LI/CL cores	3/0	0/2	0/4	1/12
Consolidated layer min. [m]	0.00	0.78	0.97	1.00
Consolidated layer avg. [m]	-	0.96	1.13	1.20
Level ice thickness [m]	0.50	0.65	0.82	0.99
Ridge snow thickness [m]	0.00	0.13	0.07	0.09
Level ice snow thickness [m]	0.02	0.11	0.02	0.05
Consolidated layer salinity [ppt]	3.8	4.2	3.8	4.1
Level ice salinity [ppt]	3.8	-	-	4.6
FDD [°d]	705	915	1228	1421

The analytical model also predicts the final consolidated layer thickness quite precise. Higher thickness values from drilling during visit 2 can be explained by the lack of a number of performed cores. Higher consolidation values from temperature profile are coming from the method overestimation when the temperature information is derived from the ridge block, not from the void. This effect is eliminated at the time of visit 4 because the consolidated layer reached the block bottom in the vertical profile of the thermistor (Figure 8b).

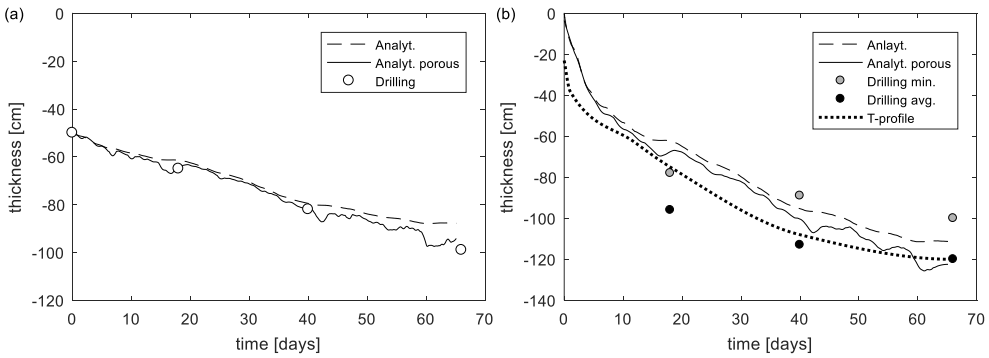

Figure 8. Level ice (a) and consolidated layer (b) thickness vs time.

The top surface temperature of ice ridges strongly depends on its elevation. Comparison of experimental heat fluxes through the sail of 15 cm height, through the consolidated layer and through level ice is presented in Figure 9a. The average heat flux in the sail was 1.8 times larger than in the consolidated layer. The analytical model is overestimating average heat flux in the consolidated layer only by 1.6 % (Figure 9b).

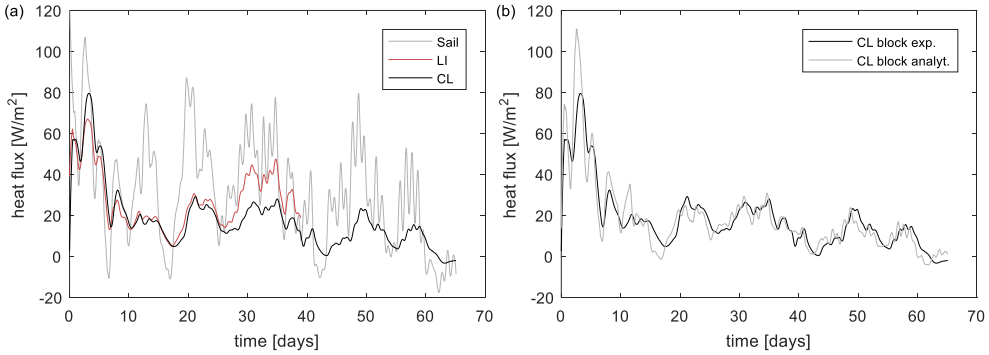

Figure 9. Vertical heat fluxes in ridge sail, consolidated layer and level ice (a) and comparison of heat fluxes in ridge block from experiment and from the analytical model (b).

Results of in-situ and laboratory uniaxial compression experiments, performed during visits 2, 3 and 4, are presented in Figure 10.

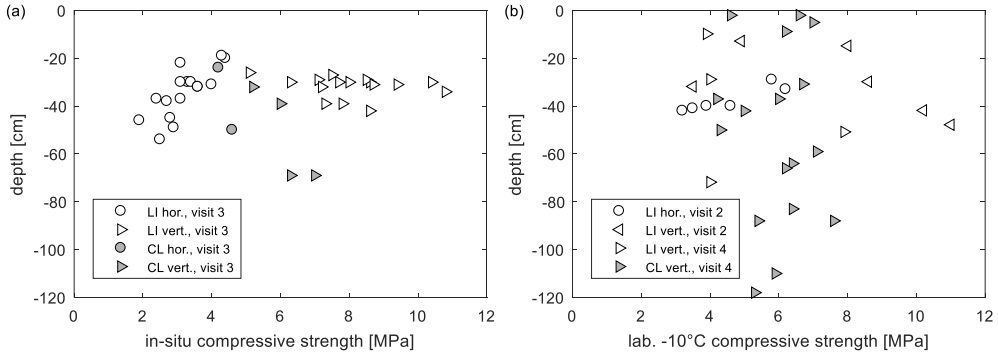

Figure 10. Uniaxial compressive strength for in-situ (a) and -10°C (b) temperatures vs depth.

In-situ during visit 3 average compression strength of horizontal level ice samples was 3.2 MPa, and 8.1 MPa for vertical level ice samples. Horizontal samples from consolidated

layer had the strength of 4.4 MPa, and 6.1 MPa for vertical samples from the consolidated layer.

In laboratory conditions at the temperature of around -10°C, the average strength of horizontal level ice samples was 4.5 MPa at visit 2, vertical strength was 7.7 MPa at visit 2 and 5.0 MPa at visit 4. Vertical consolidated layer strength was 5.9 MPa.

The strength of level ice for visit 2 was measured in different directions for horizontal samples: for EW direction it was 6.0 MPa, for NS it was 3.4 MPa, for 45° to NS it was 4.2 MPa.

The samples from the ridge had a much higher percentage of failures in a ductile way in contrast to level ice.

DISCUSSION

The increasing trend of level ice salinity can be explained by the presence of approximately 12 cm thick part of snow ice at the beginning of the experiment. The final level ice salinity profile shows that around 4 cm of ice was formed on the top during the experiment (Figure 4b). The decreasing portion of less saline snow ice is explaining the increase of level ice salinity with time.

Slightly lower ridge salinity in comparison to level ice can be explained by stronger ice desalinization after warming during initial phase according to the brine dynamics model by Griewank and Notz (2013). At the same time, according to Kovacs (1997), ice salinity depends on the ice growth rate. Vertical heat fluxes were almost equal in the consolidated layer and in level ice during the first 25 days (Figure 9a), when upper 70 cm of the consolidated layer was formed. Ridge multi-directional desalinization process requires further investigations.

Strength relations of consolidated layer and level ice in the presented experiment are in a good agreement with the results from Shafrova and Høyland (2008).

Høyland (2002) described large errors of consolidated layer thickness measurements performed by drilling and by temperature profile analysis. Obviously, at the same vertical core, thickness from temperature profile cannot be higher than from drilling. Meanwhile, temperature profiles from the ridge voids and ridge blocks are different due to the presence of strong horizontal fluxes in ridges. It is important to mention that any ridge solidification model describes new ice formation in the ridge voids. It means that the result of such a model should correspond to the minimum consolidated layer thickness, which can be obtained from drilling or from temperature profile in the ridge void. It was found from numerical modelling that thickness of consolidated layer obtained from ridge temperature profile can differ from the thickness of newly formed ice, and this difference is scale dependent.

At the level of minimum consolidated layer thickness, the temperature in the surrounding ice blocks can be significantly colder depending on their distance from the block center. Thermistor string for the described experiment was placed in the ice block. From the Figure 8b it can be seen, that thickness values from the temperature profile are always approximately 15 cm larger than of analytical solution, while vertical heat fluxes in fully consolidated part are almost equal for both the experiment and the model.

An example of the modelled temperature profile from the ridge block and void is shown in Figure 11. For that specific example from numerical simulation air ambient temperature is -15°C, sail height is 15 cm, and there is no snow. Under the assumption of a linear temperature profile, the estimated thickness in the block is 14 cm larger than in the ridge void, similar to the experimental observations.

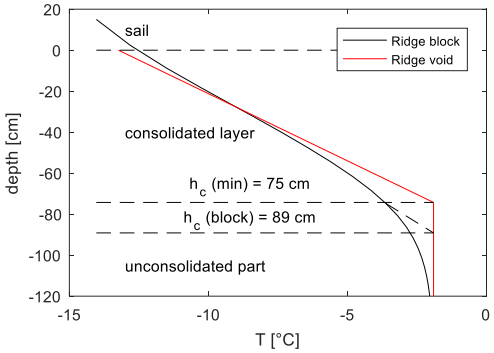

Figure 11. Ridge temperature profiles for block and void from the numerical simulation.

The heat fluxes in level ice and the consolidated layer below water level were almost equal during the first 25 days of the experiment when the snow thickness above both types of ice was in the same range (Figure 9a). Level ice thickness and corresponding thermal resistance were higher only during the first 12 days (Figure 6a). It shows the importance of coupling of air convection and conduction through snow and ice. At the same time, heat flux through the sail was 1.8 times higher than through the underwater consolidated layer. This difference corresponds to the difference in snow thermal resistance for the ridge and level ice of 2.2. The possible explanation for this difference in vertical fluxes is the existence of significant horizontal fluxes in the sail through its lateral surfaces. For the sail height of 15 cm and the block side length of 50 cm, the ratio of the area and the sail vertical projection is also equal to 2.2.

The question for future investigations is how the top flux difference from 1D and 3D models can affect the rate of ridge solidification and how it can be affected by the presence of snow.

CONCLUSIONS

This paper provides details of artificial ridge preparation and temporal investigations of its morphological, thermal and mechanical parameters. It was shown that the artificial ridge is providing sufficient information for accurate growth prediction and validation of ridge solidification models. It was confirmed that the top ridge surface temperature could be predicted only considering sail morphology.

One-dimensional analytical model using thermal resistance concept was described and applied for both level ice and ridge consolidation. A detailed description of the model application for usage with meteorological data and basic parameters from several visits of the experimental site was provided. It was shown that the ice growth for both saline level ice and the consolidated layer of saline ice ridges has significant differences from the fresh ice growth, and that accurate thickness prediction is only possible considering sea ice micro-porosity. The described analytical model can predict heat fluxes inside the consolidated layer quite accurately allowing a fast analysis of experimental data or predictions.

It was observed in the experiment, that the temperature profile could give overestimated values of consolidated layer thickness depending on the profile location. Potential reasons were described and confirmed with both experiment and numerical simulations.

REFERENCES

Adams, C. M., French D.N. and Kingery W. D., 1960. Solidification of sea ice. *Journal of Glaciology*, 3(28), 745-760.

Ashton G.D., 1989. Thin Ice Growth. *Journal of Water Resources Research*. Vol. 25, No. 3, pp. 564–566.

Blanchet, D., 1998. Ice loads from first-year ice ridges and rubble fields. *Canadian Journal of Civil Engineering*. 25 (2), pp. 206–219.

Cox, G.F.N. & Weeks, W.F., 1983. Equations for determining the gas and brine volumes in sea-ice samples. *Journal of Glaciology*, pp. 306–316.

Ervik, Å., Nord T.N., Høyland, K. V. Samardzija I., Li, H., 2019. Ice-ridge interactions with the Norströmsgrund lighthouse: Global forces and interaction modes. *Cold Region Science and Technology*, 158, pp. 195-220.

Griewank, P. J. & Notz, D., 2013. Insights into brine dynamics and sea ice desalination from a 1-D model study of gravity drainage. *Journal of Geophysical Research: Oceans*, 118(7), pp. 3370–3386.

Høyland, K.V., 2002. Consolidation of first-year sea ice ridges. *Journal of Geophysical Research*, 107 (C6), 15_1-15_7.

Kovacs, A., 1997. *Sea ice. Part 1: Bulk salinity versus ice floe thickness*. CRREL Rep. 96-7.

Leppäranta, M. & R. Hakala, 1992. The structure and strength of first-year ridges in the Baltic Sea. *Cold Region Science and Technology*, 92, pp. 295– 311.

Leppäranta, M., Lensu, M., Kosloff, P., Veitch, B., 1995. The life story of a first-year sea ice ridge. *Cold Region Science and Technology*, 23 (3), pp. 279–290.

Marchenko, A. & Morozov, E., 2013. Asymmetric tide in Lake Vallunden (Spitsbergen). *Nonlinear Processes in Geophysics*, 20, pp. 935-944.

Notz, D., 2005. *Thermodynamic and Fluid-Dynamical Processes in Sea Ice*. Ph.D. thesis, Univ. of Cambridge, Cambridge, U. K.

Petrich, C., Langhorne P. J., & Sun Z. F., 2007. Formation and structure of refrozen cracks in land-fast first-year sea ice. *Journal of Geophysical Research: Atmospheres*, 112:C04006.

Salganik, E. & Høyland, K. V., 2018. Thermodynamics and Consolidation of Fresh Ice Ridges for Different Scale and Configuration. *Proceedings of the 24th IAHR International Symposium on Ice*, Vladivostok, Russia, pp. 304-311.

Schwerdtfeger, P., 1963. The thermal properties of sea ice. *Journal of Glaciology*. 789–807.

Shafrova, S. & Høyland, K.V., 2008. Morphology and 2D spatial strength distribution in two Arctic first-year sea ice ridges. *Cold Region Science and Technology*, 51 (1), pp. 38–55.

Shestov, A. & Høyland, K. V. and Ervik, Å., 2018. Decay phase thermodynamics of ice ridges in the Arctic Ocean. *Cold Region Science and Technology*, 152, pp. 23-34.

Stefan, J., 1891. Uber die Theorie der Eisbildung, insbesondere uber die Eisbildung im Polarmeere, *Annalen der Physik und Chemie*, 42, pp. 269-286.

Timco, G. W. & L. E. Goodrich, 1988. Ice rubble consolidation. *9th International Symposium on Ice, International Association of Hydraulic Engineering*, Sapporo, Japan.

World Meteorological Organization, 1970. *WMO sea ice nomenclature* (supplement No 5.1989). Technical Report MO No. 259.TP.145. World Meteorological Organization, Geneva, Switzerland.

A.4. Paper 4

Consolidation of fresh ice ridges for different scales.

Salganik, E., Høyland, K.V., Maus, S.

Cold Regions Science and Technology. vol. 171., 2020.

https://doi.org/10.1016/j.coldregions.2019.102959

Cold Regions Science and Technology 171 (2020) 102959

Contents lists available at ScienceDirect

Cold Regions Science and Technology

journal homepage: www.elsevier.com/locate/coldregions

Consolidation of fresh ice ridges for different scales

Evgenii Salganik[a,*], Knut Vilhelm Høyland[a], Sönke Maus[b]

[a] Sustainable Arctic Marine and Coastal Technology (SAMCoT), Centre for Research-based Innovations (CRI), Norwegian University of Science and Technology, Institutt for bygg- og miljøteknikk NTNU, 7491 Trondheim, Norway
[b] Department of Civil and Environmental Engineering, Norwegian University of Science and Technology, Institutt for bygg- og miljøteknikk NTNU, 7491 Trondheim, Norway

ARTICLE INFO

Keywords:
Ice ridges
Thermodynamics
Consolidation
Laboratory
Scaling

ABSTRACT

This study characterizes the refreezing process of deformed ice. Twenty laboratory experiments in ice ridge consolidation were conducted to study the influence of ridge blocks size, initial temperature, and top surface roughness on the consolidation rate. Experiments covered a ridge block thickness range of 2–6 cm, initial block temperatures from −1 °C to −23 °C, ridge sail height up to 3 cm, and consolidated layer thickness up to 14 cm. Experiments were conducted with the average value of the convectional heat transfer coefficient of 20 W/m^{2}K. The presented analytical model for ridge solidification was able to predict the observed ice growth rates and differences between level ice and consolidated layer thicknesses at different stages of the experiments. For the provided experiments, the consolidated layer was as much as 2.2–2.8 times thicker than the surrounding ice level. The consolidation rate was lower than in the analytical solution at the start of the experiment and approached the analytical solution only when the thickness of the surrounding level ice was larger than the ridge void width. The developed numerical model confirmed the observed experimental effects from the block size, initial temperature and surface roughness. Both numerical and analytical models can predict solidification rates for previous studies at the large range of scales for both fresh and saline ice. The advantages of the simplified experimental ridge geometry include high accuracy of the main parameters governing the process, including the ridge macroporosity.

1. Introduction

1.1. Motivation

Ice covers in rivers, lakes, seas and oceans deform due to action from wind and currents, resulting in ice ridges or ice accumulations. The process may not be the same in all these cases, but as long the result is a floating accumulation of broken ice it will consolidate with time depending on the physical size of the pieces. According to the definition of the WMO (1970), an ice ridge is a line or wall of broken ice that is forced up by pressure. Ridges usually consist of a sail and a keel above and below the water level, respectively. The keel initially consists of randomly packed ice blocks separated by water-filled voids described by the ridge macroporosity. Due to cooling from the atmosphere, the keels consolidate by freezing of these voids, largely proceeding vertically downwards and forming the consolidated layer (Leppäranta et al., 1995). This layer may be thicker than the surrounding level ice and constitutes a threat to the marine, coastal or hydraulic infrastructure, such as bridges, pipelines, lighthouses, range markers, fixed and floating facilities for production of oil and gas or offshore wind, harbours and ships. Ice ridges are also key features in climate studies as they constitute a large fraction of the ice volume, and because they melt more slowly than level ice. The consolidation process occurs over different timescales; ice accumulation in rivers may persist for hours or days, ridges in lakes and seas with seasonal ice cover persist a few months and the ridges in the Arctic basin and other areas with summer ice can persist a few years. Leppäranta et al. (1995), Blanchet (1998), Høyland (2002), Strub-Klein and Høyland (2011) described the seasonal development of the consolidated layer.

Høyland and Liferov (2005) distinguished among three phases of consolidation: the initial phase, the main phase and the decay phase. During the initial phase, the broken pieces of ice are submerged in the water. As they usually have lower temperatures than water at the freezing point, the temperature in the ice increases in the initial phase. The heat comes from latent heat release in the water voids and thus implies that the ice pieces grow in all directions, decreasing the macroporosity of the layer of ice pieces. Such a change is due to faster 3D diffusion than the 1D consolidation processes, justifying the separate

* Corresponding author at: Department of Civil and Environmental Engineering, Norwegian University of Science and Technology, Høgskoleringen 7a, Trondheim 7491, Norway.
E-mail addresses: evgenii.salganik@ntnu.no (E. Salganik), knut.hoyland@ntnu.no (K.V. Høyland), sonke.maus@ntnu.no (S. Maus).

https://doi.org/10.1016/j.coldregions.2019.102959
Received 23 August 2019; Received in revised form 6 November 2019; Accepted 2 December 2019
Available online 04 December 2019

treatment of this phase. During the main phase, consolidation of this layer takes place largely one-dimensionally from top to bottom, before it starts to melt in the decay phase. Ice ridges that do not survive a summer melt are called first-year ice ridges, and the available field data on ridge morphology have been summarized by Strub-Klein and Sudom (2012).

Physical parameters of broken ice features can be studied in the field, but these investigations are time-consuming and are usually unable to provide data about the ridge formation process, initial conditions before consolidation, and potential full-scale loads on offshore structures and vessels. Thus, many of the parameters governing consolidation process are unknown or quite uncertain: initial macroporosity (liquid water content), initial size, orientation, salinity and temperature of broken ice blocks forming the ridge, and thickness of the snow above the ridge.

Predicting the thickness of the consolidated layer for these different timescales is important, and in an engineering context, scale-model testing is often conducted for this purpose. In such tests, the physical size of the problem is significantly reduced with a geometric scale factor, and the other relevant factors and processes must be scaled in such a way that the correct full-scale ice forces can be predicted (Langhaar, 1951; Palmer and Dempsey, 2009). Thus, the consolidation process should be understood not only for different timescales but also for different sizes, leading to several unsolved challenges (Høyland, 2007, Repetto-Llamazares, 2010; Høyland, 2010). Previous consolidation models did not include scale effects (Leppäranta, 1993), while in laboratory experiments (Timco and Goodrich, 1988; Blanchet, 1998) and field experiments (Leppäranta et al., 1995; Høyland, 2002), such effects were observed. However, laboratory-scale models of ice ridges also involve scaling of ice mechanical properties using dopants, which complicates the solidification process because the temperature-dependent liquid fraction and microstructure of the model ice differ from the field.

There are important differences between fresh ice and saline ice thermodynamics. However, with respect to ice growth rates, the differences are small. The numerical model of Maykut and Untersteiner (1969) provided a 7% higher equilibrium ice thickness for fresh ice. Notz (2005) presented experimental results for saline ice growth, showing that the growth rate of saline ice cooled from above is close to that of fresh ice (in contrast to saline ice cooled in a non-natural way from below due to the absence of the ice desalinization process). Petrich et al. (2007) presented both analytical and experimental analyses of the ice-opening refreezing process, showing that his model describes this process for both seawater and freshwater assuming different values of latent heat and ice thermal conductivity for both types of ice. Griewank and Notz (2013) showed that different salinity profiles could change ice thickness predictions by less than 4%. For ridges, Timco and Goodrich (1988) found no difference between level ice and ridge consolidation for fresh water and EG/AD/S water solution, and for the full scale, the ratios of the consolidated layer and surrounding level ice in almost fresh Baltic ridges compared well with those observed in saline ridges (Høyland, 2002). The physical basis for the similar growth rates for fresh and saline ice is that its growth rate is proportional to the value of the square route of thermal conductivity divided by the density and latent heat (Stefan, 1891; Leppäranta and Hakala, 1992; Petrich et al., 2007). The difference in this value between sea ice and fresh ice at the water freezing temperature is less than 4% (Schwerdtfeger, 1963; Yen, 1981; Notz, 2005).

Our research goal is to study ice ridge consolidation on laboratory scales to improve understanding of ridge thermodynamics in general. To exclude complications due to microstructure and solute rejection, we study freshwater ice and focus on ridge consolidation and macroporosity. Small-scale experiments are performed and the results compared to those from a one-dimensional analytical model and a two-dimensional numerical model. The results are interpreted in terms of their upscaling potential to larger scales.

1.2. Previous studies

The growth rate of the consolidated layer in time t is a function of the meteorological conditions (air and water freezing temperatures T_a and T_w, wind speed, long and shortwave radiation and snow thickness), the actual ice thickness and the ridge macroporosity. The oceanic flux becomes important in the decay phase but has little effect in the main phase. An easy way to allow for comparison between different temporal and physical scales is to perform a comparison with the surrounding level ice thickness. Leppäranta and Hakala (1992) assumed that level ice has the same surface flux and that the only difference is the ridge macroporosity η, and they defined a non-dimensional factor R by dividing the thickness of the consolidated layer h_c with the surrounding level ice thickness h_i:

$$R = h_c/h_i = \eta^{-0.5} \quad (1)$$

Most ridge growth models, including the international standard (ISO 19906, 2010), use this approach. The level ice surrounding a ridge can be of different origins. It may be (a) level ice from which the ridge has formed and that has continued to grow since that time, or it may be (b) level ice that started forming in a lead created by ridge formation (Fig. 1). The former will be thicker than the latter, and the ratio R and its history will differ for the cases. In case (a), R will start at a value lower than equilibrium, while in case (b), it will approach equilibrium from above. Although it is often different to determine this origin in the field, it is known in the laboratory, allowing a more concise analysis and model evaluation.

Only a couple of field studies and even fewer laboratory investigations on the growth of the consolidated layer have been conducted. Both fresh and doped ice have been used in laboratories, and both saline and Baltic ridges have been monitored in situ. Independent of the ice type, the ratio of the consolidated layer to level ice thicknesses R seems to approach a similar asymptotic value for both small-scale and full-scale measurements. The laboratory investigations provided a higher R values with a decreasing trend, whereas the trend was increasing in situ (Fig. 2).

The basin experiments (Timco and Goodrich, 1988) showed a

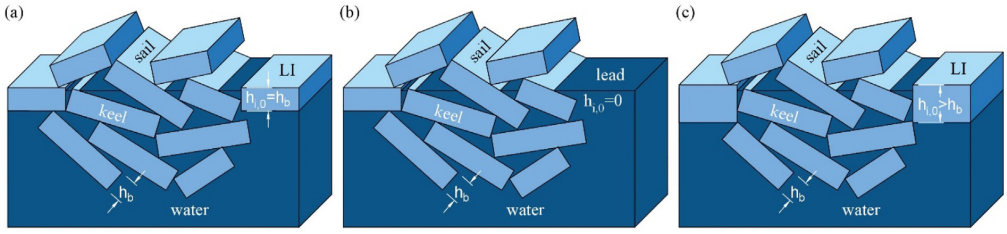

Fig. 1. Scheme of an ice ridge formed from uniform level ice with thickness $h_{i,0} = h_b$ (a), formed close to a newly formed lead with zero ice thickness $h_{i,0} = 0$ (b), and formed from closure of a lead by a thicker level ice $h_{i,0} > h_b$ (c).

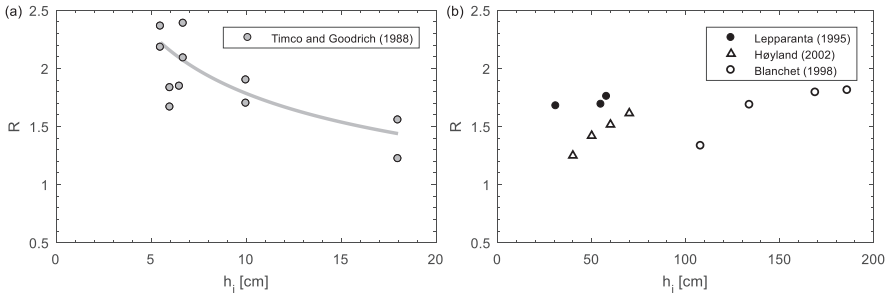

Fig. 2. The ratio of the consolidated layer to level ice thicknesses R vs level ice thickness h_i from laboratory experiments by Timco and Goodrich (1988) (a) and from field data by Leppäranta et al. (1995), Høyland (2002) and Blanchet (1998) (b).

decreasing trend and larger R values for a lower level ice thickness (Fig. 2a). The consolidation layer thickness in their experiments was in the range from 10 to 28 cm; the level ice was 5–18 cm. Ridge macroporosity was not measured, ice was both fresh and model (EG/AD/S), and wind speed was 0.2 cm/s, but the effect of additional growth from a higher local wind speed was measured. Field experiments are difficult to compare with analytical solutions due to uncertainty in the ice initial thickness. Leppäranta et al. (1995) showed increasing R values during their field experiment with an initial level ice thickness of 0.31 m and macroporosity of 0.28. Blanchet (1998) presented fieldwork results with the same increasing trend and initial level ice thickness of 0.83 m. Høyland (2002) showed increasing time R values for ridges in Svalbard and in the Baltic Sea (Fig. 2b).

Measurements of the consolidated layer are more difficult than for level ice. Three methods are mainly used: mechanical drilling, thermal drilling and analysis of vertical temperature profiles. Results using the drilling method can provide higher values than temperature profiles (Høyland, 2002). Kharitonov (2008) used the thermal drilling method and found average consolidated layer thickness values equal to 0.83–1.63 of the level ice thickness for ridges with an average keel macroporosity ranging from 0.12–0.28. Kharitonov and Morev (2009) presented an analysis of the sail height effect on ridge consolidation. Wazney et al. (2019) performed small-scale mechanical experiments with fresh deformed ice, showing that the consolidation time was the key factor for the maximum loads.

Since level ice thickness is commonly used to define the R value as in Eq. (1), it is important to provide an overview of its growth models and their scalability. The first analytical model was published by Stefan (1891) and includes only conduction and latent heat fluxes under the assumption of an ice top surface temperature equal to the air ambient temperature. To obtain accurate results with this model, ice temperatures should be accurately measured. Adams et al. (1960) added sensible heat, air convection and wind speed effect to the growth model, which made it possible to predict thin ice growth in an accurate manner. Maykut and Untersteiner (1971) presented a one-dimensional model of sea ice growth, including incoming and outgoing longwave and shortwave radiation, conduction in snow and ice, convection in water, and sensible heat. Ashton (1989) analysed the effects of wind speed on air convection and thin ice growth and compared them with field experiments. Leppäranta et al. (1995) presented a summary of analytical ice growth models. Notz (2005) conducted a detailed review of sea ice thermodynamic parameters and experiments examining sea ice desalinization.

To perform experiments evaluating small-scale ridge consolidation, it is important to analyse existing setups of basin tests to obtain useful data. According to Repetto-Llamazares (2010), key parameters of the average model first-year ridge include a keel depth of 30 cm, sail height of 7 cm, blocks of 10 × 8 × 3 cm, a porosity of 20–40%, and level ice thickness of 6 cm. For full-scale ridges, the average ratio of keel to sail heights k/s is 5.2, the average relation of sail height and block thickness is $s \cong 3.73\sqrt{w}$, the average sail height s is 2 m (Strub-Klein and Sudom, 2012), and the unconsolidated keel macroporosity also ranges from 20 to 40% (Høyland, 2007; Pavlov et al., 2016; Bonath et al., 2018).

The consolidation problem has similarities with the formation of refrozen cracks in ice, which have been described and modelled by Petrich et al. (2007). Their model has boundary conditions assuming a linear temperature profile in the surrounding ice at a certain distance. For the consolidation problem, this assumption would require one layer of horizontal blocks with a ratio of block length and thickness larger than two, which cannot be treated as the ice ridge.

2. Analytical model

2.1. Governing equations

The consolidation rate of fresh ice ridges in a laboratory is mainly governed by air temperature, wind speed, and ridge configuration. In the field, it is also affected by oceanic fluxes from the bottom, long and shortwave radiation, and presence of snow. The ridge is a porous medium consisting of ice and water. In contrast to level ice growth, its solidification cannot be accurately modelled as a one-dimensional problem without significant simplifications. Nevertheless, under the assumption of homogeneity, this problem can be solved in a single dimension, which literally means that the homogeneous ridge consists of a mixture of infinitely small ice blocks surrounded by water. The consolidated layer thickness and initial block size are on the same order for short consolidation times.

Ice growth includes heat transfer from the water via conduction through the ice into convective heat transfer in the air. The amount of newly formed ice h_i depends on the sum of the conductive heat flux q_c and the heat flux from the water q_w. It can be expressed as

$$-\rho_i L_i \partial h_i/\partial t = q_c + q_w, \tag{2}$$

where ρ_i is the ice density, L_i is the ice latent heat, and t is the time.

The oceanic heat flux q_w is an external energy source. It can be determined from an oceanic model and will be assumed to be zero for laboratory conditions. The conductive heat flux q_c depends on the ice bottom and top surface temperatures T_f and T_s, and its thickness h_i according to Fourier's law:

$$q_c = -k_i \partial T/\partial z \cong k_i (T_f - T_s)/h_i, \tag{3}$$

where k_i is the ice thermal conductivity. This equation neglects internal heat storage related to the specific heat needed to cool the ice and assumes a constant thermal conductivity.

The heat flux from the ice or snow surface into the air consists of the turbulent heat exchange with the atmosphere and the radiation balance. It depends on the atmospheric conditions, characteristics of the surface type, and surface temperature of the ice/snow system. For thin

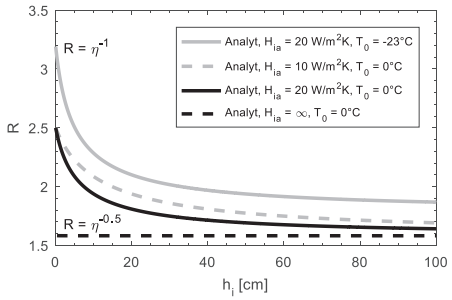

Fig. 3. Ratio of consolidated layer and level ice thicknesses $R = h_c/h_i$ vs level ice thickness h_i for the analytical solution from Eqs. (6), (8) and (9) and initial macroporosity η_0 of 0.4 for the different initial block temperatures T_0 and heat transfer coefficient H_{ia}.

ice, the turbulent heat flux is dominating (Adams et al., 1960). The convectional heat transfer is then expressed as a linear function of the temperature difference between the ice surface and the atmosphere (Newton's law of cooling):

$$q_a = H_{ia}(T_s - T_a), \tag{4}$$

where H_{ia} is the convectional heat transfer coefficient.

Assuming an insignificant effect from long and shortwave radiation, and the absence of snow, one can set $q_c = q_a$ to obtain the ice top surface temperature T_s. Setting Eq. (5) in Eq. (3), one can then integrate Eq. (2) to obtain the ice thickness h_i, Eq. (6):

$$T_s = \frac{k_i T_f + H_{ia} h_i T_a}{k_i + H_{ia} h_i}; \tag{5}$$

$$h_i = \left(\frac{2k_i}{\rho_i L_i}(T_f - T_a)t + \left(\frac{k_i}{H_{ia}}\right)^2\right)^{0.5} - \frac{k_i}{H_{ia}} \tag{6}$$

In all previous publications and engineering standards, ice ridges are implicitly assumed as a homogeneous media with small pores that are evenly distributed in its volume. For such a ridge, we can assume that we have to freeze only the liquid fraction η inside the ridge volume (Leppäranta, 1993):

$$L_c = L_i \eta \tag{7}$$

Inserting this in Eq. (6), we can obtain consolidated layer thickness analytical solution for homogeneity assumption:

$$h_c = \left(\frac{2k_i}{\rho_i L_i \eta}(T_f - T_a)t + \left(\frac{k_i}{H_{ia}}\right)^2\right)^{0.5} - \frac{k_i}{H_{ia}} \tag{8}$$

The initial phase of ridge consolidation can be included in the described analytical model by assuming a change in initial porosity from η_0 to η, where η_0 is the porosity prior to the temperature change from the initial ice temperature T_0 to the water temperature T_f:

$$\eta = \eta_0 - (1 - \eta_0)\frac{c_i(T_f - T_0)}{L_i} \tag{9}$$

This implies a relative additional ice volume $\eta - \eta_0$ be formed after the end of the initial phase of ridge consolidation. How fast is this initial change in comparison to vertical ice growth? The duration of the initial phase depends on the initial temperature T_0 and characteristic block thickness w according to the solution of the heat diffusion equation in the x-axis direction of the smallest block dimension:

$$c_i \rho_i \frac{\partial T}{\partial t} = \frac{\partial T}{\partial x}\left(k_i \frac{\partial T}{\partial x}\right) \tag{10}$$

The approximate form of the solution for the initial temperature T_0 and $t \geq 1/\pi^2$ is

$$T(x,t) \approx \frac{4T_0}{\pi} sin(\pi x) e^{-\pi^2 t} \tag{11}$$

This is a dimensionless solution, which means that dimensional time t′ can be expressed as

$$t' = \frac{c_i \rho_i w^2 t}{k_i} \tag{12}$$

The temperature at the centre of the block at time $t = 1/\pi^2$ is only 47% of the initial temperature T_0. We can assume the thermal equilibrium conditions after the initial phase when we are within 1% of the freezing point $T_{eq} = T_f - 0.01(T_f - T_0)$. For example, the equilibrium time t_{eq} for 4-cm-thick blocks is only 12 min, which means that we can assume that ice growth during the initial phase can occur immediately after the start of an experiment for the analytical model of ridge solidification.

The simplifications expressed in Eqs. (7)–(9) provide a one-dimensional solution of the consolidation problem based on the amount of freezing degree-days and the macroporosity η. We use this model to investigate the effect of the convectional heat transfer coefficient H_{ia}, introduced in Eq. (4), on the ratio R. The model shows that assuming an ice surface temperature equal to the air temperature ($H_{ia} = \infty$) significantly underestimates the R values for a level ice thickness less than 20–30 cm. In reality, the ice top surface temperature is a function of the ice thickness as well as the heat flux into the air. Accounting for this effect of finite heat transfer coefficient demonstrates a significant scale effect of the consolidated layer and level ice growth rate ratio (Fig. 3): the R value starts at η^{-1} and only approaches $\eta^{-0.5}$ for thick ice.

The convectional heat transfer coefficient H_{ia} for steady laboratory conditions can be back-calculated using Eq. (5) from the experimental level ice thickness for the corresponding temperatures:

$$H_{ia} = \frac{k_i(T_f - T_s)}{h_i(T_s - T_a)} \tag{13}$$

In summary, the R value is a function of several variables: the initial macroporosity η_0, the level ice thickness h_i, the initial ice temperature T_0, and the convectional air-ice heat transfer coefficient H_{ia}.

It is possible to normalize R with respect to some of these variables. The macroporosity may not be the same in all data, so an easy approach is to divide by the equilibrium value ${\eta_0}^{-0.5}$, which will only be correct with the infinite heat transfer coefficient H_{ia}, zero thermal inertia $c_p \Delta T$, and infinitely small block size w. In this case, the equilibrium value of $R{\eta_0}^{0.5}$ becomes one. The number of accumulated freezing degree-days $(T_f - T_a)t$ is assumed to be the same for both level ice and the consolidated layer. We may use Eqs. (6) and (8), and introduce a normalized solution, allowing for comparison between experiments with a different convective heat transfer coefficient (H_{ia}), macroporosity (η_0) and ice thickness (h_i):

$$R_{norm} = \left(\frac{h_c(h_c + 2k_i/H_{ia})}{h_i(h_i + 2k_i/H_{ia})}\eta_0\right)^{0.5} \tag{14}$$

This factor has the same dimension of [m/m] as the R value but reduces the experimental variance. The analytical solution for this factor provides a value of 1 for any macroporosity, allowing separate investigations of other factors influencing consolidation. Eq. (9) was used to account for the ice initial temperature of −23 °C, giving an R_{norm} value of 1.13. The value of the initial macroporosity η_0 was used for normalisation to experimentally and numerically assess the validity of Eq. (9) and the effect of the initial block temperature T_0 on the freezing rates.

The main geometric parameters of the model ridge are defined in Fig. 4b. Other factors influencing the values of R, including the sail height s, block thickness w and keel depth k, are not included in the analytical model and are not normalized. Their effect will be described in Section 4 based on the experimental and numerical results.

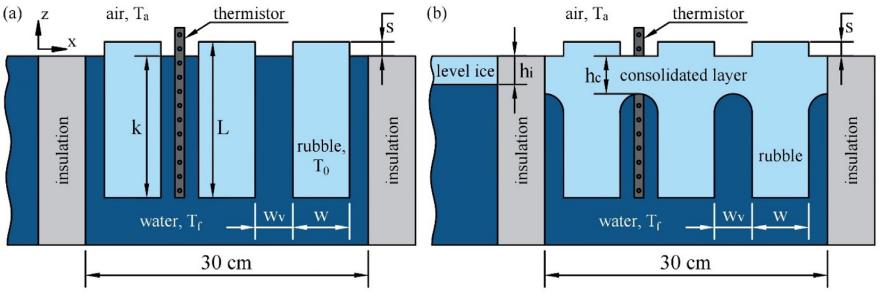

Fig. 4. Scheme of the experimental setup at the start (a) and end (b) of the experiment.

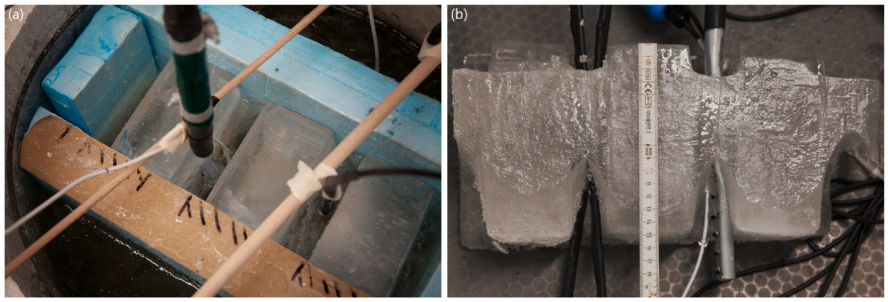

Fig. 5. Experimental setup before (a) and after (b) consolidation.

2.2. Ice growth and thermodynamics

For comparison with observations, it is useful to consider the simplifications made in the analytical model, which are as follows: neglecting specific heat and temperature dependencies (e.g., the thermal conductivity of ice); and a constant heat transfer coefficient H_{ia}. For fresh ice, most of the thermodynamic parameters are slightly temperature-dependant at atmospheric pressure. According to Pounder (1965), the density of pure ice depends slightly on temperature as follows:

$$\rho_i = 916.8 - 0.1403 \cdot T \quad (15)$$

According to Yen et al. (1991), pure ice thermal conductivity is

$$k_i = 2.21 - 1.00 \cdot 10^{-2} T + 3.44 \cdot 10^{-5} T^2 \quad (16)$$

Pure ice heat capacity from Weast (1971) can be determined as

$$c_i = 2112.2 + 7.6973 \cdot T \quad (17)$$

The latent heat of fusion L_i of water is 333.5 kJ/kg, according to Feistel and Hagen (1998). For analytical solutions, it is sufficiently accurate to use values at 0 °C corresponding to the bottom surface of the ice slab. For a temperature range between 0 °C and − 20 °C, the thermal conductivity typically changes by 1%.

As an example, we performed a comparison of the analytical solution with constant thermodynamic parameters and provided a numerical solution with temperature-dependent values of ρ_i, k_i and c_i for level ice growth with an ambient air temperature of −15 °C and heat transfer coefficient of 20 W/m^{2}K over 1000 h. The difference in final ice thickness was 1.2%. For small-scale experiments, this difference was even smaller because ice is significantly warmer. Using the simple Stefan equation, the difference in $(k_i/\rho_i L_i)^{0.5}$ was only 3.4% larger for −15 °C than for 0 °C. The difference between analytical and numerical results with constant values of ρ_i, k_i and c_i was less than 0.3%.

The heat transfer coefficient H_{ia} may vary with temperature, wind conditions, stratification and surface roughness. Practically, it has been found to vary from approximately 10 W/m^{2}K for still air to 30 W/m^{2}K for windy conditions (e.g., Ashton, 1989). In comparison to thermodynamic properties, the heat transfer coefficient dominates the uncertainty in simulations of thin ice growth.

3. Experiments

3.1. Experimental methods

Twenty tests were conducted to study the influence of the rubble block size, orientation and initial temperature on the consolidation rate. Fresh ice was cut into pieces, cooled down to the chosen temperature T_0, placed in the water tank with side thermal insulation, and frozen under laboratory conditions with an air temperature T_a of −15 °C (Fig. 4). Ice blocks were vertical or inclined by 30° from the water surface. The thickness of the ice blocks w was 2, 4 or 6 cm; the length L was 15 cm, and the depth was 10 cm through all experiments. The initial thickness for both level ice and the consolidated layer was zero (see Fig. 4b for the definition). The initial water temperature was 0 °C, and the initial ice block temperature was −1, −15 or −24 °C. The size of the side insulation box was 25 × 30 × 10 cm (Fig. 5a). The top surface roughness was characterized by the sail height s, which varied for different tests in the range from 0 to 3 cm. The keel depth value k was equal to the difference between block length L and sail height s. One longer thermistor string (100 cm long with 3 cm sensor spacing) was installed to measure air temperature, one identic thermistor together with a shorter thermistor (15 cm long with 1.5 cm spacing) were installed to measure ice and water temperatures. The initial macroporosity η_0 in the range from 0.32–0.43 was calculated as $w_v/(w + w_v)$, and values of the block and void width w and w_v were obtained from photo images taken before the consolidation. Both level ice and consolidated layer thicknesses were measured directly after each experiment. Additionally, the level ice thickness was measured during the experiment by drilling. The consolidated layer thickness was measured by drilling only in six tests to avoid ice volume disturbances.

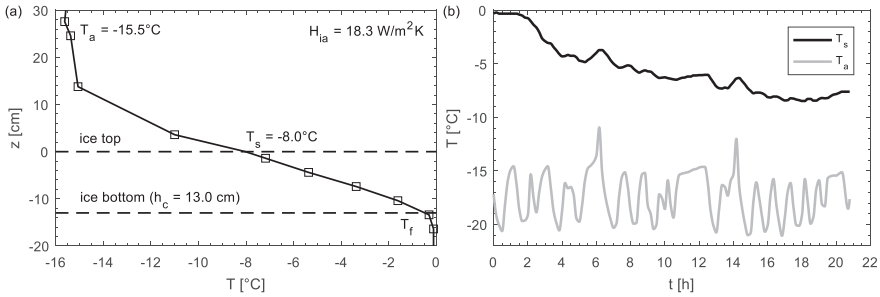

Fig. 6. Temperature vs depth after 20 h of the consolidation experiment 16 (a) and the air and consolidated layer top surface temperature vs time for experiment 16 (b).

Ridge consolidation is mainly governed by thermodynamics, and most of the information can be retrieved from thermistor strings. The temperature profile in the air above the ice was non-linear in the range of the boundary layer (Fig. 6a), and the thickness of this layer depended on the ice thickness. The boundary layer reached 15 cm in our experiments. The ice surface temperature depended on the ratio between conduction in the ice and convection in the air, so it could be estimated from the temperature gradient in ice and convectional heat transfer coefficient H_{ia} depending mainly on the air velocity (Fig. 6a). The consolidated layer thickness h_c in this paper was assumed to be the minimum thickness of newly formed ice after the ridging process (Fig. 4b).

The final thicknesses, air and ice temperatures were measured directly in the experiments. Ice top surface temperature was derived using temperature profiles with a certain accuracy depending on the sensor precision and spacing. In this paper, the following method was used: all sensors with a temperature below -0.3 °C were assumed to be within the ice. For these sensors, the average temperature gradient was calculated. It was then extrapolated at the top and bottom sensors to determine the surface temperature at $z = 0$.

The time-averaged convectional heat transfer coefficient can be obtained from the level ice thickness development using the analytical model from Eq. (6) (Fig. 7a). It can also be obtained from air, ice top and bottom surface temperatures (Eq. (13)). This parameter cannot be completely constant in the laboratory due to the cyclic work of cooling fans – thus, time averaging might be used. The duration of the full cycle of cooling and warming for the NTNU laboratory was 40 min (Fig. 8b).

3.2. Experimental results

The summary of the performed experiments is presented in Table 1, including the main initial parameters: ice block initial temperature T_0, ridge initial macroporosity η_0, block width w, sail height s, number of accumulated freezing degree-days FDD, and block inclination α; and the final values of level ice and consolidated layer thickness h_i and h_c, their ratio R, and factor R_{norm}.

An example of the vertical temperature profile is shown in Fig. 6a together with the measured consolidated layer thickness h_c, estimated air-ice interface temperature T_s and heat transfer coefficient H_{ia}. The temporal development of the air and ice top surface temperatures T_a and T_s during a single experiment is shown in Fig. 6b.

3.2.1. Level ice growth

It is quite common that experiments focused on level ice growth provide results that deviate from theoretical predictions when plotted against FDD or $\int (T_f - T_a)dt$. A significant number of tests should be performed to obtain accurate values of the time-averaged convectional heat transfer coefficient H_{ia}. It was estimated as 20 W/m^{2}K in our laboratory (Fig. 7a). Sources of error include an uneven ice thickness, non-constant convection intensity due to cycles of cooling, and extraction of sensible heat during heating at the end of an experiment. The last effect can be clearly seen in Fig. 7a: final experimental values were larger than intermediate ones. The usage of FDD for experimental comparison results in an increasing error and is more practical to avoid the conversion from level ice thickness to FDD and back to the consolidated layer thickness (Fig. 7b).

Based on our observations, we can estimate the heat flux related to ice growth in three ways: via $q_a = H_{ia}(T_s - T_a)$ by assuming a constant H_{ia} and measured air and ice surface temperature; from $q_c = -k_i \partial T/\partial z$ based on the temperature gradient in the ice; and from $q_l = -\rho_i L_i \partial h_i/\partial t$ based on the ice growth rate. Accurate estimates of the convective q_a, conductive q_c, and latent heat fluxes q_l are clearly difficult when the ice thickness is small (Fig. 8a) due to the following factors: one needs to have two frozen sensors to properly obtain temperature gradients; the

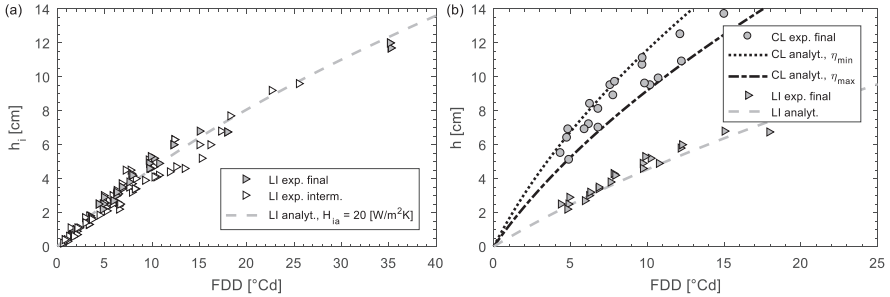

Fig. 7. Level ice thickness h_i (a) and thickness of level ice and the consolidated layer h (b) vs freezing-degree days FDD from experiments and from the analytical model for minimum and maximum experimental ridge porosities η_{min} and η_{max}.

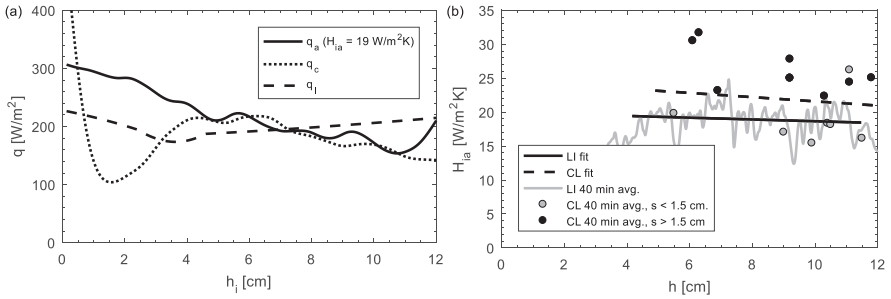

Fig. 8. Convective, conductive and latent heat fluxes q from temperature and thickness measurements vs the level ice thickness h_i (a) and heat transfer coefficient H_{ia} from temperature and thickness measurements using Eq. (13) vs the ice thickness h for the chosen level ice experiment level and for all instrumented ridge experiments (b).

assumption of linear temperature gradients may be inaccurate; ice thickness measurements from drilling are limited to an accuracy of a few mm; the heat transfer coefficient H_{ia} may not be constant over short times with relatively large temperature changes, and it may depend on the cold room cooling system.

The convectional heat transfer coefficient was estimated using Eq. (3) continuously for a single level ice experiment and for the last 40 min of each consolidation experiment due to the uncertainty of the consolidated layer thickness development (Fig. 8b). Higher values of the heat transfer coefficient H_{ia} for the consolidated layer were mostly observed when the sail height was greater than 1.5 cm. Small-scale sails added additional top surfaces for model ridges with increasing vertical heat fluxes. Several factors can change the consolidation rate, including the sail height and block thickness. Separate effects from each parameter are described in the numerical modelling results section of this paper. The level ice thickness was found to be the most accurate data for estimating the value of the convectional heat transfer coefficient (Fig. 7a).

3.2.2. Consolidation

The analytical solution from Eq. (8) significantly overestimated the R values when the level ice thickness h_i was less than the distance between blocks w_v (1.4–4.4 cm), as shown in Fig. 9a. This phenomenon will be analysed and explained using our numerical model (see Section 4). The figure further shows the effect of the initial ice temperature: colder ice consolidated faster and reached a higher maximum value. The analytical solution can be modified with Eq. (9) so that the effect of the initial temperatures is included, and the maximum values clearly correlate with the initial temperatures. Most maximum values fit in between the analytical solutions for cold and warm ice (Fig. 9b). The initial macroporosity also varied in the experiments (0.32–0.43), and most of the data fit in between these analytical solutions (Fig. 9a). Usage of R_{norm} allowed the comparison of experiments with different porosities and permitted the possibility of investigating the effects of other governing parameters. Finally, we might observe a trend of a lower value than the modelled R towards the end of the experiments, which is proposed to be an effect of the limited keel depth and will also be analysed and explained using the numerical model in Section 4.

The effect of these three parameters: sail, keel and block size – can be included only in a 2D model and will be analysed with the numerical model in Section 4. The effect of block orientation was similar to that from block thickness: the void size was higher for a higher block inclination from the vertical axis for the same block thickness. Simultaneously, experiments with inclined blocks showed a much more complicated geometry and less possibility for accurate thickness measurements. Consolidation experiments with vertical blocks of diffident thickness were found to be more convenient for scale-effect investigations.

3.3. Error sources

The described experiments include length measurements of ice

Table 1
Summary of experiments.

№	T_0 [°C]	η_0	w [cm]	s [cm]	FDD [°Cd]	α [°]	h_i [cm]	h_c [cm]	R	R_{norm}
1	−1	0.37	6.3	1.1	6.8	0	3.5	7.0	2.00	0.91
2	−1	0.36	4.6	0.0	10.7	0	4.9	9.9	2.02	0.91
3	−1	0.41	6.0	0.0	7.4	0	5.5	10.4	1.89	0.93
4	−5	0.32	6.0	0.6	12.2	0	5.8	12.5	2.16	0.97
5	−1	0.40	4.2	2.0	4.4	29	2.5	5.5	2.20	0.98
6	−1	0.40	4.8	1.7	6.8	30	3.4	8.1	2.38	1.03
7	−1	0.37	4.1	2.2	5.9	0	2.7	6.9	2.56	1.05
8	−15	0.37	4.4	0.5	4.9	39	2.9	5.1	1.76	0.84
9	−18	0.39	6.3	0.0	7.9	0	5.8	9.7	1.67	0.86
10	−15	0.33	6.0	0.0	12.3	0	6.3	11.5	1.83	0.89
11	−16	0.41	4.3	2.1	12.3	25	6.0	10.9	1.82	0.95
12	−23	0.43	4.1	0.5	10.2	0	5.2	9.5	1.83	0.99
13	−23	0.40	3.9	0.0	9.7	0	4.9	10.7	2.18	1.04
14	−23	0.35	4.2	0.5	6.3	0	3.2	8.4	2.63	1.05
15	−23	0.36	2.3	0.7	9.7	0	4.6	11.1	2.41	1.07
16	−23	0.37	4.3	2.5	15.0	26	6.8	13.7	2.01	0.97
17	−23	0.38	6.5	1.7	7.9	0	4.2	9.7	2.31	1.00
18	−23	0.43	5.7	2.4	6.2	24	3.0	7.2	2.40	1.07
19	−23	0.36	6.4	2.6	4.9	0	2.5	6.9	2.76	1.09
20	−23	0.42	4.2	2.9	7.6	0	3.8	9.5	2.50	1.10

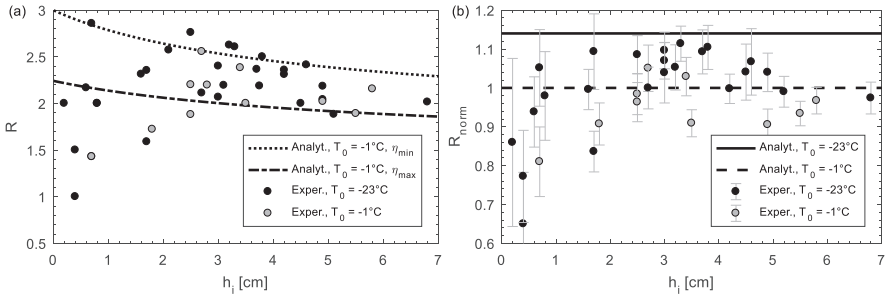

Fig. 9. Experimental results presented via R values (a) and via R_{norm} values (b) plotted against the level ice thickness h_i together with the analytical solution for the range of porosities (a) and for the range of initial block temperatures (b).

thickness, block width and sail height, leading to instrumental random error of direct and indirect measurements, which is presented using standard error bars. The known source of systematic error is the porosity irregularity when the porosity of the exact ridge void and surrounding blocks is different from the porosity of the surrounding voids. The described systematic error can be eliminated using a numerical simulation with a row of four blocks and three voids with different porosities for the central section. The local porosity is defined as the ratio of the void width and the sum of the void and half of the width of the surrounding blocks. The consolidation rate is defined by the local porosity during the initial phase. It approaches the consolidation rates for the average porosity. In the range of studied level ice thicknesses, the 10% difference in surrounding porosity results in a 5–9% difference in consolidated layer thickness in contrast to the 15–20% difference for the same change in local porosity. Another source of systematic error in porosity measurements is the presence of the thermistor with a cross-section of 1.5 cm^2 in one of the ridge voids (Fig. 5). It was accounted for by correcting the macroporosity for the thermistor cross-section.

4. Numerical simulations

Mathematical models of the solidification process can be divided into two main groups: the fixed domain and the front tracking method (Liu and Chao, 2006). The commonly used method for the first group is the effective specific heat method, which includes the latent heat in the temperature-dependent-specific heat values. This method is not very accurate when the Stefan number *Ste*, defined as $c/\Delta TL_i$, is small and when the two phases are in thermal equilibrium. The front tracking method was chosen for analysis in our experiments. For this method, two phases are solved separately and linked by the Stefan condition at the interface. The effective specific heat method is also applicable to the current problem. However, it requires a low temperature interval between phases, fine mesh, low relative errors, and a large computational time.

4.1. Governing equations and boundary conditions

The ridge consolidation process was modelled using the finite element analysis simulation software COMSOL Multiphysics 5.3a. Two materials were used: water and ice. Heat transfer in fluid and laminar flow packages were coupled for water simulation. The position of the ice-water boundary was defined by the Stefan energy balance condition (Eq. (19), where the difference in heat fluxes in two materials is equal to the amount of new solid formed or melted (Alexiades et al., 2003).

This numerical model requires the following material parameters for ice and water: thermal conductivity, heat capacity, density, coefficient of thermal expansion, latent heat of fusion and kinematic viscosity. Fresh ice thermodynamic parameter values are described in chapter 2.2. Other values were obtained using the Gibbs SeaWater Oceanographic Toolbox of TEOS−10 (Millero, 2010). Thermal boundary conditions were defined as thermal insulation at the sides and at the bottom, and as external convection with a constant heat transfer coefficient H_{ia} at the top (air-ice interface). The value of $H_{ia} = 20 W/m^2K$ was used based on the experimental level ice growth rate under the laboratory conditions. The heat transfer coefficient was assumed to be equal for level ice and consolidated layer growth. The air ambient temperature was equal to the mean experimental value of −15 °C.

The heat flux balance at the air-ice interface is described as follows:

$$H_{ia}(T_a - T_s) = k_i\left(\frac{\partial^2 T}{\partial x^2} + \frac{\partial^2 T}{\partial z^2}\right) \quad (18)$$

The heat flux balance at the ice-water interface is

$$\rho_i L_i v_n = k_i \frac{\partial T}{\partial n} - q_w, \quad (19)$$

where v_n is normal velocity of the ice-water interface, $\partial T/\partial n$ is normal derivative of the ice temperature at the interface.

Heat diffusion within the ice is described by

$$\rho_i c_i \frac{\partial T}{\partial t} = k_i\left(\frac{\partial^2 T}{\partial x^2} + \frac{\partial^2 T}{\partial z^2}\right) \quad (20)$$

Simulations of the ridge consolidation were performed to study the effect of the initial block temperature, block width and length, sail height, and porosity on ice growth. The numerical model setup was similar to the experimental setup shown in Fig. 4, except for the presence of a thin initial ice thickness of 1 mm at the air-water interface.

4.2. Comparison with the experimental and analytical results

The described numerical model is compared to experimental results and the analytical model in Figs. 10 and 11. In the following section, we discuss its capability to predict the observed development of the R value and the effects of the initial temperature T_0, block thickness w, sail height s, and keel depth k.

4.2.1. Block thickness effect

The 1D analytical solution deviated from observations, which was the most prominent at the beginning of the experiments. Running the 2D numerical model with different block thicknesses indicated that this deviation was a consequence of the variable block thicknesses, a 2D effect that was well-captured by the numerical model (Fig. 10a). The R_{norm} values approached equilibrium faster for thinner blocks. The figure indicates a peak in R_{norm} that was reached when level ice had grown to approximately the size of the pores (1.3 cm for 2-cm-thick blocks and 2.7 cm for 4-cm-thick blocks). Fig. 10b shows that the numerical model captured an important effect, in which for small block sizes, the R value increased, reached a maximum value and decreased. When the block size increased, this effect disappeared.

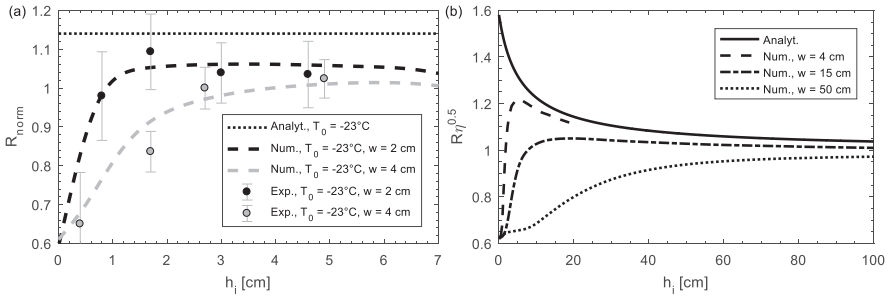

Fig. 10. Values of R_{norm} (a) and $R\eta^{0.5}$ (b) vs the level ice thickness h_i for different block thicknesses w in physical and numerical experiments.

4.2.2. Sail height (surface roughness) and initial block temperature effects

The numerical model confirmed the effect of the initial ice temperature and sail height, with increasing consolidation for increasing sail heights and decreasing initial temperatures (Fig. 11). The effect on R_{norm} values from a decreasing initial temperature of -23 °C was equivalent to the effect from an increasing sail height of 3 cm. The increasing sail height resulting in faster consolidation was due to two factors: the higher sail was due to locally thicker ice and a lower ice surface temperature and corresponding higher conductive heat flux through thin ice (Eqs. (2) and (3)). Additionally, the effective heat transfer coefficient H_{ia} increased due to an increase in the ice surface in comparison to its horizontal projection.

In contrast to our experiments, the sail height of the ice basin and natural ridges mainly depended on the ridge isostatic balance or the balance of gravity and buoyancy forces. Thus, the sail height could not be zero. In our experimental scale, the sail resembled the surface roughness and its impact on heat transfer and the increasing consolidation rate (Fig. 12a). The sail effect and the effect of the initial ice temperature depended on each other and could not be simply added (Fig. 12b).

The effect from large-scale sails in the field also included trapped air or snow volumes. This effect was more complicated and required further investigation. However, we performed additional simulations to investigate the roughness effect for thicker blocks. For simulations with a 15-cm-thick block surface, the roughness had little effect on consolidation, while for 50-cm blocks, a small sail with a height within 1–50 cm resulted in slightly lower ridge consolidation. It corresponded to the field results, as presented by Kharitonov and Morev (2009), showing no effect of a relatively small sail height on the consolidated layer thickness.

4.2.3. Porosity and turbulence effect

The macroporosity is the main parameter defining the difference between a ridge and level ice consolidation, and the effect of both macroporosity and the heat transfer coefficient is considered in R_{norm}. Lower values of the heat transfer coefficient H_{ia} led to a more significant scale effect for similar ice thicknesses (Fig. 3). Only an infinitely high H_{ia} corresponding to Stefan's equation for ice growth led to an immediate equilibrium value of $R{\sim}\eta^{-0.5}$. The numerical model was used to validate Eq. (14) with a constant void thickness w_v, and the varying porosity η_0 was obtained by changing the block size. Fig. 13 shows that both effects were well captured and only slightly overestimated by the analytical model.

The change in porosity in the range from 0.3–0.5 resulted in a 3.5% difference in R_{norm} value, which was smaller than the instrumental errors of the consolidation experiments with a similar scale. However, in the present numerical simulations, an increase in porosity implied a lower block thickness, which in turn increased R_{norm} (see Fig. 10a). Hence, Fig. 13 shows that the block thickness effects could influence the porosity effects and vice versa. The R_{norm} value was almost independent of the heat transfer coefficient H_{ia}. Usage of R_{norm} provided the possibility of comparing the experiments with different porosities and different thickness ranges expecting R_{norm} values approaching a value of 1.

4.2.4. Keel effect

The effect of the limited keel depth k is critical mainly for the experimental setup. In the field, the keel depth to block thickness ratio was often much larger than in our experiments, which resulted in a decreasing trend in R_{norm} towards the end of the experiments, approximately 2 cm before h_c reached the keel bottom (Fig. 11). When the consolidation front was approaching the bottom of the ice blocks, the consolidation rate was decreasing until the front became planar and further consolidation was identical to level ice growth (Fig. 14b). The affected region depended on the scale of the voids between blocks. The numerical modelling results explained the lower R values for the later experimental stages: the solidification rate was slower when the consolidated layer thickness h_c was approaching the values of the keel depth k.

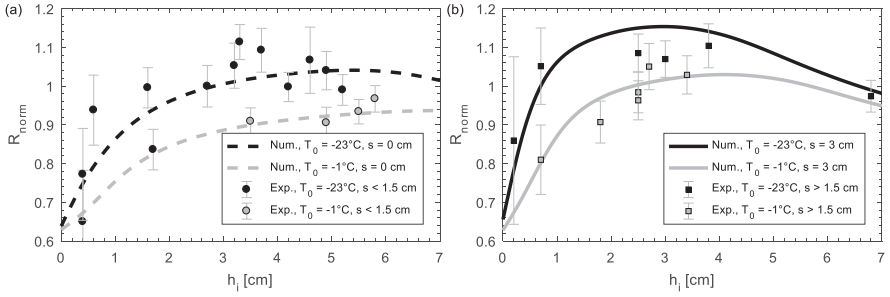

Fig. 11. Temperature effect on the R_{norm} values for experiments with a small (a) and large (b) sail.

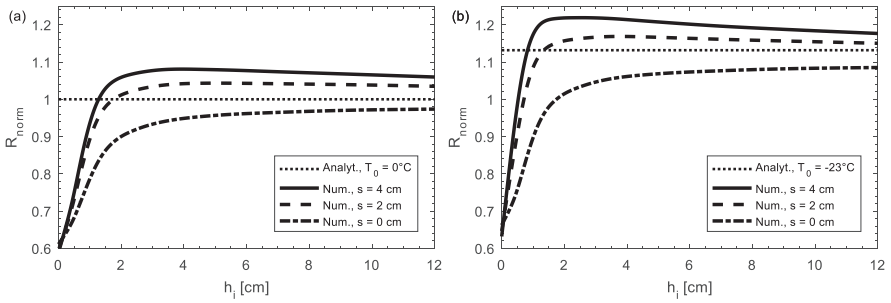

Fig. 12. Values of R_{norm} vs level ice thickness h_i for different sail height s for warm (a) and cold (b) 4-cm-thick ice blocks.

4.2.5. Ice-water interface and temperature distribution

The location of the ice-water interface at different times of the simulation is presented in Fig. 14a. Its shape was changing during the initial phase and when the consolidation front was approaching the ice block bottom. Numerical results for the temperature distribution throughout the experiment are presented in Fig. 14b.

The arch shape of the consolidation front covered the ice volume equivalent to approximately one-quarter of the consolidated layer with a thickness equal to the void width (7 mm for the 2.7-cm voids). The shape usually formed after 1 h of freezing for 4-cm-thick ice blocks. However, it should be noted that in reality, brine released during freezing may lead to different pattern and modes of haline convection, which may influence the porosity evolution due to heat and salt transfer. These convection processes, similar to the details of heat transfer in the atmospheric boundary layer, cannot be addressed herein. However, the size and 2D effects in a pure heat conduction problem can be addressed.

5. Discussion

5.1. Choice of experimental setup

Our experimental setup with a simplified ridge morphology allowed more accurate measurements of macroporosity and consolidated layer thickness in comparison to other methods, and the usage of fresh ice allowed the neglect of complications with composition-dependent thermodynamic variables. The proposed setup also dramatically reduced the preparation time of the experiments, allowing comparisons of the results of solidification with different ridge initial parameters and different scales. The effect of the change in macroporosity within the range of the described experiments was comparable to the effects of other ridge parameters, including the initial block temperature and the sail height. Verification of their effects was only possible using R_{norm}, which allowed the neglect of the effect of macroporosity. Usage of R_{norm} was only possible with high accuracy of the macroporosity measurements, which was provided by the simplified ridge geometry, as described in the experimental setup. As described in Section 1, the effect of ice chemical composition on ice growth was in the range of the ice thickness and ridge porosity measurement errors.

5.2. Comparison across scales

We suggest that the small-scale consolidation process can be divided into several phases. The initial phase starts immediately after ridging, when the level ice and consolidated layer are growing at almost the same rate, and the R value is 1. This phenomenon has also been observed during small-scale fresh ice ridge solidification by Wazney et al. (2019) and during both saline and fresh ice crack refreezing by Petrich et al. (2007). This phase ended when values of R started to approach the value of η^{-1} (Fig. 10b). The initial phase of consolidation can be described only by 2D modelling. The end of this phase usually occurs when the level ice reaches approximately the void width value and R reaches the maximum value. During the following main phase, R was defined by the presented analytical solution described in Section 2. It slowly decreased and approached its equilibrium value of $\eta^{-0.5}$.

The time for consolidation to reach analytical solution values was scale-dependent. It was observed in the large-scale field experiments (Fig. 2b). This definition of the consolidation phases differed from the original definition proposed by Høyland and Liferov (2005). We believe that the duration of the initial phase from that original definition is too small in comparison to the duration of the whole consolidation process and cannot be identified from the thickness development alone.

Analysis of field experiments during consolidation requires knowledge of the ridge macroporosity, the amount of *FDD* before and after ridging, and the thermal insulation provided mostly by snow. These data are usually unavailable, and a level ice growth model is necessary to estimate the ridging time from air temperature data, the ridge block thickness and level ice thickness development. Based on the ridging

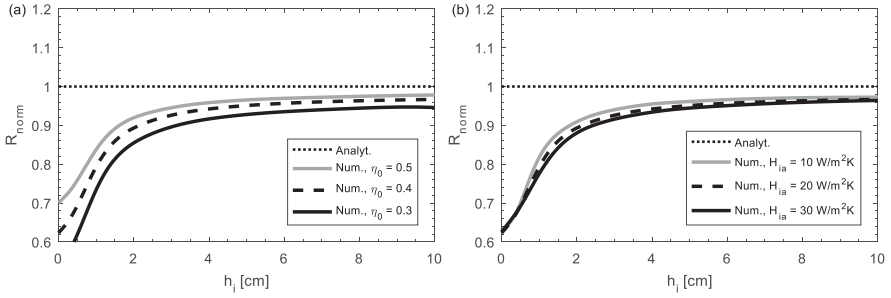

Fig. 13. R_{norm} vs the level ice thickness h_i for different porosities (a) and different heat transfer coefficients H_{ia} (b).

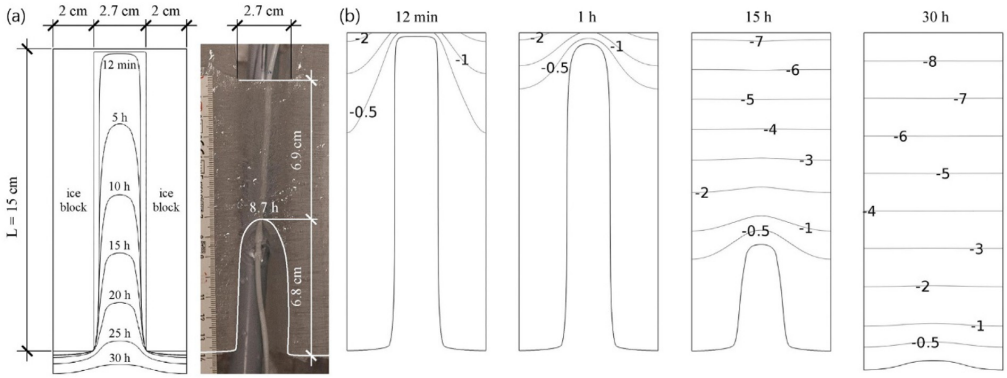

Fig. 14. Ice-water interface from the simulation and after the end of experiment 18 (a) and isotherms from simulations for different stages of the experiment.

time, air temperature, wind speed and snow thickness, the ridge consolidation model can predict its development and provide R values for any experimental time.

One of the differences between the basin and natural ridge consolidation was the presence of level ice around the natural ridge, which decreased the initial R values. The difference between the 1D analytical and 2D numerical solution is presented in Fig. 15. It was assumed that the initial level ice thickness was equal to the thickness of the ice blocks forming the ridge. The level ice initial thickness h_o resulted in changing values of R, and thick blocks caused the season to be too short to reach ${\eta_0}^{-0.5}$.

Application of the described analytical and numerical models for the experiments in different scales and different ice types, including fresh, saline and with dopants, is presented at Fig. 16a. The values of the heat transfer coefficient to simulate these experiments were determined using the level ice growth from the described experiments. The ridge porosity of 0.5 was estimated for the experiments by Timco and Goodrich (1988) from the block length and thickness ratio using the approach of Surkov and Truskov (2003). For the experiment by Blanchet (1998), the ridge porosity was assumed to be equal to the average field value for upper keels of 0.25 according to Pavlov et al. (2016). Both the snow thickness and ridge macroporosity were measured in experiments by Høyland (2002).

Both analytical and numerical models provided very accurate predictions of consolidation development. For the small-scale tests by Timco and Goodrich (1988), most of the key parameters for consolidation were unknown, including the ridge porosity, initial block temperature and surface roughness. The faster decrease in the consolidation rate observed in experiments by Timco and Goodrich (1988) in comparison to our analytical solution could be due to the surface roughness effect described in this paper and their increases with depth macroporosity values measured in the field by Pavlov et al. (2016). The similarity of the results from our experiments and those of Timco and Goodrich (1988) confirms that our experimental setup is applicable for the small-scale consolidation problem (Fig. 16b).

The final problem concerns how to compare the results of field and laboratory experiments. In general, they have different scales, different dominating heat exchange mechanisms (turbulence for smaller scales and radiation for larger scales), and different porosities, making the normalisation necessary for comparison very complicated. The R value differs for differences in wind speed, top surface insulation, and porosity and is scale-dependant for both the final thickness and the initial block thickness. The results could be reanalysed using the presented model and result in divergence from its predictions. Simultaneously, non-critical factors might be excluded from the comparison to generate a smaller experimental matrix and allow comparisons of a larger amount of field data.

5.3. Choice of boundary conditions

The analytical model is one-dimensional and cannot directly include effects from the sail. The two-dimensional numerical model is based on

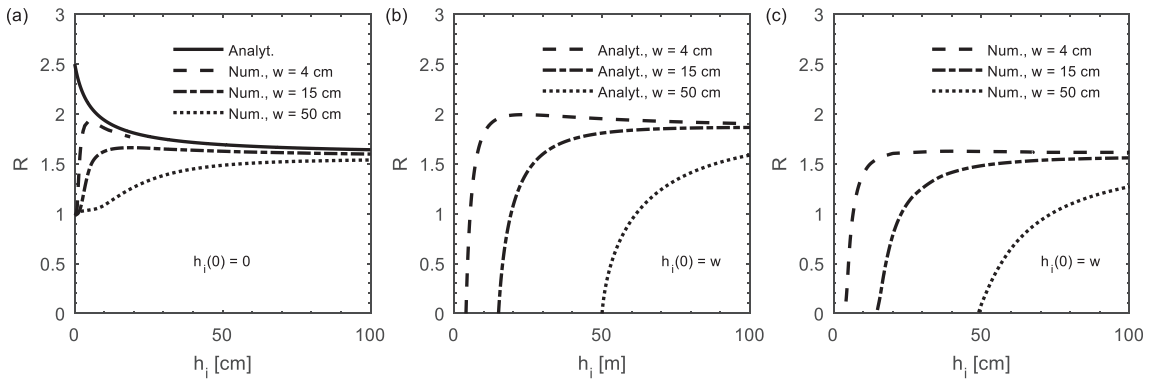

Fig. 15. R vs level ice thickness h_i for 4, 15 and 50-cm-wide blocks and a porosity of 0.4 with a 0 initial level ice thickness (a) and a ridge block initial level ice thickness from analytical solution (b) and from numerical simulations (c).

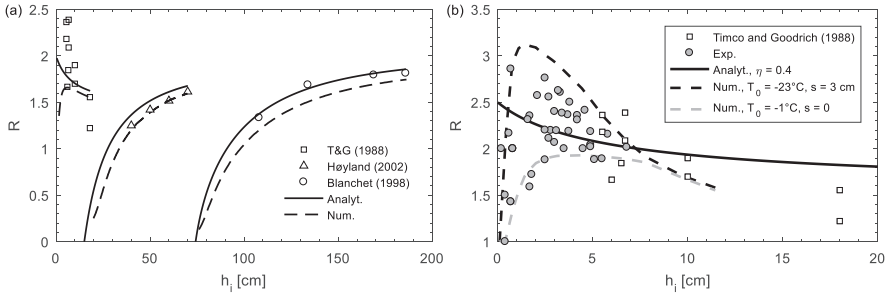

Fig. 16. Comparison of R values from experiments by Timco and Goodrich (1988), Blanchet (1998), and Høyland (2002) and from analytical and numerical solutions for initial experimental conditions for large scales (a) and small scales (b).

several assumptions, including equal values of heat transfer coefficient for the ridge and level ice top surface. It accurately describes the experimental consolidated layer growth dependence on the sail height, meaning that the same convectional heat transfer coefficient can be used for both level ice and small-scale ridge models. Using our numerical model, it was possible to use realistic ridge cross-sections with extended surfaces representing the ridge sail. For the presented level ice growth, the experiment convectional heat transfer coefficient showed significant variation with the value of 19 ± 2 W/m^{2}K based on the measured temperature profile. The heat transfer coefficient values for the ridges with small sails were in the same range as those for level ice but significantly higher than those for larger sail heights (Fig. 8b). Based on the experiments with different initial block temperatures, we can conclude that most of the sensible heat was converted into latent heat and changed the porosity after ridge formation. Considering only parameters such as the initial block temperature, macroporosity, and sail height was it possible to confirm the experimental ice growth results with numerical results (Fig. 11).

Both analytical and numerical models were able to predict consolidation rates for experiments with different scales and ice types (Fig. 16). We also showed the potential reason for consolidated layer thickness overestimation using vertical temperature profiles (Fig. 14b): ice blocks could be significantly colder than the water freezing temperature even below the minimum thickness of the consolidated layer. The relative error values could be much higher for the initial stages of the experiment, which led to the suggestion that more detailed and advanced algorithms should be described and implemented to determine the consolidated layer thickness from the temperature profiles.

6. Summary and conclusions

This paper contributes to a better understanding of ridge solidification and scale effects. Data from previous experiments on different scales were analysed, and a possible explanation of ridge consolidated layer development was described. Twenty laboratory experiments were performed to improve our understanding of factors governing consolidation of small-scale ridges. The main findings of the recent study are summarized as follows:

- The analytical model of ice ridge solidification, which is able to explain observed scale effects on consolidated layer growth, is presented. It allows the comparison of experiments for ridges with different porosities, ice block initial temperatures, subjected to air with different convectional heat transfer coefficients using the introduced normalisation factor R_{norm}. The ratio of the consolidated layer and surrounding level ice thickness based on that solution mainly depended on the ridge macroporosity η, starting at the value of η^{-1} and approaching $\eta^{-0.5}$ for thick ice.
- The new configuration of laboratory experiments in ridge consolidation was described to improve the accuracy of the main parameters governing that process. In the provided experiments, the consolidated layer reached a thickness up to 2.2–2.8 times greater than level ice for the ridge macroporosity η of 0.4, similar to the described analytical model predictions of η^{-1}.
- A numerical model, which was able to predict effects on the consolidation rates from sail height, block thickness, block initial temperature and macroporosity, was described and validated using the provided experiments. The sail height had a significant effect on the small-scale consolidation, leading to up to a 40% thicker consolidated layer for the sail height of 3 cm compared to the level area. This phenomenon was observed in both experiments and numerical simulations, and it contrasts with typical observations for large-scale ridges.
- Both experiments and numerical simulations confirmed that the consolidated layer thickness was initially growing slower than predicted by the analytical solution. The analytical solution was approached when the thickness of ice growing in voids reached the thickness of the ridge blocks.

Acknowledgements

The authors wish to acknowledge the support of the Research Council of Norway through the Centre of Research based Innovation SAMCoT grant 203471 (Sustainable Arctic Marine and Coastal Technology), the RCN PETROMAKS2 grant 243812 (Microscale Interaction of Oil with Sea Ice for Detection and Environmental Risk Management in Sustainable Operations, MOSIDEO), as well as the support of all the SAMCoT partners.

References

Adams, C.M., French, D.N., Kingery, W.D., 1960. Solidification of sea ice. J. Glaciol. 3 (28), 745–760. https://doi.org/10.3189/S0022143000018050.
Alexiades, V., Hannoun, N., Mai, T., 2003. Tin melting: effect of grid size and scheme on the numerical solution. In: Fifth Mississippi State Conference on Differential Equations and Computational Simulations, pp. 55–69. ftp://ftp.zcu.cz/pub/doc/EJDE/conf-proc/10/a5/alexiades.pdf.
Ashton, G.D., 1989. Thin ice growth. Water Resour. Res. 25 (3), 564–566. https://doi.org/10.1029/WR025i003p00564.
Blanchet, D., 1998. Ice loads from first-year ice ridges and rubble fields. Can. J. Civ. Eng. 25 (2), 206–219. https://doi.org/10.1139/l97-073.
Bonath, V., Petrich, C., Sand, B., Fransson, L., Cwirzen, A., 2018. Morphology, internal structure and formation of ice ridges in the sea around Svalbard. Cold Reg. Sci. Technol. 155, 263–279. https://doi.org/10.1016/j.coldregions.2018.08.011.
Feistel, R., Hagen, E., 1998. A Gibbs thermodynamic potential of sea ice. Cold Reg. Sci. Technol. 28 (2), 83–142. https://doi.org/10.1016/S0165-232X(98)00014-7.
Griewank, P.J., Notz, D., 2013. Insights into brine dynamics and sea ice desalination from a 1-D model study of gravity drainage. J. Geophys. Res. Oceans 118 (7), 3370–3386. https://doi.org/10.1002/jgrc.20247.
Høyland, K.V., 2002. Consolidation of first-year sea ice ridges. J. Geophys. Res. 107 (C6). https://doi.org/10.1029/2000jc000526.
Høyland, K.V., 2007. Morphology and small-scale strength of ridges in the North-western Barents Sea. Cold Reg. Sci. Technol. 48 (3), 169–187. https://doi.org/10.1016/j.

coldregions.2007.01.006.
Høyland, K.V., 2010. Thermal aspects of model basin ridges, Proc. of 20th Ice Symposium (IAHR). Lahti, Finland. http://riverice.civil.ualberta.ca/IAHR%20Proc/20th%20Ice%20Symp%20Lahti%202010/Papers/066_Hoyland.pdf.
Høyland, K.V., Liferov, P., 2005. On the initial phase of consolidation. Cold Reg. Sci. Technol. 41 (1), 49–59. https://doi.org/10.1016/j.coldregions.2004.09.003.
ISO 19906, 2010. Petroleum and natural gas industries – arctic offshore structures. Int. Stand. 2010 (50). https://doi.org/10.5594/J09750.
Kharitonov, V.V., 2008. Internal structure of ice ridges and stamukhas based on thermal drilling data. Cold Reg. Sci. Technol. 52 (3), 302–325. https://doi.org/10.1016/j.coldregions.2007.04.020.
Kharitonov, V.V., Morev, V.A., 2009. Hummocks near the North Pole 25 drifting station (in Russian). Meteorol. Gidrol. 2009 (6), 68–73.
Langhaar, H., 1951. Dimensional Analysis and Theory of Models. John Wiley and Sons 166 p.
Leppäranta, M., 1993. A review of analytical models of sea-ice growth. Atmosphere-Ocean 31 (1), 123–138. https://doi.org/10.1080/07055900.1993.9649465.
Leppäranta, M., Hakala, R., 1992. The structure and strength of first-year ice ridges in the Baltic Sea. Cold Reg. Sci. Technol. 20 (3), 295–311. https://doi.org/10.1016/0165-232X(92)90036-T.
Leppäranta, M., Lensu, M., Kosloff, P., Veitch, B., 1995. The life story of a first-year sea ice ridge. Cold Reg. Sci. Technol. 23 (3), 279–290. https://doi.org/10.1016/0165-232X(94)00019-T.
Liu, Y.C., Chao, L.S., 2006. Modified effective specific heat method of solidification problems. Mater. Trans. 47 (11), 2737–2744. https://doi.org/10.2320/matertrans.47.2737.
Maykut, G.A., Untersteiner, N., 1969. Numerical Prediction of the Thermodynamic Response of Arctic Sea Ice to Environment Changes. The Rand Corporation, Santa Monica, California RM-6093-PR. https://www.rand.org/pubs/research_memoranda/RM6093.html.
Maykut, G.A., Untersteiner, N., 1971. Some results from a time–dependent, thermodynamic model of sea ice. J. Geophys. Res. 76, 1550–1575.
Millero, F.J., 2010. History of the equation of state of seawater. Oceanography 23 (3), 18–33. https://doi.org/10.5670/oceanog.2010.21.
Notz, D., 2005. Thermodynamic and Fluid-Dynamical Processes in Sea Ice. University of Cambridge. http://mpimet.mpg.de/fileadmin/staff/notzdirk/Notz_PhD_abstract.pdf.
Palmer, A., Dempsey, J., 2009. Model tests in ice. In: Port and Ocean Engineering Under Arctic Conditions Conference (POAC 09), Lulea, Sweden, 1–10, POAC09-40. http://www.poac.com/Papers/POAC09_01-71.zip.
Pavlov, V.A., Kornishin, K.A., Efimov, Y.O., Mironov, E.U., Guzenko, R.B., Kharitonov, V.V., 2016. Peculiarities of consolidated layer growth of the Kara and Laptev Sea ice ridges. Neftyanoe Khozyaystvo – Oil Ind. 11, 49–54.
Petrich, C., Langhorne, P.J., Haskell, T.G., 2007. Formation and structure of refrozen cracks in land-fast first-year sea ice. J. Geophys. Res. Oceans 112 (4). https://doi.org/10.1029/2006JC003466.
Pounder, E.R., 1965. The Physics of Ice. Pergamon Press, Oxford, UK. https://doi.org/10.3189/S0022143000019353.
Repetto-Llamazares, A., 2010. Review in model basin ridges. In: Proc. of the 20th Ice Symposium (IAHR), Lahti, Finland.
Schwerdtfeger, P., 1963. The thermal properties of sea ice. J. Glaciol. 789–807. https://doi.org/10.3189/S0022143000028379.
Stefan, J., 1891. Ueber die Theorie der Eisbildung, insbesondere über die Eisbildung im Polarmeere. Ann. Phys. 278 (2), 269–286. https://doi.org/10.1002/andp.18912780206.
Strub-Klein, L., Høyland, K.V., 2011. One season of a 1st year sea ice ridge investigation – Winter 2009. In: Proceedings of 21th International Conference on Port and Ocean under Arctic Conditions (POAC) Montreal, Canada.
Strub-Klein, L., Sudom, D., 2012. A comprehensive analysis of the morphology of first-year sea ice ridges. Cold Reg. Sci. Technol. 82, 94–109. https://doi.org/10.1016/j.coldregions.2012.05.014.
Surkov, G.A., Truskov, P.A., 2003. Parameters of hummock-forming blocks of ice. In: Proceedings of the 17th International Conference on Port and Ocean Engineering under Arctic Conditions (POAC) 2003. Trondheim, Norway. 2. pp. 87–102. http://www.poac.com/Papers/POAC03_V2.zip.
Timco, G.W., Goodrich, L.E., 1988. Ice rubble consolidation. In: Proceedings of 9th International Symposium on Ice, International Association of Hydraulic Engineering. 1. pp. 537–548.
Wazney, L., Clark, S.P., Malenchak, J., 2019. Laboratory investigation of the consolidation resistance of a rubble river ice cover with a thermally grown solid crust. Cold Reg. Sci. Technol. 157, 86–96. https://doi.org/10.1016/j.coldregions.2018.10.001.
Weast, R.C., 1971. Handbook of Chemistry and Physics, 52 edition. Chemical Rubber Co., Cleveland, OH.
World Meteorological Organization, 1970. WMO Sea Ice Nomenclature (supplement No 5.1989). Technical Report MO No. 259.TP.145. World Meteorological Organization, Geneva, Switzerland.
Yen, Y.C., 1981. Review of Thermal Properties of Snow, Ice, and Sea Ice. CRREL Res. Rept. 81-10, U.S. Army Cold Reg. Res. and Eng. Lab., Hanover, NH, US.
Yen, Y.C., Cheng, K.C., Fukusako, S., 1991. Review of intrinsic thermophysical properties of snow, ice, sea ice, and frost. In: Zarling, J.P., Faussett, S.L. (Eds.), Proceedings 3rd International Symposium on Cold Regions Heat Transfer, Fairbanks, AK, June 11–14, 1991. University of Alaska, Fairbanks, US, pp. 187–218.

A.5. Paper 5

Medium-scale experiment in consolidation of an artificial sea ice ridge in Van Mijenfjorden, Spitsbergen.

Salganik, E., Høyland, K.V., Shestov, A.

Submitted to Cold Regions Science and Technology, under revision.

Medium-scale experiment in consolidation of an artificial sea ice ridge in Van Mijenfjorden, Svalbard

Evgenii Salganik[a,b][1], Knut Vilhelm Høyland[a][2], Aleksey Shestov[b][3]

[a] Department of Civil and Environmental Engineering, Norwegian University of Science and Technology, Trondheim, Norway

[b] The University Centre in Svalbard, Longyearbyen, Norway

Highlights

- Experiments on the consolidation of artificial ridge allow better controlling its key parameters.
- The spatial difference in the ridge temperature profiles can lead to thickness overestimation.
- Sail and rubble can be included in a ridge consolidation analytical model.
- Temperature profiles can provide values of the main snow thermodynamic parameters.
- Radiative models are more accurate than convective models in ice growth rate prediction.

Abstract

This study characterizes a consolidation of undeformed level ice and ice ridges. Field investigations were performed in the Van Mijenfjorden, Svalbard for 66 days between February and May of 2017. The thickness and properties of the level ice that was used to make the ridge were measured and thermistor-strings were installed in the ridge and the neighboring level ice. The ridge was visited four times for drilling and sampling. During our field experiment, the level ice grew from 50 to 99 cm, the consolidated layer grew up to 120 cm, and the ridge macroporosity was about 0.36. The experimental results provided enough information for accurate growth prediction and validation of ridge consolidation models.

Two analytical resistive models and two-dimensional discretized numerical models are presented. All models need general met-ocean conditions and general ice physical properties. The ridge model includes the effect of the inhomogeneous top and bottom surfaces of the consolidated layer. The models were validated against the field measurements, and the furthers details of the analytical models were validated against the numerical model.

The analytical resistive ridge model with convective atmospheric flux captures the relevant

[1] First author. Given name: Evgenii, surname: Salganik; email: evgenii.salganik@ntnu.no.
[2] Corresponding author. Given name: Knut, middle name: Vilhelm, surname: Høyland; email: knut.hoyland@ntnu.no; phone: +47 93879170.
[3] Co-author. Given name: Aleksey, surname: Shestov; email: aleksey.shestov@unis.no.

phenomena well and could be used for prediction of the consolidated layer thickness in probabilistic analysis of ice actions on structures. The model including the radiative terms predicted heat fluxes in level ice and ridge better than the convective model but required more input data. Vertical temperature profiles through the consolidated layer and further into respectively a void and an ice block may result in significantly different estimations of the consolidated layer thickness. The difference between fresh and saline ice growth is equally important for level ice and ice ridges, but its values are becoming significant only during the warming phase.

Keywords: ice ridges, thermodynamics, consolidation, field experiment, ice thickness.

1 Introduction

According to the definition of the WMO (1970), an ice ridge is a line or wall of broken ice forced up by pressure. Ridges usually consist of three parts: the sail, the consolidated layer, and the unconsolidated rubble. The thickness of level ice, the consolidated layer, and the keel depth are the main ridge parameters for ice action calculations. The level ice h_i and the consolidated layer h_c thicknesses can be measured by mechanical or thermal drilling or from the ridge vertical temperature profile. Experiments are costly and time-consuming. It is beneficial if h_i and h_c can be predicted based on models with general met-ocean data as input. Simple analytical models have the advantage of being applicable in the probabilistic approach for ice action and evaluation of structural reliability.

Advanced numerical models for ridge consolidation exist (Høyland, 2002a; Marchenko, 2008), but these are difficult to use in probabilistic design where for example different climate scenarios need to be considered and thousands of simulations should be run to quantify structural reliability. The traditional solution is based upon modifying the latent heat in Stefan's law with the rubble macro-porosity (Leppäranta and Hakala, 1992). In the simplest form, this solution neither takes into account the snow cover nor the atmospheric boundary layer (the air), but modifications to include these can easily be done. However, the effects of the real three-dimensional bottom and top surfaces of the consolidated layer are not included.

A few field studies describe the seasonal development of consolidated layer (Blanchet, 1998; Høyland, 2007; Shestov et al., 2018), and only one field study (Leppäranta et al., 1995) report observations of formation date and initial conditions. In basin-scale experiments on ridge consolidation (Høyland et al., 2001; Salganik and Høyland, 2018; Timco and Goodrich, 1988) the initial conditions can be quantified, but it is not straight forward to up-scale them to full-scale conditions. Basins are often indoors and have no snow and different ratios between the different atmospheric fluxes. Small-scale consolidation is usually controlled by turbulent fluxes, while large-scale thermodynamics mainly depends on longwave and shortwave radiation. There are also size effects (Salganik et al., 2020), and this means that ridge consolidation includes a large range of scales and ratios of thermal resistances.

The consolidation process of ice ridge is usually characterized by the ratio $R = h_c/h_i$ of thicknesses, the consolidated layer to level ice. The natural ridging process can occur at any time throughout the season. Ridge consolidation description using factor R is practical for

engineering purposes, but not helpful for consolidation model validation. The factor R is sensitive to the initial level ice thickness at the time of ridge formation. In this paper thickness of the consolidated layer h_c is defined as a minimum of newly formed ice between ice blocks (Figure 1).

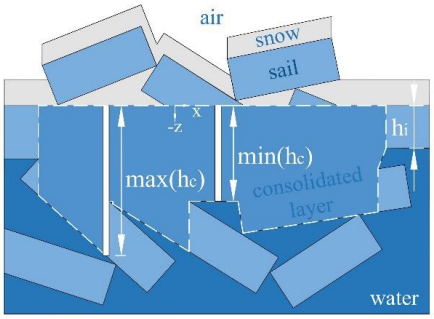

Figure 1. Ice ridge cross-section with a boundary of the consolidated layer (white dashed line) and its maximum and minimum thickness h_c.

Medium-scale consolidation experiments provide the advantage of accurately measured parameters such as initial macroporosity, initial block temperature, and salinity, and freezing time, which are normally not available in case of full-scale natural ridges. It reduces error in crucial parameters for the consolidation process, which includes radiation, air natural, and forced convection, conduction through snow and ice, and phase change. Saline ice has a polycrystalline structure with salt brine inclusions between crystals. Thus, any temperature or salinity change leads to the change of sea ice solid fraction. In this paper, we define and validate a simple analytical consolidation model suitable for transient air temperature, wind speed, and snow thickness. The field experiment was intended to compare thermodynamics and development of physical and mechanical parameters of level ice and consolidated layer.

2 Sea ice growth modelling

2.1 Basic assumptions and atmospheric fluxes

We have used two analytical and two numerical models to calculate the growth and thickness of level ice and the consolidated layer. The analytical models are one-dimensional, and they ignore thermal inertia. The two-dimensional numerical models were used to estimate the error from these simplifications. All models require the following input of material and morphological parameters:

- Snow: thickness, thermal conductivity (Calonne et al., 2011).
- Level ice: salinity and thickness.
- Ridges: macroporosity; block initial temperature, salinity, and thickness; sail size, consolidated layer salinity, and thickness.

The heat exchange with the atmosphere must be estimated and this was modelled in two ways. Firstly, with a simple convective flux, and secondly, with a more advanced model including

radiation and turbulence (Maykut, 1986).

In the convective model the atmospheric flux is given as:

$$q_{atm} = H_{ia}(T_{as} - T_a) \quad (1)$$

where the convective heat transfer coefficient H_{ia} is a function of only the wind speed V_w and can be found as (Adams et al., 1960):

$$H_{ia} = \max(11.6, 5.7V_w^{0.8}) \quad (2)$$

The radiative model is more complicated and includes longwave and shortwave radiation, sensible and latent heat fluxes. Radiation fluxes are not simply proportional to the difference between surface and air ambient temperatures $T_{as} - T_a$ and cannot be simply included in the total model in the form of temperature-independent resistance as for convective model. It requires the following meteorological data:

- LW radiation: air temperature, humidity, cloudiness (Rosati and Miyakoda, 1988).
- SW radiation: cloudiness, surface albedo (Shine, 1984).
- Turbulent fluxes: air temperature, wind speed (Smith, 1988).

The net surface heat flux can be written as (Maykut, 1986):

$$q_{LW} + q_{SW} + q_s + q_e + q_m + q_c = 0, \quad (3)$$

where q_{LW} is the net longwave radiation, q_{SW} is the net shortwave radiation, q_s is the sensible heat flux, q_e is the latent heat flux, q_m is the top surface melting heat flux, q_c is the conductive flux through the ice and snow. Details on how to calculate the different fluxes are given in Appendix A. The equilibrium snow top surface temperature T_{as} can be found numerically from Eq. (3), and the conductive flux up through the ice and the snow can be found as:

$$q_c = \frac{k_s k_i}{k_s h_i + k_i h_s}(T_f - T_{as}), \quad (4)$$

where k_s and k_i are the snow and ice thermal conductivities, h_s and h_i are the snow and ice thicknesses, T_f is the water freezing temperature.

2.2 Analytical 1-D resistive level ice model

With this model, the growth of level ice with a uniform snow cover in steady-state conditions can be simulated with a convective atmospheric flux. The growth depends on how the temperature difference between air and water is distributed between insulating layers of air, snow, and ice. For slow changes of boundary conditions, the temperature gradient at the bottom of ice depends on the ice top surface temperature and its thickness. Three thermal resistances define temperature profile: air R_a, snow R_s and ice R_i (Figure 2a).

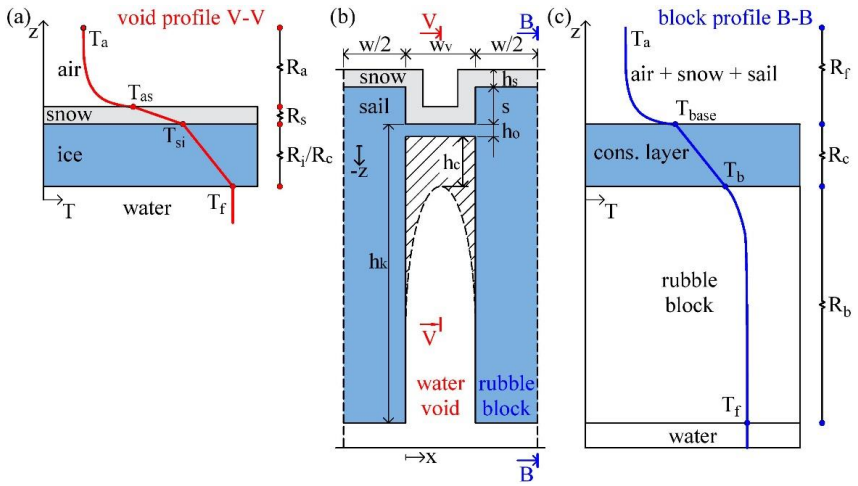

Figure 2. Sketch of geometry used in analytical and numerical models of a ridge, w is the block width, w_v is the void width, h_s is the snow thickness, s is the sail height, h_0 is the initial ice thickness for the numerical model, h_k is the keel depth, and h_c the minimum thickness of the consolidated layer (b) and thermal resistance model for the level ice and ridge void (a), and for the ridge block (c).

The total system thermal resistance is showing how much heat can be transported in time from the water to the air. To find the vertical heat flux q at any time one should know air and water temperatures T_a and T_f, and the values defining three thermal resistances namely snow thickness h_s and thermal conductivity k_s, ice thickness h_i and thermal conductivity k_i, and convective heat transfer coefficient H_{ia}:

$$q = \frac{T_a - T_{as}}{R_a} = \frac{T_{as} - T_{si}}{R_s} = \frac{T_{si} - T_f}{R_i} = \frac{T_a - T_f}{R_a + R_s + R_i}; \quad (5)$$

$$R_a = 1/H_{ia}\,; \quad (6)$$

$$R_s = h_s/k_s\,; \quad (7)$$

$$R_i = h_i/k_i, \quad (8)$$

where T_{as} and T_{si} are the air-snow and snow-ice interface temperatures.

Convective heat transfer coefficient H_{ia} can be estimated from the measured wind speed from Eq. (2), the snow thermal conductivity depends on snow density (Calonne et al., 2011), ice thermal conductivity slightly depends on its salinity and temperature (Schwerdtfeger, 1963), and the snow and ice thicknesses and should be measured manually or estimated from the measured vertical temperature profiles. The more advanced radiative model described in section 2.1 has been also used in this analytical resistive model.

Level ice thickness can be accurately estimated from the vertical temperature profile. Ice thermal conductivity development can be estimated from its temperature and periodically measured salinity profiles.

There is only a very weak dependence of drift snow temperature on its thermal conductivity

(Sturm et al., 1997). In our paper we suggest estimating snow thermal conductivity values from the measured snow thickness and vertical temperature profile in snow and ice as:

$$k_s = \frac{(T_{si} - T_f)}{(T_{as} - T_{si})} \frac{k_i h_s}{h_i} \tag{9}$$

One of the ways to validate this model is to compare the estimated and measured interface temperatures. In transient conditions, temperature distribution will be following described ratios with a time lag defined by the thermal inertia of snow and ice. Higher time lag will be corresponding to the higher thermal resistance of layers above the chosen level of temperature measurements.

The analytical resistive model with convective or radiative atmospheric flux can be used for ice growth estimation based on the knowledge of air and water temperature, ice and snow thickness and thermal conductivity, and wind speed. The results of these predictions can be validated using manually measured ice thickness. Assuming no oceanic flux from the water and no thermal inertia, the pure ice growth can be estimated as:

$$\rho_i L_i \, dh_i/dt = -k_i \, \partial T/\partial z \tag{10}$$

Gas-free fresh (pure) ice growth can be estimated from meteorological data including air temperature, wind speed, and snow thickness as:

$$\rho_i L_i \frac{dh_i}{dt} = \frac{T_f - T_a}{R_a + R_s + R_i} \tag{11}$$

Sea ice is saline and has different thermal properties and corresponding thermal response. However, the major difference is related to melting and the difference in the growth of fresh and saline ice is not considerable (Notz, 2005). The details of saline ice growth are given in Appendix B.

Such a simple analytical model, which ignores time delay in thermal diffusion, can give errors when the air temperature is quickly moving towards seawater freezing point. This error can be eliminated only by solving diffusion equations for snow and saline ice layers assuming external convection from the air. The difference between analytical and numerical predictions will be presented in the results of this study.

2.3 Analytical 1-D resistive ridge model

Ridge consolidation has many similarities with level ice growth, but there are some vital differences: a) the ridge keel is porous with a macroporosity η_m while the level ice grows from liquid and b) the spatial inhomogeneous top and bottom surfaces. The macroporosity may be adjusted by modifying the latent heat so that it becomes (Leppäranta and Hakala, 1992):

$$L_r = \eta_m L_i \tag{12}$$

This assumption is valid for homogeneous ridges with small voids so that the vertical temperature gradient is constant horizontally. In a natural real ridge, the voids are so large that the vertical temperature profiles may vary horizontally. This makes horizontal heat fluxes occur inside ice ridges (Leppäranta et al., 1995), and the ice-water interface has an ellipse shape where new ice is forming (Petrich et al., 2007). These inhomogeneities caused by the relatively

large voids/consolidated layer thickness ratios are more complicated to handle in our analytical one-dimensional models. In our simplified sketch of an ice ridge (Figure 2b) its macroporosity is defined as $w_v/(w_v + w)$.

Let us start with the top surface, or the sail, characterized by its height s. It gives a locally changing ratio of thermal resistances and the total area via which heat is extracted to the air. But ridge sails also change the distribution of snow, creating accumulations and snow-free surfaces. It is making top surface conduction to be a 2D or even 3D problem in contrast to level ice. These factors are changing thermal resistance of ridge sail and its top surface temperature, making the analysis of field data much more complicated due to the difference in temperatures of different parts of the consolidated layer. The top surface in natural ridges can be colder while the sail temperature at the water level can be warmer than in sail free consolidated layer (Leppäranta et al., 1995).

In this model, we assume that snow thickness is the same on the top and on the sides of ice ridge blocks. It is important to mention that when snow is thick enough and its top surface is even, other models to handle sail thermodynamics might be used. Snow may accumulate in different ways on and around a ridge sail and the choice of the model requires detailed investigations of snow thickness spatial distribution.

Thermodynamics of ridge sail, not covered by a thick layer of snow, is mainly affected by two factors: additional thermal resistance from the thicker ice layer, which should decrease heat flux below water level, and additional air-snow or air-ice interface area, which should increase heat flux below water level. Both factors should be considered to predict heat flux and temperature profile in ice ridge. For example, an initial thickness equal to the sail height can decrease vertical heat flux during the starting period of consolidation.

We have applied the theory of extended surfaces (Incropera et al., 2013). Fin performance defines an effective heat flux q_f and a corresponding thermal resistance R_f through the snow-covered sail (Figure 2c), and it assumes a spatially constant base temperature T_{base}. The theory compares the effective heat flux through the fins with that of a flat surface and defines a fin performance:

$$\epsilon_f = \frac{q_f}{HA_c(T_{base} - T_a)}, \tag{13}$$

where H is the combined heat transfer coefficient of air and snow.

The thermal resistance of the snow-covered sail becomes

$$R_f = (T_{base} - T_a)A_c/q_f \tag{14}$$

The vertical heat flux through the sail and the snow q_f gives information about the total thermal resistance of the system consisting out of ice, snow, and air above the consolidated layer. Fin performance ϵ_f can tell how much presence of sail increase or decrease the consolidation rate.

When ice is snow-free, the thermal resistance of air is equal to the turbulence resistance $1/H_{ia}$. When there is snow on the top of the ice, the heat transfer coefficient H can be estimated as:

$$H = \left(\frac{1}{H_{ia}} + \frac{h_s}{k_s}\right)^{-1} \quad (15)$$

The bottom surface is also inhomogeneous and here we simply define two different vertical one-dimensional heat fluxes, up from a void (Figure 2a) and through a block (Figure 2c). The model assumes that sail exists only on top of blocks and the heat flux up from a ridge void q_v can be found as:

$$q_v = \frac{T_f - T_a}{R_a + R_s + R_c}; \quad (16)$$

$$R_c = h_c/k_i, \quad (17)$$

where R_c is the thermal resistance of the consolidated layer.

The heat flux in the ridge block q_b with sail can be found as:

$$q_b = \frac{T_f - T_a}{R_f + R_c + 0.5 \cdot R_b}, \quad (18)$$

where R_f is the thermal resistance of finned surface (a sail), R_b is the rubble block thermal resistance that can be expressed as:

$$R_b = \frac{w}{4k_i}\left(\frac{\pi}{2} - 1\right) \quad (19)$$

This additional thermal resistance is changing the temperature at the bottom level of the consolidated layer, making blocks colder than the water freezing point.

The effective, or total heat flux in the ridge is equal to the latent flux from consolidation:

$$q_r = q_v\eta_t + q_b(1 - \eta_m) = \rho_i L_r \frac{dh_c}{dt} \quad (20)$$

The estimation of ice thickness from temperature profile usually requires several assumptions. It is a common practice to assume that temperature profile in solid ice is linear beyond the upper layer of approximately 20 cm, where the temperatures depend on daily temperature variations (Leppäranta et al., 1995). The difference in temperature profiles between ridge voids and blocks is making experimental thickness estimation from the measured temperature profile more complicated, as well as analysis of experimental heat fluxes due to ridge inhomogeneity.

2.4 Numerical model of level ice and ridge

The numerical simulations of level ice and ridge consolidation were performed with finite element analysis simulation software COMSOL Multiphysics 5.3a using the front tracking method. The position of the ice-water boundary was defined by Stefan's energy balance condition (Eq. (22), where the difference of heat fluxes in two materials is equal to the amount of new solid formed or melted.

This numerical model requires the following material parameters for ice and water: thermal conductivity, heat capacity, density, coefficient of thermal expansion, latent heat of fusion and water kinematic viscosity. Saline ice thermodynamic parameter values are described in Appendix B. Other values were obtained using the Gibbs SeaWater Oceanographic Toolbox

of TEOS-10 (Millero, 2010). Thermal boundary conditions were defined as thermal insulation at the sides and at the liquid bottom (Figure 2b). The air-ice interface has a temperature-dependent incoming heat flux based on either convectional model with a constant heat transfer coefficient H_{ia} or on radiative heat balance for both level ice and the ridge.

The heat flux balance at the air-snow interface for the convective model is described as follows:

$$H_{ia}(T_a - T_{as}) = k_s \left(\frac{\partial^2 T_s}{\partial x^2} + \frac{\partial^2 T_s}{\partial z^2} \right) \tag{21}$$

The top surface heat flux balance for the radiative numerical model is described in Eq. (3). The heat flux balance at the ice-water interface is

$$\rho_i L_i v_n = k_i \frac{\partial T_i}{\partial n} - q_w, \tag{22}$$

where v_n is the normal velocity of the ice-water interface, $\partial T_i / \partial n$ is the normal derivative of the ice temperature at the interface, and q_w is the heat flux from the water.

Heat diffusion within the snow and ice is described by

$$\rho_{s,i} c_{s,i} \frac{\partial T_{s,i}}{\partial t} = k_{s,i} \left(\frac{\partial^2 T_{s,i}}{\partial x^2} + \frac{\partial^2 T_{s,i}}{\partial z^2} \right) \tag{23}$$

The numerical model includes a thin initial ice thickness h_0 of 5 cm at the air-water interface.

In numerical modelling, we used an average snow density value of 374 kg/m^3, obtained from measurements taken during the winter end on Svalbard (Sand et al., 2003) and the thermal conductivity value of 0.21 Wm^{-2} obtained from the temperature measurements analysis.

3 Field measurements

3.1 Methods and preparations

The field experiment in the consolidation of artificial ice ridge was performed during 66 days from 25 February 2017 until 2 May 2017 in seawater Vallunden lagoon in the Van Mijenfjorden in Svalbard (Figure 3).

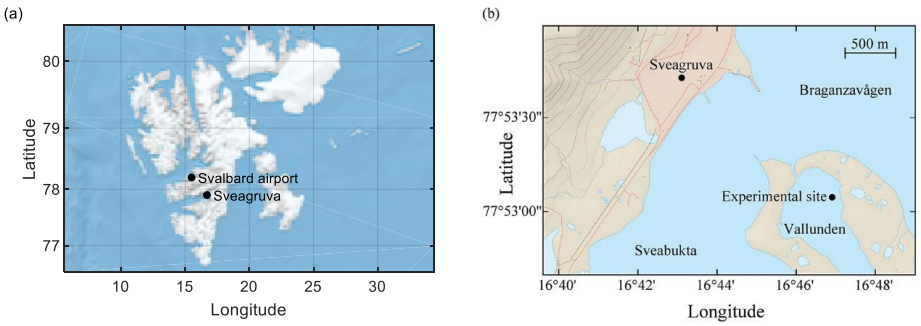

Figure 3. Location of weather stations in Svalbard (a) and location of the experimental site in Van Mijenfjorden (b) on the map by Norwegian Polar Institute.

The ridge was made of 55 blocks from 50 cm thick ice, totally 11.4 m^3 of ice. The average initial level ice salinity was 3.8 ppt and the average initial block temperature was -7.8 °C. A basin 3.0 m by 4.9 m was made in the level ice cover, and the blocks were dumped into the basin. The ice blocks were cut in the feeding channel using a trencher. After that, the blocks were placed into the water basin using rope, ramp, and snowmobile (Figure 4).

The following information was collected during 4 visits: temperature, salinity, density profiles, and uniaxial compressive strength. We collected 3 vertical cores during the visit 1 and 12 vertical cores at visit 4 to investigate ridge morphology. The value of initial macroporosity was estimated based on the volume of ice blocks measured during visit 1 and final ridge volume measured during visit 4. The initial volume of ice was calculated using measured dimensions of all 55 blocks that were used for the ridge creation. The final volume of ice was estimated using keel depth values from 12 cores drilled during visit 4.

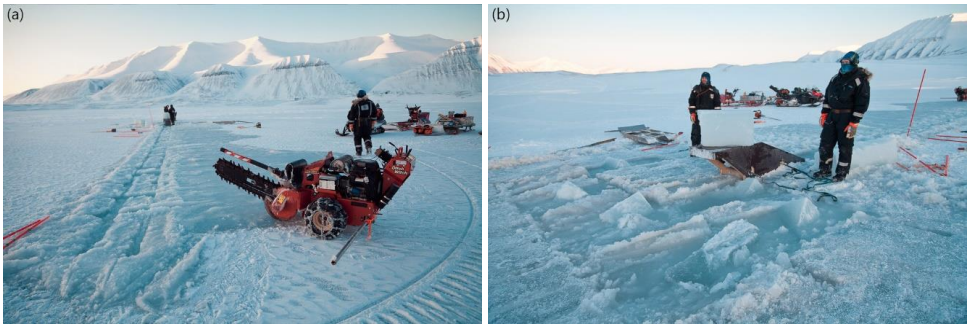

Figure 4. Feeding channel (a) and ridge building using the ramp (b).

Both level ice and ridge were instrumented with thermistor strings. In the ridge, the thermistor was in the sail with 15 cm freeboard and logged continuously until May 4. Level ice had 7 cm freeboard and its temperature profile was logged until March 18.

Three cores were used to measure initial parameters of level ice from which the ridge was formed during visit 1. One core of the level ice and of the ridge were used for salinity and density profiles at visit 4. The vertical resolution of salinity and density profiles was 5 cm.

During all 4 visits of the experimental site from 25 February 2017 until 4 May 2017 following parameters were measured for level ice and model ridge: ice and snow thickness, ice salinity and density vertical profiles. A comparison of uniaxial compressive strength is presented in Appendix D.

Models input data includes two main groups of parameters: atmospheric data from weather stations or remote sensors, and physical parameters of ice and snow. Sea ice thermodynamic parameters including heat capacity, thermal conductivity, latent heat and solid fraction were calculated from Notz (2005). Data from weather stations in Svalbard were collected using web services yr.no and eklima.no provided by the Norwegian Meteorological Institute. Most information for the top surface heat balance was received from the closest weather station 99760 Sveagruva, located 2 km from the experimental site. Sveagruva weather station is providing information about air temperature, humidity and wind speed. Cloudiness data was received from 99840 Svalbard airport weather station in 40 km from the experimental site. The

number of clear and overcast days at Sveagruva and Svalbard airport weather stations was similar from the 1970s until the 1990s (Førland et al., 1997). Local cloudiness at the experimental site was received from the Icosahedral Nonhydrostatic (ICON) Modelling Framework from the German Weather Service. Coefficients for sensible and latent heat fluxes were found from (Smith, 1988).

Ice thickness estimation from temperature profile was based on the temperature data below the upper 20 cm, where values are sensible to daily air temperature variations. All the sensors with temperature values lower than a chosen threshold of 1 °C were considered frozen, and the highest and lowest measurement points were used for linear extrapolation of temperature profile to obtain ice thickness value. The sensitivity of this method to the chosen threshold will be described in the paper results.

3.2 Measurements

In the following sections we will describe input data and results of our thermodynamic models' application. Input data includes two main group of parameters: atmospheric data from weather stations or remote sensors, and physical parameters of ice and snow. The average cloudiness c measured at Svalbard airport weather station near Longyearbyen was 0.63 during the experimental time. The Icosahedral Nonhydrostatic (ICON) Modelling Framework from German Weather Service showed the average cloud cover of 0.57 for Longyearbyen airport and 0.58 for Sveagruva.

The average air temperature in Sveagruva during the experiment was -12.6 °C, which was only 0.3 °C warmer than the historical value for March and April (Førland et al., 1997). The average relative humidity RH was 0.75 for both Sveagruva and Longyearbyen, 0.06 lower than the historical average. The average wind speed at Sveagruva during our experiment was 4.7 m/s.

Sea ice thermodynamic parameters depend on its salinity. Cores drilled from level ice and model ridge during visit 1 and visit 4 were used to obtained salinity profiles (Figure 5). Comparing level ice salinity profiles, it can be argued that about 4 cm of ice formed above the initial top surface between two visits. The level ice salinity after 66 days changed from 3.8 ppt to 4.6 ppt, consolidated layer final salinity was 4.1 ppt.

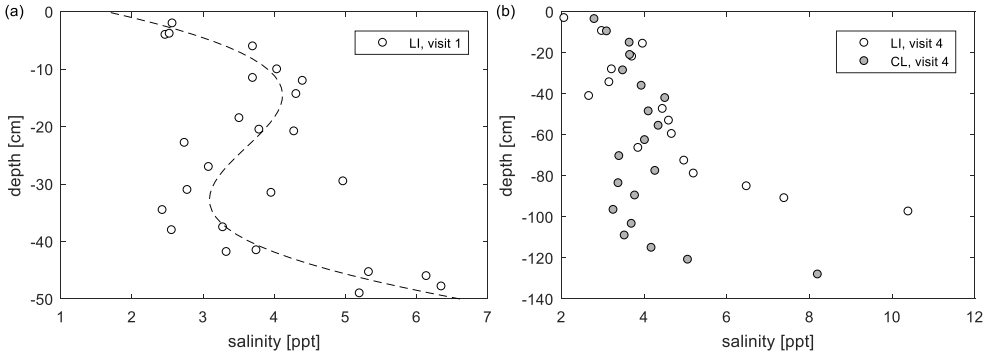

Figure 5. Salinity profiles for visit 1 (a) and for visit 4 (b).

Relative brine volume was estimated using in-situ direct measurements of ice temperature

salinity, density, and water freezing temperature T_f (Cox and Weeks, 1983). Values of the relative brine volume are presented for level ice at visit 1 (Figure 6a) and both for level ice and consolidated layer at visit 4 (Figure 6b).

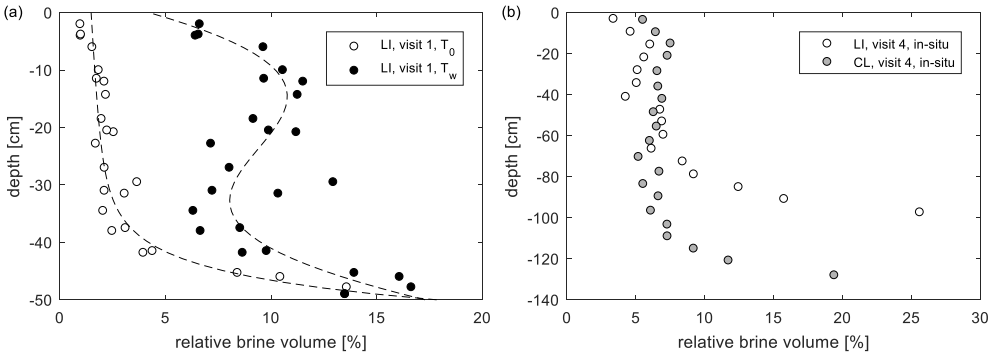

Figure 6. Relative brine volume profile for in-situ and water temperatures for visit 1 (a) and for in-situ temperatures and visit 4 (b).

Level ice grew from 50 cm to 99 cm, while the consolidated layer grew from 0 until 120±12 cm. The average freeboard after the experiments was 7 cm for level ice and 8 cm for the consolidated layer. The temporal development of level ice and consolidated layer draft is presented in Figure 7a: from the drilling during 4 visits and from the vertical temperature profiles measured by thermistors. During visit 4 salinity, density and temperature of level ice and consolidated layer were measured, giving 8 % of liquid volume fraction (Figure 6b) and 2 % of gas volume fraction.

Snow thickness above the level ice varied in the range 2–11 cm, while snow thickness above the ridge was 0–13 cm. For measured snow thickness and estimated snow thermal conductivity at the ridge, the heat transfer coefficient H of air and snow varied in the range 1.4–21 W/m^{2}K.

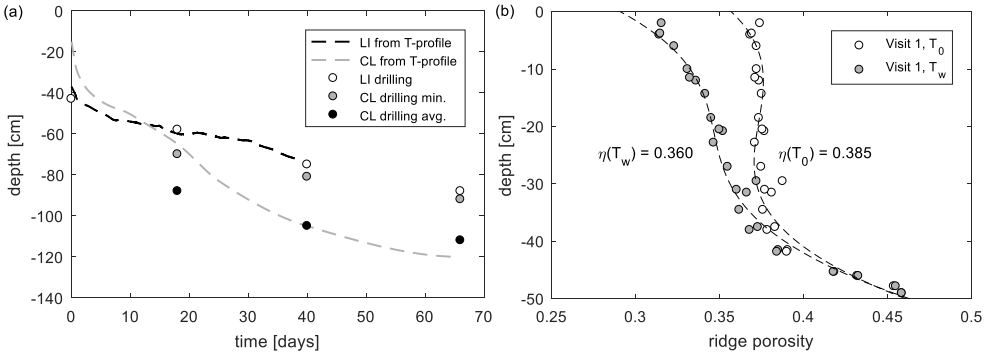

Figure 7. Ice draft development (a) and ridge porosity profile for visit 1 at in-situ and water temperature (b).

Ridge total porosity values estimated for measured level ice in-situ and water temperature, salinity, and density are presented in Figure 7b. Due to the block average initial temperature of -7.8 °C, the ridge total porosity should decrease from 0.39 to 0.36. Ridge initial macroporosity was found from its morphology at visit 1 and 4 (Figure 8).

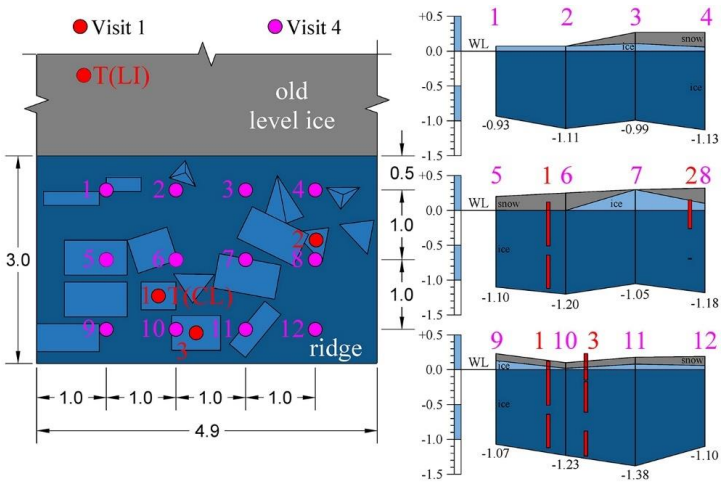

Figure 8. Ridge vertical profiles during visit 1 and 4.

Table 1. Evolution of the main level ice and consolidated layer parameters

Parameter	Visit			
	1	2	3	4
Number of LI/CL cores	3/0	0/2	0/4	1/12
Min. CL thickness [m]	0.00	0.78	0.97	1.00
Avg. CL thickness [m]	-	0.96	1.13	1.20
LI thickness [m]	0.50	0.65	0.82	0.99
CL snow thickness [m]	0.00	0.13	0.07	0.09
LI snow thickness [m]	0.02	0.11	0.02	0.05
CL salinity [ppt]	3.8	4.2	3.8	4.1
LI salinity [ppt]	3.8	-	-	4.6
FDD [°d]	705	915	1228	1421
Ridge macroporosity	0.36	-	-	0.00

4 Results

Before the analysis of the provided fieldwork experiment, we will present more general results of our analytical and numerical investigations, where we will try to improve understanding of ridge thermodynamics and validation methods for ridge models. We will focus on thermodynamic effects from the main differences between level ice and ice ridge including ridge sail, snow on its top, ridge rubble, and ridge inhomogeneity (section 4.1). After that, we will describe details of the consolidation experiment and how general conclusions can help with its analysis and model validation (sections 4.2–4.5).

4.1 Sail and rubble effects

The presence of the sail has two different effects, its thickness provides additional insulation and delays consolidation while the irregular surface gives a higher exposed area and enhances the consolidation. The snow cover is a key factor here as it strongly affects the heat transfer coefficient H from Eq. (15) and with this the sail effect. Below we will examine how the snow

cover affects the analytical solution of the surface flux (by the fin performance ϵ_s in Eq. (13) and further, apply the two-dimensional numerical solution (Section 2.4). The solution for the fin performance shows that it increases with increasing snow thickness, and for snow thicknesses above 1 cm it predicts that the presence of a sail increases the heat flux compared to the same snow cover of flat ice (Figure 9). This solution (Appendix C) assumes that the temperature below the sail T_{base} (base temperature) is not affected by the surface conditions and this is not strictly true. Numerical simulations confirm the general trend of increasing the effect of thicker snow but modifies the effect for thin snow covers.

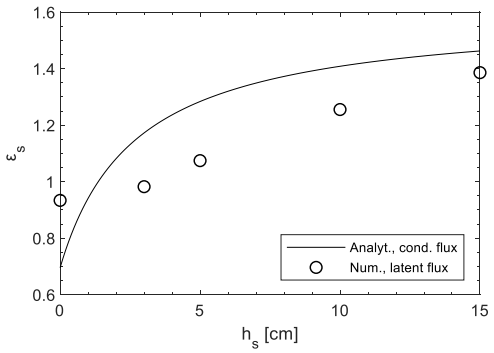

Figure 9. Sail performance vs snow thickness for 15 cm sail height and 50 cm sail width from the analytical sail model and its effect on consolidated layer thickness from the numerical convective model.

Defining lower boundary of the consolidated layer in the ridge is also complicated by its inhomogeneity. In our consideration, the thickness of the consolidated layer is defined by newly formed ice in the void (Figure 2b). In the void the consolidated layer thickness similarly to the level ice thickness can be estimated from temperature profiles as the ice temperature is always less than equal to T_f, and the water below is always warmer or equal to T_f similar (Figure 2a). In the block, the boundary of the consolidated layer is somewhere inside the block (Figure 2c) and the temperature profile cannot be used the same way as above to define the thickness of the consolidated layer. The spatial resolution of temperature measurements combined with the non-linear temperature profile close to the bottom of the block and the daily variations in the top makes it necessary to extrapolate. A linear section of temperature profile for extrapolation was chosen by cutting off upper nodes affected by daily temperature changes and bottom nodes in the non-linear part. We cut off nodes in the upper 20 cm of the profile below the snow-ice interface and nodes in the bottom part of the profile where the temperature is higher than equal to $T_f - \Delta T$. Threshold ΔT can be set for example 1 °C or 0.5 °C. Further, a linear temperature profile is extrapolated to T_f, and the thickness of the consolidated layer in the block is defined.

Figure 10 shows temperature profiles through the void and block at two different time moments of our numerical simulation. Defined according to the description above, the boundary of the consolidated layer in a void and a block are shown on the plots. The figure illustrates that there may be significant differences in the estimated thicknesses of the consolidated layer (Δh_c up to 0.2 m) for the chosen threshold ΔT of 1 °C. Considering our minimum definition of the

consolidated layer (Figure 1), which corresponds with the one derived from a void, we call the difference in estimated thicknesses as an overestimation.

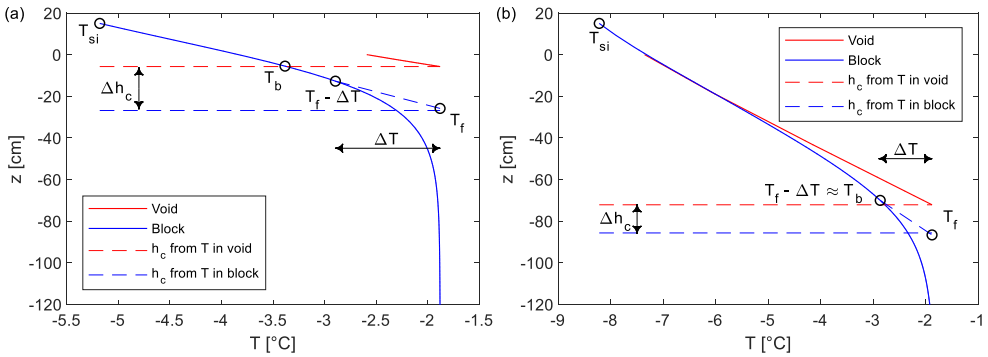

Figure 10. Temperature profiles in ridge void and block after 1 day (a) and after 25 days (b) of consolidation from the numerical model.

Numerical simulations of this overestimation were done without sail and snow, and with 15 cm high sail and 7 cm thick snow to check how temperature profiles are affected by snow and sail. The ice thickness overestimation decreased with increasing consolidated layer thickness and depended on sail and snow (Figure 11a). It also depended on the ice temperature (not shown in the figure). A dimensionless block temperature θ_b can be defined as:

$$\theta_b = \frac{T_b - T_f}{T_{si} - T_f} = \frac{\Delta T_b}{\Delta T_c + \Delta T_b}, \tag{24}$$

where T_b is the temperature at the center of the block at the bottom level of the consolidated layer with a minimum thickness (Figure 10a).

The thickness overestimation Δh_c depends on the block temperature T_b (Figure 10a) as:

$$\frac{\Delta h_c}{h_c}(\Delta T = \Delta T_b) = \theta_b \tag{25}$$

From the resistive analytical model described in section 2.3, the dimensionless block temperature θ_b is defined by the block thickness w, and the consolidated layer thickness h_c as:

$$\theta_b = \frac{R_b}{R_c + R_b} = \left(1 + \frac{7h_c}{w}\right)^{-1} \tag{26}$$

The condition $\Delta T = \Delta T_b$ is complicated to use for the thickness estimation in experiments because it requires knowledge of the consolidated layer thickness. For the smaller thresholds $\Delta T < \Delta T_b$ the values of the thickness overestimation are larger and cannot be described by the resistive model. The larger thresholds $\Delta T > \Delta T_b$ correspond with smaller overestimations but can dramatically increase errors of the temperature profile extrapolation, especially for the initial phase of the consolidation. Thus, it is recommended to use threshold range close to the ΔT_b for the later stages of the consolidation. For our experiments ΔT_b lays in the range between $(T_f - T_{si})/5$ and $(T_f - T_{si})/10$ during the most of the time (Figure 11b).

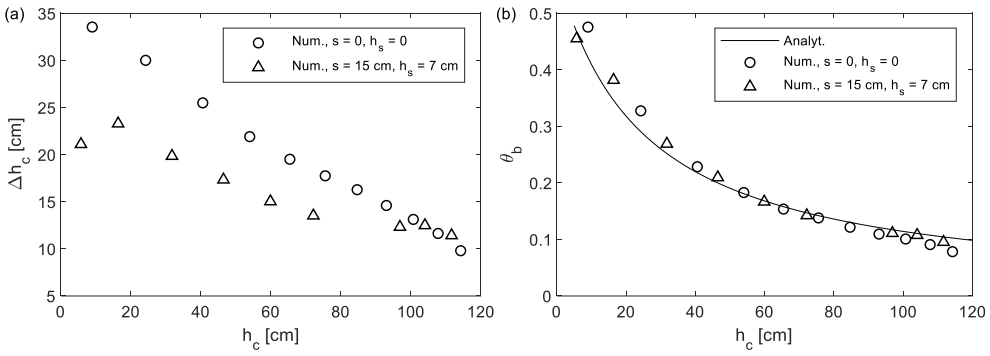

Figure 11. Thickness overestimation Δh_c based on temperature profiles from numerical modelling using $\Delta T = 1$ ℃ (a) and block bottom dimensionless temperature θ_b based on analytical and numerical models (b).

In comparison to thickness measurements, which are representing average heat transfer over ridge void and surrounding blocks, temperature profile measurements are representing only local vertical heat transfer. As can be seen from Figure 10, large-scale ridges are inhomogeneous and vertical temperature gradient can be significantly different for different parts of a ridge. It can be important for the validation of an analytical consolidation model because almost any analytical model is only able to describe average heat flow through different parts or the whole ice ridge.

4.2 Top surface heat balance

The air and snow-ice interface temperature of level ice and the ridge are shown in Figure 12. The ridge top surface was colder than of level ice during the first 20 days of our experiment. The thermal resistance of air was much smaller than thermal resistances of both ice and snow: the average air temperature was only 0.3 °C lower than the measured top surface temperature of snow, while the average difference between the top and bottom surface temperatures was 8.3 °C for ice and 4.1 °C for snow.

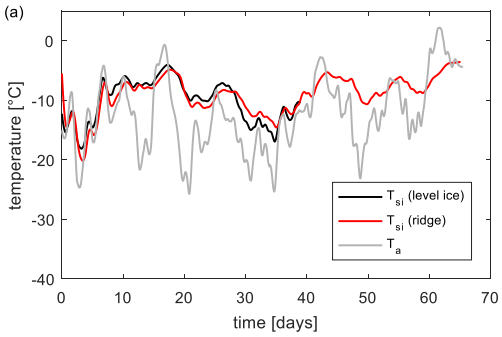

Figure 12. Snow-ice interface temperature T_{si} and air ambient temperature T_a development for level ice and the ridge.

Let us proceed with examining how the analytical models (Section 2.3) with the two different

atmospheric fluxes (simple convective or more advanced radiative) predict the air-snow temperature T_{as}. We assume that the air temperature was known and define a temperature difference over the air boundary layer $\Delta T_a = T_{as} - T_a$. The radiative model is more complicated and to estimate its sensitivity, the uncertainty of the three following aspects were examined:

- Longwave radiation model: Maykut (1986), Rosati and Miyakoda (1988).
- Cloudiness: from the weather station in Longyearbyen, from the ICON model for Svea.
- Turbulent heat transfer coefficient: Smith (1988), Rosati and Miyakoda (1988).

The analytical dependence of the air-snow temperature on the ice thickness for the average experimental meteorological conditions is given in Figure 13a and shows that the convective model predicts a warmer snow surface. The convective model does, by definition, predict a snow or ice top surface temperature T_{as} warmer than the air temperature T_a (if T_a is colder than water). In nature, the snow surface can be colder than the air temperature (Figure 13 b) and this is known as ground inversion This phenomenon can only be predicted by the radiative model. Figure 13b shows ΔT_a derived directly from the level ice measurements and for the two models based on meteorological data and experimentally measured conductive heat flux q_c and not including snow parameters using Eq. (3) and Eq. (5).

The turbulent heat transfer coefficient has relatively little effect of 2 % of the heat flux. Averaged over time difference between analytical and experimental values of ΔT_a was in the range of -2.5…0.6 °C for different parametrisation giving the best fit for the models of Maykut (1986), Smith (1988), and cloudiness data from the Longyearbyen weather station. A simple convective model by Adams et al. (1960) gave a difference of 1.7 °C (Figure 13b).

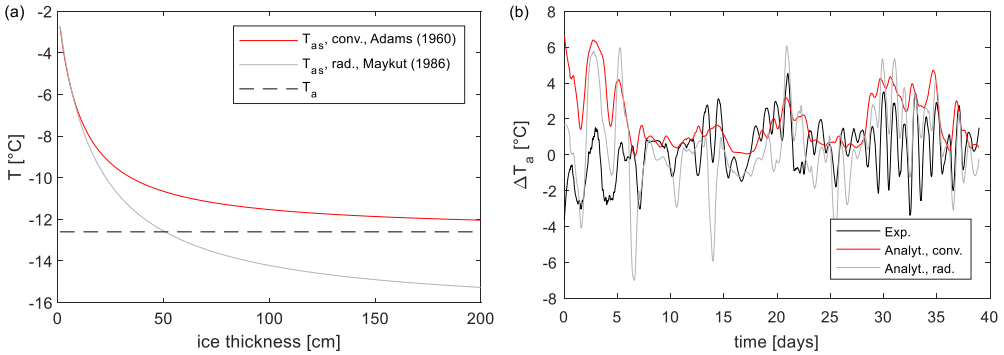

Figure 13. Surface temperature T_{as} vs ice thickness h_i for the average experimental meteorological conditions (a) and the difference between the top surface and air temperatures ΔT_a from the level ice experiment, radiative and convective analytical models based on experimentally measured conductive heat flux q_c and meteorological data (b).

As a conclusion, it can be said that while radiative models can predict top surface temperatures more accurately, an error of the convective model is small enough considering its simplicity and applicability for resistive thermodynamic models.

4.3 Snow conditions

Snow thickness between visits was estimated using Eq. (9). In the first approach snow thermal conductivity value was chosen arbitrarily. From the values of snow thickness, time moments of snow thickness transition were found. Snow thickness values were linearly interpolated to fit the shape of estimated values and measured snow thickness values. After that thermal conductivity values were estimated based on assumed snow thickness in time. The final value of snow thermal conductivity was obtained using statistical analysis of estimated values, based on conductive heat flux balance in snow and ice.

The snow layer has thermal resistance comparable with ice; also, it is a material with high uncertainties in its thermodynamic characteristics. Snow thickness was measured directly only during four visits. The snow thermal conductivity value of 0.21 Wm^{-2} was obtained based on the level ice temperature profile and four in-situ measurements of snow thickness, requested the fit of thermal resistance values Eq. (9). Further, the reverse task can be solved. Assuming a constant snow thermal conductivity and knowing ice temperature profile, snow thickness in time during the experiment was estimated (Figure 14) and further used in numerical modelling. Both for level ice and model ridge snow thickness was considerably low except days 12–21.

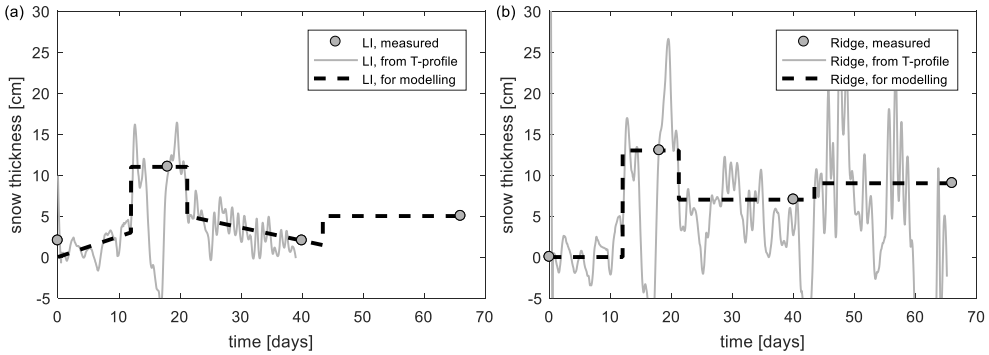

Figure 14. Snow thickness above level ice (a) and consolidated layer (b) vs time.

The analysis of snow thickness effects on heat transfer in the ridge is more complicated than for pure one-dimensional level ice. The temperature profile in ridge blocks is non-linear even under steady-state ambient conditions: temperature gradient is slightly lower in sail (Eq. (48) and is also decreasing towards the block bottom. With our measured snow thickness and estimated snow thermal conductivity, the heat transfer coefficient H varied in the range 1.4–21 W/m^2K according to Eq. (15).

4.4 Vertical heat fluxes

In two previous sections we estimated the main parameters of air and snow models fitting our field observations. It is of interest to see how these models can predict heat fluxes found experimentally from ice temperature, density, and salinity vertical profiles. Analytically and numerically estimated heat fluxes are only based on meteorological data and measured or estimated ice and snow thermodynamic parameters. The average level ice heat flux from convective and radiative models are 7 % and 3 % lower than from the experiment (Figure 15a).

Modelling and validation of heat fluxes for ridges are much more complicated due to its inhomogeneity and corresponding different boundary conditions at different vertical profiles. Figure 15b shows the results of the simplest “flat” analytical models of ridge consolidation. In that model there is no sail. Our experimental temperature profile was measured in the ridge block. Experimental values from the first 4 days are not presented because not enough sensors were frozen for heat flux estimation. The “flat” analytical radiative model gives 6 % higher flux than experimentally estimated, the convective model gives 5 % lower flux for days 5–66 of our experiment.

There is a difference between average fluxes in voids and blocks. In our numerical radiative model heat flux in the void was 22.6 W/m^2, while average flux in the block was 19.3 W/m^2, significantly closer to the experimental heat flux of 19.0 W/m^2. As it was described in the sail effect section, the largest heat flux increase is only observed in the vicinity of sail walls, while heat fluxes in the middle of block and void are almost equal.

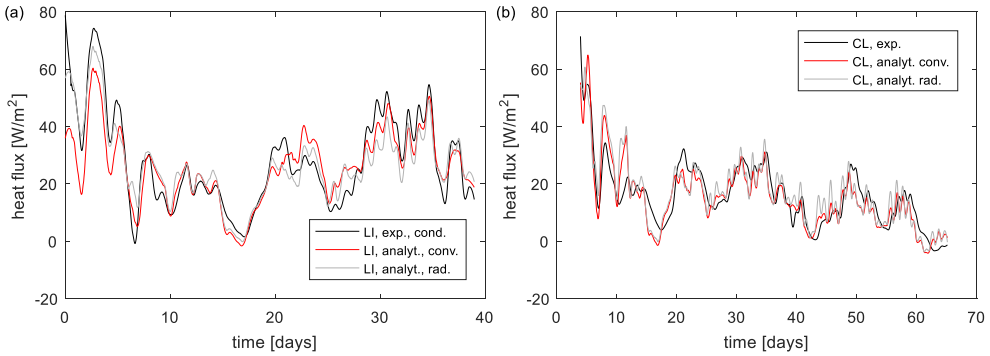

Figure 15. Vertical heat fluxes from experiment, convectional and radiative analytical models in level ice (a) and in the ridge (b).

As a summary, our analytical and numerical models are predicting heat fluxes equally accurate for level ice and ridges, while the more advanced radiative model is performing slightly better than convective (Table 2).

4.5 Ice thickness

Level ice thickness from direct measurements at visit 4 was 99 cm including 4 cm of top surface growth. Our convective and radiative analytical models predicted the thickness of 95 cm and 102 cm correspondingly (Figure 16a), while numerical models gave 94-95 cm. The measured consolidated layer thickness was 120 cm, while convective and radiative analytical models gave 113 cm and 123 cm (Figure 16b). The numerical model predicted a slightly lower thickness due to considering thermal inertia and ridge initial phase. For both level ice and consolidated layer, the numerical radiative model gave the closest values to the experimental thickness.

Higher consolidation values from the temperature profile are coming from the method overestimation when the temperature information is derived from the ridge block, not from the void. This effect is eliminated at the time of visit 4 because the consolidated layer reached the

block bottom in the vertical profile of the thermistor (Figure 16b). Similarly, there was no significant thickness overestimation in the range of 50-65 cm which corresponds to the void depth, measured during visit 1 (Figure 8).

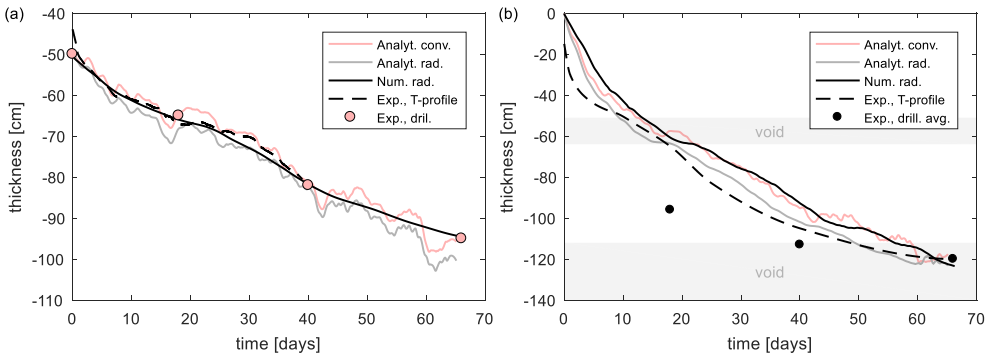

Figure 16. Level ice (a) and consolidated layer (b) thickness vs time. The grey shaded area corresponds to the voids found from drilling during visit 1.

It is convenient to compare growth prediction from different models and experimental sources in one table (Table 2). Results of model application are quite similar for both types of ice: convective models are underestimating ice growth, while radiative models are giving values closer to experimental thicknesses.

Table 2. Ice thickness and mean vertical heat flux values after visit 4 (visit 3)

Ice type	Model	s [m]	h analyt. [m]	h num. [m]	h exp. [m]	q analyt. [W/m^2]	q num. [W/m^2]	q exp. [W/m^2]
LI	Conv.	0	0.95	0.94	0.95	20.3 (25.9)	19.9 (27.0)	(27.9)
	Rad.	0	1.02	0.95		21.2 (27.0)	20.9 (28.3)	
CL	Conv.	0	1.13	1.14	1.20	20.3	20.3	19.0
	Rad.	0	1.23	1.20		21.6	21.0	
	Conv.	0.15	1.21	1.16		21.4	19.4	
	Rad.	0.15	-	1.23		-	22.2	

It is of interest to evaluate thickness overestimation for the described experiment. We should assume as reference results of the numerical modelling using a radiative balance (Figure 16b). As it was described for the general case, thickness overestimation mainly depends on ice temperature and its thickness (Figure 17a). The first part of our experiment (days 0–35) with a thinner consolidated layer was performed at significantly lower air temperatures than the second part (days 35–66). The temperature effect on thickness overestimation was almost constant, and the scale effect was considerably low (Figure 17b).

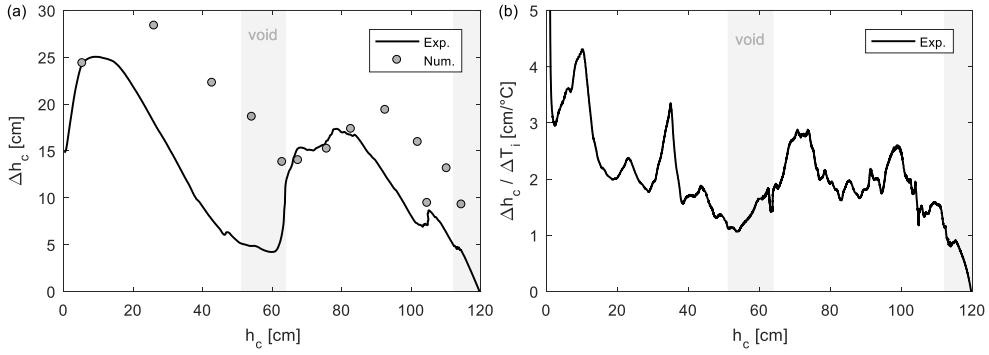

Figure 17. Total thickness overestimation Δh_c (a) and its values per temperature difference in ice $\Delta T_i = T_f - T_{si}$ (b) vs consolidated layer thickness. The grey shaded area corresponds to the voids found from drilling during visit 1.

The calculated thickness overestimation was in the range of 0–25 cm or 0–5 cm/°C with a significant drop when the consolidated layer was growing in voids.

5 Discussion

5.1 Validation of consolidation models

There are two main options for validation of a model using field experiments in ridge consolidation: to compare temperature profiles or coring profiles. The accuracy of both methods is influenced by the inhomogeneity of the bottom surface of the consolidated layer. As was observed in previous studies (Blanchet, 1998; Høyland, 2002b; Timco and Burden, 1997), the consolidated layer thickness measurements from coring have too large variability and errors to be suitable for consolidation model validation. Høyland (2002) reported a 26 % difference in consolidated layer thickness measurements performed by drilling and by temperature profile analysis. Timco and Burden (1997) analyzed maximum, minimum and average thickness of the consolidated layer for 25 ridges and found thickness variability larger than 3. This study attempted to show limitations and errors which can be observed in the analysis of ridge temperature and estimated thickness.

Consolidated layer thickness, as the key engineering parameter of an ice ridge, is one of the most important outputs of any fieldwork or modelling. Meanwhile, any consolidation model can give a value of minimum thickness not including the thickness of ice blocks, partly frozen into a consolidated layer. Because of that a simple condition of an ice and water boundary, where the temperature is equal to the water freezing point, would give thickness including ice blocks, inside which ice temperature is exponentially approaching freezing temperature. This condition is impractical because it is not providing values of interest (minimum consolidated layer thickness) and it also requires accurate equipment to distinguish small temperature differences. As it was shown in the paper, it is possible to use more advanced conditions of the ice-water interface, but even such algorithms can give overestimated values of consolidated layer thickness.

Another way to validate the consolidation model is to compare values of vertical heat fluxes or corresponding vertical temperature gradients. But heat fluxes are much more than thickness are affected by local conditions. And to analyse the temperature profile, it is important to know its exact location, which is especially complicated for underwater ridge parts. Vertical heat flux under sail, below upper 20 cm affected by daily temperature deviations, and above bottom part of the consolidated layer can give a good estimate of heat transfer after the initial phase of consolidation. It is important to consider that large-scale ridges are not homogenous media and because of that heat fluxes are not only converting in vertical ice growth but also horizontal growth and thermal inertia.

As a conclusion, one should consider that thickness estimation from a temperature profile is more complicated for ridges and can give significant errors. At the same time, measured heat fluxes are also not always equal to the latent heat fluxes related to the change of consolidated layer thickness.

Radiative models are predicting faster ice growth under any conditions. Meanwhile, the difference between radiative and convective models' predictions can be significantly lowered due to the presence of the shortwave radiation. This explains why both radiative and convective numerical models accurately predict ice growth.

5.2 Thickness overestimation

At the level of minimum consolidated layer thickness, the temperature in the surrounding ice blocks can be significantly colder depending on their distance from the block center. The thermistor string for the described experiment was placed in the ice block. From Figure 16b it can be seen, that thickness values from the temperature profile are always approximately 15 cm larger than of analytical solution, while vertical heat fluxes in fully consolidated parts are almost equal for both the experiment and the model.

The heat fluxes in level ice and the consolidated layer below water level were almost equal during the first 25 days of the experiment when the snow thickness above both types of ice was in the same range. Level ice thickness and corresponding thermal resistance were higher only during the first 12 days. It shows the importance of coupling of air convection and conduction through snow and ice.

Even though thickness estimation with a smaller threshold is giving overestimated values, it is still preferable over usage of only temperature measurements from the top part of the consolidated layer. Accuracy of such a method is highly dependent on the accuracy of the temperature measuring device and even small error can lead to high errors in thickness.

Another uncertainty to be considered is the drilling diameter of a borehole for the thermistor. The presence of such unfrozen void around thermistor can decrease values of thickness overestimation and to make temperature profile analysis more complicated. During the consolidation process, such a void will be frozen only after a front of significant temperature gradients reached that part of the drill hole. This can explain slightly lower thickness overestimation in our experiment in comparison to the numerical model result since it is not considering the presence of any voids around the virtual thermistor.

When first-year ridges get older the rubble changes so that it becomes more porous. This process will reduce the thickness overestimation or the different temperature distributions in void and block.

5.3 Ice salinity

The increasing trend of level ice salinity can be explained by the presence of approximately 12 cm thick part of snow ice at the beginning of the experiment. The decreasing portion of less saline snow ice can explain the increase of level ice salinity with time.

Slightly lower ridge salinity in comparison to level ice can be explained by stronger ice desalinization after warming during the initial phase according to the brine dynamics model by Griewank and Notz (2013). It is well known that ice salinity depends on the ice growth rate (Kovacs, 1996). Vertical heat fluxes were almost equal in the consolidated layer and in level ice during the first 25 days when the upper 70 cm of the consolidated layer was formed. Ridge multi-directional desalinization process requires further investigations.

We observed a significant ice growth between visits 3 and 4 during relatively warm temperatures (Figure 16): 27 % of level ice thickness change occurred together with 35 % of FDD, increased solar radiation, and relatively thick snow. According to our modelling results, it was partly caused by the growth of the ice microporosity during its warming, which depends on its salinity. Similar growth was not observed at the modelling results with a thermodynamic model of fresh ice.

5.4 Errors sources

Authors are aware that there are numerous ways of snow thickness distribution over an ice ridge which can influence effects from a sail on consolidation rates. We presented both results of analytical and numerical models with and without a sail. At the same time, to analyse the temperature profile above the waterline, it is necessary to have a physical model of a ridge sail.

There are two main parameters used for consolidation model validation: heat fluxes and ice thickness. The accuracy of heat flux measurements is limited by the accuracy of thermistors and the evaluation of thermal conductivity value from the ice temperature, salinity, and gas volume. The accuracy of consolidated layer thickness is mainly limited by the ridge inhomogeneity and accounting of unconsolidated rubble into total ice thickness.

6 Summary and conclusions

A medium-scale sea ice ridge was produced ridge in the Van Mijenfjorden, Svalbard in the winter of 2017. The thickness and properties of the level ice that was used to make the ridge were measured and thermistor-strings were installed in the ridge and the neighboring level ice. The ridge was visited four times for drilling and sampling. The experimental results provided enough information for accurate growth prediction and validation of ridge consolidation models.

Two analytical resistive models and two two-dimensional discretized numerical models are

presented. All models need general met-ocean conditions and general ice physical properties. Both analytical models account for the air-snow-sail layer, but only the ridge model includes the effect of the inhomogeneous top and bottom surfaces of the consolidated layer. The models were validated against the field measurements, and the furthers details of the analytical models were validated against the numerical model.

The main conclusion is:

- The analytical resistive ridge model with convective atmospheric flux captures the relevant phenomena well and could be used for prediction of the consolidated layer thickness in probabilistic analysis of ice actions on structures.

Additional important conclusions are:

- During our field experiment, the level ice grew from 50 to 99 cm, the consolidated layer grew up to 120 cm, and the macroporosity was about 0.36.
- The model including the radiative terms predicted heat fluxes in level ice and ridge better than the convective model but required more input data.
- Vertical temperature profiles through the consolidated layer and further into respectively a void and an ice block may result in significantly different estimations of the consolidated layer thickness.
- The difference between fresh and saline ice growth is equally important for level ice and ice ridges, but its values are becoming significant only during the warming phase.

Acknowledgments

The authors wish to acknowledge the support of the Research Council of Norway through the Centre of Research based Innovation SAMCoT grant 203471 (Sustainable Arctic Marine and Coastal Technology) and the University Centre in Svalbard (UNIS). We also would like to thank Sveinung Løset, Wenjun Lu, and Anne-Niekolai Heijkoop for the help with fieldwork organization.

Appendix A. Radiative model

The net longwave radiation from the ocean surface can be found as (Rosati and Miyakoda, 1988):

$$q_{LW} = -\delta\sigma T_a^3 \left(T_a \left(0.254 - \frac{0.0066}{132.22} e_a \right) (1 - C_l c) + 4(T_{as} - T_a) \right), \quad (27)$$

where $\delta = 0.95$ is the emissivity of the sea surface relative to the black body, σ is the Stefan-Boltzmann constant, e_a is the near-surface vapour pressure at air ambient temperature T_a, $C_l = 0.8$ is the cloud coefficient, c is the fractional cloud factor.

Alternatively, the net longwave radiation can be calculated as (Maykut, 1986):

$$q_{LW} = \varepsilon\sigma T_{as}^4 - \varepsilon^*\sigma T_a^4, \quad (28)$$

where $\varepsilon = 0.99$ is the snow longwave emissivity, and ε^* is the effective emissivity for the atmosphere, which can be found as (Maykut, 1986):

$$\varepsilon^* = 0.7855(1 + 0.2232\, c^{2.75}) \quad (29)$$

The net shortwave radiation q_{SW} can be found as (Shine, 1984):

$$q_{SW} = (1 - \alpha)\Phi_c \frac{S\cos^2 Z}{0.0455 + 1.2\cos Z + (1 + \cos Z)10^{-5}e_a}, \quad (30)$$

where α is the albedo of ice or snow, Φ_c is the cloud correction factor, S is the solar constant, and Z is the solar zenith angle.

Cloud correction factor Φ_c can be calculated as (Laevastu, 1960):

$$\Phi_c = 1 - 0.6c^3 \quad (31)$$

Sensible and latent heat fluxes can be found as (Maykut, 1986):

$$q_s = \rho_a c_a C_s V_w (T_a - T_{as}), \quad (32)$$

$$q_e = 0.622\rho_a L_e C_e V_w\, (e_a - e_{s0})/P, \quad (33)$$

where ρ_a is the density of the air, c_a is the specific heat of the air, C_s and C_e are the bulk transfer coefficients for sensible and latent heat, V_w is the wind speed at the reference height, L_e is the latent heat of vaporization, RH is the relative humidity, e_{s0} is the saturation vapour pressure at surface temperature T_{as}, P is the total atmospheric pressure.

The vapour pressure e can be expressed through the saturation vapour pressure e_s at the given temperature and relative humidity RH as:

$$e = \mathrm{RH} \cdot e_s \quad (34)$$

The saturation vapour pressure e_s at the given temperature T can be found as (Tsonis, 2007):

$$e_s = 611\exp(19.83 - 5417/(T + 273.15)) \quad (35)$$

The bulk transfer coefficients for sensible and latent heat C_s and C_e mainly depends on wind speed and the temperature difference between surface and air $T_{as} - T_a$. For surfaces warmer than air these coefficients are usually in the range of $(1 \ldots 2) \cdot 10^{-3}$ for the elevation of 10 m (Smith, 1988).

Appendix B. Saline ice growth

Prediction of saline ice growth includes additional complications connected to its temperature-dependent latent and sensible heat. Thermal inertia for saline ice can be divided into specific heat of pure ice and brine, and change of solid fraction at different temperatures, which requires freezing or melting of pure ice inside sea ice. The sum of both effects can be presented via the enthalpy of sea ice:

$$H_{si} = -L_i m_i - m_i \int c_i dT - (1 - m_i) \int c_b dT \quad (36)$$

Enthalpy values at different temperatures illustrate the difference from pure ice growth model: depending on ice temperature and salinity only a certain mass fraction should be frozen, while additional negative heat should be spent to adjust ice temperature to a certain temperature profile. The zero value of enthalpy can be chosen arbitrarily and assumed zero at sea ice freezing point.

The sea ice solid mass fraction can be found as:

$$m_i = 1 - \frac{S_i}{S_b} \tag{37}$$

The sea ice solid volume fraction can be found as:

$$v_i = \frac{1 - \frac{S_i}{S_b}}{1 + \frac{S_i}{S_b}\left(\frac{\rho_i}{\rho_b} - 1\right)} \tag{38}$$

The thermal conductivity of sea ice is equal to (Notz, 2005):

$$k_{si} = v_i k_i + (1 - v_i) k_b, \tag{39}$$

The heat capacity of sea ice per unit mass c_{si} can be found as (Notz, 2005):

$$c_{si} = c_i - L_i \frac{\alpha S_i}{T^2}, \tag{40}$$

where $\alpha = -0.05411$ is the slope of the liquidus.

The density of sea ice was found as (Notz, 2005):

$$\rho_{si} = v_i \rho_i + (1 - v_i) \rho_b, \tag{41}$$

The density of pure can be found from (Pounder, 1966) as:

$$\rho_i = 916.8 - 0.1403 \cdot T \tag{42}$$

The thermal conductivity of pure ice cab found from Yen (1991) as:

$$k_i = 2.21 - 1.00 \cdot 10^{-2} T + 3.44 \cdot 10^{-5} T^2 \tag{43}$$

Pure ice heat capacity can be found as (Weast, 1977):

$$c_i = 2112.2 + 7.6973 \cdot T \tag{44}$$

The latent heat of fusion L_i of water is 333.5 kJ/kg (Feistel and Hagen, 1998). The enthalpy value for ice with any temperature and salinity distribution is defining how much energy should be extracted from the water for its consolidation and cooling (Figure 18). As can be seen, enthalpy difference can be higher or lower than pure ice latent heat. Pure ice and brine sensible heat are decreasing sea ice growth at low temperatures in comparison to Stefan's equation. In contrast, the low solid fraction of warm sea ice can lead to faster growth in comparison to Stefan's equation and pure ice growth. For salinity of 5 ppt warm ice at water freezing temperature requires 15 % less negative energy to be formed.

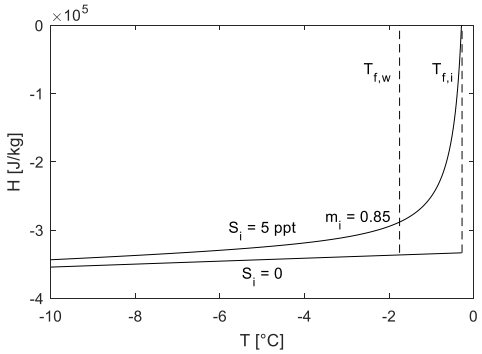

Figure 18. Saline and fresh ice enthalpy vs temperature.

The difference between the top and bottom heat fluxes in ice is spent on ice heating or cooling. When ice is thick enough, the bottom heat flux depends only on average top surface temperature.

For the field data analysis, usage of the bottom ice boundary for heat flux calculation can be impractical due to high uncertainties in salinity and temperature profiles, while only the change of total ice volume is the main value of interest. The thickness of saline ice including sensible heat can be estimated from pure ice thickness without sensible heat from the solid volume fraction as:

$$h_{si} = h_i \frac{\rho_i L_i}{\rho_{si} \Delta H_{si}} \tag{45}$$

Appendix C. Extended surface theory

Any finned surface includes thermal conduction through the fin and thermal convection at its surfaces. Fin can be described by its thickness w and length l, which define two main parameters: top perimeter $P = 2(w + l)$ and cross-section area $A_c = wl$. Heat transfer equation of a uniform fin cross-section in the vertical direction can be found as (Incropera et al., 2013):

$$\frac{d}{dz}\left(A_c \frac{dT}{dx}\right) - \frac{HP}{k_i A_c}(T - T_a) = 0 \tag{46}$$

This equation is convenient to present using dimensionless form using constant $m^2 = HP/k_i A_c$. To solve that equation boundary condition should be specified including the temperature at the base of the fin $T(0) = T_{base}$ and boundary condition at the top surface $HA_c(T(s) - T_a) = -k_i A_c dT/dx|_{z=s}$. Vertical heat flux through the sail is equal to (Incropera et al., 2013):

$$q_f = \sqrt{HPk_i A_c}(T_{base} - T_a) \frac{\sinh ms + (H/mk_i)\cosh ms}{\cosh ms + (H/mk_i)\sinh ms} \tag{47}$$

For analysis of temperature profiles, which are one of the primary measurements of any field experiments, it is also useful to know the temperature distribution above the consolidated layer,

which can be expressed as (Incropera et al., 2013):

$$\frac{T - T_a}{T_{base} - T_a} = \frac{\cosh m(s - z) + (H/mk_i) \sinh m(s - z)}{\cosh ms + (H/mk_i) \sinh ms} \tag{48}$$

This equation can quantify the difference between heat flux at the water level and the snow-ice interface.

Appendix D. Mechanical parameters

12 vertical and horizontal level ice samples for uniaxial compression were collected during visit 2. 4 vertical level ice and 17 vertical ridge samples were also collected during visit 4. Tests with these samples were performed in the lab at a temperature near -10 °C. 38 in-situ compression tests were performed during visit 3, including 32 for level ice and 6 for the ridge.

Results of in-situ and laboratory uniaxial compression experiments, performed during visits 2, 3 and 4, are presented in Figure 19. The in-situ average compression strength of horizontal level ice samples during visit 3 was 3.2 MPa, and 8.1 MPa for vertical level ice samples. Horizontal samples from the consolidated layer had a strength of 4.4 MPa, and 6.1 MPa for vertical samples from the consolidated layer.

In laboratory conditions at the temperature of around -10 °C, the average strength of horizontal level ice samples was 4.5 MPa at visit 2, vertical strength was 7.7 MPa at visit 2 and 5.0 MPa at visit 4. The vertical consolidated layer strength was 5.9 MPa.

The strength of level ice for visit 2 was measured in different directions for horizontal samples: for EW direction it was 6.0 MPa, for NS it was 3.4 MPa, for 45° to NS it was 4.2 MPa.

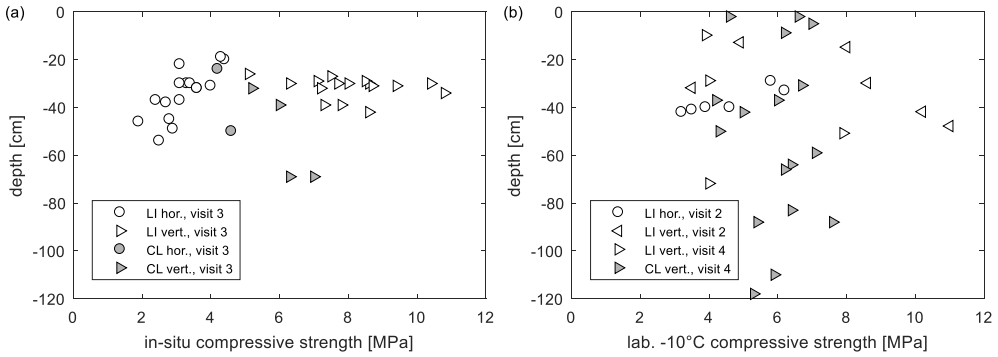

Figure 19. Uniaxial compressive strength for in-situ (a) and -10 °C (b) temperatures vs depth.

The samples from the ridge had a much higher percentage of failures in a ductile way in contrast to level ice. Strength relations of consolidated layer and level ice in the presented experiment are in good agreement with the results from Shafrova and Høyland (2008). The results of the splitting test for the ridge is described in Lu et al., 2019.

References

Adams, C.M., French, D.N., Kingery, W.D., 1960. Solidification of Sea Ice. J. Glaciol. 3, 745–761. https://doi.org/10.3189/S0022143000018050

Armstrong, T., 1972. World Meteorological Organization. WMO sea-ice nomenclature. Terminology, codes and illustrated glossary. Edition 1970. Geneva, Secretariat of the World Meteorological Organization, 1970. [ix], 147 p. [including 175 photos] + corrigenda slip. (WMO/OMM/BMO. J. Glaciol. https://doi.org/10.1017/s0022143000022577

Blanchet, D., 1998. Ice loads from first-year ice ridges and rubble fields. Can. J. Civ. Eng. 25, 206–219. https://doi.org/10.1139/l97-073

Calonne, N., Flin, F., Morin, S., Lesaffre, B., Du Roscoat, S.R., Geindreau, C., 2011. Numerical and experimental investigations of the effective thermal conductivity of snow. Geophys. Res. Lett. 38, 1–6. https://doi.org/10.1029/2011GL049234

Cox, G.F.N., Weeks, W.F., 1983. Equations for Determining the Gas and Brine Volumes in Sea-Ice Samples. J. Glaciol. 29, 306–316. https://doi.org/10.3189/S0022143000008364

Feistel, R., Hagen, E., 1998. A Gibbs thermodynamic potential of sea ice, Cold Regions Science and Technology. https://doi.org/10.1016/S0165-232X(98)00014-7

Førland, E.J., Hanssen-Bauer, I., Nordli, P.Ø., 1997. Climate statistics and longterm series of temperature and precipitation at Svalbard and Jan Mayen, DNMI-Rapport, Klima.

Griewank, P.J., Notz, D., 2013. Insights into brine dynamics and sea ice desalination from a 1-D model study of gravity drainage. J. Geophys. Res. Ocean. 118, 3370–3386. https://doi.org/10.1002/jgrc.20247

Høyland, K.V., Jensen, A., Liferov, P., Heinonen, J., Evers, K.-U., Løset, S., Määttänen, M., 2001. Physical Modelling of First-Year Ice Ridges - Part I: Production, Consolidation and Physical Properties, in: Proceedings of the 16th International Conference on Port and Ocean Engineering under Arctic Conditions. pp. 1483–1492.

Høyland, K. V., 2007. Morphology and small-scale strength of ridges in the North-western Barents Sea. Cold Reg. Sci. Technol. https://doi.org/10.1016/j.coldregions.2007.01.006

Høyland, K. V., 2002a. Simulations of the consolidation process in first-year sea ice ridges. Cold Reg. Sci. Technol. 34, 143–158. https://doi.org/10.1016/S0165-232X(02)00002-2

Høyland, K. V., 2002b. Consolidation of first-year sea ice ridges. J. Geophys. Res. 107, 3062. https://doi.org/10.1029/2000JC000526

Incropera, F.P., DeWitt, D.P., Bergman, T.L., Lavine, A.S., 2013. Principles of heat and mass transfer, Water. https://doi.org/10.1016/j.applthermaleng.2011.03.022

Kovacs, A., 1996. Part I . Bulk Salinity Versus Ice Floe Thickness. CRREL Rep. 96, 1–16.

Laevastu, T., 1960. Factors affecting the temperature of the surface layer of the sea. Comment. Phys. Math. 25.

Leppäranta, M., Hakala, R., 1992. The structure and strength of first-year ice ridges in the Baltic Sea. Cold Reg. Sci. Technol. 20, 295–311. https://doi.org/10.1016/0165-232X(92)90036-T

Leppäranta, M., Lensu, M., Kosloff, P., Veitch, B., 1995. The life story of a first-year sea ice ridge. Cold Reg. Sci. Technol. 23, 279–290. https://doi.org/10.1016/0165-232X(94)00019-T

Lu, W., Shestov, A., Løset, S., Salganik, E., Høyland, K., 2019. Medium-scale Consolidation of Artificial Ice Ridge-Part II: Fracture Properties Investigation by a Splitting Test, Proceedings of the 25th International Conference on Port and Ocean Engineering under Arctic Conditions, Delft, The Netherlands.

Marchenko, A., 2008. Thermodynamic consolidation and melting of sea ice ridges. Cold Reg. Sci. Technol. 52, 278–301. https://doi.org/10.1016/j.coldregions.2007.06.008

Maykut, G.A., 1986. The Surface Heat and Mass Balance, in: The Geophysics of Sea Ice. Springer US, Boston, MA, pp. 395–463. https://doi.org/10.1007/978-1-4899-5352-0_6

Millero, F.J., 2010. Equation of State of Seawater. Oceanography 23, 18–33. https://doi.org/10.5670/oceanog.2010.21.COPYRIGHT

Notz, D., 2005. Thermodynamic and fluid-dynamical processes in sea ice. University of Cambridge.

Petrich, C., Langhorne, P.J., Haskell, T.G., 2007. Formation and struture of refrozen cracks in land-fast first-year sea ice. J. Geophys. Res. Ocean. 112, 1–13. https://doi.org/10.1029/2006JC003466

Pounder, E.R., 1966. The Physics of Ice. Am. J. Phys. https://doi.org/10.1119/1.1973537

Rosati, A., Miyakoda, K., 1988. A General Circulation Model for Upper Ocean Simulation. J. Phys. Oceanogr. 18, 1601–1626. https://doi.org/10.1175/1520-0485(1988)018<1601:agcmfu>2.0.co;2

Salganik, E., Høyland, K.V., 2018. Thermodynamics and Consolidation of Fresh Ice Ridges for Different Scale and Configuration, Proceedings of 24th IAHR International Symposium on Ice.

Salganik, E., Høyland, K.V., Maus, S., 2020. Consolidation of fresh ice ridges for different scales. Cold Reg. Sci. Technol. 171. https://doi.org/10.1016/j.coldregions.2019.102959

Sand, K., Winther, J.G., Maréchl, D., Bruland, O., Melvold, K., 2003. Regional variations of snow accumulation on Spitsbergen, Svalbard, 1997-99. Nord. Hydrol. https://doi.org/10.2166/nh.2003.0026

Schwerdtfeger, P., 1963. The Thermal Properties of Sea Ice. J. Glaciol. 4, 789–807. https://doi.org/10.1017/S0022143000028379

Shestov, A., Høyland, K., Ervik, Å., 2018. Decay phase thermodynamics of ice ridges in the Arctic Ocean. Cold Reg. Sci. Technol. 152, 23–34. https://doi.org/10.1016/j.coldregions.2018.04.005

Shine, K.P., 1984. Parametrization of the shortwave flux over high albedo surfaces as a function of cloud thickness and surface albedo. Q. J. R. Meteorol. Soc. https://doi.org/10.1002/qj.49711046511

Smith, S.D., 1988. Coefficients for sea surface wind stress, heat flux, and wind profiles as a function of wind speed and temperature. J. Geophys. Res. Ocean. 93, 15467–15472. https://doi.org/10.1029/JC093iC12p15467

Sturm, M., Holmgren, J., König, M., Morris, K., 1997. The thermal conductivity of seasonal snow. J. Glaciol. 43, 26–41. https://doi.org/10.1017/S0022143000002781

Timco, G.W., Burden, R.P., 1997. An analysis of the shapes of sea ice ridges. Cold Reg. Sci. Technol. https://doi.org/10.1016/S0165-232X(96)00017-1

Timco, G.W., Goodrich, L.E., 1988. Ice rubble consolidation. Proc. 9th Int. Symp. Ice, Int. Assoc. Hydraul. Eng. 1, 537–548.

Tsonis, A.A., 2007. An Introduction to Atmospheric Thermodynamics, An Introduction to Atmospheric Thermodynamics. Cambridge University Press, Cambridge. https://doi.org/10.1017/CBO9780511619175

Weast, R.C., 1977. CRC Handbook of Chemistry and Physics, 57th Edition, Handbook of Chemistry and Physics.

A.6. Paper 6

Experiments in scaled ice ridge and structure interaction in Aalto ice tank: thermodynamics of ethanol ice.

Salganik, E., Ervik, Å., Heinonen, J., Høyland, K.V., Perälä, I., Puolakka, O., Shestov, A., van den Berg, M.

Submitted to Proceedings of the 25th International Association for Hydro-Environment Engineering and Research (IAHR) International Symposium on Ice, Trondheim, Norway, under revision.

25th IAHR International Symposium on Ice

Trondheim, Norway, June 14 to 18, 2020

Experiments in scaled ice ridge and structure interaction in Aalto ice tank: thermodynamics of ethanol ice

Evgenii Salganik

Norwegian University of Science and Technology, Trondheim, Norway
E-mail: evgenii.salganik@ntnu.no

Åse Ervik

Multiconsult, Tromsø, Norway
E-mail: ase.ervik@multiconsult.no

Jaakko Heinonen

VTT Technical Research Centre of Finland Ltd., Espoo, Finland
E-mail: Jaakko.Heinonen@vtt.fi

Knut Vilhelm Høyland

Norwegian University of Science and Technology, Trondheim, Norway
E-mail: knut.hoyland@ntnu.no

Ilkka Perälä

VTT Technical Research Centre of Finland Ltd., Espoo, Finland
E-mail: Ilkka.Perala@vtt.fi

Otto Puolakka

Aalto University School of Engineering, Espoo, Finland
E-mail: otto.puolakka@aalto.fi

Aleksey Shestov

The University Centre in Svalbard, Longyearbyen, Norway
E-mail: Aleksey.Shestov@unis.no

Marnix van den Berg

Norwegian University of Science and Technology, Trondheim, Norway
E-mail: marnix.berg@ntnu.no

1 Abstract

This study characterizes the refreezing process of the deformed dopant ice. Both basin and laboratory experiments were conducted to study the influence of ethanol dopant on level ice and ice ridge consolidation rate and their mechanical properties. Experiments covered a ridge block thickness of 4 cm, ethanol concentration of 0.3% and freezing time of 7-12 hours at the temperature of -12 °C, experiments measuring flexural and compressive strength, and ice-structure interaction with cylindrical and conical structures. Study presents the influence of freezing and warming time on the mechanical parameters of model ice as well as differences between growth, temperature profile, and structure of ice from water-ethanol mixture and from pure water. The freezing process results for ethanol and fresh level and deformed ice were compared with developed thermodynamic models for fresh and dopant ice.

2 Introduction

2.1 Motivation

Ice ridge often represent the design loads for coastal and offshore structures. Ridge loads are usually estimated using basin tests, analytical and numerical models. For a full-scale measurement a structure should be equipped with load measuring devices, while ridge morphological parameters should be measured before the interaction, which is practically impossible. Basin tests are almost the only physical way to validate a model. But basin tests require a choice of scaling method for both mechanics and thermodynamics, which are often interconnected, because ice mechanical parameters are temperature dependent.

Basin tests are providing a unique chance to study interaction of ice ridges and structures. Geometrical scaling of such interaction under generally accepted scaling rules requires scaling of ice mechanical parameters and microstructure which is only possible using dopants and spraying. While mechanical parameters of a model level ice produced by spraying is well studied for conditions of a specific ice basin, it is little known about mechanical parameters of refrozen ice or as called consolidated layer of ice ridges. This layer cannot be produced by spraying so its microstructure is different from the model ice.

This study attempts to investigate process of consolidation of ethanol ice ridges and to find similarities and differences with freshwater ice ridges. It is also aiming to provide an accurate thermal and morphological data for further analysis of ice-structure interaction during test in Aalto ice tank. For that purpose, we performed a series of laboratory experiments aiming:

- To compare growth of LI and CL from pure water and ethanol solution.
- To find ice thicknesses of LI and CL for similar to basin test thermal conditions.
- To find connection between ice thickness and its temperature profile.

2.2 Previous studies

There are several different types of model ice. In some basins including Hamburg Ship Model Basin, Krylov State Research Centre, and Aker Arctic, natrium-chloride water solution is used together with bottom ice growth. Ethylene-glycol-aliphatic-detergent-sugar (AG/AD/S) dopant is used at NRC Ottawa Ice tank (Timco, 1986), ethanol dopant is used at the Aalto university ice basin (von Bock und Polach et al., 2013), where ice is growing from the top.

There is a limited amount of studies dealing with the consolidation of basin scale ridges. Timco and Goodrich (1988) presented results of AG/AD/S model ice ridge consolidation with the range of thickness of 10-30 cm and compared thickness values from direct measurements and from temperature profiles analysis. ITTC (1999) recommend scaling the consolidation time as the square of the geometric scaling factor similar to the Stefan equation of ice growth.

There is also a small number of studies presenting results of level ice solidification from different water-based solutions. It can be explained by only 4% difference between sea ice growth predictions with different salinity profiles (Griewank and Notz, 2013). Meanwhile, saline level ice cooled from below due to the absence of the ice desalinization process is growing faster than fresh ice in laboratory scales (Notz, 2005).

3 Methods

3.1 Methods of laboratory experiments

Laboratory experiments in consolidation of ice ridges formed from freshwater and ethanol solution were performed at the cold laboratory of NTNU at the air temperature of -17 °C. Ice was grown in two identical acrylic cylindrical water tanks with a diameter of 30 cm and side insulation. Ice ridges were grown using additional insulation forming water voids of 18x10 cm horizontal cross-section. Thickness of vertical blocks, forming ridges, was around 4 cm, similar to the performed basin experiments, the ridge macroporosity was around 33%. In one of the water tanks ethanol concentration was 0.3%, while other one was filled with freshwater. 9 level ice and 16 ridge experiments were performed to study freezing process of both liquids under the same external thermal conditions.

Both ice ridges were equipped with two thermistor strings: one in the middle of the void and one in the middle of the block. For the half of the ridge experiments ice blocks had initial temperature of -15 °C, other half of the ridges were made of worm blocks at -1 °C. After the end of each experiment ice was taken away from the water tank, thickness of consolidated layer and surrounding level ice was measured.

Growth of ice from ethanol solution is not a well-studied process according to authors knowledge. It has some similarities with saline ice growth, it also consists of liquid and solid parts whose proportions are temperature and concentration dependent. But there are also significant differences, especially at the ice bottom surface boundary conditions. Saline ice is expelling salt, so its bulk salinity is significantly lower than salinity of the water from which it was formed. This process is mainly driven by the difference in densities between more dense and saline brine and less dense underlying water. Mixture of water and ethanol is lighter than pure water, so there is no reason to expect significant differences in ethanol concentration in solid and liquid. This might lead to very high liquid fraction at the bottom of ethanol ice and faster ice growth.

In order to model growth of ice from ethanol solution its liquidus temperature should be set as a thermal boundary condition at the interface of solid and liquid parts.

3.2 Methods of basin tests

The model tests were performed on the ice tank of Aalto University. It is a 40 m by 40 m basin with 2.8 m water depth equipped with a cooling system and a carriage. The model ice for ridge creation was granular fine-grained ice produced by spraying the basin water from the moving carriage at -10°C. After reaching a design ice thickness of 40 mm, the air temperature is lowered to -12°C. A target model ice strength is obtained by warming ice. A Froude scaling was used with a geometric scale factor as well as flexural strength scale factor as 15. A total of three level ice sheets were produced, one ridge per ice sheet was built.

Table 1. Main parameters of ice tank experiments for basin and full scale

Parameter	Basin scale	Full scale
Level ice thickness h_i	4 cm	0.6 m
Keel depth h_k	40 cm	6 m
Sail height h_s	8 cm	1.2 m
Target flexural strength σ_f	50 kPa	0.75 MPa
Cylinder diameter d	50 cm	7.5 m

Ice was produced from pure water with 0.3% fraction of ethanol. Liquid solution density was 1000 kg/m^3, ice density for the floe 1 was 950 kg/m^3. Ridge block thickness was 4 cm for all 3 ice floes. Structure moving speed was 4 cm/s. Cylinder diameter was 50 cm. Ethanol-water liquidus temperature is -0.12°C.

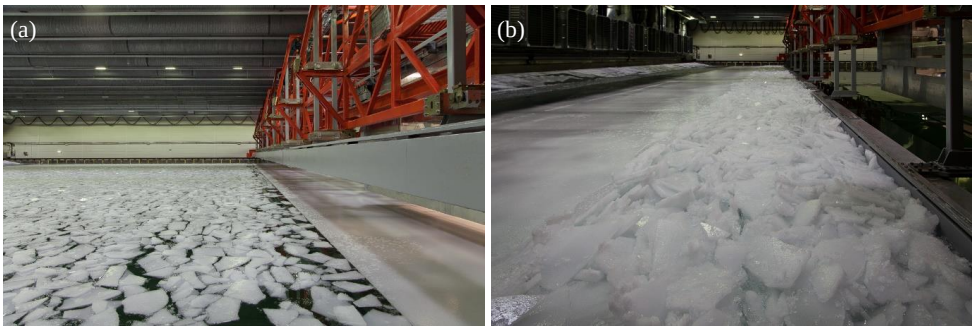

Figure 1. Ridge produced from floe 1 before (a) and after (b) ridge building.

Air temperature development is presented for different stages of experiment together with measured values of level ice flexural strength (Figure 2 and Figure 3). The first stage is spraying, when model ice is produced and cooled down to reach a certain mechanical property. After the measurement of the flexural strength, level ice can be tempered at freezing temperature or warmed to reach a preferable value of strength. When the strength is close to the needed value, a part of level ice can be broken with carriage (Figure 1a), and a ridge can be produced from that ice by pushing broken ice using pushing plates and anchoring surrounding level ice (Figure 1b). After that ice-structure interaction test with unconsolidated ice ridge can be performed. It follows by ridge consolidation at -12°C and ridge warming. When level ice flexural strength is measured again, ice-structure interaction test can be performed again with consolidated ridge.

Ridge keel depth of 40 cm was measured for the floe 3 by vertical profiling. Average measured sail height was 8 cm. Ridge 3 was produces from 40 m by 24 m ice floe with 4 cm thickness. Based on the volume of sail, keel and initial ice for the ridge production we estimated ridge initial macroporosity of 0.31.

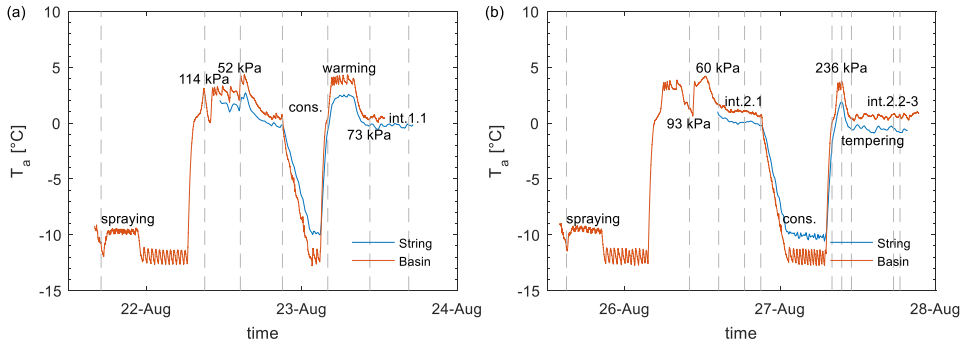

Figure 2. Air temperature timeline for ice floe 1 (a) and 2 (b).

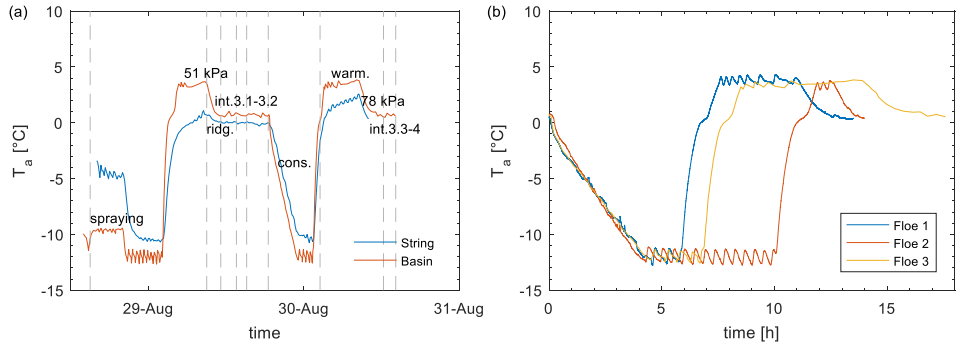

Figure 3. Air temperature timeline for ice floe 3 (a) and for ridge consolidation (b).

The main thermal values of interest are:

- Block initial temperature before ridging.
- Surface temperature of CL in comparison to of old LI.
- LI and CL thickness from T-profile.

In order to get temperature measurements two thermistors were installed in the old and new level ice and two thermistor strings were installed in the ridge. The length of each thermistor string is 40 cm, the minimum sensor spacing is 1.3 cm, time step was set to 10 minutes. We used strings from GeoPrecision GmbH with TNode EX sensors with 0.1°C accuracy in the temperature range from -20°C to +25°C. Heat flux above ice top surface was manually measured using heat flux plate Hukseflux HFP01-05 for the ice floe 3.

Temperature data can provide an information about heat transfer during ridge consolidation, temperature profile of level ice during mechanical testing and ridge temperature profile during ice-structure interaction.

Analysis of temperature data from the basin tests involves two main objectives: estimation of thickness development and vertical heat fluxes. A series of laboratory experiments were performed to develop and confirm algorithms for estimations of these parameters in the controlled environment.

Both laboratory and basin test results will be compared with results of our analytical and numerical models of level ice and ridge solidification. Analytical values of freshwater ice thickness were estimated as:

$$h_c = \left(\frac{2k_i}{\rho_i L_i \eta}(T_f - T_a)t + \left(\frac{k_i}{H_{ia}}\right)^2\right)^{0.5} - \frac{k_i}{H_{ia}}, \quad (1)$$

where k_i is the ice thermal conductivity, ρ_i is the ice density, L_i is the ice latent heat, η is the macroporosity (1 for level ice), T_f is the liquid freezing temperature, T_a is the air ambient temperature, t is the time.

For basin tests the value of heat transfer coefficient H_{ia} was found from the manually measured convective flux q_a and ice thickness h_i assuming equal convective and conductive fluxes as:

$$H_{ia} = \left(\frac{T_f - T_a}{q_a} - \frac{h_i}{k_i}\right)^{-1} \quad (2)$$

Freshwater model is described in detail in (Salganik et al., 2020), model for saline ice is described in Salganik et al. (2019).

4 Results

4.1 Results of laboratory experiments

Before the analysis of the temperature data of the performed basin test, it is important to understand, which ice thicknesses we might expect to observe in ice, grown form water-ethanol solution (alcohol ice). During our tank experiments we had ridge consolidation with freezing indexes of 50, 62 and 101 FDH at the air ambient temperature of -12°C (Figure 3b). Heat flux above level ice measured during spraying is giving heat transfer coefficient value of approximately 10 W/m^{2}K. For these values according to our analytical solution we can expect freshwater level ice thickness of 6 and 12 mm for 50 and 100 FDH respectively. For the ridge porosity of 0.31 (like in our basin and laboratory tests) estimated thickness of the freshwater consolidated layer is 17 and 34 mm for 50 and 100 FDH.

Freshwater level ice growth is a well-studied process. Thin ice growth is governed by the value of the heat transfer coefficient H_{ia}, which can be found experimentally for laboratory conditions using Eq. (1). Additional laboratory experiments were performed to check the relation between fresh and ethanol ice growth for both level ice and ridges. It was found that level ice grown from the ethanol solution is growing 15% faster and consists of two parts: strong consolidated upper part and weak dendritic lower part. Thickness of the bottom dendritic layer had thickness of approximately half of the total ice thickness (Figure 6a). Measured thickness was 6 mm and 9 mm (50 FDH), 12 mm and 16 mm (100 FDH) correspondingly for freshwater and ethanol level ice. For the same conditions consolidated layer was 23 mm and 27 mm (51 FDH), 50 mm and 48 mm (100 FDH) for freshwater and ethanol solution. Average ridge macroporosity for these laboratory experiments was 0.32. Opposite to level ice, ridges from ethanol solution didn't have weak dendritic layer and were growing as fast as fresh ice (Figure 6b).

4.1.1 Ice growth comparison

To analyse and compare conditions in the NTNU laboratory and Aalto ice basin, it is necessary to estimate the average in time heat transfer coefficient H_{ia}. For the NTNU laboratory its value was estimated from the level ice growth observation to be 13 W/m^{2}K (Figure 4a). For level ice growth in vicinity of the model ridge, the heat transfer was around 15 W/m^{2}K, slightly higher due to surface roughness. The heat transfer coefficient for the Aalto ice basin, estimated from the measured heat flux and ice thickness, was around 10 W/m^{2}K.

Table 2. Laboratory and basin experimental values of ice thickness compared with analytical and numerical thickness estimation using heat transfer coefficient H_{ia}=10 W/m^{2}K.

Floe	Type	FDH	Solution	h, basin	h, lab.	h, analyt.	h, num.
-	-	[°Ch]	-	[mm]	[mm]	[mm]	[mm]
1	LI	50	w.	-	8	6	6
			w.-eth.	20	9	8	8
2		101	w.	-	12	12	11
			w.-eth.	20	16	15	15
3		62	w.	-	8	7	7
			w.-eth.	20	9	9	10
1	CL	50	w.	-	23	17	11
			w.-eth.	15	27	20	16
2		101	w.	-	50	34	26
			w.-eth.	40	48	39	36
3		62	w.	-	23	21	14
			w.-eth.	25	27	24	21

For the considered scale of experiments, the higher value of the heat flux coefficient will give around 30 % faster growth for laboratory conditions than for ice tank. For example, for 50 and 100 FDD level ice thickness would be 7.5 mm instead of 5.8 mm and 14.7 mm instead of 11.5 mm. Measured in laboratory conditions consolidated layer thickness was 27 mm and 48 mm for ethanol solution and the same freezing indexes (Table 2). These values are larger than temperature sensor spacing of 13 mm so we can expect to measure ice thickness in the basin experiment with a reasonable accuracy (Figure 5).

4.1.2 Ice thickness estimation and ice structure

For large scale experiments indirect thickness estimation from the vertical temperature profile is a trivial process due to a significant temperature difference between ice top and bottom surfaces. For smaller scales the most of temperature changes are occurring in the air inside thermal boundary layer. Thickness estimation from the temperature profile is limited by temperature sensors spacing. At least two sensors should be frozen and be considerably colder than the liquid freezing point. As it can be clearly seen, achievable sensor spacing (13 mm in our experiment) can be easily not enough to estimate thicknesses of newly formed level ice for the considered range of freezing time. Fortunately, thickness of newly formed level ice is not of a significant interest for the ice basin ridge experiments. But for the accurate estimation of freezing rates this problem was approached for the more controlled laboratory experiments.

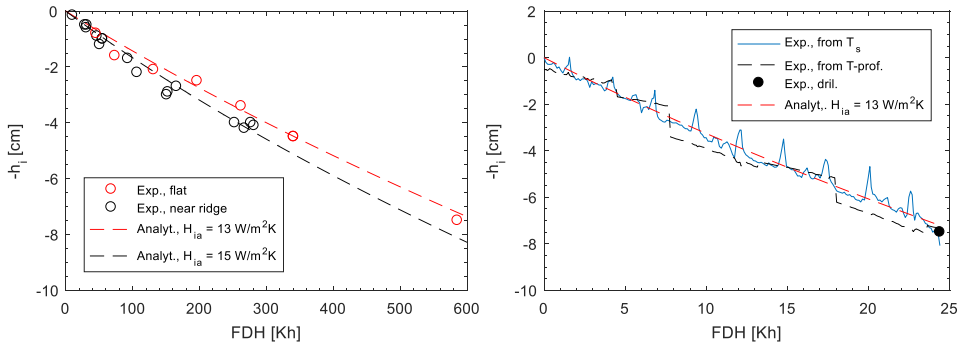

Figure 4. Freshwater level ice thickness vs FDH for experiments with different surface roughness using direct thickness measurements (a) and from different thickness estimation algorithms during single experiment (b).

Assuming constant value of heat transfer coefficient it is possible to estimate ice thickness from its measured surface temperature for almost any thickness range (Figure 4b). Examples of temperature profiles for 50 and 100 FDH at the end of experiments are presented in Figure 5. It shows the difference between temperatures in the ridge voids and blocks, that can lead to the thickness overestimation of approximately 2 cm for the block profiles.

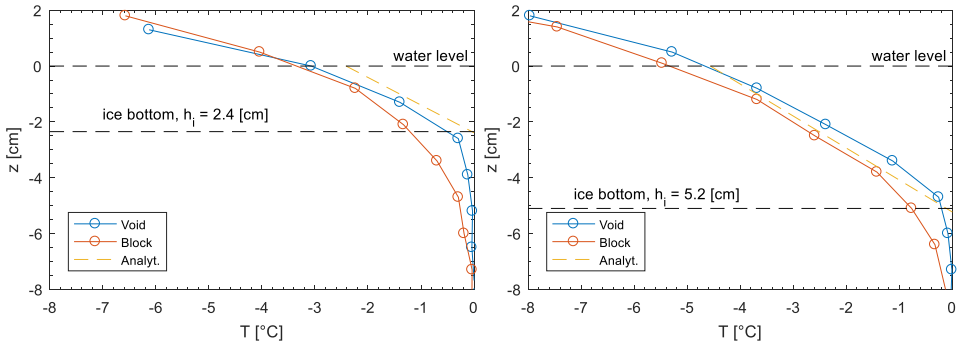

Figure 5. Temperature profiles of freshwater ridges at the end of laboratory experiments with 50 FDH (a) and 100 FDH (b).

We performed comparison of level ice growth from freshwater and from 0.3 % ethanol solution in identic thermal conditions. It was found that ethanol ice is growing approximately 15 % faster than freshwater ice (Figure 6a). This difference was close to the difference between saline and fresh ice growth based on our numerical model for 0.3 % salinity for both liquid and solid parts.

Additionally, ethanol ice has a dendritic structure with dendrites occupying approximately 50 % of the total ice thickness, while freshwater ice has a planar thermodynamically stable interface. The same ice structure was nor observed during experiments with ethanol ridges: consolidated layer didn't have a large layer of dendrites. According to the performed thin sections and similarly

to the numerical simulations ice growth in ridges occurs mostly in a horizontal direction, allowing to overcome supercooled layer of liquid.

Values of consolidated layer thickness as a function of FDH from experiments and from our numerical model is shown in Figure 6b. We haven't found any significant difference in consolidation rates between freshwater and ethanol ridges based on our laboratory results. Both ridges produced from warm (-1 °C) and cold (-15 °C) blocks were freezing close to the results of our analytical and numerical models for the FDH lower than 200 °Ch.

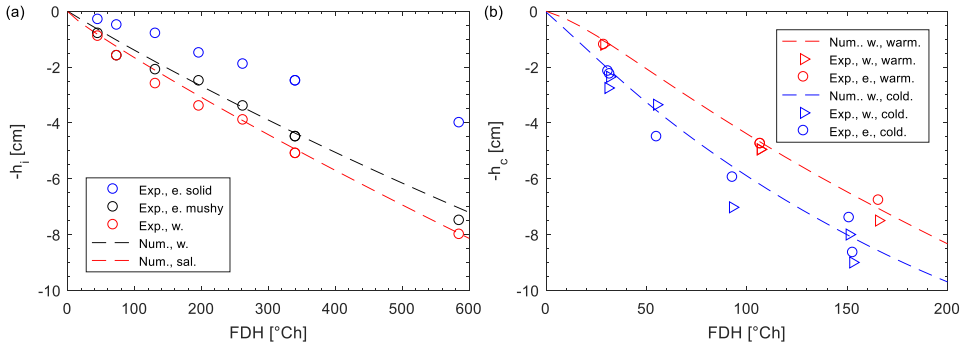

Figure 6. Level ice (a) and consolidated layer thickness (b) vs FDH for experimental, analytical and numerical experiments.

The experiments with warm blocks can be well described by analytical solution even for larger scales. For the cold blocks consolidated layer thickness is usually underestimated analytically for the initial stages of experiments and overestimated for the larger scales (Figure 7a).

The results of laboratory experiments for cold blocks can be only explained if some part of initial block sensible heat goes not to porosity change but to consolidated layer growth (Figure 7b). For the analysis we used two factors: ratio of consolidated layer and level ice thickness $R = h_c/h_i$ and corresponding normalized factor R_n defined as (Salganik et al., 2020):

$$R_n = \left(\frac{h_c(h_c + 2k_i/H_{ia})}{h_i(h_i + 2k_i/H_{ia})} \eta_0 \right)^{0.5} \quad (3)$$

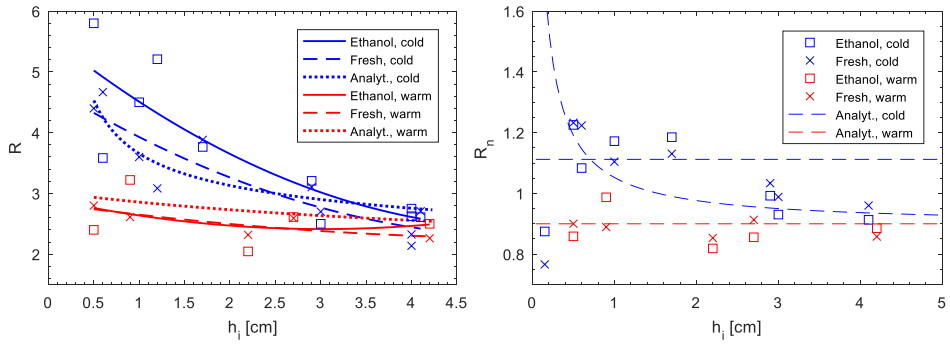

Figure 7. R (a) and R_n (b) factors vs level ice thickness from the lab. experiments and from analytical solution.

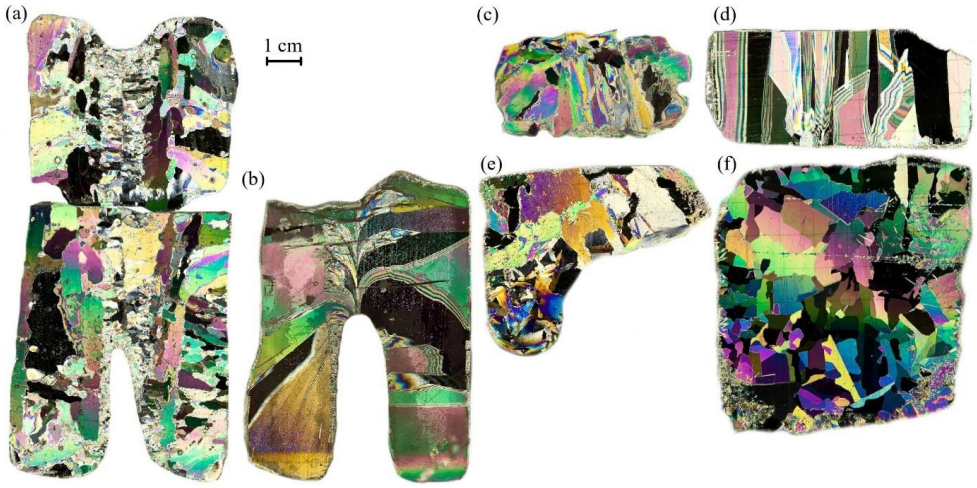

Figure 8. Vertical thin section of ethanol ridge (a), freshwater ridge (b), ethanol level ice (c), freshwater level ice (d), horizontal thin section of ethanol level ice (e), freshwater level ice (f).

Grain size was estimated using thin sections presented in Figure 8. Freshwater level ice had grains around 5 mm, ethanol level ice had slightly smaller grains of 4 mm. Newly formed ice in consolidated layer had much finer grains around 1 mm for both freshwater and ethanol ridges.

4.2 Results of basin test experiments

Temperature profiles were measured in the model ice produced by spraying. Its directly measured thickness was in the range of 40–45 mm. Temperature profiles in that ice confirms those values (Figure 9a). During the end of consolidation time there was a thin layer of supercooled water under the old level ice, which disappeared after the start of warming phase.

Table 3. Measured and estimated ice thickness for basin tests [mm]

Ice type / Ice sheet	Sheet 1	Sheet 2	Sheet 3
New LI	22 / 20 (T)	20 (T)	20 (T)
Old LI	41-45	40-41 / 35 (cam.)	40-42
CL	15 / 20 (T)	40 / 40 (T)	25 / 25 (T)

Estimated from temperature profile consolidated layer thickness is 20 mm for floe 1, 40 mm for floe 2 and 25 mm for floe 3 (Figure 9b).

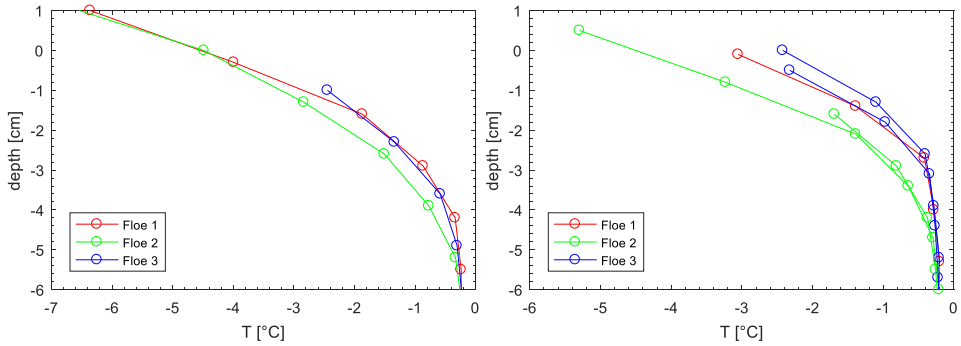

Figure 9. Old level ice (a) and ridge (b) coldest temperature profiles during consolidation.

Thickness values of different ice types measured directly, estimated from camera photos (cam.) and from temperature profiles (T) are presented in Table 3. Those measured and estimated thickness values are in a good agreement with the results of numerical modelling (Table 2).

5 Discussion

5.1 Accuracy of ridge basin tests

Estimation of ice top surface temperature and ice thickness for small scale experiments involves several complications. At least two sensors should be frozen in order to accurately quantify ice thickness and temperature gradient. Meanwhile, the sensor located between air and solid ice can provide incorrect values of the ice top surface temperatures due to their non-zero size and location.

Basin tests with ice-structure interaction are providing unique chance to have a scaled experiment with load measurements. But there are many uncertainties in ridge morphological parameters, which can make analysis of the interaction in comparison to the full scale complicated. One of these parameters is a thickness of consolidated layer. Laboratory experiments validated with analytical and numerical modelling were performed to provide more accurate predictions of consolidation rates for similar conditions to the performed basin experiment.

Measurements of consolidated layer thickness for ridges produced in ice basins includes a lot of uncertainties due to the high ratio of measuring methods errors and ranges of thickness. Direct measurements are almost impossible because basin scale ridge from ethanol ice is too fragile so it

can’t be elevated from the liquid. Model ice is also not providing enough resistance to perform ice drilling suitable for the ridge profiling.

Temperature profiles can also be used, but their measurements could be influenced by several factors: local sail height, local keel depth and vertical position of thermistor. The sail height is believed to be the key factor: it is hard to measure during installation, while sail height is usually several times larger than consolidated layer thickness. Presence of keel blocks submerged into consolidated layer can make the temperature profile non-linear. Both sail and keel underestimation can lead to an overestimation of the consolidated layer thickness.

Another important value which is hard to measure with a good precision is a ridge macroporosity. For our basin tests it was estimated from the cross-sectional profiles of keel depth, average sail height and initial ice volume before ridge production. Tuhkuri (2002) showed a large variability of ridge macroporosity values for similar ridging conditions in Aalto ice basin.

6 Summary and conclusions

Thickness estimation of consolidated layer thickness can give only an idea of thickness range, but both accuracy and number of experiments is not enough to make a good correlation between freezing time and ice growth.

Additional laboratory experiments were performed to compare solidification of freshwater and ethanol level ice and ice ridges, to validate analytical and numerical models of ridge consolidation, and to provide more accurate thickness values for further analysis of basin test results.

Main results of the study can be summarized as:

- Laboratory experiments confirm a significant difference in temperature profiles in ridge voids and blocks, that can lead to thickness overestimation by the half block thickness.
- Validation of ridge consolidation model can be performed only in laboratory conditions with well-known key parameters including ridge macroporosity, heat transfer coefficient and position of thermistors.
- Level ice grown from 0.3% water-ethanol solution is growing 15% faster and has smaller grain size than level ice from pure water.
- Ice ridges grown from pure water and from water-ethanol solution have similar consolidation rate and similar grain size of newly formed ice.
- In order to keep the value of level ice flexural strength before consolidation, basin ice ridges must be warmed after the consolidation for approximately the same time.

References

Griewank, P.J., Notz, D., 2013. Insights into brine dynamics and sea ice desalination from a 1-D model study of gravity drainage. J. Geophys. Res. Ocean. 118, 3370–3386. https://doi.org/10.1002/jgrc.20247

Notz, D., 2005. Thermodynamic and fluid-dynamical processes in sea ice. University of Cambridge.

Salganik, E., Høyland, K.V., Maus, S., 2020. Consolidation of fresh ice ridges for different scales. Cold Reg. Sci. Technol. 171. https://doi.org/10.1016/j.coldregions.2019.102959

Salganik, E., Høyland, K.V., Shestov, A., Løset, S., Heijkoop, A.-N., 2019. Medium-scale consolidation of artificial ice ridge-Part I: surface temperature, thickness and mechanical properties, in: Proceedings of the 25th International Conference on Port and Ocean Engineering under Arctic Conditions, Delft, The Netherlands.

Tests, M., Predictions, F.S., Wake, F.S., Factors, M.C., Data, I., Data, O., Example, T., Analysis, U., With, C., Scale, F., 1999. ITTC – Recommended Procedures ITTC – Test Methods for Model Ice Properties. ReVision.

Timco, G.W., 1986. EG/AD/S: A new type of model ice for refrigerated towing tanks. Cold Reg. Sci. Technol. https://doi.org/10.1016/0165-232X(86)90032-7

Timco, G.W., Goodrich, L.E., 1988. Ice rubble consolidation. Proc. 9th Int. Symp. Ice, Int. Assoc. Hydraul. Eng. 1, 537–548.

Tuhkuri, J., 2002. Laboratory tests on ridging and rafting of ice sheets. J. Geophys. Res. 107, 1–14. https://doi.org/10.1029/2001jc000848

von Bock und Polach, R., Ehlers, S., Kujala, P., 2013. Model-scale ice - Part A: Experiments. Cold Reg. Sci. Technol. 94, 74–81. https://doi.org/10.1016/j.coldregions.2013.07.001